ANALYSIS AND MODELLING OF THE ELECTRICAL CONTROL ACTIVITY IN HUMAN COLON

By

BERJ LUTHER BARDAKJIAN, M.A.Sc.

A Thesis

Submitted to the School of Graduate Studies

in Partial Fulfilment of the Requirements

for the Degree

Doctor of Philosophy

McMaster University

September 1978

ELECTRICAL CONTROL ACTIVITY IN HUMAN COLON

to arshalous
the dawn
of my
awakening
and
a stem
of transcendent
connectivity
culminating in
the twilight
of encompassing
empathy

DOCTOR OF PHILOSOPHY (1978)
(Electrical Engineering)

McMASTER UNIVERSITY
Hamilton, Ontario

TITLE: Analysis and Modelling of the Electrical Control Activity in Human Colon

AUTHOR: Berj Luther Bardakjian, M.A.Sc. (University of Toronto)

SUPERVISOR: Dr. S.K. Sarna

NUMBER OF PAGES: xvii, 307

ABSTRACT

The electrical control activity in human colon was analyzed using an interactive processor, which was developed and implemented on a NOVA 830 minicomputer, for the analysis of a biological rhythm. The characteristics of the human colonic electrical control activity varied in time and space. The colonic control waves were continuously present with waxing and waning of their amplitudes and they were not continuously phase-locked in either the longitudinal or the circumferential directions. Furthermore, multiple fundamental frequencies along with harmonic frequencies were present whereby the intensity of a harmonic frequency could be larger than that of a fundamental frequency.

An interactive processor for modelling of a biological rhythm by a population of coupled relaxation oscillators was developed and implemented on a NOVA 830 minicomputer, whereby each oscillator could be selectively stimulated.

A tubular structure of bidirectionally coupled rings of bidirectionally coupled synthesized relaxation oscillators was used to model the human colonic electrical activity. The computer model qualitatively reproduced the observed characteristics of human colonic electrical control activity. A mathematical investigation of a population of coupled synthesized relaxation oscillators elucidated the nature of waxing and waning of the amplitudes of control waves. Furthermore, it provided the conditions of synchronization of the population which led to the derivation of conditions of entrainment of a synthesized relaxation oscillator by different external stimuli.

ACKNOWLEDGEMENTS

The author wishes to express his sincere gratitude to Dr. S.K. Sarna for his expert guidance and helpful suggestions throughout the course of this work. Special thanks are due to Dr. J.F. Lind and Dr. W.E. Waterfall for implanting the electrodes during surgery. The author also wishes to thank Dr. J.W. Bandler, Dr. E.E. Daniel and Dr. E. Della Torre for their valuable suggestions and constructive criticisms.

The varied cooperation and help received from Dr. C. Charalambous, J.H.K Chen, K. Clark, Dr. J. Fox, T. Kung, P. Liu, J.R. Popovic and L. Wright is gratefully appreciated. Also, Ms. V. Bharatha is thanked for typing this thesis.

The financial support provided by the Medical Research Council of Canada, the National Research Council of Canada and the Department of Electrical Engineering at McMaster University is gratefully acknowledged.

The author is greatly indebted to his mother and brothers for providing the moral and emotional support which formed a key element in sustaining the stamina to carry out this work.

TABLE OF CONTENTS

		Page
CHAPTER 1 -	INTRODUCTION	1
	1.1 - A General Perspective	1
	1.2 - Scope and Objectives	10
	1.3 - Points of Investigation and Their Organization	10
CHAPTER 2 -	COMPUTER-AIDED DESIGN OF IIR DIGITAL FILTERS	13
	2.1 - Introduction	13
	2.1.1 - Regarding IIR Digital Filters with Large-Word-Length Coefficients	13
	2.1.2 - Regarding IIR Digital Filters with Finite-Word-Length Coefficients	15
	2.2 - Least pth Optimization of IIR Digital Filters with Large-Word-Length Coefficients	17
	2.2.1 - Description of the Problem	17
	2.2.2 - Problem Formulation	18
	2.2.3 - Stability Constraints	19
	2.2.4 - Description of a Computer Program for IIR Digital Filter Design	21
	2.2.5 - Examples	23
	2.3 - Design of IIR Digital Filters with Finite-Word-Length Coefficients	41
	2.3.1 - Description of the Problem	41
	2.3.2 - Problem Formulation	42
	2.3.3 - Examples	44
	2.4 - Discussion	57
CHAPTER 3 -	AN OPTIMAL PROCESSOR FOR MULTISTAGE DECIMATION AND FILTERING	59
	3.1 - Introduction	59
	3.2 - A Multistage Decimator	60
	3.2.1 - Derivation of Bounds on D_1, D_T, N and α	67

3.2.2 - An Optimal Multistage Decimator 69
3.2.3 - An Algorithmic Implementation of a Multiple-Input Multistage Decimating IIR Digital Filter 72
3.2.4 - Example 3.1 77

3.3 - Discussion 80

CHAPTER 4 - INTERACTIVE PROCESSORS FOR ANALYSIS AND MODELLING OF BIOLOGICAL RHYTHMS 84

4.1 - Introduction 84
4.2 - An Interactive Processor for Analysis of Biological Rhythms 86

4.2.1 - Formulation of the Discrete-Time and Discrete-Frequency Processes 88
4.2.2 - Tuneable IIR Digital Filters 92
4.2.3 - A Modular Structure for the Multichannel Analysis Processor 98
4.2.4 - Control of the Multichannel Analysis Processor 104
4.2.5 - Examples 106

4.3 - An Interactive Processor for Modelling of Biological Rhythms 108

4.3.1 - A General Structure of the Modelling Processor 114
4.3.2 - Example 4.3 117

4.4 - Discussion 118

CHAPTER 5 - MATHEMATICAL INVESTIGATION OF POPULATIONS OF COUPLED SROs 125

5.1 - Introduction 125
5.2 - The Generic Equation of a Population of Coupled SROs 125
5.3 Synchronization of a Population of Coupled SROs 134
5.4 - Entrainment of a SRO by an External Stimulus 138
5.5 - Discussion 143

CHAPTER 6 - ANALYSIS OF THE ECA IN HUMAN COLON 145

6.1 - Introduction 145

6.2 - Methods 148

6.2.1 - Acquisition of Biological Data 148
6.2.2 - Computer-Aided Analysis of Biological Data 150

6.3 - Results 151

6.3.1 - Characteristics of Human Colonic ECA 151
6.3.2 - Relationship Between ECA Frequency and Repetition Rate of Response Potentials in Human Colon 186
6.3.3 - Effects of Morphine and Feeding 197

6.4 - Discussion 197

CHAPTER 7 - A MODEL OF THE ECA IN HUMAN COLON 204

7.1 - Introduction 204
7.2 - The Generic Equation 205
7.3 - The Model Structure 206
7.4 - The Simulation Program 208
7.5 - Simulation Results 212

7.5.1 - Effects of Recording Instruments 222
7.5.2 - Effects of External Stimulation 234
7.5.3 - Effects of Transection 234

7.6 - An Extension of ECA Model to Include ERA 246
7.7 - Discussion 249

CHAPTER 8 - CONCLUSIONS 252

APPENDIX I - PARTIAL DERIVATIVES OF THE GENERALIZED LEAST PTH OBJECTIVE FUNCTION WITH RESPECT TO THE IIR DIGITAL FILTER COEFFICIENTS 259

APPENDIX II - THE OUTPUTS OF ALL OSCILLATORS IN A POPULATION OF COUPLED SROs 263

APPENDIX III - THE OUTPUTS OF ALL OSCILLATORS IN A POPULATION OF UNCOUPLED SROs 275

APPENDIX IV - A DIGITAL SIMULATOR OF AN ANALOG INPUT COUPLER 287

APPENDIX V - AN EXTENSION OF THE GENERIC EQUATION OF ECA MODEL TO INCLUDE ERA 290

REFERENCES 293

LIST OF FIGURES

Figure		Page
Fig. 2.1	A general structure of CADRDF	22
Fig. 2.2 a	Passband response for Example 2.1	29
Fig. 2.2 b	Stopband response for Example 2.1	30
Fig. 2.2 c	Pole-zero configuration of H(z) for Example 2.1	31
Fig. 2.3	More densely sampled magnitude response of the filter given by Steiglitz. (a) Passband response. (b) Stopband response.	33
Fig. 2.4	Magnitude response for Example 2.2. (a) Passband response. (b) Stopband response. (c) Pole-zero configuration of H(z).	40
Fig. 2.5 a	The feasible region for Example 2.3	46
Fig. 2.5 b	Tree structure for Example 2.3	48
Fig. 2.5 c	Contours of the unconstrained minimax objective function for Example 2.3, where $r_2 = q_2 = 1$	49
Fig. 2.6	Magnitude response for Example 2.4. (a) Passband response. (b) Stopband response.	53
Fig. 2.7	Magnitude response for Example 2.5. (a) Passband response. (b) Stopband response.	54
Fig. 3.1	An M-input multistage decimating filter	61
Fig. 3.2	Stage i of an M-input multistage decimating filter	64
Fig. 3.3	Parameters prescribing (a) magnitude swuared characteristics of elliptic low-pass IIR digital filters and (b) magnitude characteristics of optimal low-pass IIR digital filters, ψ is a normalized frequency equal to twice the frequency divided by the sampling frequency.	65
Fig. 3.4	Contours of the objective funtion U along with the constrainst $\alpha \geq 4.5\beta$	79

Figure		Page
Fig. 3.5	Electrical activity recorded from 3 sets of bipolar electrodes E1, E2 and E3 placed subserosally on the taenia coli of ascending colon. For each electrode, the activity before and after filtering and decimation is shown in the top and bottom traces, respectively.	82
Fig. 4.1	A schematic representation of a multiple-input processor for the analysis of biological rhythms	87
Fig. 4.2	Charting symbols for analysis processor	99
Fig. 4.3	A schematic representation of a modular structure of the Generator (GMPC) of Multichannel Processor's Controlling data files (DF0-DF6)	100
Fig. 4.4	A schematic representation of a modular structure of the command (EMP) to Execute Multichannel Processing	102
Fig. 4.5	Human Colonic Electrical Activity recorded from 4 sets of bipolar electrodes E1, E2, E3 and E4 placed subserosally on the taenia coli of descending (E1, E2) and sigmoid (E3, E4) colon. The top trace depicts the respiration signal.	107
Fig. 4.6	User-Computer dialogue for Example 4.1	109
Fig. 4.7	The frequency spectrum of the signal recorded from E4 and computed with a frequency resolution of 0.293 cpm	110
Fig. 4.8	(a) The cross-spectrum of a signal pair recorded from E2 and E3 and computed with a frequency resolution of 0.293 cpm (b) The cross-correlation function of signal pair recorded from E2 and E3 and computed with a time resolution of 0.2 sec	111
Fig. 4.9	User-Computer dialogue for Example 4.2	112
Fig. 4.10	Human Colonic Electrical Activity recorded from a (out of 3) sets of bipolar electrodes E1 and E2 placed subserosally on the taenia coli of ascending colon. The activity before (the two upper traces) and after (the two lower traces) band-pass filtering (2-4 cpm) is shown. Continuous lines join the zero crossings of waveforms.	113

Figure		Page
Fig. 4.11	Charting symbols for modelling processor	115
Fig. 4.12	A general structure of the modelling processor	116
Fig. 4.13	User-supplied programs (a) Main program for dimensioning (b) Subroutine Opus 5 for prescribing the population of oscillators	119
Fig. 4.14	User-computer dialogue for Example 4.3	120
Fig. 4.15	Listing of parameters. The stimulation parameters per oscillator consist of a flag to indicate presence and type of stimulus, application time in sec, removal time in sec, a time-shift factor equal to application time plus one half the pulse width, highest harmonic component in truncated fourier series, average value, angular frequency and pulse width, respectively.	121
Fig. 4.16	Outputs of the two coupled oscillators of Example 4.3	122
Fig. 5.1	A transformational synthesis approach	127
Fig. 5.2	Representation of the state of the fundamental nth oscillator. (a) When isolated from its neighborhood. (b) When coupled to its neighborhood.	129
Fig. 5.3	Two unidirectionally coupled SROs representing external stimulation of a SRO	139
Fig. 5.4	Theoretical strength-duration curve for a SRO	142
Fig. 6.1	Diagram of the colon	146
Fig. 6.2	Arrangement of electrodes	149
Fig. 6.3 a	Human colonic electrical activity recorded from 3 sets of bipolar electrodes placed subserosally on the taenia coli of ascending colon. Electrode sets E1 and E2 were placed in the longitudinal direction whereas E1 and E3 were placed in the circumferential direction.	153

Figure		Page
Fig. 6.3 b	Human colonic electrical activity recorded from the ascending colon of the same patient of Fig. 6.3, a. For each electrode, the activity before and after low-pass filtering (f_c = 0.275 Hz) and decimation is shown in the top and bottom traces, respectively.	154
Fig. 6.4 a	The power spectrum of a signal recorded from E1 in the ascending colon of the patient of Fig. 6.3, computed with a frequency resolution of 0.293 cpm	155
Fig. 6.4 b	The power spectrum of a signal recorded from E2 in the ascending colon of the patient of Fig. 6.3, computed with a frequency resolution of 0.293 cpm	156
Fig. 6.4 c	The power spectrum of a signal recorded from E3 in the ascending colon of the patient of Fig. 6.3, computed with a frequency resolution of 0.293 cpm	157
Fig. 6.4 d	The cross spectrum of signal pair recorded from E1 and E2 in the ascending colon of the patient of Fig. 6.3, computed with a frequency resolution of 0.293 cpm	158
Fig. 6.5	Phase-lag variation of human colonic ECA recorded from the ascending colon of the patient of Fig. 6.3 and band-pass filtered (2-4 cpm). E1 and E3 were in the circumferential direction whereas E1 and E2 were in the longitudinal direction.	159
Fig. 6.6	Human colonic electrical activity recorded from 3 sets of bipolar electrodes placed subserosally, in the longitudinal direction, on the taenia coli of ascending colon	160
Fig. 6.7	The power spectrum of a signal recorded from E2 in the ascending colon of the patient of Fig. 6.6, computed with a frequency resolution of 0.293 cpm	161
Fig. 6.8	Human colonic electrical activity recorded from 6 sets of bipolar electrodes placed subserosally on the taenia coli of transverse colon	164
Fig. 6.9	The power spectrum of a signal recorded from E2 in the transverse colon of the patient of Fig. 6.8, computed with a frequency resolution of 0.293 cpm	165

Figure		Page
Fig. 6.10	Human colonic electrical activity recorded from 6 sets of bipolar electrodes placed subserosally on the taenia coli of transverse colon. Electrode sets E1-E5 were placed in the longitudinal direction whereas E5 and E6 were placed in the circumferential direction.	166
Fig. 6.11 a	The power spectrum of a signal recorded from E2 in the transverse colon of the patient of Fig. 6.10	167
Fig. 6.11 b	The power spectrum of a signal recorded from E1 in the transverse colon of the patient of Fig. 6.10, computed with a frequency resolution of 0.293 cpm	168
Fig. 6.11 c	The power spectrum of a signal recorded from E1 in the transverse colon of the patient of Fig. 6.10, computed with a frequency resolution of 0.293 cpm	169
Fig. 6.11 d	The power spectrum of a signal recorded from E1 in the transverse colon of the patient of Fig. 6.10, computed with a frequency resolution of 0.293 cpm	170
Fig. 6.11 e	The cross spectrum of signal pair recorded from E3 and E4 in the transverse colon of the patient of Fig. 6.10, computed with a frequency resolution of 0.293 cpm.	171
Fig. 6.12	Human colonic electrical activity recorded from 4 sets of bipolar electrodes placed subserosally on the taenia coli of descending colon	175
Fig. 6.13	The power spectrum of a signal recorded from E4 in the descending colon of the patient of Fig. 6.12, computed with a frequency resolution of 0.293 cpm	176
Fig. 6.14	Human colonic electrical activity recorded from 4 sets of bipolar electrodes placed subserosally on the taenia coli of descending and sigmoid colon. E1 and E2 were placed in the descending colon whereas E3 and E4 were placed in the sigmoid colon.	177
Fig. 6.15	The power spectrum of a signal recorded from E1 in the descending colon of the patient of Fig. 6.14, computed with a frequency resolution of 0.293 cpm	178
Fig. 6.16	Human colonic electrical activity recorded from 4 sets of bipolar electrodes placed subserosally on the taenia coli of sigmoid colon	181

Figure		Page
Fig. 6.17 a	The power spectrum of a signal recorded from E2 in the sigmoid colon of the patient of Fig. 6.16, computed with a frequency resolution of 0.293 cpm	182
Fig. 6.17 b	The power spectrum of a signal recorded from E4 in the sigmoid colon of the patient of Fig. 6.16, computed with a frequency resolution of 0.293 cpm	183
Fig. 6.18 a	Human colonic electrical activity recorded from 4 sets of bipolar electrodes placed subserosally on the taenia coli of descending and sigmoid colon. E1 and E2 were placed in the descending colon whereas E3 and E4 were placed in the sigmoid colon.	187
Fig. 6.18 b	Band-pass filtering (2-5 cpm) of the human colonic electrical activity of Fig. 6.18 a	188
Fig. 6.18 c	High-pass filtering (f_c = 20 cpm) of the human colonic electrical activity of Fig. 6.18 a	189
Fig. 6.19 a	The power spectrum of a signal recorded from E1 in the descending colon of the patient of Fig. 6.18, computed with a frequency resolution of 0.293 cpm	190
Fig. 6.19 b	The power spectrum of a signal recorded from E2 in the descending colon of the patient of Fig. 6.18, computed with a frequency resolution of 0.293 cpm	191
Fig. 6.19 c	The power spectrum of signal recorded from E2 in the descending colon of the patient of Fig. 6.18, computed with a frequency resolution of 0.293 cpm	192
Fig. 6.20	Human colonic electrical activity recorded from E1 in the descending colon of the patient of Fig. 6.14	193
Fig. 6.21 a	The power spectrum of the signal recorded from E1 of Fig. 6.20 computed over a 0.5 minute time segment in the first quarter time interval	194
Fig. 6.21 b	The power spectrum of the signal recorded from E1 of Fig. 6.20 computed over a 0.5 minute time segment in the second quarter time interval	195
Fig. 6.21 c	The power spectrum of the signal recorded from E1 of Fig. 6.20 computed over a 0.5 minute time segment in the third quarter time interval	196

Figure		Page
Fig. 6.22 a	Human colonic electrical activity recorded from the ascending colon 10 minutes after an intra-muscular injection of morphine (10 mg). For each electrode, the middle trace is low-pass filtered (f_c = 0.275 Hz) whereas the lower trace is high-pass filtered (f_c = 20 cpm).	198
Fig. 6.22 b	The power spectrum of a signal recorded from E2, before the morphine injection, computed with a frequency resolution of 0.293 cpm	199
Fig. 6.22 c	The power spectrum of a signal recorded from E2, after the morphine injection, computed with a frequency resolution of 0.293 cpm	200
Fig. 6.23 a	Human colonic electrical activity recorded from the descending and sigmoid colon, of the patient of Fig. 6.16, before food	201
Fig. 6.23 b	Human colonic electrical activity recorded from the descending and sigmoid colon, of the patient of Fig. 6.16, immediately after eating	202
Fig. 7.1	Arrangement of oscillators in model of human colonic ECA	207
Fig. 7.2	Intrinsic frequency gradients in the longitudinal (along the r axis) and circumferential directions of ECA model	211
Fig. 7.3	A general structure of the simulation program SISYPHUS	213
Fig. 7.4	Oscillator outputs from the coupled population. For each oscillator output, the maximum amplitude is normalized to unity and the simulated time segment is of 2 minutes duraiton.	214
Fig. 7.5 a	The power spectrum of an output from oscillator 2 in the model's ascending colon, computed with a frequency resolution of 0.234 cpm	215
Fig. 7.5 b	The power spectrum of an output from oscillator 5 in the model's ascending colon, computed with a frequency resolution of 0.234 cpm	216

Figure		Page
Fig. 7.5 c	The power spectrum of an output from oscillator 46 in the model's transverse colon, computed with a frequency resolution of 0.234 cpm	217
Fig. 7.5 d	The power spectrum of an output from oscillator 49 in the model's transverse colon, computed with a frequency resolution of 0.234 cpm	218
Fig. 7.5 e	The power spectrum of an output from oscillator 66 in the model's descending colon, computed with a frequency resolution of 0.234 cpm	219
Fig. 7.5 f	The power spectrum of an output from oscillator 91 in the model's sigmoid colon, computed with a frequency resolution of 0.234 cpm	220
Fig. 7.6	Limit cycles of oscillators from the coupled population. (a) osc. 2 (b) osc. 5 (c) osc. 46 (d) osc. 49 (e) osc. 63 (f) osc. 66 (g) osc. 88 and (h) osc. 91	221
Fig. 7.7	Phase-lag variations in the model's ascending colon. Osc. 23 & osc. 24 are in the circumferential direction whereas osc. 24 & osc. 27 are in the longitudinal direction. Continuous lines join the zero crossings of waveforms.	225
Fig. 7.8	Oscillator outputs from the uncoupled population. For each oscillator output, the maximum amplitude is normalized to unity and the simulated time segment is of 2 minutes duration.	226
Fig. 7.9 a	The power spectrum of an output from intrinsic oscillator 2 in the uncoupled population, computed with a frequency resolution of 0.234 cpm	227
Fig. 7.9 b	The power specturm of an output from intrinsic oscillator 5 in the uncoupled population, computed with a frequency resolution of 0.234 cpm	228
Fig. 7.9 c	The power spectrum of an output from intrinsic oscillator 66 in the uncoupled population, computed with a frequency resolution of 0.234 cpm	229
Fig. 7.9 d	The power spectrum of an output from intrinsic oscillator 91 in the uncoupled population, computed with a frequency resolution of 0.234 cpm	230

Figure		Page
Fig. 7.10	Limit cycles of oscillators from the uncoupled population. (a) osc. 2 (b) osc. 5 (c) osc. 46 (d) osc. 49 (e) osc. 63 (f) osc. 66 (g) osc. 88 and (h) osc. 91	231
Fig. 7.11	Oscillator outputs from the coupled population after processing by a simulator of an RC input coupler. For each oscillator output, the maximum amplitude is normalized to unity and the simulated time segment is of 2 minutes duration.	232
Fig. 7.12	Oscillator output from the coupled population recorded by a Beckman recorder after conversion to an analog form via a digital-to-analog converter	233
Fig. 7.13	Effects of stimulation of oscillator 44 in the coupled population by a rectangular stimulus (amplitude 0.8, period = 1 sec and pulse width = 0.3 sec). For each oscillator output, the maximum amplitude is normalized to unity and the simulated time segment is of 1 minute duration.	235
Fig. 7.14	Effects of a partial longitudinal transection between oscillators 37 & 38, 40 & 41, 43 & 44, 46 & 47 and 49 & 50 in the coupled population. For each oscillator output, the maximum amplitude is normalized to unity and the simulated time segment is of 1.5 minutes duration.	237
Fig. 7.15	Effects of a complete circumferential transection in the model's transverse colon between oscillators 43 & 46, 45 & 47 and 44 & 48 in the coupled population. For each oscillator output, the maximum amplitude is normalized to unity and the simulated time segment is of 2 minutes duration.	239
Fig. 7.16	Effects of a complete circumferential transection in the model's distal colon between oscillators 85 & 88, 86 & 89 and 87 & 90 in the coupled population. For each oscillator output, the maximum amplitude is normalized to unity and the simulated time segment is of 2 minutes duration.	242
Fig. 7.17	Effects of a simulated partial colectomy (oscillators 28-81 removed) and an end-to-end anastomosis (oscillators 25 & 82, 26 & 83 and 27 & 84 coupled back together with a coupling factor of 0.05). For each oscillator output, the maximum amplitude is normalized to unity and the simulated time segment is of 2 minutes duration.	244

Figure		Page
Fig. 7.18	The four state variables of an oscillator exhibiting ECA and ERA. For each state variable the maximum amplitude is normalized to unity and the simulated time segment is of 15 sec duration.	247
Fig. 7.19	Limit cycles of an oscillator exhibiting ECA and ERA.	248

CHAPTER 1

INTRODUCTION

1.1 A General Perspective

Many biological rhythms are attributable to populations of interacting relaxation oscillators (Van der Pol 1940; Winfree 1967; Pavlidis 1973; Sarna 1975a) for example, the males of some species of the south-east Asian fireflies had been reported (Buck 1935, 1938, 1966; Harvey 1940; Hameda 1955) to produce a spectacle as they tended to flash at regular intervals but the event could be delayed or triggered precociously by the sight of a neighbor flashing, consequently, whole treefulls of the insects ignited and lapsed back into darkness quite regularly portraying synchronous flashing of the aggregation. On the other hand, the Jamaican fireflies had been reported (Buck 1937) to produce another type of luminous display on trees since each firefly, while walking along the twigs, tended to flash regularly but indepedendently of other flashing neighbors, consequently, the aggregation flashed asynchronously. Van der Pol and Van der Mark (1928) drew explicit parallels between normal and abnormal functioning of the vertebrate heart and the behavior of three coupled relaxation oscillators. Roberge and Nadeau (1966) provided further experimental evidence to support the hypothesis that the electrical activity of the sinus and atrioventricular (A-V) nodes behaves like a system of coupled relaxation oscillators, by destroying the sinus node (in dogs) and replacing

it by an electronic relaxation oscillator coupled to the beating heart. The output of the electronic oscillator was used to stimulate the right atrium, while the vertricular electrical activity was fed back to the input of the electronic oscillator forming a closed-loop system in which examination of the frequency and phase variations demonstrated the possibility for the entrainment of the electronic oscillator and the A-V node electrical activity above or below their spontaneous free-running frequency. They also demonstrated the reciprocal frequency pulling of one pacemaker by the other, and the gradual change in the phase between the two pacemakers which takes place during transitions from one driving mode to the other. Tissue-culture experiments (De Haan 1967) showed that the developmental primordia of chick pacemaker nodes are populations of many spontaneously beating cells, as these individual unicellular pacemakers creep into contact, they begin to synchronize each other so that eventually the population behaves as a single oscillator. In the hagfish branchial heart, a rhythmic electrical activity responsible for muscular contractions was found throughout the myocardium (Jensen 1966), yet tiny transected segments of the heart tissue were found to oscillate at different inherent rates with the fastest rate being in the sinus venosus. Furthermore, each of the four hagfish hearts (branchial, portal, cardinal, and caudal) was found to beat at its own pace without any apparent coordination with others.

Alvarez and Mahoney (1922) reported the presence of a rhythmic electrical activity (which they called "action currents") in the smooth muscle layers of stomach, small intestine, cecum, colon, and rectum, their illustrative records were acquired from cat (stomach, small intestine), dog (stomach, small intestine, colon) and rabbit (small intestine, cecum, colon, rectum). They also demonstrated the existence of frequency gradients in excised stomach and bowel, and pointed out that the rhythmic electrical activity persisted at all time. Puestow (1933) confirmed the presence of a rhythmic electrical activity (which he called "waves of altered electrical potential") and a frequency gradient in isolated canine small intestinal segments. He also demonstrated the presence of an electrical spike activity (which he associated with muscular contractions) superimposed on the rhythmic electrical activity. He implied that the rhythmic electrical activity persisted at all times whereas the electrical spike activity was of an intermittent nature. Bozler (1938b, 1939, 1941) confirmed the occurrence of an electrical spike activity associated with muscular contractions both in vitro, in isolated longitudinal muscle strips from guinea pig (colon, small intestine, uterus, ureter), rabbit (small intestine) and cat (uterus, ureter) and in situ, in exposed loops of small intestine of anesthetized cat, dog and rabbit as well as in cat stomach. He also suggested that the strength of a spontaneous muscular contraction is proportional to the frequency and duration of the spikes associated with it. Furthermore, he (Bozler 1938a) demonstrated that isolated longitudinal muscle strips from both uterus and ureter of cat and rabbit can be electrically

stimulated directly without recourse to any nerve supply within the tissue and, presented strength-duration curves for the electrical stimulation of isolated longitudinal strips from rabbit ureter. The presence of two types of electrical activity in the smooth muscle cells of the gastrointestinal tract in several species had been established (Milton and Smith 1956; Bülbring, Burnstock and Holman 1958; Burnstock, Holman and Prosser 1963; Daniel and Chapman 1963; Bass 1965; Gillespie 1962a; Duthie 1974; Christensen 1975; Daniel 1975; Sarna 1975b), one of these activities is rhythmic and omnipresent, its origin is myogenic (Burnstock Holman and Prosser 1963) and its function is to control the appearance in time and space of the spike activity which does not persist at all time and is associated with muscular contractions. Isolation of a distal segment of canine small intestine from a proximal segment (using surgical transection or clamping) had been reported to produce a decrease in the frequency of both the rhythmic muscular contractions (Douglas 1949; Milton and Smith 1956) and the rhythmic electrical activity (Milton and Smith 1956) of the distal segment, suggesting some sort of frequency entrainment or pulling of the distal segment by the proximal one. Milton and Smith (1956) also demonstrated that the repetition rate of spikes changed in the same manner as that of the rhythmic electrical activity, thus confirming a one to one temporal relationship between the frequency of the rhythmic electrical activity, the repetition rate of spikes and the frequency of the rhythmic muscular contractions (when all are present at any one site).

Nelson and Becker (1968) suggested that the rhythmic electrical activity of the small intestine behaves like a system of loosely coupled relaxation oscillators.

Throughout this thesis the following terminology will be adopted to describe the gastrointestinal electrical activity (Sarna 1975b) and the relaxation oscillators used in modelling its features.

Control cycle: denotes one depolarization and repolarization of the membrane potential.

Control wave: denotes the continuing rhythmic electrical activity recorded at any one site and is assumed to be generated by the smooth muscle cells behaving like a relaxation oscillator at that site. The size of a relaxation oscillator could be one smooth muscle cell or it could be a number of cells oscillating together as a functional unit.

Intrinsic frequency: denotes the frequency of the control wave at any one site which is electrically isolated from its neighbouring segments (Sarna 1975a).

Electrical Control Activity (ECA): denotes the totality of the continuing rhythmic electrical activity in any part (i.e. the control waves recorded at several sites from any part). The ECA is assumed to control the appearance of the electrical spike activity and hence of muscular contractions in time and space.

Response potentials: denote the rapid oscillations of membrane potential (spikes) in the depolarized state of smooth muscle cell and are associated with a muscular contraction. Their occurrence is assumed to be in

response to a control cycle when other influences, such as neural and hormonal factors (Christensen 1975) are favourable [for example, Daniel (1963) cited the presence of acetylcholine].

Repetition rate of response potentials: denotes the rate at which response potentials occur at any one site in response to a sequence of control cycles at that site. The maximum repetition rate of response potentials can not exceed the control wave frequency at that site.

Electrical Response Activity (ERA): refers to the totality of the groups of response potentials at any one site or in any part.

Phase-lock: denotes the one to one relationship between two or more control waves at different sites and implies that they have the same frequency. Since biological rhythms and factors responsible for phase-locking [for example, Sarna (1975b) cited close contacts among cells and extracellular flow of currents] are inherently slightly variable, therefore, two control waves are said to be phase-locked if over a certain period of time the maximum deviation in time lag from the initial time lag does not exceed one control wave period.

Phase lag: denotes the time lag between the occurrence of corresponding control cycles in two control waves expressed as a proportion of a control wave period.

Van der Pol oscillator: denotes a nonlinear oscillator represented by a second order differential equation proposed by Van der Pol (1926).

Bonhoeffer-Van der Pol (BVP) oscillator: denotes a nonlinear oscillator prescribed by two first order differential equations obtained by using

Lienard's transformation (Lienard 1928; Minorsky 1962) of Van der Pol's equation with added terms in the form reported by Fitzhugh (1961).
Synthesized Relaxation Oscillator (SRO): denotes a nonlinear oscillator which is synthesized using a transformational synthesis method proposed by Chua and Green (1974).

Nelson and Becker (1968) used two forward-coupled Van der Pol oscillators, having different intrinsic frequencies, to simulate the frequency gradient of the ECA in the canine small intestine and demonstrated frequency entrainment or pulling (depending on the degree of coupling) of the distal oscillator (having the lower intrinsic frequency) by the proximal one. Uncoupling of the two oscillators caused a decrease in the frequency of the distal oscillator simulating the effect of transection of the canine small intestine.

Diamant and Bortoff (1969a) reported that the ECA frequency in cat, dog and rhesus monkey small intestine, in situ, decreased aborally in stepwise fashion with each frequency plateau having a variable length and being separated from the next frequency plateau by a zone of waxing and waning. When the small intestine was transected, in vitro, into short segments (1-3 cm long), the frequency of the control waves in adjacent segments tended to decrease aborally in a successive manner. Sarna, Daniel and Kingma (1971) found only one stable frequency plateau (extending over the entire duodenum and part of the jejunum) in the ECA frequency of dog small intestine in vivo, and when the small intestine was divided, in vivo, into small segments (15 cm long), the intrinsic

frequency in consecutive segments tended to decrease aborally in an exponential manner. A single transection of duodenum in dog small intestine in situ (Diamant and Bortoff 1969b; Sarna, Daniel and Kingma 1971) caused a decrease in the ECA frequency distal to the transection, along with the formation of a distal frequency plateau (the plateau frequency being related to the distal intrinsic frequency), while the ECA frequency proximal to the transection was generally unaffected. Diamant, Rose and Davison (1970) presented a digital computer simulation of the ECA frequency gradient in canine small intestine using ten forward-coupled Van der Pol oscillators having successively decreasing intrinsic frequencies. Their model displayed an aborally decreasing step-wise in situ frequency gradient with each frequency plateau being separated from the next by an area of waxing and waning. In each frequency plateau, the plateau length increased with the increase of coupling since more oscillators got entrained. Furthermore, increasing the degree of coupling between adjacent oscillators decreased the phase lag between them with the oscillator having the highest intrinsic frequency being always in the lead. But although a frequency plateau was formed distal to a simulated transection of the computer model, the plateau frequency dropped to the intrinsic frequency of the first oscillator distal to the simulated transection which was not consistent with reported transection effects (Diamant and Bortoff 1969b). Sarna, and Daniel and Kingma (1971) proposed that both forward and backward coupling of relaxation oscillators were necessary to simulate the

observed characteristics of the ECA in small intestine and they presented an analog computer simulation of the ECA in canine small intestine using sixteen bidirectionally coupled generalized BVP oscillators. Their model displayed an aborally decreasing exponential intrinsic frequency gradient, one frequency plateau in the proximal part in which control waves were phase-locked, a plateau frequency higher than the intrinsic frequency of the most proximal oscillator in the plateau region, a temporal variation of the frequencies distal to the frequency plateau and the capability of showing oral and aboral phase lags. A simulated transection of the computer model caused the formation of a frequency plateau distal to the transection whose plateau frequency was related to the intrinsic frequency of the oscillator distal to the transection. Oscillators aboral to the new frequency plateau displayed temporal variations of their frequencies which was consistent with the observed experimental data. Sarna, Daniel and Kingma (1972) also, proposed an array of bidirectionally coupled relaxation oscillators as a model of the ECA in canine stomach and they presented an analog and hybrid computer simulation of the canine gastric ECA using an array of thirteen bidirectionally coupled generalized BVP oscillators. Their model featured an intrinsic frequency decline from the corpus to the pylorus and from the greater curvature to the lesser curvature, phase-locking of all oscillators at a frequency close to that of the highest intrinsic frequency oscillator and a distal decrease in phase lag. A simulated circumferential transection caused the formation of another frequency

plateau with a lower plateau frequency distal to the transection while the frequency plateau proximal to it remained unaffected which was consistent with the observed experimental data.

1.2 Scope and Objectives

This thesis centers around three main objectives, namely

a. Development and implementation of interactive processors for the analysis and simulation of biological rhythms using a digital computer (NOVA 830).

b. A mathematical investigation of a population of interacting SROs to provide an insight into the nature of interaction among the different members and also, to elucidate the effect of external stimulation of an isolated member.

c. Analysis and modelling of the ECA in human colon to elucidate the nature of the myogenic control system which, in conjunction with the neural and hormonal control systems, are responsible for mixing and propulsive movements of the colonic lumenal contents by controlling the sequence of colonic muscular contractions in time and space.

1.3 Points of Investigation and Their Organization

Objectives (a), (b), and (c) are further subdivided as follows:

a.1 Design of optimal IIR digital filters using a least pth optimization strategy.

a.2 Design of IIR digital filters with finite word length coefficients.

a.3 Development of an optimal processor for decimation and filtering

using an optimal IIR digital filter.

a.4 Design of tuneable IIR digital filters via parameter transformations.

a.5 Modular implementation of an interactive processor for the analysis of biological rhythms.

a.6 Development and implementation of an interactive processor for simulation of biological rhythms using populations of interacting oscillators.

b.1 Entrainment of a SRO by an external stimulus.

b.2 Synchronization of a population of interacting SROs.

c.1 Determination of the characteristics and organizational patterns of human colonic ECA.

c.2 Modelling of the ECA in human colon using a population of interacting SROs.

The first objective is covered in chapters two, three and four where chapter two deals with (a.1) and (a.2), while chapter three deals with (a.3) and chapter four deals with (a.4) to (a.6). The second objective is covered in chapter five which deals with (b.1) and (b.2), whereas, the third objective is covered in chapters six and seven with chapter six dealing with (c.1) and chapter seven with (c.2). The introduction of chapters two to seven, sketches some of the work that had been reported in the literature along with what was done in the course of this thesis regarding the subject matter of the chapter in question.

The numerical computations for (a.1), (a.2) and contour plotting for (a.3) were performed on a CDC 6400 computer, otherwise a NOVA 830 minicomputer was used.

CHAPTER 2

COMPUTER-AIDED DESIGN OF IIR DIGITAL FILTERS

2.1 Introduction

When a recorded biological signal of essentially low frequency content is contaminated with wideband noise (e.g. recording artifacts), then an IIR (infinite impulse response) digital filter can be efficiently used to extract the signal of interest. For example, IIR digital filters have been used to filter out most of the contaminating noise from recorded electrocardiograms (Weaver et al. 1968; Lynn 1971) and from recorded electrical activity of the human colon (Bardakjian and Sarna 1978a). Furthermore, IIR digital filters can be used to decimate biological signals (Bardakjian and Sarna 1978a) and also, to extract a frequency component of interest from recorded biological signals to investigate their spontaneous phase relations, hence determine whether or not they are phase-locked (Bardakjian et al. 1976a).

2.1.1 Regarding IIR Digital Filters with Large-Word-Length Coefficients

Two main approaches have been taken to approximation problems in IIR digital filter design, the first of these is an analytical approach through classical approximation theories (Kaiser 1966; Gold and Rader 1969; Sablatash 1971; Haykin 1972), whereas the second is an iterative approach that is particularly appropriate for use on a digital computer (Steiglitz 1970; Helms 1971; Deczky 1972; Bandler and Bardakjian 1973a, 1973b; Charalambous

1974a, 1975). Oppenheim and Schafer (1975) gave a general picture of the wide range of possibilities available for digital filter design along with details to enable the implementation of some of the surveyed techniques.

Haykin (1972) presented a unified treatment of IIR digital filtering by using the convolution integral to derive an integro-difference equation for defining the input-output relation of a linear time invariant filter, then he used that equation to obtain various analog-to-digital filter transformations for the discretization of a continuous-time transfer function, with each transformation corresponding to a specific way of approximating the continuous-time excitation. An iterative method for designing IIR digital filters with arbitrary prescribed magnitude characteristics was described by Steiglitz (1970), the method uses the Fletcher-Powell algorithm (Fletcher and Powell 1963) to minimize a square-error criterion in the frequency domain and a strategy was described whereby stability and minimum phase constraints were observed, while still using the unconstrained optimization algorithm. Helms (1971) reviewed and occasionally extended techniques for determining the coefficients of digital filters which have equiripple or minimax errors, whereas Charalambous (1974a, 1975) described minimax optimization of IIR digital filters. Deczky (1972) outlined a method for the design of IIR digital filters using a weighted minimum p-error criterion, where the largest value of p tried was reported to be 40.

A practical approach to computer-aided design optimization was presented by Bandler and Charalambous (1972) whereby least pth approximation using extremely large values of p (typically 10^3 to 10^6) was applied and it was shown how suitable and reasonably well-conditioned objective functions could be formulated, giving particular emphasis to general approximation

problems as, for example, in filter design. Also it was demonstrated how easily and efficiently extremely near minimax results could be achieved on a discrete set of sample points.

In this Chapter, an optimal choice of the coefficients of an IIR digital filter to meet arbitrary specifications on the magnitude characteristics using a least pth optimization strategy (Bandler and Charalambous 1972) in conjunction with a powerful function minimization method Fletcher (1970, 1972) to solve the approximation problem in the z-domain, is described. The local optimality of the least pth solution is checked by perturbation whereas the order of the filter can be increased through growing second-order filter sections to meet the prescribed specifications and a pole inversion technique (Steiglitz 1970) is implemented to meet the stability requirements.

2.1.2 Regarding IIR Digital Filters with Finite-Word-Length Coefficients

The problem of designing IIR digital filters with a priori specified finite-word-length for the representation of the coefficients, can be formulated as a nonlinear discrete optimization problem. Many approaches using random search optimization algorithms were proposed (Steiglitz 1971; Avenhaus 1972; Suk and Mitra 1972) to solve this problem. Störzbach (1972) proposed a zero-one programming approach, whereas Charalambous and Best (1974) proposed an approach using a branch and bound technique in conjunction with an optimization algorithm for linearly constrained problems. Another approach (Bandler, Bardakjian and Chen 1974a,1975b) would be to formulate the continuous (large-word-

length)nonlinear programming problem as an unconstrained minimax problem (Bandler and Charalambous 1974b) and use Dakin's branch and bound technique (Dakin 1966) in conjunction with Fletcher's unconstrained minimization program (Fletcher 1972) to discretize the solution. The main features of this approach were implemented in a general computer program package DISOPT (Chen 1974; Bandler and Chen 1975a). A formulation utilizing this approach is given in this chapter along with an illustrative example.

As the cost of a digital filter, if implemented as a special-purpose computer, depends heavily on the word-length of the coefficients it should be reduced as much as possible (Avenhaus 1972). On the other hand when the coefficients of a digital filter, initially specified with unlimited accuracy (large-word-lengths) are quantized by rounding or truncation, then coefficient quantization error occurs which affects the digital filter's response (Rabiner et al. 1972). Therefore, it is desirable to incorporate the word-lengths as additional parameters of the approximation problem in IIR digital filter design.

In this chapter, the problem of designing IIR digital filters with optimized-word-length coefficients to meet arbitrary, prescribed magnitude characteristics in the frequency domain, is formulated (Bandler, Bardakjian and Chen 1974a, 1975b) as a nonlinear integer programming problem, where the parameter vector consists essentially of the word-lengths of the coefficients and the multipliers of the quantization step sizes. A function of the word lengths is minimized, subject to the prescribed constraints on the magnitude characteristics, while constraining all the constituents

of the parameter vector to be integers.

2.2 Least pth Optimization of IIR Digital Filters with Large-Word-Length Coefficients

2.2.1 Description of the Problem

Suppose that upper and/or lower bounds on the magnitude characteristics of an IIR digital filter are prescribed at a discrete set of frequencies $f_1, f_2, \ldots, f_m$ corresponding to a discrete set of values of the complex variable z evaluated on the unit circle in the z-domain such that

$$z_i = e^{j\psi_i \pi}, \qquad i = 1, 2, \ldots, m \tag{2.1a}$$

where

$$\psi_i = \frac{2f_i}{f_s}, \qquad i = 1, 2, \ldots, m \tag{2.1b}$$

and f_s is the sampling frequency.

The transfer function of an IIR digital filter is chosen usually to be either of the cascade form or the parallel form (Helms 1971), namely

$$H(z) = c_{4K+1} \prod_{k=1}^{K} \frac{1 + c_{4k-3} z^{-1} + c_{4k-2} z^{-2}}{1 + c_{4k-1} z^{-1} + c_{4k} z^{-2}} \tag{2.2a}$$

or

$$H(z) = c_{4K+1} + \sum_{k=1}^{K} \frac{c_{4k-3} + c_{4k-2} z^{-1}}{1 + c_{4k-1} z^{-1} + c_{4k} z^{-2}} \qquad (2.2b)$$

All the poles of the transfer function should lie inside the unit circle in the z-domain for the filter to be stable.

2.2.2 Problem Formulation

Find the n-dimensional parameter vector $\underset{\sim}{c}$ where n = 4K+1 and K is the number of second-order IIR digital filter sections, to minimize the generalized least pth objective function (Bandler and Charalambous 1972; Bandler et al. 1976)

$$U(\underset{\sim}{c},\psi,\xi,p) = M(\underset{\sim}{c},\xi)\left[\sum_{i\in K_u}\left\{\frac{e_u(\underset{\sim}{c},\psi_i) - \xi}{M(\underset{\sim}{c},\xi)}\right\}^g + \sum_{i\in K_\ell}\left\{\frac{-e_\ell(\underset{\sim}{c},\psi_i) - \xi}{M(\underset{\sim}{c},\xi)}\right\}^g\right]^{1/g}, \quad M(\underset{\sim}{c},\xi) \neq 0 \qquad (2.3a)$$

or $$U(\underset{\sim}{c},\psi,\xi,p) = 0, \qquad M(\underset{\sim}{c},\xi) = 0 \qquad (2.3b)$$

where

$$e_u(\underset{\sim}{c},\psi) \triangleq w_u(\psi)\,[|H(\underset{\sim}{c},\psi)| - S_u(\psi)] \qquad (2.3c)$$

$$e_\ell(\underset{\sim}{c},\psi) \triangleq w_\ell(\psi)\,[|H(\underset{\sim}{c},\psi)| - S_\ell(\psi)] \qquad (2.3d)$$

$$H(\underset{\sim}{c},\psi) \triangleq H(z)\Big|_{z=e^{j\psi\pi}} \qquad (2.3e)$$

$$M(\underset{\sim}{c},\xi) \triangleq \max_{i\epsilon I_u,\ j\epsilon I_\ell} [e_u(\underset{\sim}{c},\psi_i)-\xi,\ -e_\ell(\underset{\sim}{c},\psi_j)-\xi] \tag{2.3f}$$

$$K_u \triangleq \begin{cases} J_u \triangleq \{i \mid e_u(\underset{\sim}{c},\psi_i)-\xi \geq 0,\ i\epsilon I_u\}, & M(\underset{\sim}{c},\psi) > 0 \\ I_u, & M(\underset{\sim}{c},\psi) < 0 \end{cases} \tag{2.3g}$$

$$K_\ell \triangleq \begin{cases} J_\ell \triangleq \{i \mid -e_\ell(\underset{\sim}{c},\psi_i)-\xi \geq 0,\ i\epsilon I_\ell\}, & M(\underset{\sim}{c},\xi) > 0 \\ I_\ell, & M(\underset{\sim}{c},\xi) < 0 \end{cases} \tag{2.3h}$$

$$g \triangleq \frac{M(\underset{\sim}{c},\xi)}{|M(\underset{\sim}{c},\xi)|}\, p, \qquad p > 1 \tag{2.3i}$$

whereby $S_u(\psi)$, and $S_\ell(\psi)$ are the upper and lower specifications on the magnitude response, $w_u(\psi)$ and $w_\ell(\psi)$ are upper and lower error weighting functions, I_u and I_ℓ are index sets representing the upper and lower sampled approximation intervals, respectively, and ξ is an artificial margin of errors.

The partial derivatives of the objective function (2.3) with respect to the IIR digital filter coefficients, for both the cascade and parallel forms, are given in Appendix I.

2.2.3 Stability Constraints

Suppose that H(z) has a pole at $z=z_p$ located outside the unit circle in the z-domain, such that

$$H(z) = \frac{N(z)}{z - z_p}$$

Consider the function

$$Q(z_p) = \frac{z - z_p}{z - \frac{1}{\tilde{z}_p}}$$

where $\tilde{z}_p$ denotes the complex conjugate of z_p, and where

$|Q(z_p)| = |z_p|$ when $|z| = 1$. Let

$$H'(z) = H(z)Q(z_p) = \frac{N(z)}{z - \frac{1}{\tilde{z}_p}}$$

Hence, the inversion of real or complex conjugate pairs of poles of the transfer function with respect to the unit circle in the z-domain is equivalent to multiplying the transfer function by a particular all pass function, implying that the inversion of such poles of the transfer function with respect to the unit circle does not affect the shape of the magnitude characteristics. Thus, all such poles that do not lie within the unit circle in the z-domain can be inverted with respect to the unit circle to insure the stability of the filter. It is to be noted that the magnitude characteristics of the stable filter should be divided by the magnitude of each inverted pole, that is, if there are r poles $z_{p1},\ldots,z_{pr}$ that do not lie within the unit circle in the z-domain, then, after their inversion, one gets

$$|H(z)| = \frac{|H'(z)|}{\prod_{i=1}^{r} |z_{pi}|} \qquad (2.4)$$

2.2.4 Description of a Computer Program for IIR Digital Filter Design

A general computer program package CADRDF was developed utilizing the aforementioned ideas. Fig. 2.1 depicts a general arrangement of the package. A Fortran listing is given elsewhere (Bardakjian 1978b). The user should specify, in the MAIN program, the desired form of the transfer function, the initial number of second-order filter sections, the maximum acceptable number of filter sections, the required precision and an option for local optimality checking either by perturbation of the parameters or by increasing ξ and then restarting the optimization process. The user should specify also the upper and lower bounds on the magnitude response, $S_u(\psi)$ and $S_\ell(\psi)$ in function subroutine FUNCS, the upper and lower weighting functions $w_u(\psi)$ and $w_\ell(\psi)$ in function subroutine W and the discrete set of frequency points along with the required function minimization algorithm, the Fletcher method (Fletcher 1972) or the Fletcher-Powell method (Fletcher and Powell, 1963), in a DATA DECK.

Starting with the initial number of filter sections, the coefficients of the digital filter are evaluated by minimizing the objective function (2.3) via the chosen minimization algorithm. Package ULPFM, which is a slightly modified version of a general package FMLPO described elsewhere (Popovic and Bandler 1973; Popovic, Bandler and Charalambous 1974), sets the objective function (2.3) using function subroutines FUNCS and W

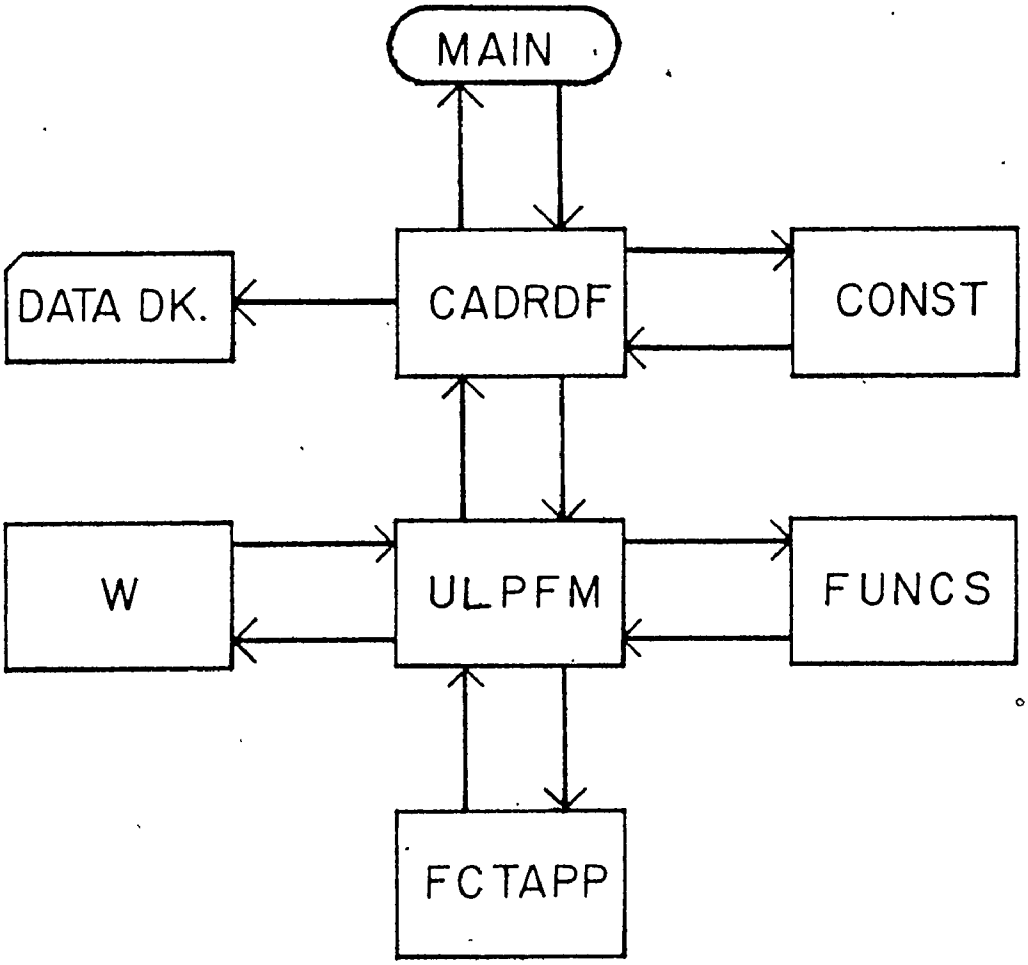

Fig. 2.1 A general structure of CADRDF

along with subroutine FCTAPP which prescribes the approximating function $|H(\underset{\sim}{c},\psi)|$ and its first partial derivatives with respect to $\underset{\sim}{c}$, and then searches for a local minimum of the objective function using the Fletcher and Powell or the Fletcher method. It is to be noted that the value of p is increased successively and the optimization is carried out for each value of p, until the absolute value of the relative change in maximum error $\left|\frac{\Delta M(\underset{\sim}{c},\xi)}{M(\underset{\sim}{c},\xi)}\right|$ becomes less than some small quantity (taken to be 0.001). To insure the stability of the filter a stability checking is provided, through subroutine CONST, whereby all the poles that do not lie within the unit circle in the z-domain are inverted with respect to the unit circle, as discussed in section 2.2.3. Local optimality of the solution $\hat{\underset{\sim}{c}}$ is checked by either perturbing $\hat{\underset{\sim}{c}}$ or increasing ξ, restarting the optimization process using the highest attained value of p and comparing the solutions before and after perturbation. It is to be noted that a minimax optimum will not be affected by increasing ξ (Bandler, and Charalambous 1973c). If the specifications are not satisfied and the maximum specified number of second-order filter sections has not been exceeded, a second-order filter section is grown by increasing the number of the independent parameters n by 4, assigning a starting value of zero for each of the grown filter coefficients c_{4k-3}, c_{4k-2}, c_{4k-1} and c_{4k}, then repeating the whole design process.

2.2.5 Examples

Example 2.1

Consider the design of a low-pass IIR digital filter of the cascade

form whose ideal magnitude response is specified by

$$\text{Ideal magnitude response} = \begin{cases} 1 & \psi \epsilon W_p \\ 0 & \psi \epsilon W_s \end{cases}$$

where $W_p = [0., 0.09]$ is the passband and $W_s = [0.11, 1.0]$ is the stopband.

Let

$$S_u(\psi) = S_\ell(\psi) = 1 \quad \psi \epsilon W_p$$

$$S_u(\psi) = 0 \quad \psi \epsilon W_s$$

$$w_u(\psi) = w_\ell(\psi) = 1 \quad \psi \epsilon W_p \cup W_s$$

All the functions of ψ will be evaluated at a finite discrete set of values of ψ taken from the closed intervals W_p and W_s as follows

ψ = 0.0, 0.08 (0.01) ; $S_u(\psi_i) = S_\ell(\psi_i) = 1$; i = 1,...,9

ψ = 0.0801, 0.09 (0.00045); $S_u(\psi_i) = S_\ell(\psi_i) = 1$; i = 10,...,32

ψ = 0.11 , 0.2 (0.01) ; $S_u(\psi_i) = 0$; i = 33,...,42

ψ = 0.3, 1 (0.1) ; $S_u(\psi_i) = 0$; i = 43,...,50

A starting point $c^o = [0 \quad 0 \quad 0 \quad -0.25 \quad 0.1]^T$ was taken for a second-order filter section of the cascade form. Test quantities for the Fletcher and Fletcher-Powell methods were 10^{-6}, and $\xi = 0$.

Optimization using both the Fletcher method and the Fletcher-Powell method in accordance with the aforementioned ideas gave the results

shown in Table 2.1, while growing another filter section and restarting the optimization process gave the results shown in Table 2.2. The passband and the stopband of the magnitude response are depicted in Figs. 2.2a and 2.2b respectively whereas the pole-zero configuration of the transfer function is depicted in Fig. 2.2c.

It is to be noted that 201 equidistant values of ψ were used for response evaluation and plotting in each frequency band, whereas local optimality checking, as depicted in Table 2.3, was provided through perturbation of $\hat{c}$ namely, replacing the obtained solution $\hat{c}$ by $1.0001\hat{c}$ and restarting the optimization process. The computational execution time on the CDC 6400 was in the order of 20 seconds for a one section filter and 2 minutes for a two section filter (using the Fletcher method).

Discussion

The results of the low-pass filter reported by Steiglitz (1970) were reproduced using the package CADRDF (taking the transition region specification into account), however, using the set of sample points given by Steiglitz in the optimization process and then evaluating the magnitude response of the obtained solution at 201 equidistant values of ψ in the passband and, similarly, for the stopband, an error peak was detected in the interval [0.08, 0.09] that was not taken into account by the previous scheme of specified sample points. The passband and the stopband of the magnitude response are depicted in Figs. 2.3a and 2.3b respectively.

TABLE 2.1

OPTIMIZATION RESULTS FOR EXAMPLE 2.1 USING ONE SECTION

g = p	Maximum Error	Objective Function	Solution $\hat{c}$	Number of Function Evaluations: Fletcher Method	Number of Function Evaluations: Fletcher-Powell Method
2	0.446136	0.905656	-1.672551 1. -1.790717 0.850218 0.151727	106	393
10	0.278126	0.308162	-1.799881 1 -1.831101 0.889290 0.221937	33	68
100	0.248415	0.251337	-1.815636 1. -1.836826 0.895616 0.240215	27	97
1000	0.246809	0.247100	-1.816441 1. -1.837210 0.896016 0.241345	37	48
10000	0.246713	0.246741	-1.816464 0.999999 -1.837254 0.896054 0.241338	29	38

TABLE 2.2

OPTIMIZATION RESULTS FOR EXAMPLE 2.1 USING TWO SECTIONS

g = p	Maximum Error	Objective Function	Solution $\hat{c}$	Number of Function Evaluations Using Fletcher Method
2	0.094612	0.183426	-1.858902 0.999999 -1.864459 0.945603 -1.304232 0.999999 -1.739599 0.775075 0.028496	130
10	0.046434	0.055707	-1.870517 0.999999 -1.872787 0.952596 -1.480946 0.999999 -1.750330 0.785957 0.040564	80
100	0.043999	0.044486	-1.870794 1. -1.873968 0.953359 -1.517114 1. -1.752070 0.787578 0.043228	58
1000	0.043639	0.043688	-1.870747 1. -1.874085 0.953433 -1.520148 0.999999 -1.752504 0.787952 0.043373	49

contd.....

Table 2.2 (continued)

g = p	Maximum Error	Objective Function	Solution $\hat{c}$	Number of Function Evaluations Using Fletcher Method
10000	0.043610	0.043614	-1.870741 0.999999 -1.874095 0.953439 -1.520276 1. -1.752557 0.787996 0.043369	52

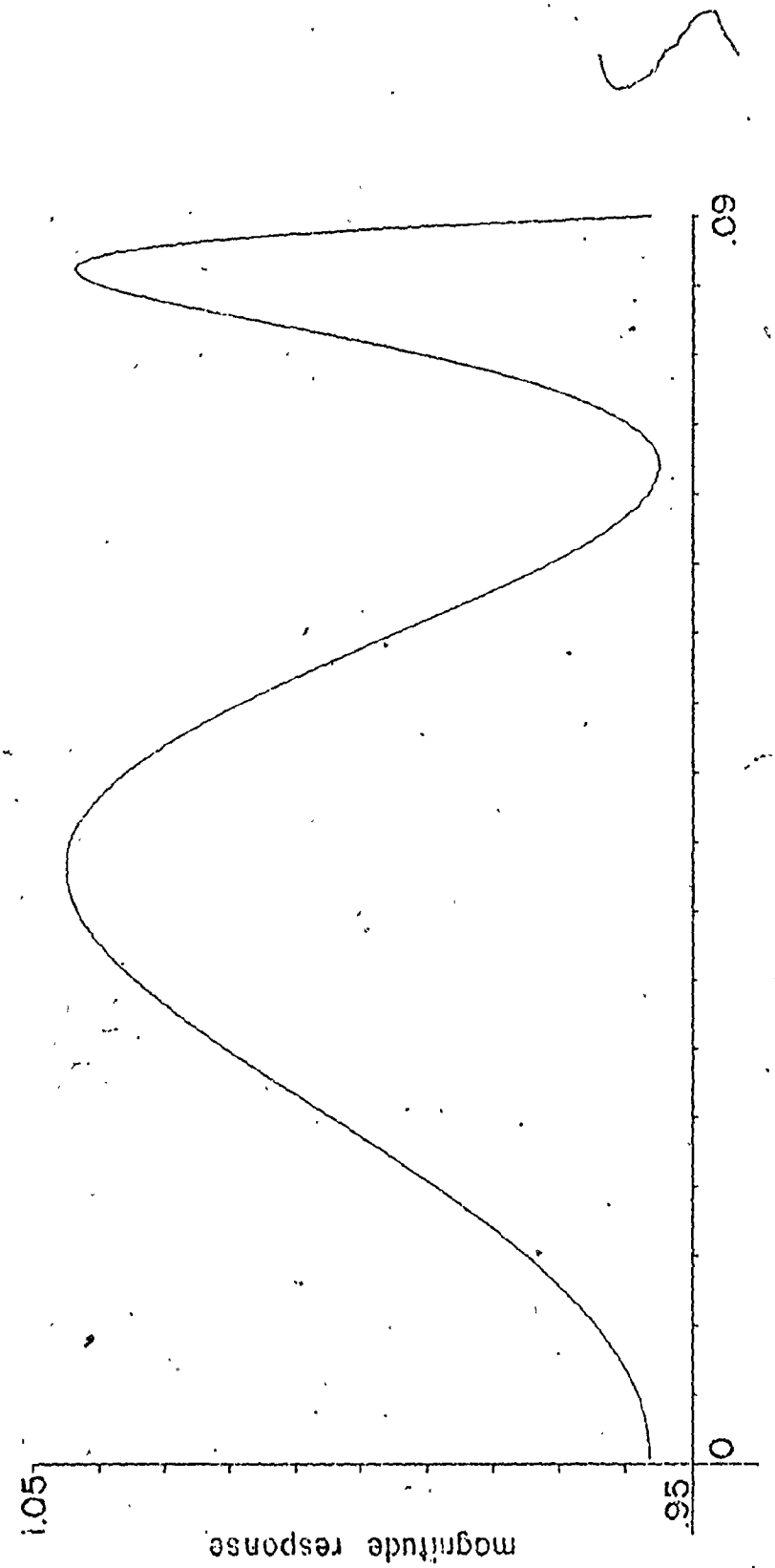

Fig. 2.2 a Passband response for Example 2.1

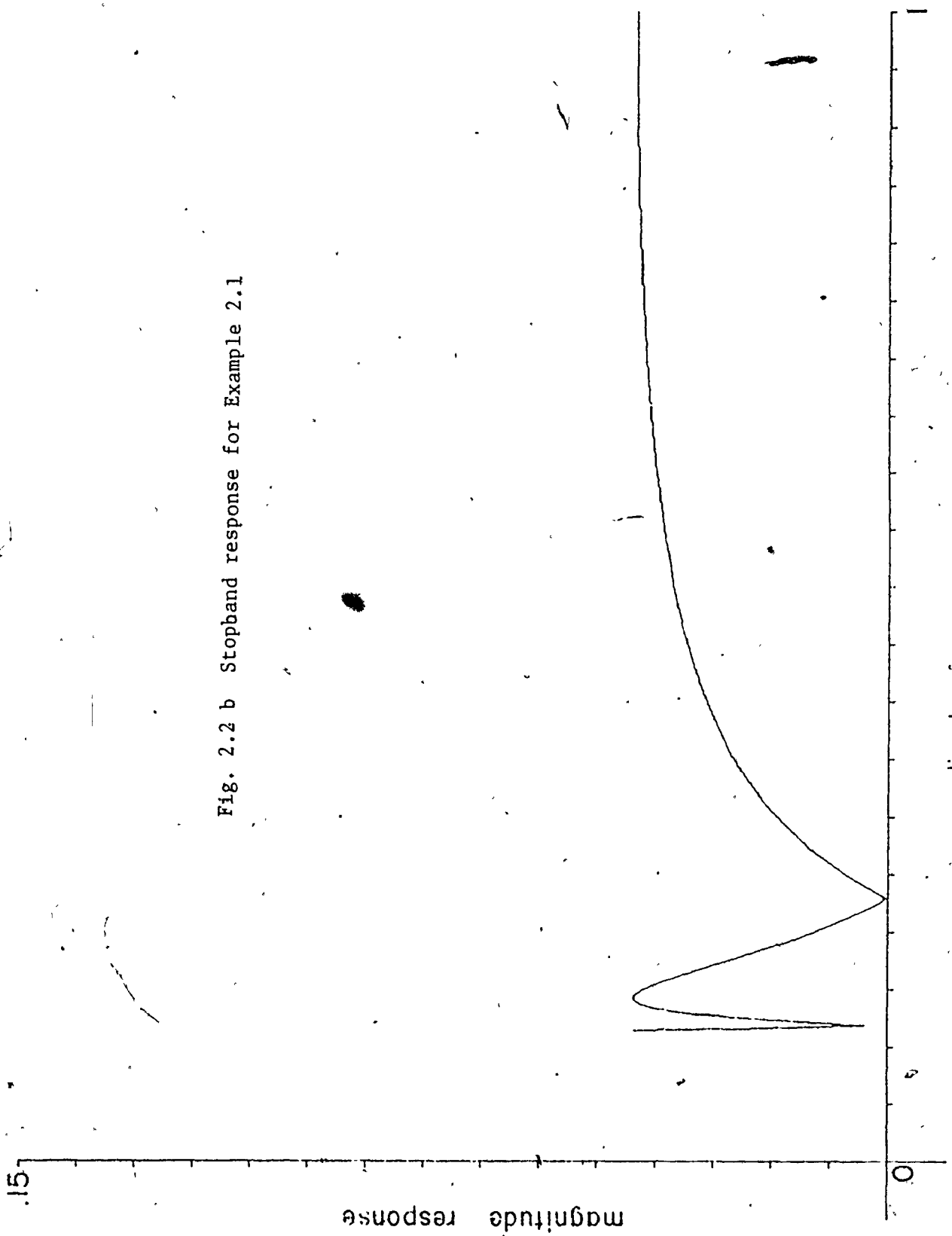

Fig. 2.2 b Stopband response for Example 2.1

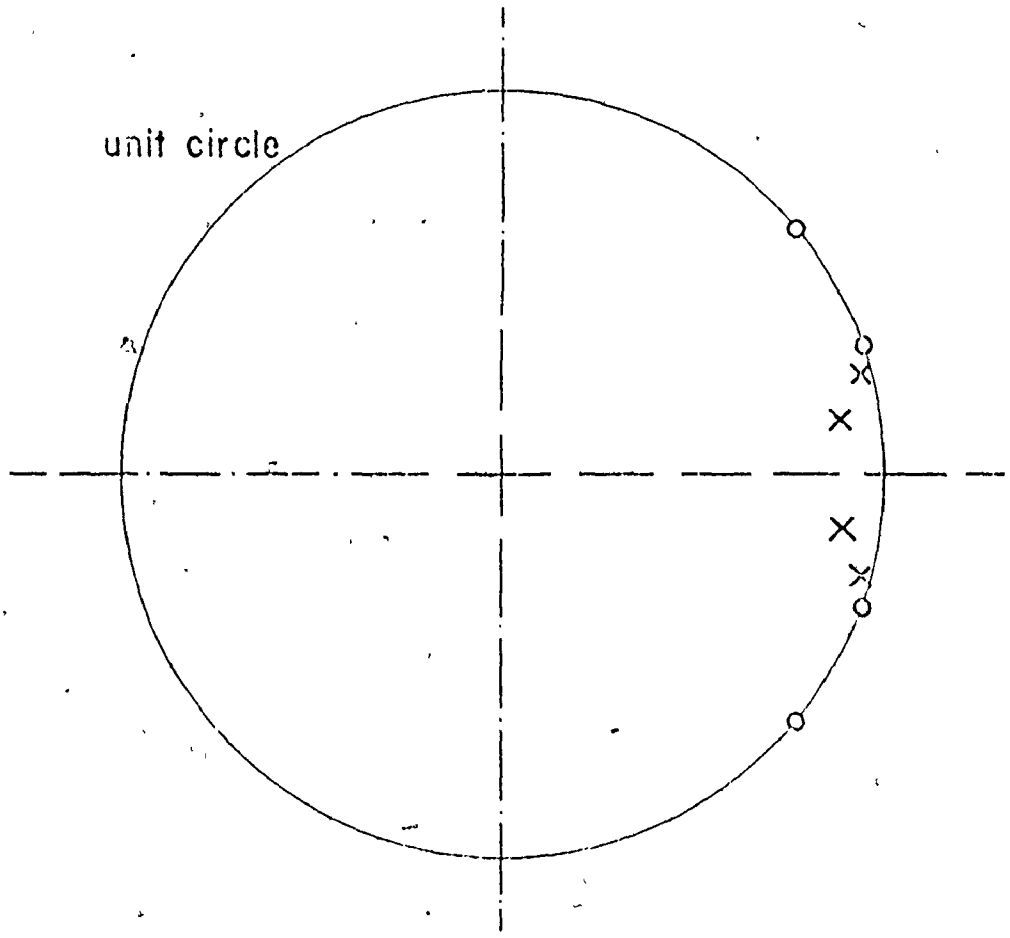

Fig. 2.2 c Pole-zero configuration of H(z) for Example 2.1

TABLE 2.3

LOCAL OPTIMALITY TABLE FOR EXAMPLE 2.1

Solution before perturbation $\hat{c}$	Starting point after perturbation	Solution after perturbation $\hat{c}^*$	Absolute differences in components of $\hat{c}$ & $\hat{c}^*$
-1.870741	-1.870928	-1.870741	0.0
0.999999	1.000100	1.	10^{-6}
-1.874095	-1.874283	-1.874095	0.0
0.953439	0.953534	0.953439	0.0
-1.520276	-1.520428	-1.520280	4×10^{-6}
1.	1.000100	1.000004	4×10^{-6}
-1.752557	-1.752732	-1.752557	0.0
0.787996	0.788075	0.787996	0.0
0.043369	0.043373	0.043368	10^{-6}
Maximum Error			
0.043610	0.046658	0.043610	0.0

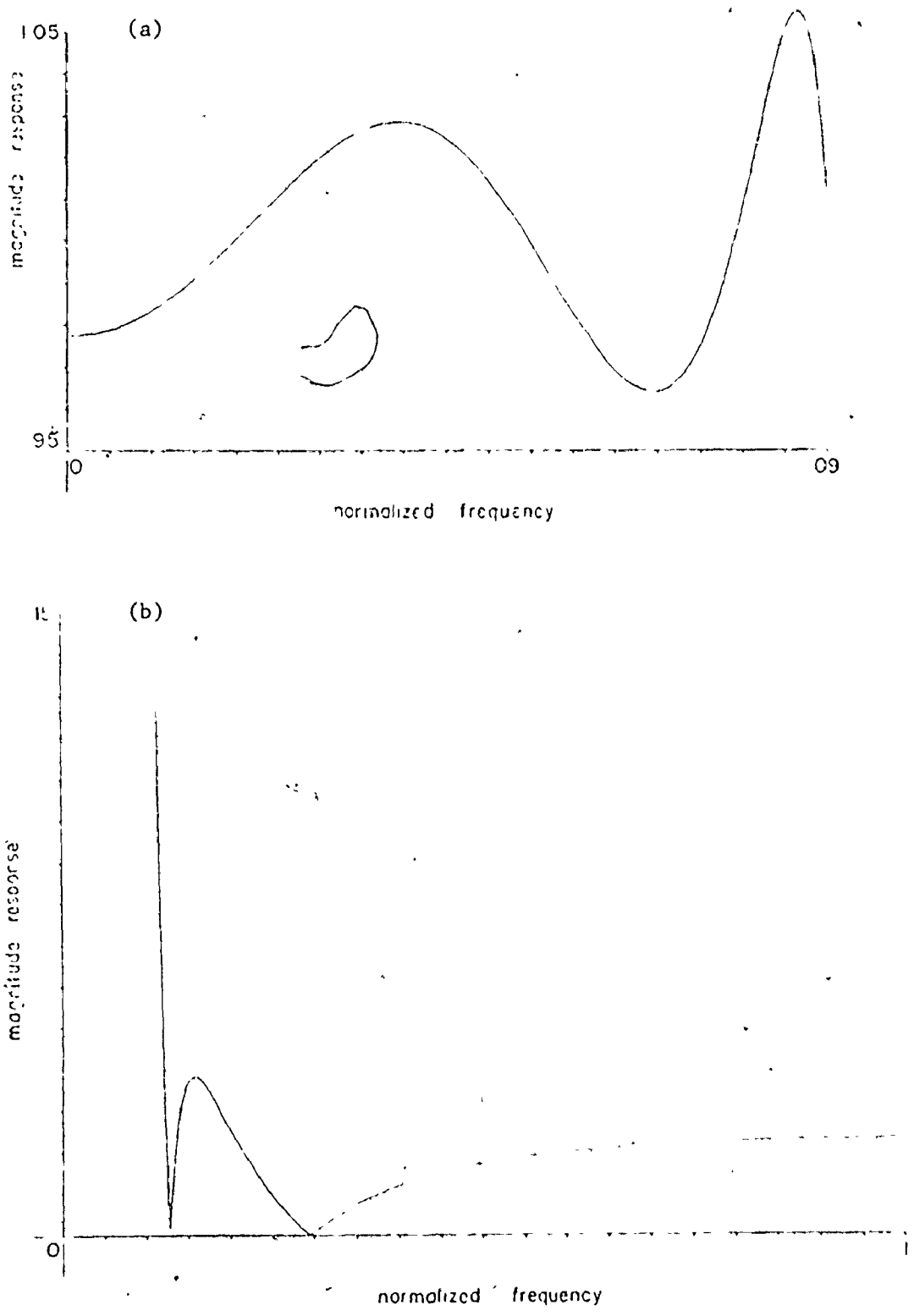

Fig. 2.3 More densely sampled magnitude response of the filter given by Steiglitz. (a) Passband response. (b) Stopband response.

From the results of Table 2.1, it can be seen that for this example, the Fletcher method (with a total of 232 function evaluations) was more efficient than the Fletcher-Powell method (with a total of 644 function evaluations) in the sense that it required a smaller number of function evaluations to produce each least pth solution and when the number of independent variables was increased to 9 through growing the second filter section, the Fletcher-Powell method was remarkably slower than the Fletcher method, as it ran into computational time limit without yielding even the least squares solution, while for the same specified computational time, the Fletcher method gave the least 10000th solution. As the magnitude response was specified on a closed continuous interval, it was plotted along the specified closed continuous interval in Figs. 2.2a and 2.2b.

Example 2.2

Consider the design of a low-pass IIR digital filter of the cascade form, for a 10 kHz sampling rate, whose upper and lower magnitude response bounds are specified by

$f = 0, 900\ (100)$; $S_u(f) = 1.1$; $S_\ell(f) = 0.9$

$f = 1200$; $S_u(f) = 0.1$

$f = 1500,\ 5000\ (500)$; $S_u(f) = 0.1$

The specifications can be prescribed in terms of ψ as follows

ψ = 0 , 0.18 (0.02) ; $S_u(\psi_i) = 1.1$; $S_\ell(\psi_i) = 0.9$; i=1,....,10

ψ = 0.24 ; $S_u(\psi_i) = 0.1$; i=11

ψ = 0.3, 1. (0.1) ; $S_u(\psi_i) = 0.1$; i=12,...,19

The same starting point as that used by Suk and Mitra (1972), namely, $\underset{\sim}{c}^o = [0\ 1\ -1\ 0.5\ 0.1]^T$ was taken for a second-order filter section of the cascade form. Weighting factors, test quantity for the Fletcher method and ξ were as in Example 2.1. Optimization using the Fletcher method gave the results shown in Table 2.4 while growing another filter section of the cascade form from the one section locally optimal solution and restarting the optimization process gave the results shown in Table 2.5. The computational execution time on the CDC 6400 was of the same order of magnitude as in Example 2.1. The passband and the stopband of the magnitude response are depicted in Figs. 2.4a and 2.4b respectively, whereas the pole-zero configuration of the transfer function is depicted in Fig. 2.4c.

Discussion

The sign of g was positive so long as the magnitude response did not lie within the specified bounds, but a change of sign of g to negative, occurred, when the specifications were met, but that did not stop the optimization process as it went on to produce a locally optimal solution for the case when the specifications were met. As the magnitude response was initially specified at a discrete set of frequency points, the magnitude response of the final solution was depicted only at that discrete set of

TABLE 2.4

OPTIMIZATION RESULTS FOR EXAMPLE 2.2 USING ONE SECTION

g = p	Maximum Error	Objective Function	Solution $\hat{c}$		Number of Function Evaluations Using Fletcher Method	
			Cascade Form	Parallel Form	Cascade Form	Parallel Form
2	0.192456	0.244387	-0.858152 1. -1.500265 0.709050 0.157547	-0.064648 0.198152 -1.500265 0.709050 0.222195	44	75
10	0.109918	0.121980	-1.147287 0.999999 -1.540582 0.759644 0.206694	-0.065399 0.182045 -1.540582 0.759644 0.272094	60	26
100	0.101718	0.102881	-1.165964 1. -1.544701 0.764404 0.210503	-0.064878 0.179944 -1.544701 0.764404 0.275382	27	26
1000	0.101302	0.101417	-1.166416 0.999999 -1.545169 0.764763 0.210425	-0.064725 0.179711 -1.545169 0.764763 0.275151	43	34

contd.....

Table 2.4 (continued)

g = p	Maximum Error	Objective Function	Solution $\hat{c}$		Number of Function Evaluations Using Fletcher Method	
			Cascade Form	Parallel Form	Cascade Form	Parallel Form
10000	0.101271	0.101282	-1.166418 1.000001 -1.545223 0.764801 0.210399	-0.064702 0.179681 -1.545223 0.764801 0.275102	24	34

TABLE 2.5

OPTIMIZATION RESULTS FOR EXAMPLE 2.2 USING TWO SECTIONS

$g^c=-p$	Maximum Error	Objective Function	Solution $\hat{c}$	Number of Function Evaluations Using Fletcher Method
-2	-0.062826	-0.016925	-1.412375 1. -1.575303 0.882915 0.618033 0.999999 -1.430463 0.562704 0.026034	182
-10	-0.068650	-0.059397	-1.407856 1. -1.578990 0.885035 0.082835 0.999999 -1.438495 0.570015 0.032027	85
-100	-0.073797	-0.072980	-1.404770 0.999999 -1.584958 0.888081 -0.207829 0.999999 -1.453960 0.582477 0.035615	94

contd.....

Table 2.5 (continued)

g = −p	Maximum Error	Objective Function	Solution $\hat{c}$	Number of Function Evaluations Using Fletcher Method
-1000	-0.074321	-0.074240	-1.404186 1. -1.585726 0.888448 -0.226099 0.999999 -1.456176 0.584152 0.035719	58
-10000	-0.074369	-0.074361	-1.404118 0.999999 -1.585808 0.888486 -0.227133 0.999999 -1.456438 0.584344 0.035707	71

(a)

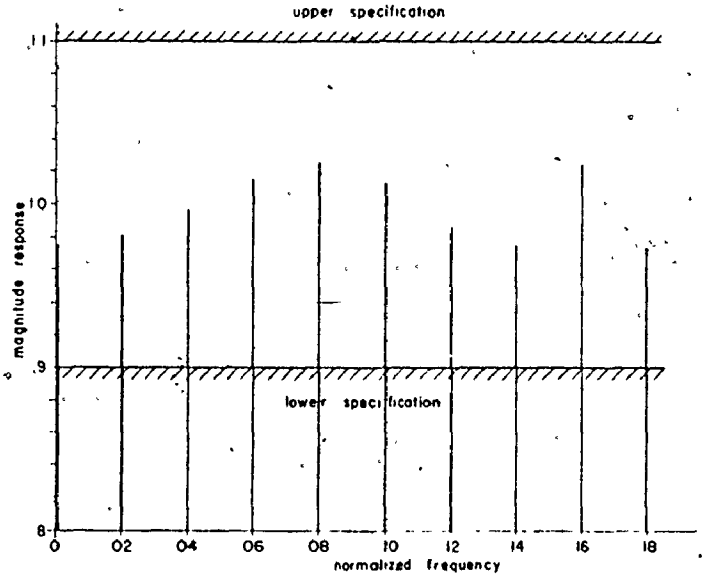

(b)

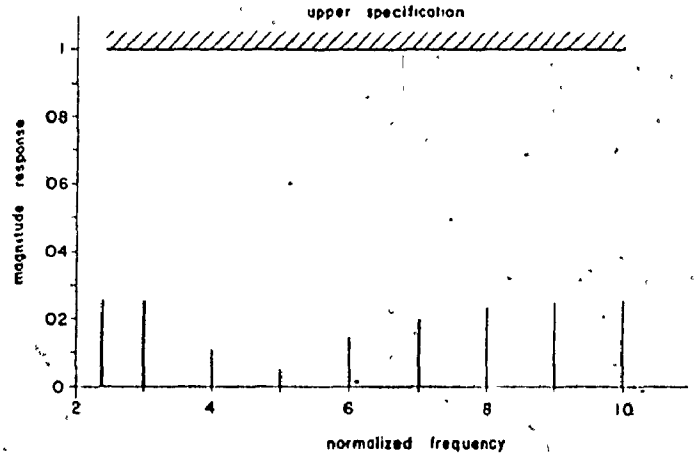

(c)

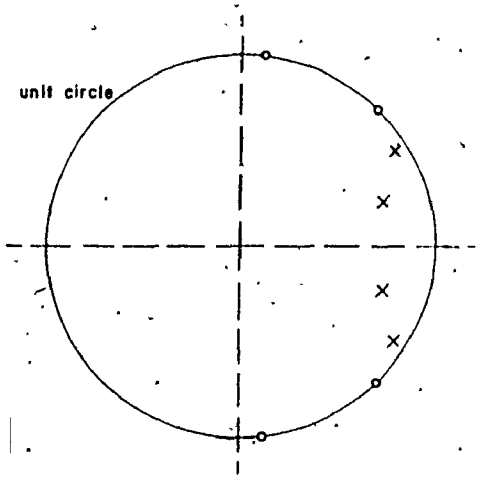

Fig. 2.4 Magnitude response for Example 2.2. (a) Passband response. (b) Stopband response. (c) Pole-zero configuration of H(z).

frequency points as shown in Figs. 2.4a and 2.4b. Increasing the value of ξ did not affect the least 10000th solution. To compare the design of second-order filter sections of the cascade and parallel forms with regards to the required number of function evaluations, a second-order filter section of the parallel form was designed using the same starting conditions as the second-order filter section of the cascade form. Optimization results using the Fletcher method for both forms are given in Table 2.4 for comparison. It is to be noted that the total number of function evaluations needed to reach a least 10000th solution was approximately the same for both forms (198 for the cascade form as compared with 195 for the parallel form), also, the same value of the objective function was reached at each pth solution using both forms.

The results shown in Tables 2.1, 2.2, 2.4 and 2.5 are computed on the basis that the least squares solution is used as a starting point to obtain the least 10th solution, then the least 10th solution is used as a starting point to obtain the least 100th solution, and so on.

2.3 Design of IIR Digital Filters with Finite-Word-Length Coefficients

2.3.1 Description of the Problem

Suppose that the magnitude characteristics of an IIR digital filter, of the cascade form whose coefficients are represented exactly using finite-word-lengths, are specified to lie within given upper and/or lower bounds at a prescribed discrete set of frequencies $f_1, f_2, \ldots f_m$ corresponding to a discrete set of values of the complex variable z evaluated on the unit circle in the z-domain as in (2.1a) and (2.1b). One

approach to this problem is to specify the word-lengths required to represent the coefficients and optimize the magnitude characteristics of the filter, whereas a second approach is to optimize the word-lengths required to represent the coefficients subject to the constraints that the magnitude characteristics lie within the specified upper and/or lower bounds. If necessary, stability constraints may be dealt with either by the pole inversion approach or by imposing the appropriate set of linear inequalities on c_{4k-1} and c_{4k} (Steiglitz 1971, Charalambous and Best 1974b).

2.3.2 Problem Formulation

Let a coefficient, which is to be represented exactly using a finite-word-length be $c_i = r_i 2^{-q_i}$, $i = 1, \ldots, n$, where r_i is an integer, q_i is a nonnegative integer, 2^{-q_i} is the coefficient quantization step-size and q_i+1 is the word-length of the coefficient.

Case 1: A Priori Specified Word Lengths

Find the n-dimensional parameter vector $\underset{\sim}{c}$ representing the finite-word-length coefficients of the IIR digital filter, given the n word-lengths prescribing $\underset{\sim}{q}$, to minimize an appropriately chosen objective function comprising the deviations of the magnitude response $|H(\underset{\sim}{c},\psi)|$ from its prescribed upper and lower bounds $S_u(\psi)$ and $S_\ell(\psi)$ respectively, that is find $\underset{\sim}{c}$ for a given $\underset{\sim}{q}$ to minimize an objective function $U(|H(\underset{\sim}{c},\psi)|, S_u(\psi), S_\ell(\psi))$ subject to

$$c_i/2^{-q_i} \in I, \quad i = 1,2,\ldots,n$$

where n = 4K+1 and I is the set of integers.

Case 2: Optimal Word Lengths

Find a 2n-dimensional parameter vector $\underset{\sim}{c}'$ representing the optimal word-length coefficients of an IIR digital filter to minimize an appropriately chosen objective which is a function of the word-lengths of the n coefficients, such that the magnitude response $|H(\underset{\sim}{c}',\psi)|$ lies within its prescribed upper and lower bounds $S_u(\psi)$ and $S_\ell(\psi)$ respectively, that is find

$$\underset{\sim}{c}' = \begin{bmatrix} q_1 \\ q_2 \\ \vdots \\ q_n \\ r_1 \\ r_2 \\ \vdots \\ r_n \end{bmatrix}$$

to minimize an objective function

$$U(q_1, q_2, \ldots, q_n)$$

subject to

$$S_\ell(\psi) \leq |H(\underset{\sim}{c}',\psi)| \leq S_u(\psi)$$

and

$$q_i, r_i \in I, \quad i = 1,2,\ldots,n$$

where n = 4K+1 and I is the set of integers.

A practical appraoch to the numerical solution of the discrete optimization problems formulated in cases 1 and 2 is to use a branch and bound technique such as Dakin's tree-search algorithm (Dakin 1966) whereby each continuous nonlinear programming problem is transformed into an unconstrained minimax problem (Bandler and Charalambous 1974b) which in turn is solved by using one of several least pth optimization algorithms (Bandler and Charalambous 1972; Charalambous and Bandler 1973, 1976; Bandler et al.1976) in conjunction with Fletcher's unconstrained function minimization method (Fletcher 1972), as implemented in a general user-oriented computer program package DISOPT (Chen 1974; Bandler and Chen 1975a) whose Fortran listing is given by Chen (1974).

2.3.3 Examples

Of the several algorithms and options implemented in DISOPT (Chen 1974; Bandler and Chen 1975a), the following were used in the examples presented in this section

Algorithm 1: Nonlinear minimax optimization as a least pth optimization with a large value of p (Bandler and Charalambous 1972).

Algorithm 2: Nonlinear minimax optimization as a sequence of least pth optimizations with increasing values of p (Bandler and Charalambous 1972).

Algorithm 3: Application of an extrapolation technique to a sequence of least pth optimizations with geometrically increasing values of p (Chu 1974).

Option 1 : In the search for a discrete solution, reduce the dimensionality

of the problem by 1 through fixing a variable at its added discretizing constraint value.

Option 3 : Check the vertices, about the continuous solution, for an initial discrete solution.

Option 4 : Check the existence of a feasible solution before searching for an optimal one.

Option 7 : Search for only one discrete optimal solution.

The computational execution time on the CDC 6400 was in the order of 20 seconds for Example 2.3 and 1-5 minutes for the other examples, and the magnitude responses of Examples 2.4 and 2.5 are depicted on closed continuous intervals in Figs. 2.6a, 2.6b, 2.7a and 2.7b, for convenience, in spite of being prescribed initially, at a discrete set of frequencies.

Example 2.3

Find two optimal-word-length numbers x_1 and x_2 such that

$$0.2 \leq x_1 \leq 0.4$$

and

$$0.2 \leq x_2 \leq 0.8$$

The feasible region in the x_1-x_2 space is depicted in Fig. 2.5a.

Let

$$x_1 = r_1 2^{-q_1} \quad \text{and} \quad x_2 = r_2 2^{-q_2}$$

Starting with $\underline{c}'^{0} = [1 \quad 1 \quad 1 \quad 1]^T$ and using the Case 2 formulation whereby taking

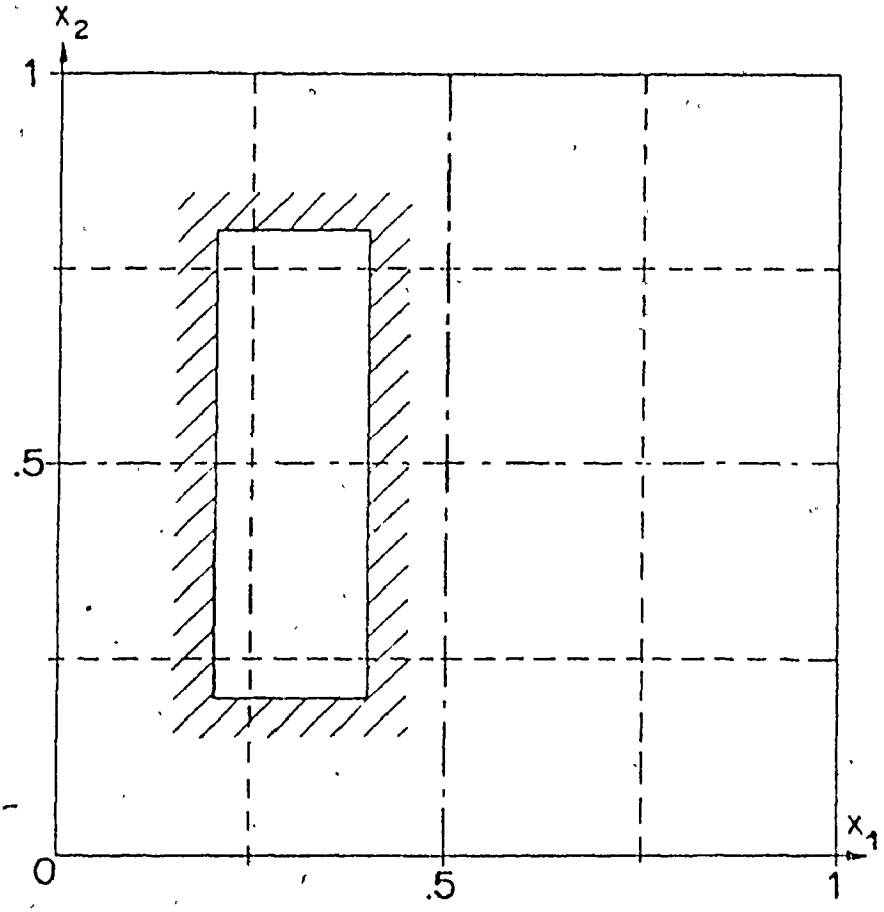

Fig. 2.5a The feasible region for Example 2.3

TABLE 2.6

TREE-SEARCH RESULTS FOR EXAMPLE 2.3

Node number	Objective Function $U(\underset{\sim}{c}')$	Solution $\underset{\sim}{c}'$	Description
0	0	$[0\ 0\ .2\ \ .781]^T$	continuous
1	-	-	nonfeasible
2	1.322	$[1.322\ 0\ 1\ \ .358]^T$	feasible
3	-	-	nonfeasible
4	2	$[2\ \ 0\ \ 1.201\ \ .51]^T$	feasible
5	2	$[2\ \ 0\ \ 1\ \ .51]^T$	feasible
6	-	-	nonfeasible
7	2.322	$[2\ \ .322\ \ 1\ \ 1]^T$	feasible
8	-	-	nonfeasible
9	3	$[2\ 1\ 1\ 1\ \ .554]^T$	feasible
10	3	$[2\ 1\ 1\ 1]^T$	discrete
11	$\geq$ 3	-	abandoned
12	2.322	$[2.322\ \ 0\ 2\ \ .28]^T$	feasible
13	-	-	nonfeasible
14	$\geq$ 3	-	abandoned

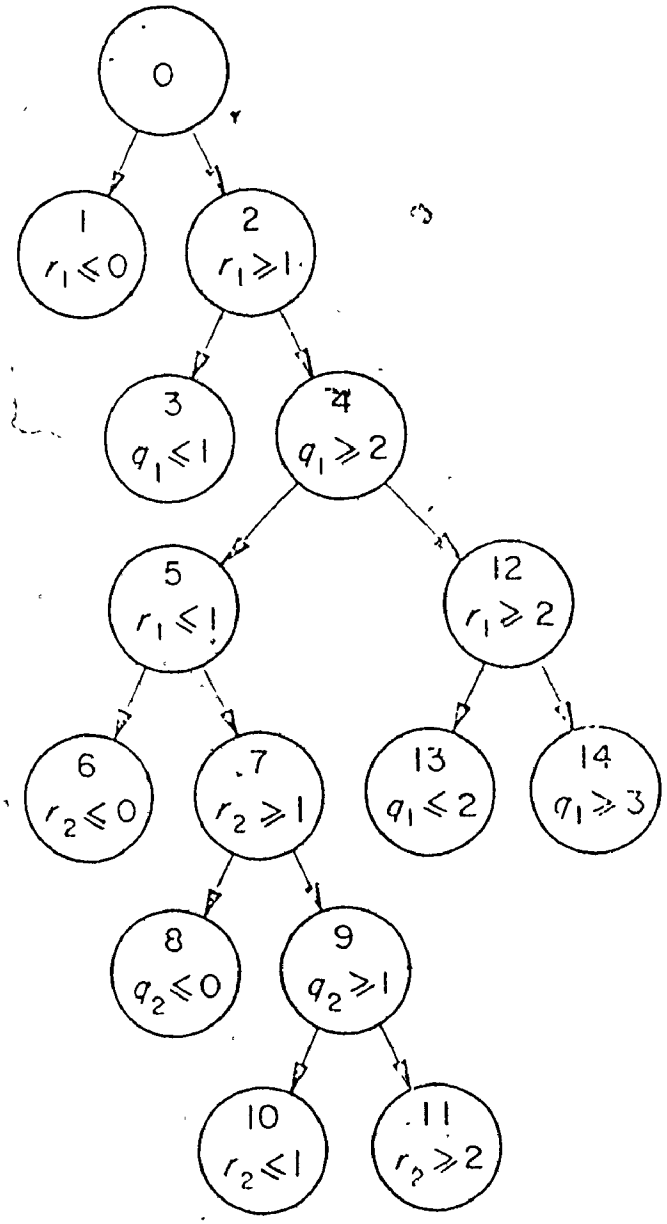

Fig. 2.5b Tree structure for Example 2.3.

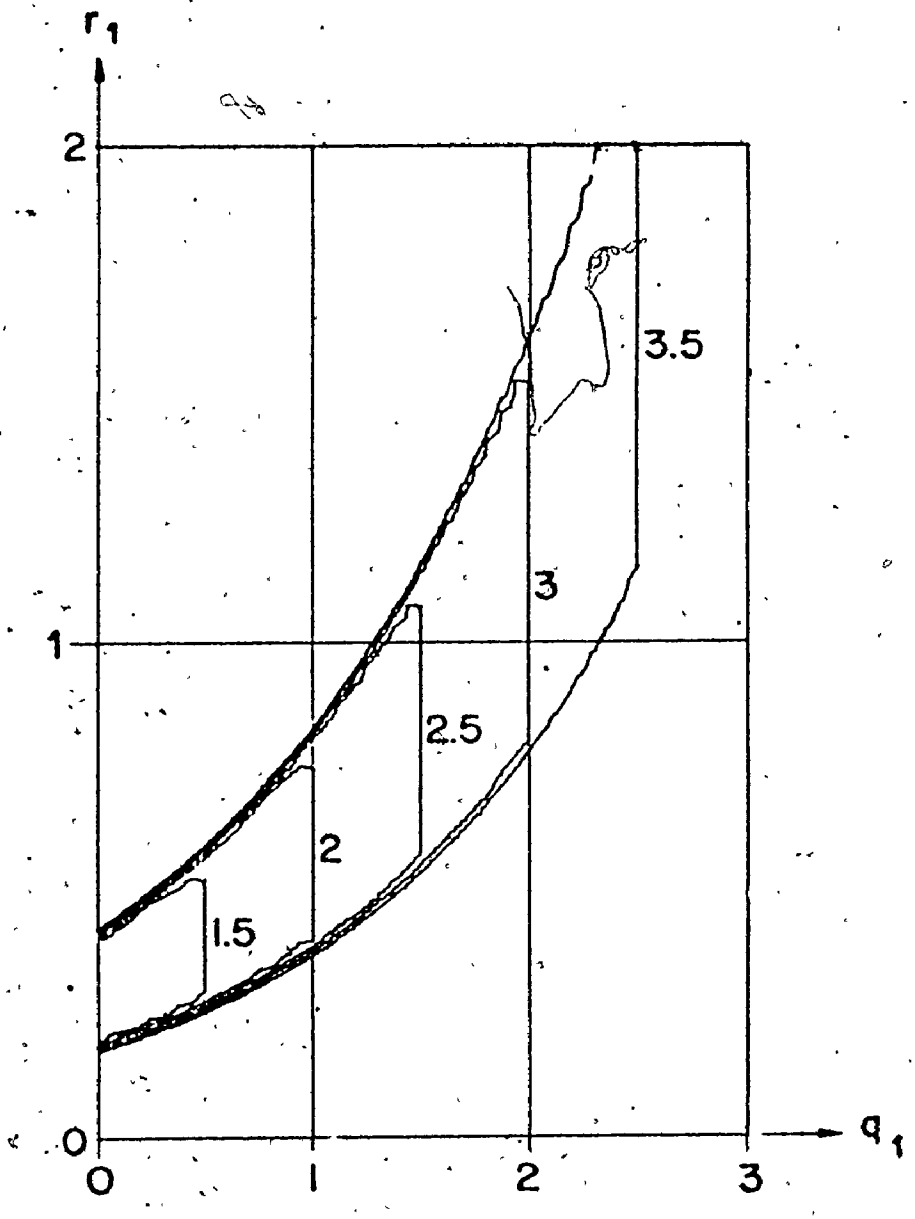

Fig. 2.5c Contours of the unconstrained minimax objective function for Example 2.3, where $r_2 = q_2 = 1$

$$U(q) = q_1 + q_2$$

DISOPT produced the results shown in Table 2.6 and Fig. 2.5b using Algorithms 3 with a third order extrapolation, initial value of p = 4, multiplying factor for p of 4 and options 3, 4, and 7. Fig. 2.5c depicts the contours of the unconstrained minimax objective function (Bandler and Charalambous 1974), as incorporated into DISOPT for $r_2 = q_2 = 1$. The discrete solution $\hat{c}' = [2\ 1\ 1\ 1\ ]^T$ at note 10 in Table 2.6 corresponds to

$$x_1 = 0.25 \quad \text{and}$$
$$x_2 = 0.5$$

Example 2.4

Consider the design of a low-pass IIR digital filter of the cascade form, having a 7-bit word length, whose magnitude response is specified by

f = 0, 900 (100)	S(f) =1
f = 1000	S(f) =1/ 2
f = 1200	S(f) = 0
f = 1500, 5000 (500)	S(f) = 0

Using a second-order filter section of the cascade form for a sampling frequency of 10kHz and the starting point of Suk and Mitra (1972) namely, $c^0 = [0\ 1\ -1\ -0.5\ 0.1]^T$ with the Case 1 formulation whereby taking

$$U(c, \psi) = \sum_{i=1}^{20} (|H(c, \psi_i)| - S(\psi_i))^2$$

DISOPT gave the results shown in Table 2.7, using Algorithm 1 with $p = 10^7$ and options 1, 3, 4, and 7. The passband and the stopband of the magnitude

TABLE 2.7

COMPARISON OF DISCRETE SOLUTIONS FOR EXAMPLE 2.4

Parameters	Suk and Mitra	DISOPT	
		Early Solution	Final Solution
c_1	-.25	-.296875	-.328125
c_2	1.3125	1.015625	1.015625
c_3	-1.4375	-1.4375	-1.43125
c_4	.65625	0.640625	.65625
c_5	.09375	0.109375	.109375
Objective Function	.31535	.29138	.29059
Maximum Error	.41345	-	.36685
Number of Function Evaluations	139	306	574 (terminated at 1030)

response are depicted in Figs. 2.6a and 2.6b respectively.

Example 2.5

Consider the design of a low-pass IIR digital filter of the cascade form, having an optimal word length whose upper and lower magnitude response bounds are specified by

$$\psi = 0,\ .18\ (.02),\ S_u(\psi_i) = 1.3,\ S_\ell(\psi_i) = .7,\quad i = 1,2,\ldots,10$$

$$\psi = .24\ ,\ S_u(\psi_i) = .3\ ,\quad i = 11$$

$$\psi = .3,\ 1\ (.1)\ ,\ S_u(\psi_i) = .3\ ,\quad i = 12, 13,\ldots,19.$$

Using one second-order filter section of the cascade form and the starting point $\underline{c}'^{o} = [q_1^o\ r_1^o\ r_2^o\ r_3^o\ r_4^o\ r_5^o\ ]^T = [1\ 0\ 2\ -2\ 1\ .2]^T$ with the Case 2 formulation whereby taking

$$q_1 = q_2 = \ldots = q_5$$

and

$$U(\underline{q}) = q_1$$

DISOPT gave the solutions $[2\ -6\ 5\ -6\ 3\ 1]^T$, $[2\ -4\ 3\ -6\ 3\ 1]^T$ and $[2\ -5\ 4\ -6\ 3\ 1]^T$ using Algorithm 2 with a sequence of p values $\{2, 10, 10^2, 10^3, 10^4\}$ and options 3 and 4. The corresponding IIR digital filter coefficients sets are $\{-1.5, 1.25, -1.5, .75, .25\}$, $\{-1, .75, -1.5, .75, .25\}$ and $\{-1.25, 1, -1.5, .75, .25\}$ respectively. The passband and the stopband of the magnitude response for the last coefficient set are depicted in Figs. 2.7a, and 2.7b respectively.

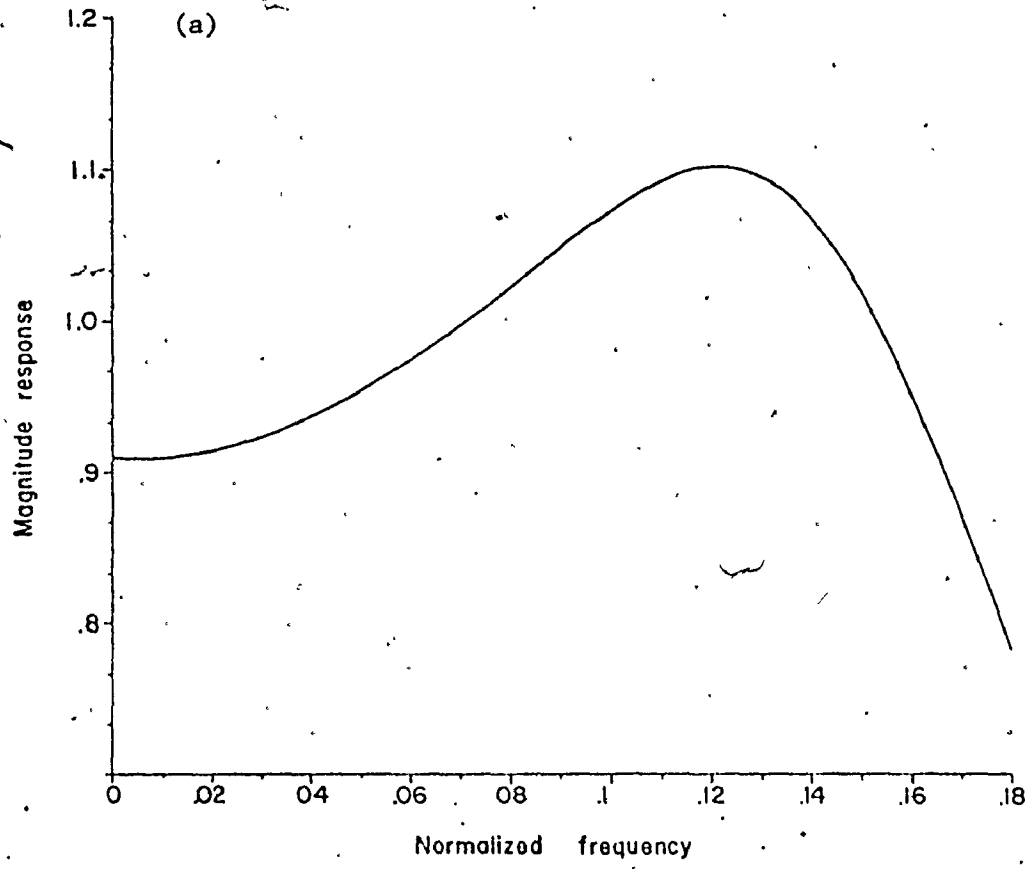

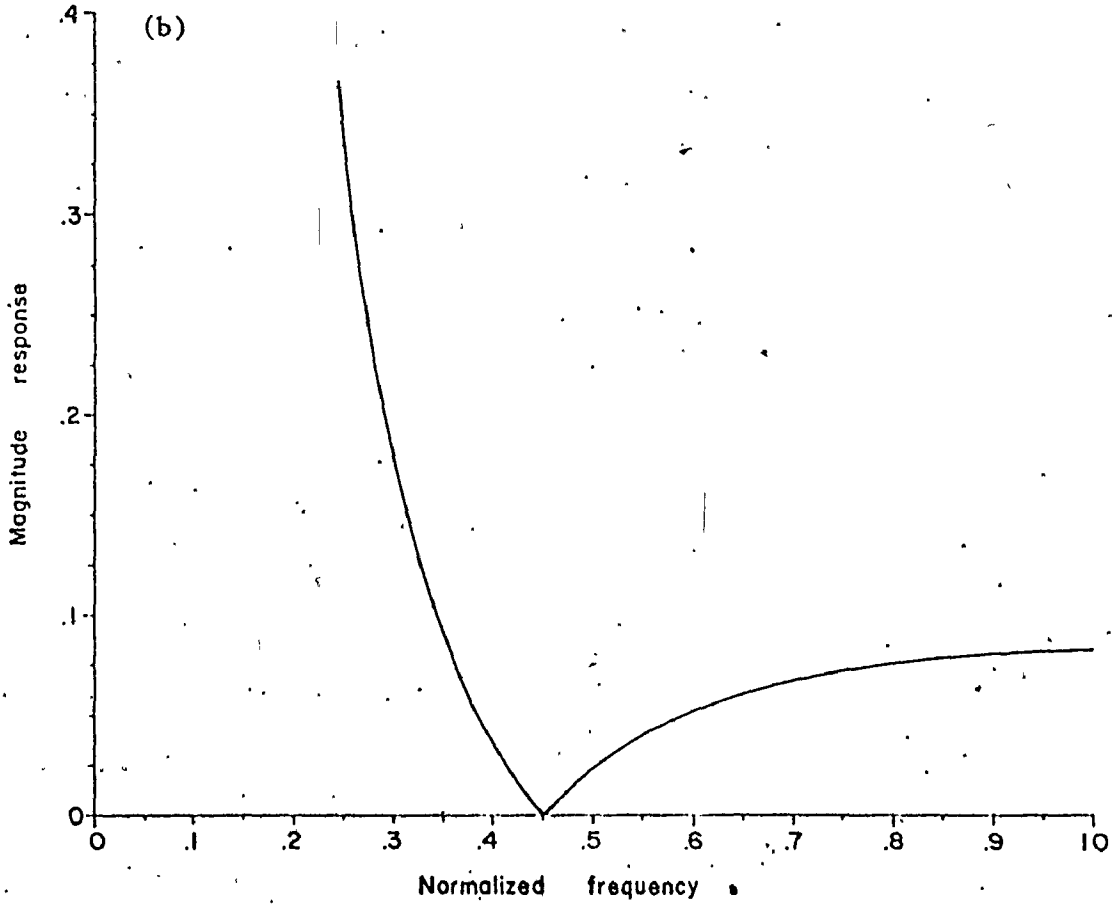

Fig. 2.6 Magnitude response for Example 2.4. (a) Passband response. (b) Stopband response.

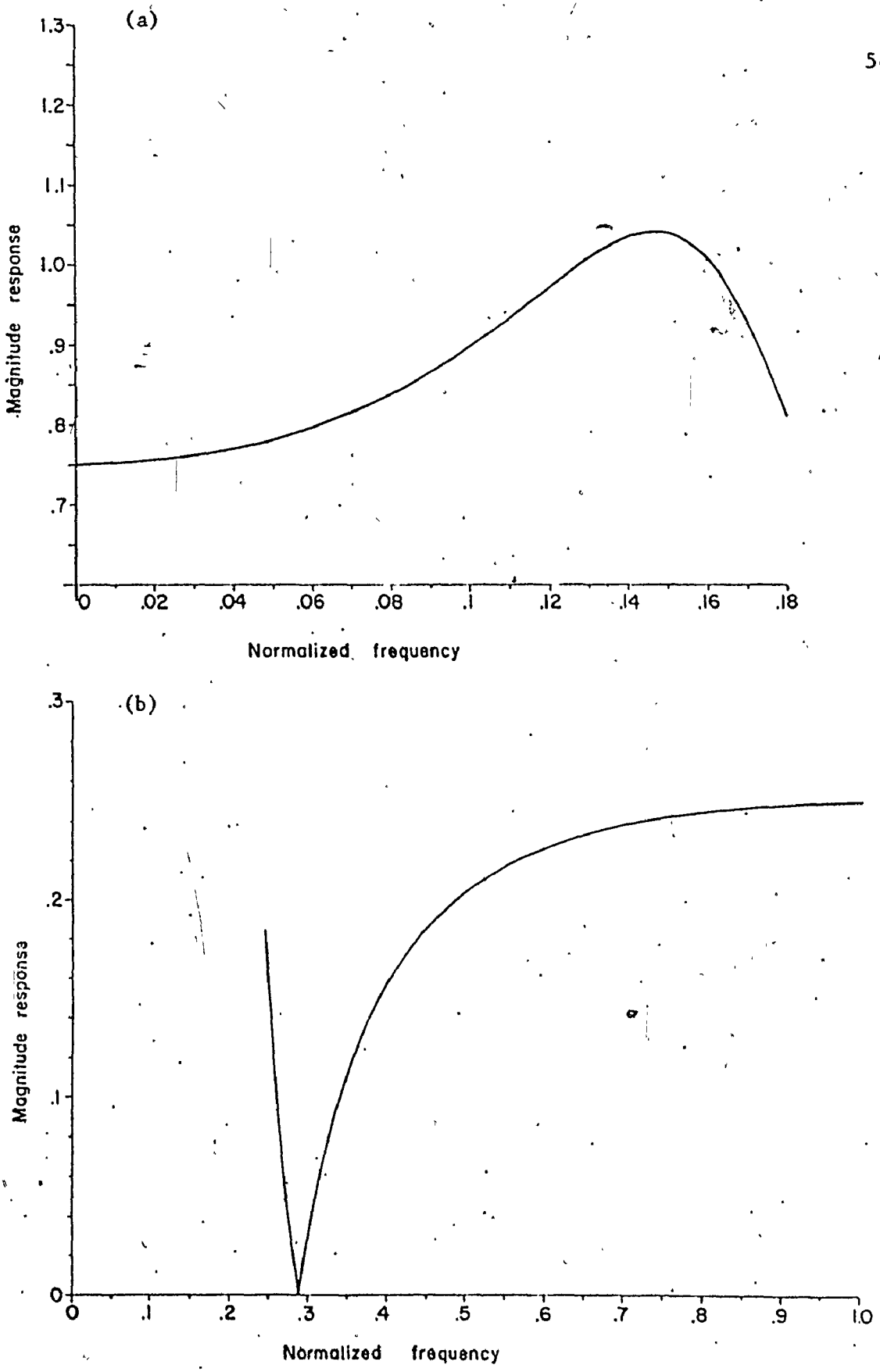

Fig. 2.7 Magnitude response for Example 2.5. (a) Passband response. (b) Stopband response.

Example 2.6

This is the same as Example 2.5, except that all q_i's can vary and

$$U(\underset{\sim}{q}) = q_1+q_2+q_3+q_4+q_5.$$

Starting with $[q_1q_2q_3q_4q_5r_1r_2r_3r_4r_5]^T = [2\ 0\ 1\ 2\ 2\ 0\ 1\ -2\ 2\ .4]^T$, DISOPT gave a solution $[2\ 0\ 1\ 2\ 2\ -5\ 1\ -3\ 3\ 1]^T$, which corresponds to the last coefficient set in Example 2.5 using the same algorithm and options as in Example 2.3.

When a uniform (all q_i's equal) word-length was optimized in Example 2.5 and all feasible discrete solutions were sought, then an optimal nonuniform (all q_i's need not be equal) word-length solution may be deduced from the uniform word-length solutions since for each

$$c_i = r_i\, 2^{-q_i}, \qquad i = 1, \ldots, n \qquad (2.5a)$$

let r_i be represented in terms of its factors which are multiples of 2, i.e., let

$$r_i' = r_i'\, 2^{v_i}, \qquad i = 1, \ldots, n \qquad (2.5b)$$

then

$$c_i = r_i'\, 2^{v_i}\, 2^{-q_i} = r_i'\, 2^{-(q_i' - v_i)} = r_i'\, 2^{-q_i'}, \qquad i = 1, \ldots n \qquad (2.5c)$$

where v_i, r_i, q_i, r_i' and q_i' are integers and q_i' corresponds to the nonuniform word-length solution. For example, the last uniform-word-length solution reached in Example 2.5 can be represented as

$$c_1 = -5 \times 2^{-2} = -5 \times 2^0 \times 2^{-2} = -5 \times 2^{-2}$$

$$c_2 = 4 \times 2^{-2} = 1 \times 2^2 \times 2^{-2} = 1 \times 2^0$$

$$c_3 = -6 \times 2^{-2} = -3 \times 2^1 \times 2^{-2} = -3 \times 2^{-1}$$

$$c_4 = 3 \times 2^{-2} = 3 \times 2^0 \times 2^{-2} = 3 \times 2^{-2}$$

$$c_5 = 1 \times 2^{-2} = 1 \times 2^0 \times 2^{-2} = 1 \times 2^{-2}$$

wherefrom

$$\underset{\sim}{r} = [-5 \quad 4 \quad -6 \quad 3 \quad 1]^T$$

$$\underset{\sim}{q} = [2 \quad 2 \quad 2 \quad 2 \quad 2]^T$$

$$\underset{\sim}{v} = [0 \quad 2 \quad 1 \quad 0 \quad 0]^T$$

hence

$$\underset{\sim}{q}' = [2 \quad 0 \quad 1 \quad 2 \quad 2]^T$$

and

$$\underset{\sim}{r}' = [-5 \quad 1 \quad -3 \quad 3 \quad 1]^T$$

which is the optimal-nonuniform-word-length solution reached in Example 2.6. Hence, although a uniform-word-length was optimized in Example 2.5, it was possible to deduce the corresponding nonuniform-word-length-solution through factors of r_1 which are multiples of 2.

2.4 Discussion

In solving the approximation problem of IIR digital filters, having large-word-length coefficients, with arbitrary specifications on the magnitude characteristics, the application of a least pth optimization strategy using extremely large values of p, typically 10000, yields reasonably well-conditioned objective functions, where effectively negative values of p can be used to obtain the coefficients of an IIR digital filter that meets or exceeds the prescribed magnitude specifications (as in Example 2.2). Both the cascade and parallel forms seem to be identical in so far as the value of the objective function at a least pth solution and the number of function evaluations required to reach that solution are concerned, whereas the use of the Fletcher method in conjunction with least pth optimization seems to be more efficient than that of the Fletcher-Powell method. Local optimality of the least pth solution may be checked by perturbing the obtained solution or increasing ξ and then restarting the optimization process, whereas stability requirements of the filter transfer function can be met by using a pole inversion technique, and the order of the filter can be increased to meet the prescribed magnitude specifications by growing second-order filter sections. The results of Examples 2.1 and 2.2 indicate that the zeros of the transfer function tend to lie on the unit circle in the z-domain, thus it seems that the efficiency of the computation may be improved by using a starting or fixed value of 1 for each of the coefficients c_{4k-2} of a biquadratic second-order filter section of the cascade form.

One approach to the design of IIR digital filters, having finite-

word-length coefficients may be summarized as follows, firstly, a continuous large-word-lengths feasible solution is sought to determine the minimum necessary order of the filter, secondly, if the word-lengths are specified then the optimal corresponding magnitude response is sought using the Case 1 formulation, whereas if the word-lengths are to be optimized then the Case 2 formulation may be used where initially, a uniform variable word-length may be optimized (as in Example 2.5) and all feasible discrete solutions are sought wherefrom the optimal-word-lengths solution is obtained, or alternatively only one discrete solution is found, then the word-lengths are allowed to differ (as in Example 2.6) and a suitable function of these word-lengths is minimized. Finally, if desired, the magnitude response corresponding to the optimal-word-lengths solution could be optimized using the Case 1 formulation.

CHAPTER 3

AN OPTIMAL PROCESSOR FOR MULTISTAGE DECIMATION AND FILTERING

3.1 Introduction

Schafer and Rabiner (1973) have shown that sampling rate reduction and sampling rate increase are basically interpolation processes and can be efficiently implemented using FIR (finite impulse response) digital filters. Crochiere and Rabiner (1975) have presented a general theory of multistage decimators and interpolators, they also presented the necessary relations for optimally designing multistage decimators utilizing a multiple of FIR digital filters implemented in a direct form.

Rabiner et al. (1974) made some comparisons between equivalent optimal FIR and elliptic IIR digital filters based on the number of multiplications per sample required to realize these filters. They concluded that in the case of low-pass filters with quasi-equiripple magnitude characteristics, elliptic IIR filters could generally be realized more efficiently than equivalent linear phase FIR filters, but when the additional requirement of constant group delay in the passband was added to the specifications, the linear phase FIR filters were found to be more efficient than group-delay-equalized elliptic IIR filters. However, their comparisons excluded IIR filters which are designed, using modern optimization procedures, to meet frequency domain specifications

on both magnitude and group delay responses, where the number of poles and zeros of the filter transfer function are unequal.

This chapter presents an optimal processor for multistage decimation and filtering utilizing a single low-pass IIR digital filter coefficient set, but having a different cut-off frequency at each decimation stage because the cut-off frequency is determined by the sampling frequency at each stage. The IIR filter is implemented in a cascade form. The upper bound on the decimation ratio per stage is presented along with an upper bound on the overall decimation ratio and a lower bound on the number of stages.

3.2 A Multistage Decimator

A multistage decimator is shown in Fig. 3.1 where

$\eta_{1i}(n\tau_o), \ldots\ldots, \eta_M(n\tau_o)$ are the input sequences to the multistage decimator

$\hat{\mu}_{1i}(n\tau_N), \ldots\ldots, \hat{\mu}_M(n\tau_N)$ are the output sequences of the multistage decimator

$\mu^o_{1i}(n\tau_{i*}), .., \mu^o_{Mi}(n\tau_{i*})$ are the input sequences to ith decimation stage

$\mu^p_{1i}(n\tau_{i*}), \ldots, \mu^p_{Mi}(n\tau_{i*})$ are the sequences at the output of the low-pass filter of ith decimation stage.

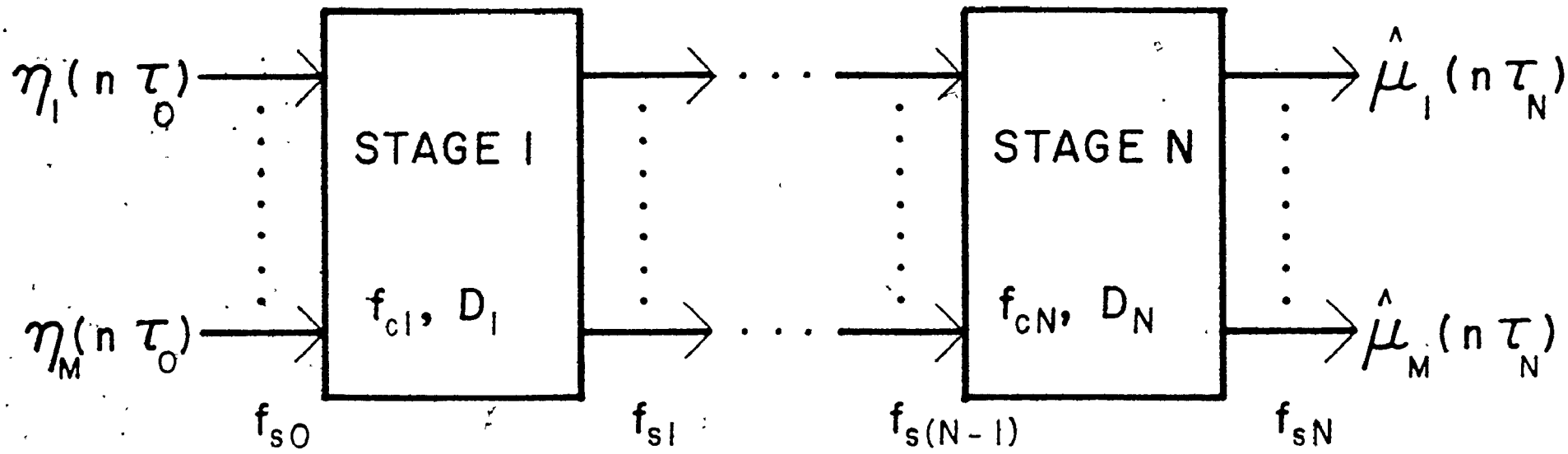

Fig. 3.1 An M-input N-stage decimating filter

M is the multiplicity of the input

N is the number of the decimation stages

τ_o is the original sampling period

τ_i is the ith sampling period

f_{so} is the initial sampling frequency

f_{si} is the sampling frequency at the output of ith decimation stage

$f_{ci} = f_{pi} + \Delta_i$ is the cut-off frequency of ith decimation stage

f_{pi} is the passband upper frequency of ith decimation stage

Δ_i is the transition band of ith decimation stage

D_i is the decimation ratio of ith decimation stage

$i^* = i - 1$ denotes the (i-1)th decimation stage

The final sampling frequency is

$$f_{sN} = \frac{f_{so}}{\prod_{i=1}^{N} D_i} \tag{3.1a}$$

where

$$D_i = \frac{f_{si^*}}{f_{si}}, \qquad i = 1, \ldots, N \tag{3.1b}$$

To avoid aliasing at the lower sampling rates it is necessary to ensure that at each stage of decimation, the input sequences are appropriately band limited. This is achieved by low-pass filtering at a

cut-off frequency f_{ci}. Then, the sample rate reduction can be achieved by extracting every D_ith sample of the filtered sequence as shown in Fig. 3.2.

Let frequency band limiting at each decimation stage be achieved through a low-pass IIR digital filter and let the governing equations for the passband upper frequency f_{pi} and the transition band Δ_i of the IIR low-pass filter be specified by

$$f_{pi} = \alpha f_{si^*}, \quad i = 1, \ldots, N \tag{3.2a}$$

$$\Delta_i = \beta f_{si^*}, \quad i = 1, \ldots, N \tag{3.2b}$$

hence,

$$f_{ci} = (\alpha + \beta) f_{si^*}, \quad i = 1, \ldots, N \tag{3.2c}$$

An approximate relationship for the order N_f of an elliptic-filter (Gold and Rader 1969) whose magnitude squared response $|H_e|^2$ is shown in Fig. 3.3a is

$$N_f \simeq \frac{2}{\pi^2} \ln \frac{4A}{\epsilon_o} \ln \frac{8 \tan(\pi\alpha)}{\tan(\pi\alpha + \pi\beta) - \tan(\pi\alpha)} \tag{3.3a}$$

If the magnitude response $|H_o|$ of an optimal IIR filter is specified as in Fig. 3.3b, then an approximate expression for N_f can be obtained by relating δ_1 and δ_2 to ϵ_o and A as follows (Rabiner et al. 1974)

$$\epsilon_o = \frac{2\sqrt{\delta_1}}{1 - \delta_1} \tag{3.3b}$$

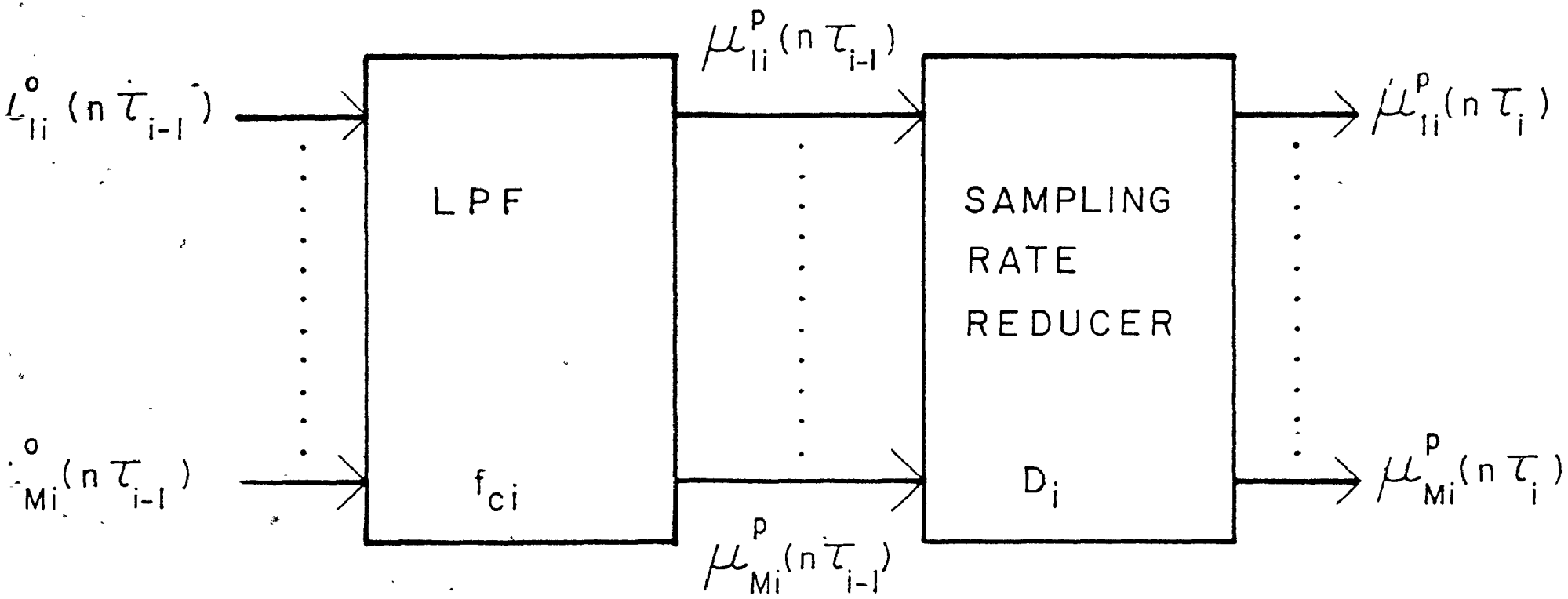

Fig. 3.2 Stage i of an M-input multistage decimating filter

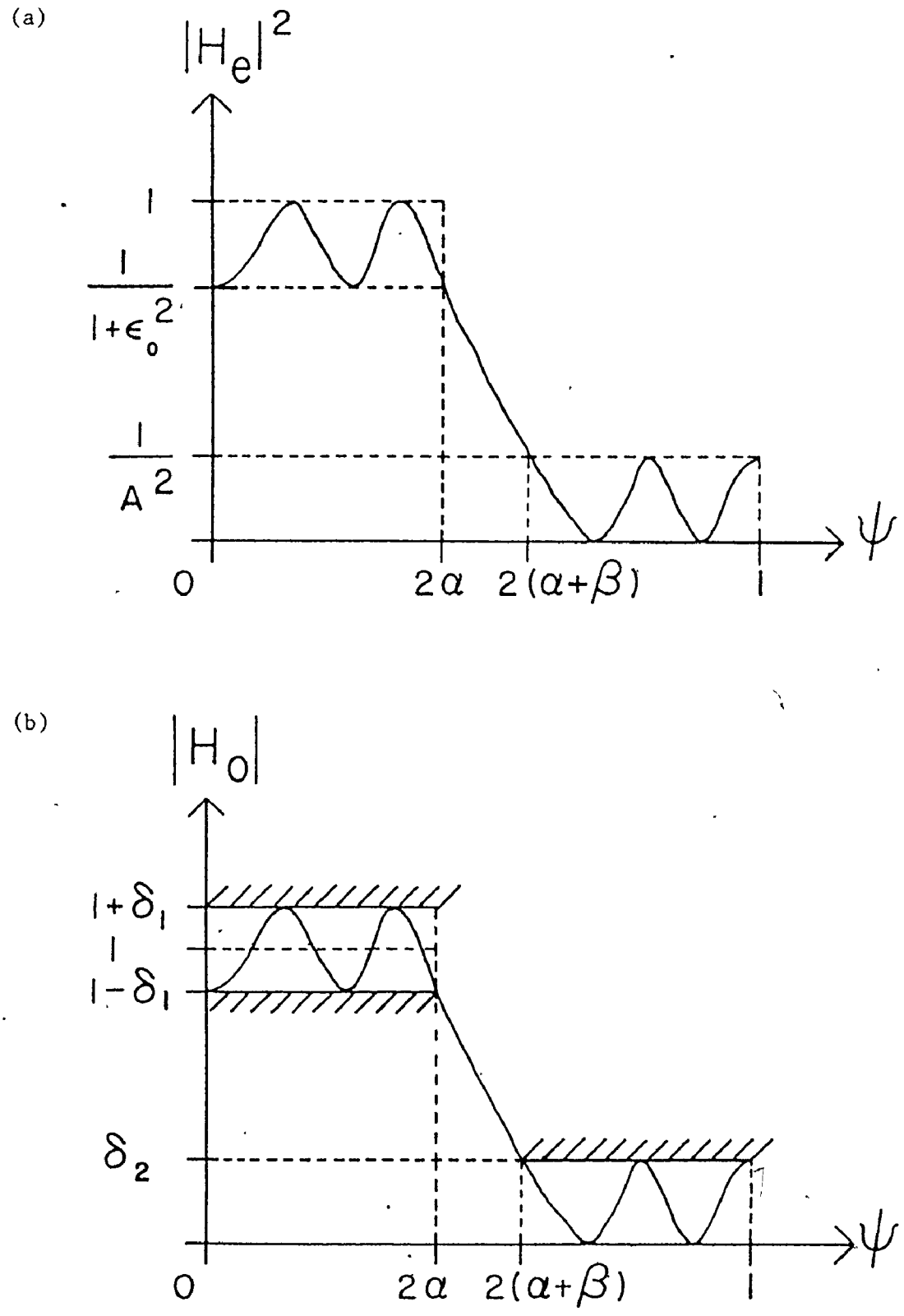

Fig. 3.3 Parameters prescribing (a) magnitude squared characteristics of elliptic low-pass IIR digital filters and (b) magnitude characteristics of optimal low-pass IIR digital filters, ψ is a normalized frequency equal to twice the frequency divided by the sampling frequency.

$$A = \frac{1 + \delta_1}{\delta_2} \tag{3.3c}$$

hence,

$$N_f \simeq \frac{2}{\pi^2} \ln \frac{2(1-\delta_1)^2}{\delta_2\sqrt{\delta_1}} \ln \frac{8 \tan(\pi\alpha)}{\tan(\pi\alpha+\pi\beta)-\tan(\pi\alpha)} \tag{3.3d}$$

The linear relationship between f_{ci} and f_{si*} enables the same digital filter to operate at different cut-off frequencies proportional to the different sampling frequencies implicit in a multistage decimation process. Thus, on the one hand, low-pass filtering can be used to satisfy the sampling theorem requirements on decimation and on the other hand, decimation can be used to adjust the cut-off frequency of a low-pass filter and to reduce the number of samples from which a deduction of some desired information is possible. The final passband upper frequency, transition band and cut-off frequency of the N stage decimator are

$$f_{pN} = \alpha \frac{f_{so}}{\prod_{i=1}^{N-1} D_i} \tag{3.4a}$$

$$\Delta_N = \beta \frac{f_{so}}{\prod_{i=1}^{N-1} D_i} \tag{3.4b}$$

$$f_{cN} = (\alpha+\beta) \frac{f_{so}}{\prod_{i=1}^{N} D_i} \tag{3.4c}$$

3.2.1 Derivation of Bounds on D_i, D_T, N and α

Consider a signal having frequency contents up to f_{ho} and sampled at a frequency f_{so}. Assume the desired information to lie within a frequency band up to f_h. Define a decimation index m_d such that

$$m_d = \frac{f_{ho}}{f_h}, \quad 1 \leq m_d < \infty \tag{3.5a}$$

The initial upper bound on the overall decimation ratio is

$$D_{uo} = \frac{f_{so}}{2 f_{ho}} \tag{3.5b}$$

After appropriate low-pass filtering the upper bound on the overall decimation ratio increases to

$$D_u = \frac{f_{so}}{2 f_h} = m_d D_{uo} \tag{3.5c}$$

An upper bound D_{us} on the decimation ratio per stage can be derived for the given low-pass filter by invoking the requirement of the sampling theorem

$$f_{si} \geq 2 f_{ci}, \quad i = 1, \ldots, N \tag{3.6a}$$

$$f_{si} \geq 2(\alpha+\beta) f_{si*}, \quad i = 1, \ldots, N \tag{3.6b}$$

Therefore,

$$D_i \leq \frac{1}{2(\alpha+\beta)}, \quad i = 1, \ldots N \tag{3.6c}$$

and

$$D_{us} = \frac{1}{2(\alpha+\beta)} \tag{3.6d}$$

This upperbound on the decimation ratio per stage (D_{us}) constitutes a major factor in determining the number of decimation stages needed for a specified sampling rate reduction. Let the specified overall decimation ratio be

$$D_T = \prod_{i=1}^{N} D_i \tag{3.7a}$$

where

$$D_T \leq D_u \tag{3.7b}$$

A lower bound N_ℓ on the number of stages can be obtained from the inequality

$$D_T \leq (D_{us})^N \tag{3.8a}$$

substituting from equation (3.6d) into (3.8a) it follows that

$$N \geq \frac{\ell n\ D_T}{\ell n\ 0.5 - \ell n(\alpha+\beta)} \tag{3.8b}$$

hence,

$$N_\ell = \frac{\ell n\ D_T}{\ell n\ 0.5 - \ell n(\alpha+\beta)} \tag{3.8c}$$

A lower bound on α can be obtained from the inequality

$$f_{pN} \geq W_o \, f_h \quad , \quad W_o \geq 1 \tag{3.9a}$$

where W_o is a weighting factor used to compensate for discretization effects on the sampling frequencies. Substituting from equations (3.4a) and (3.5c) into (3.9a), it follows that

$$\alpha \geq \frac{W_o \, D_T}{2 \, D_u \, D_N} \tag{3.9b}$$

since

$$D_N \leq \frac{1}{2(\alpha+\beta)} \tag{3.9c}$$

therefore, substituting from (3.9c) into (3.9b) it follows that

$$\alpha \geq \frac{\beta \, W_o \, D_T}{D_u - W_o \, D_T} \tag{3.9d}$$

hence

$$\alpha_\ell = \frac{\beta \, W_o \, D_T}{D_u - W_o \, D_T} \tag{3.9e}$$

3.2.2 An Optimal Multistage Decimator

Let

$$U_1 = \frac{1}{\ell n \ 0.5 - \ell n(\alpha + \beta)} \tag{3.10a}$$

and

$$U_2 = \ell n \frac{8 \tan(\pi\alpha)}{\tan(\pi\alpha+\pi\beta) - \tan(\pi\alpha)} \qquad (3.10b)$$

It can be seen from (3.8c), (3.3a) and (3.3d) that U_1 and U_2 are proportional to N_ℓ and N_f respectively. Furthermore, as β is a fraction N_ℓ is minimum if β is minimum while N_f is minimum if β is maximum. Hence, the multistage decimator can be considered optimal, in a minimax sense, if the specified decimation requirement is met at a minimum of the maximum of N_ℓ and N_f. Thus, an optimization problem can be formulated as follows:

Find α and β to minimize

$$U = \max \{W_1 U_1, W_2 U_2\} \qquad (3.10c)$$

subject to

$$\alpha \geq \frac{\beta W_o D_T}{D_u - W_o D_T}$$

$$\alpha + \beta < 0.5 \qquad (3.10d)$$

$$\alpha, \beta > 0 \qquad (3.10e)$$

where W_1 and W_2 are weighting factors to be chosen in such a way as to portray the relative importance of the number of stages with respect to the filter order. Constraints (3.10d) and (3.10e) are imposed to insure that U_1 and U_2 are finite. This weighted-constrained-minimax

optimization problem can be solved using a simple 2-dimensional grid search and plotting the contours of the objective function U, along with its linear constraints, since it involves only two parameters.

After determining α and β, for specified ripple and attenuation parameters (such as ε_o and A or δ_1 and δ_2 in Fig. 3.3), the coefficients of the IIR digital filter can be optimally chosen either by using conventional frequency-domain design techniques for elliptic IIR digital filters in conjunction with the bilinear z-transformation (Kaiser 1966; Gold and Rader 1969; Sablatash 1971) or by using an optimization strategy (such as least pth (Bandler and Bardakjian 1973b) or minimax,(Charalambous 1974a, 1975) in conjunction with a powerful function minimization method (such as the Fletcher method (Fletcher 1970, 1972) to solve the approximation problem in the z-domain directly.

To find the optimal set of decimation ratios to meet a decimation requirement D_T, the set S_T of all the J factors d_j of D_T is found where

$$S_T \triangleq \{d_j \mid D_T = \prod_{j=1}^{J} d_j,\ d_j > 1,\quad d_j \text{ integer},\ J \geq 1\} \qquad (3.11a)$$

then the set S_T is subdivided into N separate subsets such that $N-N_\ell$ is minimum and subject to the constraint that within each subset S_i having B_i members, the product D_i of the members is less than or equal to D_{us} that is

$$S_T = \bigcup_{i=1}^{N} S_i \qquad (3.11b)$$

such that $N - N_\ell$ is minimum

$$\sum_{i=1}^{N} B_i = J \tag{3.11c}$$

$$S_i \triangleq \{d_j \mid D_i = \prod_{j=1}^{B_i} d_j,\ D_i \leq D_{us},\ B_i \geq 1\} \tag{3.11d}$$

Hence,

$$D_i = \prod_{j=1}^{B_i} d_j;\quad d_j \in S_i;\quad i = 1, \ldots, N \tag{3.11e}$$

3.2.3 An Algorithmic Implementation of a Multiple-Input Multistage Decimating IIR Digital Filter

The IIR digital filter is implemented as a cascade of second-order biquadratic filter sections (and a first order filter section if the filter order N_f is odd) of the form

$$\mu_{ji}^{r}(n\,\tau_{i*}) = \mu_{ji}^{r-1}(n\,\tau_{i*}) + \sum_{k=1}^{2} c_{k+4r-4}\,\mu_{ji}^{r-1}(n\,\tau_{i*} - k\,\tau_{i*}) - \sum_{k=1}^{2} c_{k+4r-2}\,\mu_{ji}^{r}(n\tau_{i*} - k\tau_{i*}) \tag{3.12a}$$

where

$$\mu_{ji}^{o}(n\,\tau_{i*}) = c_K\,\mu_{ji*}^{p}(n\,\tau_{i*}) \tag{3.12b}$$

$$\mu_{jo}^{p}(n\,\tau_o) = \eta_j(n\,\tau_o) \tag{3.12c}$$

$$\hat{\mu}_j(n\,\tau_N) = \mu_{jN}^{p}(n\,\tau_N) \tag{3.12d}$$

$\mu_{ji}^{r}(n\,\tau_{i*})$ are intermediate outputs

n is a non-negative integer

$\{c_k \mid k=1, \ldots, K\}$ is the set of filter coefficients

$c_{4r-2} = 1$ for zeros of transfer function to lie on the unit circle in the z-domain

$i = 1, \ldots, N$; $j=1, \ldots, M$ and $r = 1, \ldots, R$

Case 1: If N_f is even, then

$$R = \frac{N_f}{2} \tag{3.12e}$$

$$K = 4R+1 \tag{3.12f}$$

$$p = R \tag{3.12g}$$

Case 2: If N_f is odd, then

$$R = \frac{N_f - 1}{2} \tag{3.12h}$$

$$K = 4R + 3 \tag{3.12i}$$

$$p = R + 1 \tag{3.12j}$$

$$\mu_{ji}^{p}(n\tau_i^*) = \mu_{ji}^{R}(n\tau_{i*}) + c_{K-2}\mu_{ji}^{R}(n\tau_{i*} - \tau_{i*}) - c_{K-1}\mu_{ji}^{p}(n\tau_{i*} - \tau_{i*}) \tag{3.12k}$$

To implement the algorithm efficiently, the filter coefficients that are unity are excluded from the filter coefficient set to reduce storage requirements.

Let

$K^* = 3R + 1$ for N_f even

$= 3R + 3$ for N_f odd

$R^* = R - 1$ for N_f even

$= R$ for N_f odd

$\{c_k^* \mid k=1, \ldots, K^*\}$ be the set of filter coefficients excluding unity coefficients

$\underset{\sim}{\mu}_o$ be an M-dimensional input array

$\underset{\sim}{\mu}_p$ be an M-dimensional output array

$\{\underset{\sim}{\mu}_r \mid r = 1, \ldots, R^*\}$ be a set of M-dimensional intermediate output arrays

$\{\underset{\sim}{\sigma}_k \mid k = 1, \ldots, N_f + 2\}$ be a set of M-dimensional working arrays

Then the algorithm (Bardakjian and Sarna 1976b) can be described as follows:

Read N, M, $\{D_i \mid i=1, \ldots, N\}$, $\{c_k^* \mid k=1, \ldots, K^*\}$, $\alpha, \beta, f_{so}, f_h, N_f$

if N_f even, $R \leftarrow N_f/2$, $R^* \leftarrow R-1$

if N_f odd, $R \leftarrow (N_f-1)/2$, $R^* \leftarrow R$

$D_{us} \leftarrow 1/2(\alpha+\beta)$

$D_u \leftarrow f_{so}/2\ f_h$

$\tau_{so} \leftarrow 1/f_{so}$

$D_T \leftarrow 1$

$i \leftarrow 1$

1. if $D_i > D_{us}$, go to 8

$D_T \leftarrow D_T D_i$

$i \leftarrow i + 1$

If $i \leq N$, go to 1

If $D_T > D_u$, go to 8

2. $\underset{\sim}{\tau}_o \leftarrow \underset{\sim}{0}$

$\underset{\sim}{\sigma}_k \leftarrow \underset{\sim}{0} \quad k = 1, \ldots, N_f + 2$

Kount $\leftarrow$ 1

$i \leftarrow 1$

3. Read $\underset{\sim}{\mu}_o$ from input data file

if $N_f \neq 1$, go to 4

$\underset{\sim}{\mu}_p \leftarrow c_3^* \underset{\sim}{\mu}_o + c_1^* \underset{\sim}{\sigma}_1 - c_2^* \underset{\sim}{\sigma}_2$

$\underset{\sim}{\sigma}_1 \leftarrow \underset{\sim}{\mu}_o$

$\underset{\sim}{\sigma}_2 \leftarrow \underset{\sim}{\mu}_p$

go to 6

4. if $N_f \neq 2$, go to 5

$\underset{\sim}{\mu}_p \leftarrow c_4^* \underset{\sim}{\mu}_o + c_1^* \underset{\sim}{\sigma}_1 + \underset{\sim}{\sigma}_2 - c_2^* \underset{\sim}{\sigma}_3 - c_3^* \underset{\sim}{\sigma}_4$

$\underset{\sim}{\sigma}_{k+1} \leftarrow \underset{\sim}{\sigma}_k \quad k = 1, 3$

$\underset{\sim}{\sigma}_1 \leftarrow \underset{\sim}{\mu}_o$

$\underset{\sim}{\sigma}_3 \leftarrow \underset{\sim}{\mu}_p$

go to 6

5. $\underset{\sim}{\mu}_1 \leftarrow c_K^* \underset{\sim}{\mu}_o + c_2^* \underset{\sim}{\sigma}_1 + \underset{\sim}{\sigma}_2 - c_2^* \underset{\sim}{\sigma}_3 - c_3^* \underset{\sim}{\sigma}_4$

$\underset{\sim}{\mu}_r \leftarrow \underset{\sim}{\mu}_{r-1} + c^*_{3r-2} \underset{\sim}{\sigma}_{2r-1} + \underset{\sim}{\sigma}_{2r} - c^*_{3r-1} \underset{\sim}{\sigma}_{2r+1} - c_3^* \underset{\sim}{\sigma}_{2r+2}$;

$r=2,\ldots,R^*$

if N_f even, $\underset{\sim}{\mu}_p \leftarrow \underset{\sim}{\mu}_{R-1} + c^*_{3R-2} \underset{\sim}{\sigma}_{2R-1} + \underset{\sim}{\sigma}_{2R} - c^*_{3R-1} \underset{\sim}{\sigma}_{2R+1} - c^*_{3R} \underset{\sim}{\sigma}_{2R+2}$

if N_f odd, $\underset{\sim}{\mu}_p \leftarrow \underset{\sim}{\mu}_R + c^*_{3R+1} \underset{\sim}{\sigma}_{2R+1} - c^*_{3R+2} \underset{\sim}{\sigma}_{2R+3}$

$\underset{\sim}{\sigma}_{k+1} \leftarrow \underset{\sim}{\sigma}_k \quad k= 1, 3, \ldots, 2R+1$ (3.12l)

$\underset{\sim}{\sigma}_1 \leftarrow \underset{\sim}{\mu}_o$ (3.12m)

$\underset{\sim}{\sigma}_{2r+1} \leftarrow \underset{\sim}{\mu}_r \; ; r = 1, 2, \ldots, R^*$ (3.12n)

if N_f even $\underset{\sim}{\sigma}_{2R+1} \leftarrow \underset{\sim}{\mu}_p$ (3.12o)

if N_f odd $\underset{\sim}{\sigma}_{2R+3} \leftarrow \underset{\sim}{\mu}_p$ (3.12p)

6. Kount ← Kount + 1

If Kount $\leq$ D_i, go to 3

Write $\underset{\sim}{\mu}_p$ in output data file

Kount ← 1

If stopping criteria is met, go to 7

Go to 3

7. $i \leftarrow i + 1$

Delete input data file

If $i > N$, go to 8

Input data file ← output data file

Delete output data file

Go to 2

8. Stop

The stopping criterion can be either a test for a maximum allowable number of samples per input sequence, or a test for an end of file indicator at the end of the input data file. It is to be noted that the delay operation required for filtering is achieved by array shifting in assignments (3.12l) to (3.12p).

3.2.4 Example 3.1

Design an optimal decimator with an overall decimation ratio of 100 to process electrical signals acquired from the human colon (See chapter 6), where f_{ho} = 30 Hz, f_{so} = 100 Hz and f_h = 0.2045 Hz.

To choose α and β let

$$W_o = 2$$

$$W_1 = 8$$

$$W_2 = 1$$

Then, the solution of the weighted-constrained-minimax problem specified by (3.10c), (3.9d), (3.10d) and (3.10e), (which can be found by using a 2-dimensional grid search), is

$$\alpha = 0.045$$

and

$$\beta = 0.01$$

as can be seen from Fig. 3.4 which depicts the contours of the objective function U along with the active linear constraint ($\alpha \geq 4.5\beta$). Substituting in (3.6d) and (3.8c)

$$D_{us} = 9$$

and

$$N_{\ell} = 2.086$$

To optimally choose the coefficients of the IIR digital filter for a magnitude specification prescribed by choosing $\delta_1 = \delta_2 = 0.05$ (hence, $N_f \simeq 3.746$), a least pth optimization strategy was used and the coefficients of a fourth order, low-pass IIR digital filter were estimated (Example 2.1 of Chapter 2) to be

$$\{c_k \mid k=1, \ldots,9\} = \{-1.870741, 1, -1.874095, 0.953439, -1.520276, 1, -1.752557, 0.787996, 0.043369\}$$

The passband response, the stopband response and the pole-zero configuration of the transfer function are depicted in Figs. 2.2a, 2.2b and 2.2c respectively.

To find an optimal set of decimation ratios, the set S_T of all the J factors of D_T is found to be

$$S_T = \{2, 2, 5, 5\} \quad , J = 4$$

For N = 2, the set S_T cannot be subdivided into 2 subsets according to (3.11b) - (3.11d).

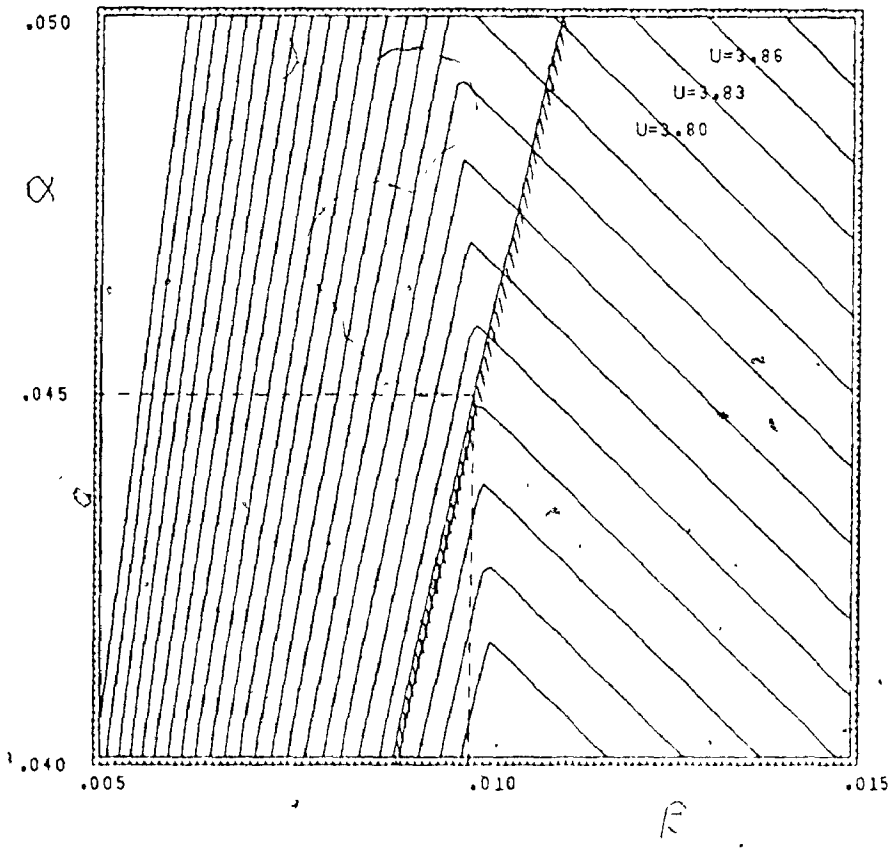

Fig. 3.4 Contours of the objective function U along with the constraint $\alpha \geq 4.5\beta$

For N = 3, the set S_T can be subdivided into the following 3 subsets according to (3.11b) - (3.11d)

$$S_1 = \{5\}\ ,\ B_1 = 1\ ,\quad D_1 = 5$$

$$S_2 = \{2,2\},\ B_2 = 2\ ,\quad D_2 = 4$$

$$S_3 = \{5\}\ ,\ B_3 = 1\ ,\quad D_3 = 5$$

Table 3.1 portrays the progression of filtering and decimation for 3 stages, whereas Fig. 3.5 depicts electrical signals obtained from human colon before and after filtering and decimation.

3.3 Discussion

An optimal processor for multistage digital filtering and decimation, its algorithmic implementation, upper bounds on the decimation ratio per stage and the overall decimation ratio along with a lower bound on the number of stages have been presented. The use of filtering for decimation and decimation for filtering allowed for flexibility in using the proposed processor. Multistage decimation and filtering can be used to reduce the number of samples that contain a "cleaned up" version of the "sought after" information and it allows the use of the same set of filter coefficients to produce different cut-off frequencies [as can be seen from equations (3.2a)-(3.2c) and (3.4a)-(3.4c)].

Generally, to meet any decimation requirement, where a linear phase constraint is not too critical, the feasibility of the requirement should be checked by ensuring that inequality (3.7b) holds. The parameters governing the passband upper frequency and the transition band of the lowpass IIR filter can be chosen by solving a weighted-constrained

Table 3.1

Progression of Filtering and

Decimation for 3 Stages

i	D_i	f_{si} in Hz	f_{pi} in Hz	Δ_i in Hz	f_{ci} in Hz	N_S
1	5	20	4.5	1	5.5	2048
2	4	5	0.9	0.2	1.1	512
3	5	1	0.225	0.05	0.275	102

where N_S is the number of samples per input sequence

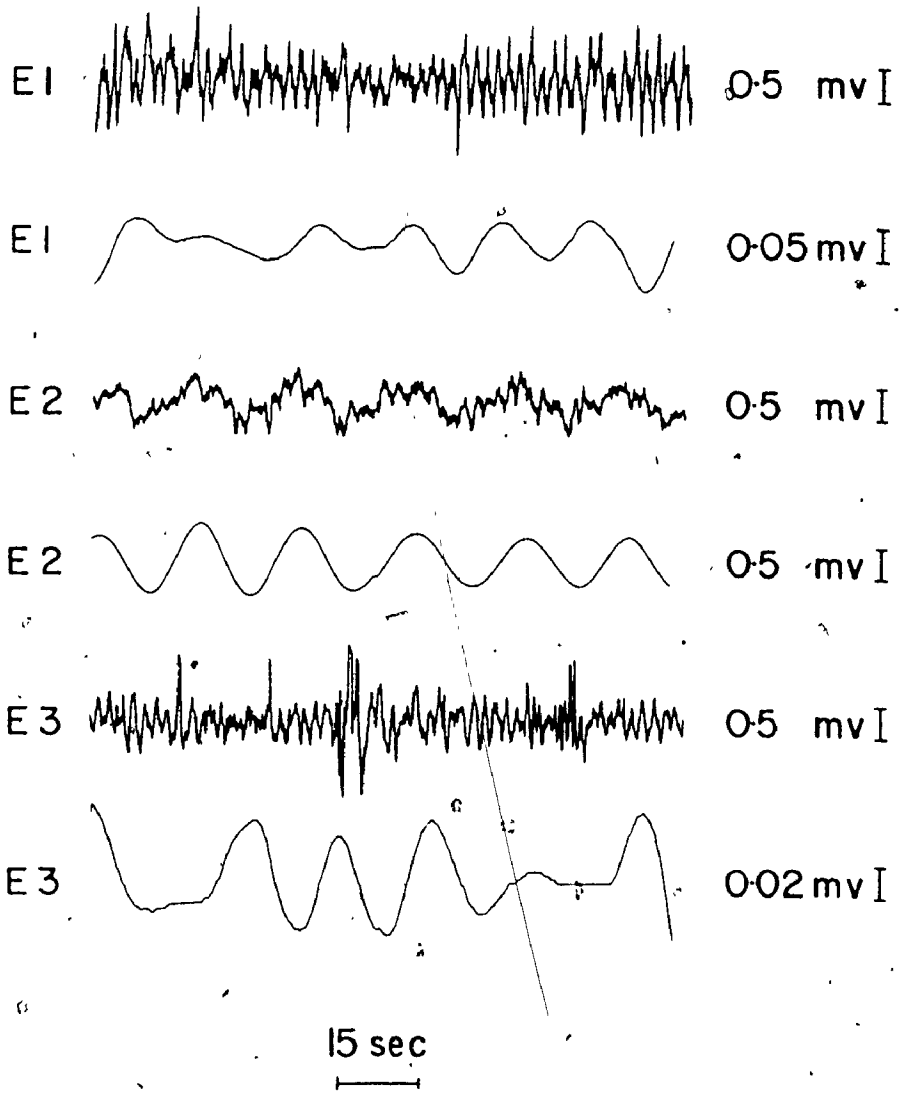

Fig. 3.5 Electrical activity recorded from 3 sets of bipolar electrodes E1, E2 and E3 placed subserosally on hte taenia coli of ascending colon. For each electrode, the activity before and after filtering and decimation is shown in the top and bottom traces, respectively.

minimax problem specified by (3.10c), (3.9d), (3.10d) and (3.10e). Then the coefficients of the low-pass IIR filter are chosen, for specified ripple and attenuation characteristics, either by conventional frequency domain design techniques for elliptic IIR digital filters or by using an optimization strategy such as that described in Chapter 2 where the approximation problem is solved in the z-domain directly. The number of stages and the decimation ratios are then determined from (3.11a) - (3.11e). To implement the multiple-input IIR multistage decimating filter, the filter coefficients that are unity are excluded from the filter coefficient set, and the delay operation required for filtering is achieved by array shifting, to reduce storage requirements.

CHAPTER 4

INTERACTIVE PROCESSORS FOR ANALYSIS AND MODELLING OF BIOLOGICAL RHYTHMS

4.1 Introduction

Interactive analysis and modelling of rhythmic biological signals may be used to elucidate the nature of their rhythmicity and their effects on the functions of organs or systems originating them. Linkens and Cannell (1974b) described an interactive graphical analysis of gastrointestinal electrical signals where the correlation option used was a mean-lagged products algorithm (taking about 1 sec/point) and the digital filtering option was fulfilled by superimposing ideal passbands on the amplitude-squared FFT display, hence, their digital filtering option exhibits the same averaging effects implicit in a FFT procedure. Schüssler and Winkelnkemper (1970) suggested an approach to implementation of a tuneable low-pass or high-pass digital filter in which the cutoff frequency could be controlled through a single parameter. In their approach, which is an implementation of the frequency transformation of digital filters as outlined by Constantinides (1967, 1968), each of the delay elements in a prototype low-pass digital filter is replaced by a first order all-pass network. As the parameter of the all-pass network is varied, the filter cutoff frequency is varied. For a prototype low-pass IIR digital filter, the tuneable low-pass or high-pass filter will contain delay-free feedback loops which are not

digitally realizable, whereas for a prototype low-pass FIR digital filter such delay-free feed-back loops in the tuneable filter will be avoided but the tuneable filter will have an infinite impulse response (since the all-pass networks have infinite impulse responses), hence, a possible linear phase property of the prototype FIR filter will not be preserved in the tuneable IIR filter. Oppenheim, Mecklenbräuker and Mersereau (1976) described an approach to implementation of a tuneable FIR digital filter whose cutoff frequency is controlled through a small number of parameters. In this chapter, two approaches to the implementation of a tuneable low-pass or high-pass IIR digital filtering stage whose cut-off frequency is varied through transforming all the coefficients of a prototype low-pass analog or IIR digital filter, are described.

This chapter presents an interactive processor of continuous-time rhythmic signals using IIR digital filters for multistage decimation (as described in Chapter 3) and tuneable multistage low-pass and/or high-pass (hence bandpass) filtering, also a Fast Fourier Transform algorithm for computation of power spectra and for "high speed" correlation along with a spectral digital filter for spectral smoothing. A mathematical formulation of the processor is presented along with a modular structure suitable for implementation on a digital computer. A modular interactive approach to programming is used to allow an easy "tailoring" of the processor to meet a particular need. It is to be noted that as far as the user is concerned, the "tailoring" of the processor consists of a "dialogue" with the digital computer where the user responds with yes, no or a numeral. Also, narrow bandpass filtering can be used to investigate the phase relationships between different frequency components of two or more signals. This type of processing enables a numerical approach

to the spectral analysis of spontaneous rhythmicity which exists in, for example, smooth muscle cells (Golenhofen 1970, 1976; Basar and Eroglu 1976), rhythms in insect populations, cell populations, biochemical oscillators and oscillations in cultures of Fungi (Pavlidis 1973), whereas it is particularly useful in analyzing the gastrointestinal ECA (Sarna, Daniel and Kingma 1971, 1972; Bardakjian et al. 1976a; Prosser, Weems, and Connor 1976).

This chapter also presents an interactive processor for modelling of biological rhythms which enables an interactive investigation of the main features of the dynamic properties of coupled nonlinear biological oscillators (Bardakjian and Sarna 1977). The modelling processor is compatible with the analysis processor thus allowing a uniform analysis of both simulated and biological data. Since the interactive modelling processor is geared specifically towards biological rhythms, it provides some attractive features (such as stimulation by a user-specified regime) that are not readily available in the more general simulation languages [such as MIMIC, CSSL (Stephenson 1971) and CSMP (Speckhart and Green 1976)].

4.2 An Interactive Processor for Analysis of Biological Rhythms

A schematic representation of a multiple-input processor for the analysis of biological rhythms is shown in Fig. 4.1 where

$\underset{\sim}{\eta}(t)$ are M continuous-time input signals

$\underset{\sim}{\eta}(n\tau_o)$ are M discrete-time signals obtained by sampling $\underset{\sim}{\eta}(t)$ at τ_o intervals

$\hat{\underset{\sim}{\mu}}(n\tau_N)$ are M discrete-time decimated and low-pass filtered signals

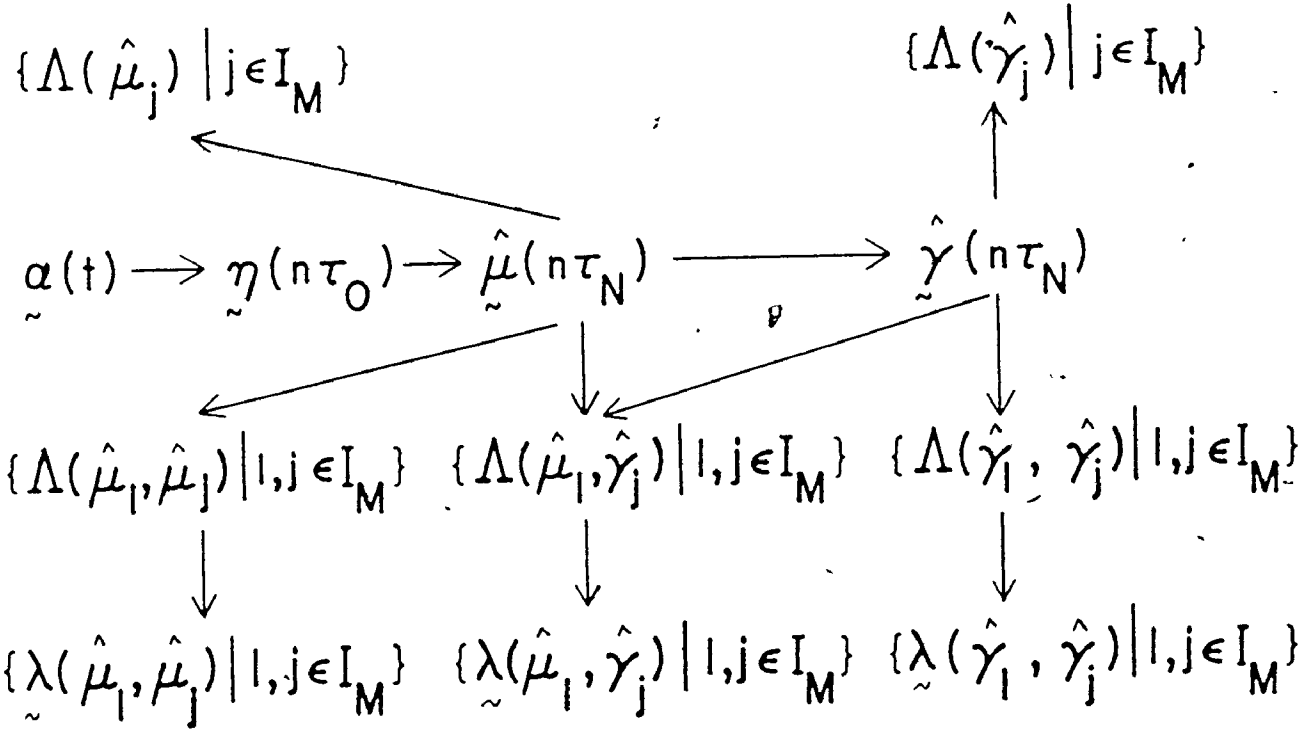

Fig. 4.1 A schematic representation of a multiple-input processor for the analysis of biological rhythms

$\hat{\gamma}(n\tau_N)$ are M discrete-time low-pass and/or high-pass filtered signals

$\Lambda(\hat{\mu}_\ell, \hat{\mu}_j)$ denotes the cross spectrum of the discrete-time signals $\hat{\mu}_\ell(n\tau_N)$ and $\hat{\mu}_j(n\tau_N)$

$\underset{\sim}{\lambda}(\hat{\mu}_\ell, \hat{\mu}_j)$ $\triangleq \{\lambda_1(\hat{\mu}_\ell, \hat{\mu}_j), \lambda_2(\hat{\mu}_\ell, \hat{\mu}_j), \lambda_3(\mu_\ell, \mu_j)\}$

$\lambda_1(\hat{\mu}_\ell, \hat{\mu}_j)$ denotes the phase lag spectrum, in degrees, of the discrete-time signals $\hat{\mu}_\ell(n\tau_N)$ and $\hat{\mu}_j(n\tau_N)$

$\lambda_2(\hat{\mu}_\ell, \hat{\mu}_j)$ denotes the time delay spectrum, in seconds of the discrete time signals $\hat{\mu}_\ell(n\tau_N)$ and $\hat{\mu}_j(n\tau_N)$

$\lambda_3(\hat{\mu}_\ell, \hat{\mu}_j)$ denotes the cross correlation of the discrete-time signals $\hat{\mu}_\ell(n_N)$ and $\hat{\mu}_j(n_N)$

M is the multiplicity of the input

N is the number of decimation stages

V is the number of tuneable filtering stages

τ_o is the initial sampling period

τ_N is the final sampling period

I_M is an index set consisting of integers 1 to M.

4.2.1 Formulation of the Discrete-Time and Discrete-Frequency Processes

The discrete-time and discrete-frequency processes shown in Fig. 4.1 can be formulated in terms of difference equations and Discrete Fourier Transform pairs as follows

$$\mu_{ji}^{r}(n\tau_{i*}) = \mu_{ji}^{r-1}(n\tau_{i*}) + \sum_{k=1}^{2} c_{k+4r-4}\ \mu_{ji}^{r-1}(n\tau_{i*}-k\tau_{i*}) - \sum_{k=1}^{2} c_{k+4r-2}\ \mu_{ji}^{r}(n\tau_{i*} - k\tau_{i*}) \qquad (4.1a)$$

$$\mu^{o}_{ji}(n\tau_{i*}) = c_{4R+1}\,\mu^{R}_{ji*}(n\tau_{i*}) \tag{4.1b}$$

$$\mu^{R}_{jo}(n\tau_{o}) = \eta_{j}(n\tau_{o}) \tag{4.1c}$$

$$\hat{\mu}_{j}(n\tau_{N}) = \mu^{R}_{jN}(n\tau_{N}) \tag{4.1d}$$

$$\gamma^{q}_{jv}(n\tau_{N}) = \gamma^{q-1}_{jv}(n\tau_{N}) + \sum_{k=1}^{2} d_{k+4q-4,v}\,\gamma^{q-1}_{jv}(n\tau_{N} - k\tau_{N}) - \sum_{k=1}^{2} d_{k+4q-4,v}\,\gamma^{q}_{jv}(n\tau_{N} - k\tau_{N}) \tag{4.2a}$$

$$\gamma^{o}_{jv}(n\tau_{N}) = d_{4Q+1,v}\,\gamma^{Q}_{jv*}(n\tau_{N}) \tag{4.2b}$$

$$\gamma^{Q}_{jo}(n\tau_{N}) = \hat{\mu}_{j}(n\tau_{N}) \tag{4.2c}$$

$$\hat{\gamma}_{j}(n\tau_{N}) = \gamma^{Q}_{jV}(n\tau_{N}) \tag{4.2d}$$

$$F_{j}(m) = \begin{cases} \sum_{n=0}^{N_s-1} \omega_{o}(n\tau_{N})\,\hat{\mu}_{j}(n\tau_{N})\exp(-j\,\frac{2\pi mn}{N_s}), & 0 \le m \le N_s-1 \\ 0, & \text{otherwise} \end{cases} \tag{4.3a}$$

$$F_{j}(m) = \sum_{k=1}^{K_W} W_{k}\,[\,F_{j}(m+k-K_W+1) + F_{j}(m-k+K_W-1)\,], \qquad K_W \ge 1 \tag{4.3b}$$

$$\omega_{o}(n\tau_{N}) = \begin{cases} \omega_{1}(n\tau_{N}), & n=0,\ 1,\ \ldots\ldots,\ N_s - N_z - 1 \\ 0, & \text{otherwise} \end{cases} \tag{4.3c}$$

$$\Lambda(\hat{\mu}_j) \triangleq \{F_j(m)\}, \qquad 0 \le m \le N_s-1 \tag{4.3d}$$

$$F_{\ell j}(m) = \begin{cases} F_\ell(m)\ F_j(-m), & 0 \le m \le N_s-1 \\ 0, & \text{otherwise} \end{cases} \tag{4.4a}$$

$$\Lambda(\hat{\mu}_\ell, \hat{\mu}_j) \triangleq \{F_{\ell j}(m)\}, \qquad 0 \le m \le N_s-1 \tag{4.4b}$$

$$\lambda_1(\hat{\mu}_\ell, \hat{\mu}_j) \triangleq \{\frac{180}{\pi} \arctan\left[\frac{\text{Im } F_{\ell j}(m)}{\text{Re } F_{\ell j}(m)}\right]\}, \qquad 0 \le m \le N_s-1 \tag{4.4c}$$

$$\lambda_2(\hat{\mu}_\ell, \hat{\mu}_j) \triangleq \{\frac{N_s \tau_N}{2\pi m} \arctan\left[\frac{\text{Im } F_{\ell j}(m)}{\text{Re } F_j(m)}\right]\}, \qquad 0 \le m \le N_s-1 \tag{4.4d}$$

$$f_{\ell j}(n) = \begin{cases} \frac{\omega_2(n\tau_N)}{N_s} \sum_{m=0}^{N_s-1} F_{\ell j}(m) \exp\left(j \frac{2\pi mn}{N_s}\right), & 0 \le n \le N_s-1 \\ 0, & \text{otherwise} \end{cases} \tag{4.5a}$$

$$\lambda_3(\hat{\mu}_\ell, \hat{\mu}_j) \triangleq \{f_{\ell j}(n)\}, \qquad 0 \le n \le N_s-1 \tag{4.5b}$$

$i^* = i - 1$

$v^* = v - 1$

$i = 1, \ldots, N$

$j = 1, \ldots, M$

$\ell = 1, \ldots, M$

$v = 1, \ldots, V$

$r = 1, \ldots, R$

$q = 1, \ldots, Q$

where

R	is the number of second-order filter sections per decimation stage
Q	is the number of second-order filter sections per tuneable stage
K_W	is the number of coefficients of the spectral filter
N_s	is the number of points used in a Discrete Fourier Transformation
N_z	is the number of padding zeros
$\{c_k \mid k=1,\ldots,4R+1\}$	is the coefficient set for the multistage decimating IIR digital filter
$\{d_{k,v} \mid k=1,..,4Q+1$ and $v = 1,..,V\}$	is the coefficient set for the multistage tuneable IIR digital filter
$\{W_k \mid k=1,\ldots, K_W\}$	is the coefficient set for the spectral digital filter
ω_o	is a discrete-time window for providing a weighted finite-duration sequence that can be augmented by N_z padding zeros.
ω_1 , ω_2	are weighting sequences for data smoothing

and $\Lambda(\hat{\gamma}_j)$, $\Lambda(\hat{\gamma}_\ell, \hat{\gamma}_j)$, $\Lambda(\hat{\mu}_\ell, \hat{\gamma}_j)$, $\underset{\sim}{\lambda}(\hat{\mu}_\ell, \hat{\gamma}_j)$, $\underset{\sim}{\lambda}(\hat{\gamma}_\ell, \hat{\gamma}_j)$, are formulated in a similar manner to equations (4.3) - (4.5).

Spectral smoothing (Bruce 1968; Beauchamp 1973) represented by the spectral digital filter implementation (4.3b) is utilized to reduce the spectral sidelobe amplitudes resulting from using finite-

duration sequences in Discrete Fourier Transformations.

4.2.2 Tuneable IIR Digital Filters

Tuneability is achieved, in a software sense, through spectral transformations (Constantinides 1970) of a prototype low-pass IIR digital filter or, alternatively, by a bilinear z-transformation (Steiglitz 1965; Kaiser 1966; Gold and Rader 1969; Oppenheim and Schafer 1975), of a prewarped analog filter obtained by algebraic transformations (Guillemin 1957) of a prototype analog low-pass elliptic filter whose transfer function may be chosen from analog filter tables (Christian and Eisenmann 1966).

Let the transfer function of the vth stage of the tuneable IIR digital filter be

$$H_{tv}(Z) = d_{4Q+1,v} \prod_{k=1}^{Q} \frac{1 + d_{4k-3,v} Z^{-1} + d_{4k-2,v} Z^{-2}}{1 + d_{4k-1,v} Z^{-1} + d_{4k,v} Z^{-2}} \qquad (4.6)$$

also,

τ_N be the sampling period of the tuneable IIR digital filter

and

f_{pv} be the passband (upper or lower) frequency of the vth (low-pass or high-pass) stage of the tuneable IIR digital filter

where

$$v \in I_V \triangleq \{ i \mid i=1, \ldots, V\}$$

Method 1 : Spectral Transformations of a Prototype Low-Pass IIR Digital Filter

Let the transfer function of the prototype low-pass IIR digital filter be

$$H_p(z) = \hat{c}_{4Q+1} \prod_{k=1}^{Q} \frac{1 + \hat{c}_{4k-3} z^{-1} + \hat{c}_{4k-2} z^{-2}}{1 + \hat{c}_{4k-1} z^{-1} + \hat{c}_{4k} z^{-2}} \tag{4.7}$$

also,

f_{pp} be the passband upper frequency of the prototype low-pass IIR digital filter

and

$\{\hat{c}_k \mid k=1,..,4Q+1\}$ be the coefficient set of the prototype IIR digital filter

Case 1 : Low-Pass to Low-Pass Transformation

$H_{tv}(Z)$ is obtained from $H_p(z)$ via the transformation (Constantinides 1970)

$$H_{tv}(Z) = H_p(z)\Big|_{z^{-1} = \frac{Z^{-1} - \phi_v}{1 - \phi_v Z^{-1}}} \tag{4.8a}$$

where

$$\phi_v = \frac{\sin \pi\tau_N(f_{pp} - f_{pv})}{\sin \pi\tau_N(f_{pp} + f_{pv})} \tag{4.8b}$$

Also, substituting from (4.7) into (4.8a) and equating with (4.6), then

$$d_{4Q+1,v} = \hat{c}_{4Q+1} \prod_{k=1}^{Q} \frac{1+ \phi_v(\hat{c}_{4k-2}\ \phi_v - \hat{c}_{4k-3})}{1+ \phi_v(\hat{c}_{4k}\ \phi_v - \hat{c}_{4k-1})} \tag{4.8c}$$

$$d_{4k-3,v} = \frac{\phi_v(\hat{c}_{4k-3}\ \phi_v - 2 - 2\hat{c}_{4k-2}) + \hat{c}_{4k-3}}{1 + \phi_v(\hat{c}_{4k-2}\ \phi_v - \hat{c}_{4k-3})} \tag{4.8d}$$

$$d_{4k-2,v} = \frac{\phi_v(\phi_v - \hat{c}_{4k-3}) + \hat{c}_{4k-2}}{1 + \phi_v(\hat{c}_{4k-2}\ \phi_v - \hat{c}_{4k-3})} \tag{4.8e}$$

$$d_{4k-1,v} = \frac{\phi_v(\hat{c}_{4k-1}\ \phi_v - 2\ \hat{c}_{4k} - 2) + \hat{c}_{4k-1}}{1 + \phi_v(\hat{c}_{4k}\ \phi_v - \hat{c}_{4k-1})} \tag{4.8f}$$

$$d_{4k,v} = \frac{\phi_v(\phi_v - \hat{c}_{4k-1}) + \hat{c}_{4k}}{1 + \phi_v(\hat{c}_{4k}\ \phi_v - \hat{c}_{4k-1})} \tag{4.8g}$$

$k = 1, \ldots, Q$ and $v \in I_v$

Case 2 : Low-Pass to High-Pass Transformation

$H_{tv}(Z)$ is obtained from $H_p(z)$ via the transformation (Constantinides 1970)

$$H_{tv}(Z) = H_p(z)\Big|_{z^{-1}} = -\frac{Z^{-1} + \phi_v}{1 + \phi_v Z^{-1}} \tag{4.9a}$$

where

$$\phi_v = -\frac{\cos\pi\tau_N(f_{pp} - f_{pv})}{\cos\pi\tau_N(f_{pp} + f_{pv})} \tag{4.9b}$$

Also, substituting from (4.7) into (4.9a) and equating with (4.6), then

$$d_{4Q+1,v} = \hat{c}_{4Q+1} \prod_{k=1}^{Q} \frac{1 + \phi_v(\hat{c}_{4k-2}\,\phi_v - \hat{c}_{4k-3})}{1 + \phi_v(\hat{c}_{4k}\,\phi_v - \hat{c}_{4k-1})} \tag{4.9c}$$

$$d_{4k-3,v} = \frac{\phi_v(2 + 2\,\hat{c}_{4k-2} - \hat{c}_{4k-3}\,\phi_v) - \hat{c}_{4k-3}}{1 + \phi_v(\hat{c}_{4k-2}\,\phi_v - \hat{c}_{4k-3})} \tag{4.9d}$$

$$d_{4k-2,v} = \frac{\phi_v(\phi_v - \hat{c}_{4k-3}) + \hat{c}_{4k-2}}{1 + \phi_v(\hat{c}_{4k-2}\,\phi_v - \hat{c}_{4k-3})} \tag{4.9e}$$

$$d_{4k-1,v} = \frac{\phi_v(2 + 2\hat{c}_{4k} - \hat{c}_{4k-1}\,\phi_v) - \hat{c}_{4k-1}}{1 + \phi_v(\hat{c}_{4k}\phi_v - \hat{c}_{4k-1})} \tag{4.9f}$$

$$d_{4k,v} = \frac{\phi_v(\phi_v - \hat{c}_{4k-1}) + \hat{c}_{4k}}{1 + \phi_v(\hat{c}_{4k}\,\phi_v - \hat{c}_{4k-1})} \tag{4.9g}$$

$k = 1, \ldots, Q$ and $v \in I_v$

Method 2 : Algebraic Transformations of A Prototype Analog Low-Pass Elliptic Filter In Conjuction With The Bilinear Z-Transformation

Let the transfer function of the prototype analog low-pass elliptic filter, whose upper passband angular frequency ω^a_{pp} is unity, be

$$H^a_p(s) = g_{3K+1} \prod_{k=1}^{Q} \frac{s^2 + g_{3k-2}}{s^2 + g_{3k-1}s + g_{3k}} \tag{4.10a}$$

also

$H^{a}_{tv}(S)$ be the transfer function of the tuneable analog filter

and

$\{ g_k \mid k=1,\ldots, 3Q+1 \}$ be the coefficient set of the prototype analog filter whereas $H_{tv}(Z)$ is obtained from $H^{a}_{tv}(S)$ via the bilinear z-transformation (Steiglitz 1965; Kaiser 1966; Gold and Rader 1969; Oppenheim and Schafer 1975)

$$H_{tv}(Z) = H^{a}_{tv}(S)\Big|_{S = \frac{2}{\tau_N}\left(\frac{1-Z^{-1}}{1+Z^{-1}}\right)} \tag{4.10b}$$

and the prewarped analog passband (upper or lower) frequency is

$$f^{a}_{pv} = \frac{1}{\pi \tau_N} \tan\left(\pi \tau_N f_{pv}\right) \tag{4.10c}$$

Case 1 : Low-Pass to Low-Pass Transformation

$$H^{a}_{tv}(S) = H^{a}_{p}(s)\Big|_{s = \frac{S\tau_N}{\phi_v}} \tag{4.11a}$$

where

$$\phi_v = 2\pi f^{a}_{pv} \tau_N \tag{4.11b}$$

and substituting from (4.10c) into (4.11b) then,

$$\phi_v = 2 \tan(\pi \tau_N f_{pv}) \tag{4.11c}$$

Also, substituting from (4.11a) into (4.10b) and equating with (4.6) then,

$$d_{4Q+1,\, v} = g_{3Q+1} \prod_{k=1}^{Q} \frac{4 + g_{3k-2}\phi^2}{4 + 2g_{3k-1}\phi + g_{3k}\phi^2} \tag{4.11d}$$

$$d_{4k-3,\,v} = \frac{2\,g_{3k-2}\,\phi_v^2 - 8}{g_{3k-2}\,\phi_v^2 + 4} \tag{4.11e}$$

$$d_{4k-2,\,v} = 1 \tag{4.11f}$$

$$d_{4k-1,\,v} = \frac{2\,g_{3k}\,\phi_v^2 - 8}{g_{3k}\,\phi_v^2 + 2g_{3k-1}\phi_v + 4} \tag{4.11g}$$

$$d_{4k,\,v} = \frac{g_{3k}\,\phi_v^2 - 2g_{3k-1}\,\phi_v + 4}{g_{3k}\,\phi_v^2 + 2g_{3k-1}\phi_v + 4} \tag{4.11h}$$

$k=1, \ldots, Q$ and $v \in I_v$

Case 2 : Low-Pass to High-Pass Transformation

$H^a_{tv}(S)$ is obtained from $H^a_p(s)$ via the algebraic transformation (Guillemin 1957)

$$H^a_{tv}(S) = H^a_p(s)\Big|_{s = \frac{\phi_v}{S\tau_N}} \tag{4.12a}$$

where

$$\phi_v = 2\pi f^a_{pv} \tau_N \tag{4.12b}$$

and substituting from (4.10c) into (4.12b) then

$$\phi_v = 2 \tan (\pi \tau_N f_{pv}) \tag{4.12c}$$

Also, substituting from (4.12a) into (4.10b) and equating with (4.6), then,

$$d_{4Q+1} = g_{3Q+1} \prod_{k=1}^{Q} \frac{\phi_v^2 + 4g_{3k-2}}{\phi_v^2 + 2g_{3k-1}\phi_v + 4g_{3k}} \tag{4.12d}$$

$$d_{4k-3,v} = \frac{2\phi_v^2 - 8g_{3k-2}}{\phi_v^2 + 4g_{3k-2}} \tag{4.12e}$$

$$d_{4k-2,v} = 1 \tag{4.12f}$$

$$d_{4k-1,v} = \frac{2\phi_v^2 - 8g_{3k}}{\phi_v^2 + 2g_{3k-1}\phi_v + 4g_{3k}} \tag{4.12g}$$

$$d_{4k,v} = \frac{\phi_v^2 - 2g_{3k-1}\phi_v + 4g_{3k}}{\phi_v^2 + 2g_{3k-1}\phi_v + 4g_{3k}} \tag{4.12h}$$

$k = 1, \ldots, Q$ and $v \in I_v$

4.2.3 A Modular Structure for the Multichannel Analysis Processor

A modular structure is used for interactive computer-aided analysis of biological rhythms. Each module is an independent unit on its own but the structure of the data files is compatible for all modules, hence, an operating modular scheme can be "tailored" to meet a particular need. The modules are controlled by controlling data files which are generated by an interactive dialogue between the user and the computer. Fig. 4.2 depicts charting symbols, whereas, Fig. 4.3 depicts a modular structure of the generator (GMPC) of multichannel processor's controlling

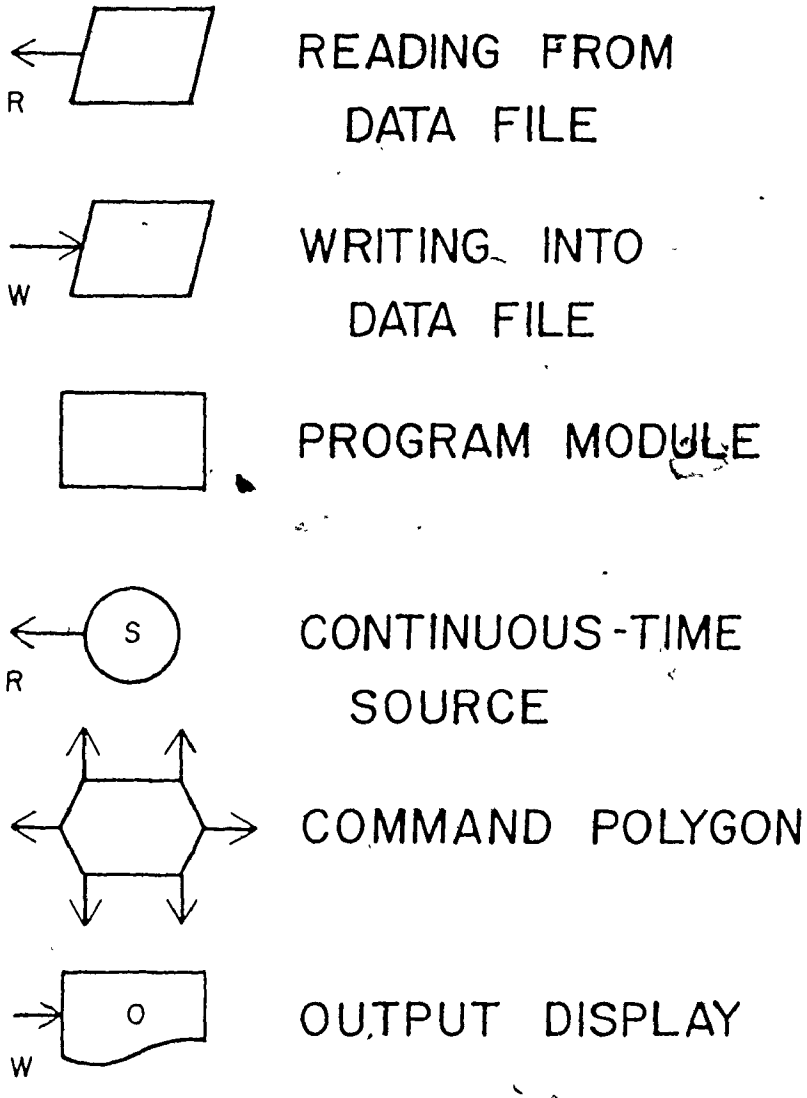

Fig. 4.2 Charting symbols for analysis processor

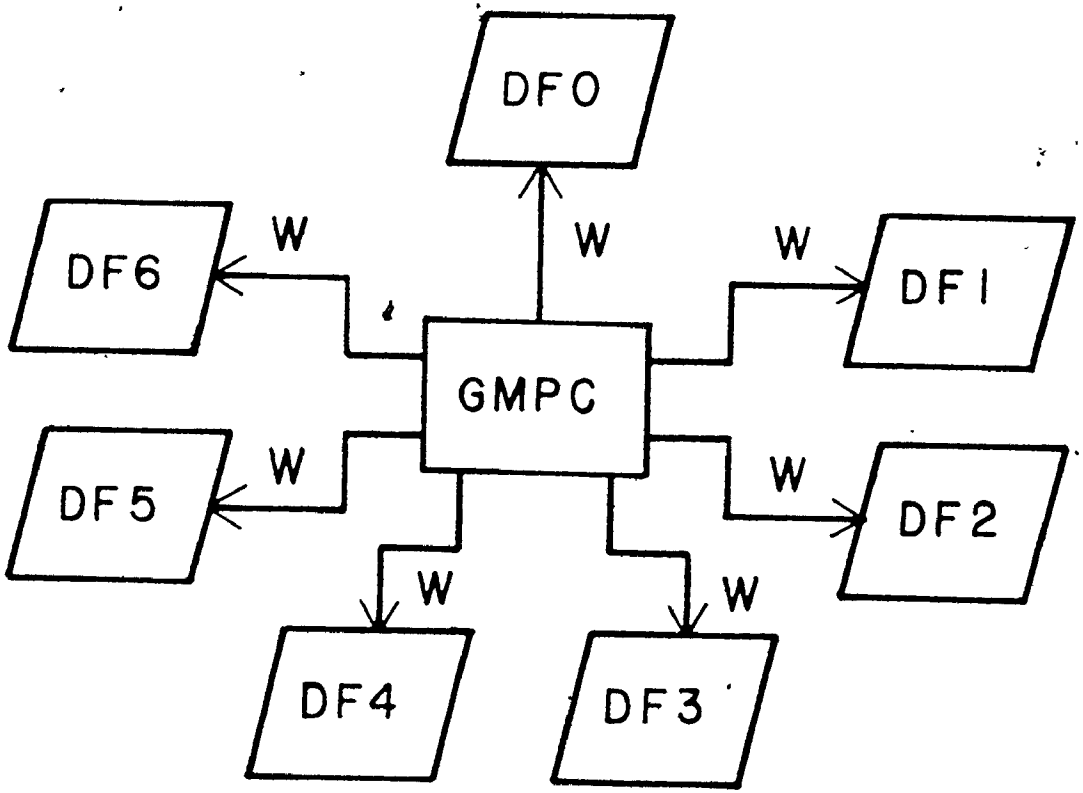

Fig. 4.3 A schematic representation of a modular structure of the Generator (GMPC) of Multichannel Processor's Controlling data files (DF0-DF6)

data files (DF0-DF6), and Fig. 4.4 depicts a modular structure of the command (EMP) to execute multichannel processing.

Module 1 is for analog to digital conversion, the input to this module is a multichannel analog source (e.g. a tape recorder) while the output is a data file (IDATA) comprising of integer numbers.

Module 2 is a module for multichannel multistage decimation and low-pass filtering to reduce the sampling rate of module 1, if necessary. A description of the theory and implementation of multi-channel multi-stage decimating IIR digital filters is given in Chapter 3. The input to this module is data file (IDATA) while the output is decimated and filtered data file (B1) comprising of real numbers.

Module 3 is a module for interfacing data file (IDATA) into data file (B1) compatible with the requirements of other modules, it is used if decimation is not required.

Module 4 is a module for multichannel multistage tuneable IIR digital filtering where each filtering stage can be chosen to be either of low-pass or high-pass type. For tuneablilty which is to be achieved using *Method 1*, the fourth-order low-pass IIR digital filter of Example 2.1 (presented in Chapter 2), having a passband ripple of 0.76 db, minimum stopband attenuation of 27.58 db and a transition bandwidth (normalized with respect to the passband upper frequency) of 0.22 was chosen as a prototype low-pass IIR digital filter. Whereas for tuneability which is to be achieved using *Method 2*, a prototype fourth-order analog low-pass elliptic filter (C 04 A 25 42) , having a passband ripple of 0.27 db, minimum stopband attenuation of 33.45 db and a transition bandwidth (normalized with respect to the passband upper

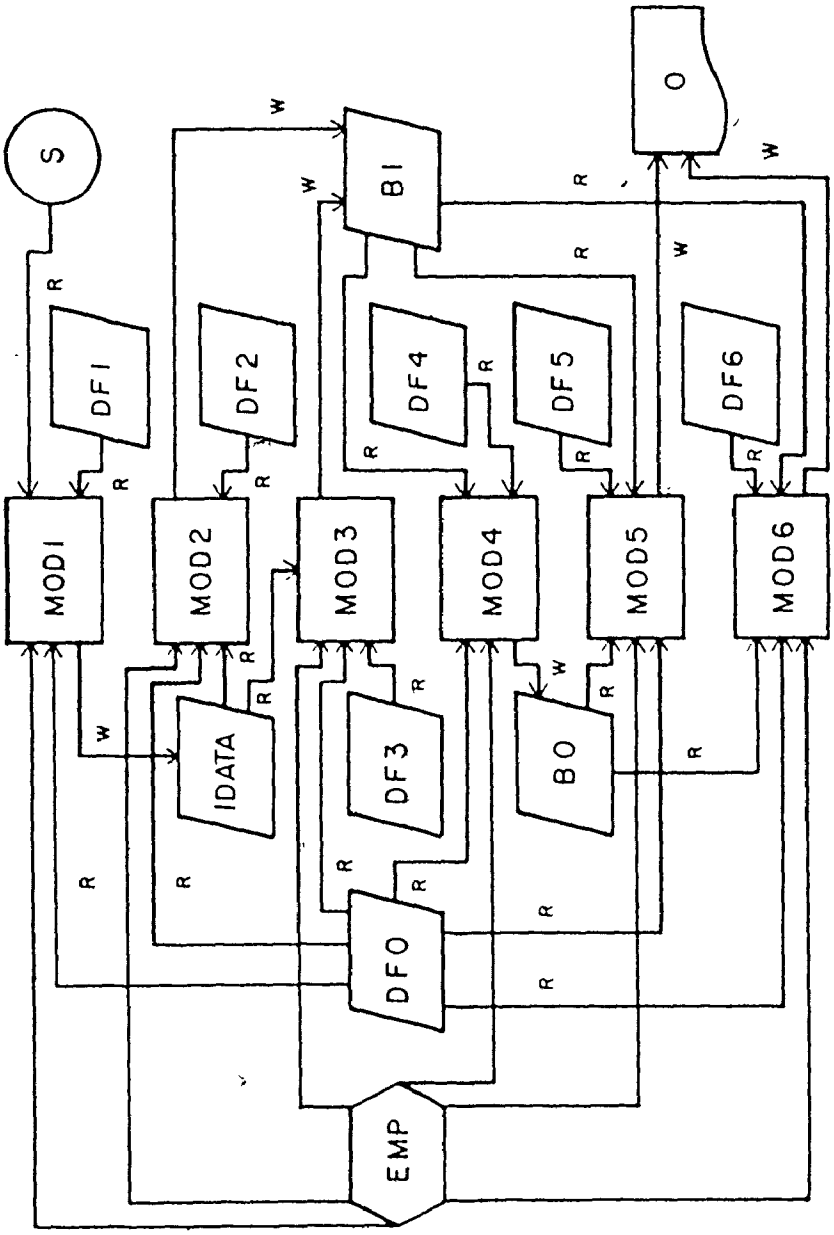

Fig. 4.4 A schematic representation of a modular structure of the command (EMP) to Execute Multichannel Processing

frequency) of 0.49448, was chosen from analog filter tables (Christian and Eisenmann 1966) wherein the filter parameters were tabulated as $\{\hat{g}_k \mid k=1, \ldots 7\}$ which are related to the filter coefficient set $\{g_k \mid k = 1, \ldots\ldots, 7\}$ as follows:

$$g_7 = \frac{1}{(1 + \hat{g}_7^2)^{1/2}}$$

$$g_{3k-2} = \hat{g}_{3k-2}^2$$

$$g_{3k-1} = 2\,\hat{g}_{3k-1}$$

$$g_{3k} = \hat{g}_{3k-1}^2 + \hat{g}_{3k}^2$$

$$k = 1, 2 \text{ where}$$

$$\{\hat{g}_k \mid k = 1, \ldots\ldots, 7\} = \{1.5862005153,\ 0.1449516451,$$
$$1.0495148487,\ 3.4616283819,$$
$$0.5430445193,\ 0.5427411948,$$
$$47.049128\ \}$$

The input to this module is data file (B1) and the output is filtered data file (B0) comprising of real numbers. This module can be used for narrow band-pass filtering of multichannel signals to investigate their phase lag variations with time (Bardakjian et al. 1976a).

Module 5 is a module for multichannel multisegment frequency analysis using a sequential application of a Decimation-in-Time Fast Fourier Transform algorithm for in place computations of periodograms (Cooley and Tukey 1965; Steiglitz 1974; Chapter 6 of Oppenheim and Schafer 1975; Rabiner and Gold 1975). A spectral filter [whose corresponding discrete-time window resembles a Hamming window (Oppenheim and Schafer 1975)]described by Bruce (1968), where $K_W = 2$ and

$\{W_1, W_2\} = \{0.25, -0.25\}$ may be used for spectrum smoothing. The input to this module is data file (B1) and/or data file (B0), this enables the computation of the frequency spectra of chosen segments from different channels of both processed data files, while the output is directed to an output device such as a line printer, or a CRT screen where the frequency spectra are displayed in a graphical and (if desired) numeric form.

Module 6 is a module for multichannel multisegment correlations using a sequential application of a Fast Fourier Transform algorithm making use of the properties of the Discrete Fourier Transforms of real signals (Chapter 3 of Oppenheim and Schafer 1975;Rabiner and Gold 1975) to, efficiently, compute cross spectra and correlations of corresponding data segments from different channels or different data segments from a particular channel or different data segments from different channels. Auto spectra and correlations can, also, be computed. The input to this module is data file (B1) and/or data file (B0), and the output is directed to an output device such as a line printer, or CRT screen where the cross spectra and cross correlation functions are displayed in a graphical and (if desired) numeric form. A Fortran listing of the analysis processor is given elsewhere (Bardakjian 1978).

4.2.4 Control of the Multichannel Analysis Processor

The multichannel processor is controlled by seven controlling data files as shown in Figures 4.3 and 4.4. DF0 is an initialization file determining whether or not a particular module is to be summoned, it contains the initialization flags. DF1 is a controlling data file for module 1, it contains the number of input channels, the sampling

frequency, the decimation factor of the system clock and the duration of the continuous-time data to be digitized (per channel). DF2 is a controlling data file for module 2, it contains the analog-to-digital conversion gain, the number of input channels, the number of decimation stages and the decimation ratios. DF3 is a controlling data file for module 3, it contains the number of input channels. DF4 is a controlling data file for module 4, it contains the number of input channels, the number of channels to be filtered, the number of filtering stages, the sampling frequency, the channel numbers that are to be filtered, flags indicating whether a filtering stage is of the low-pass or high-pass type and the cut-off frequencies of the filtering stages. DF5 is a controlling data file for module 5, it contains the number of input channels, the number of filtered channels, the number of samples per FFT analysis, the number of input samples per FFT analysis (to allow for zero padding), the number of filtered channels to be analyzed, a flag for removal of d.c. components, a flag for a time-window, a flag for a spectral filter, the sampling frequency, a parameter describing a spectral filter, the maximum data segment number, the number of channels to be analyzed, the channel numbers to be analyzed, the number of spectrum points to be plotted for each analyzed channel, flags to print the numerical values of the frequency spectrum for each analyzed channel, data segment numbers for each channel to be analyzed and flags to indicate whether each channel to be analyzed has been filtered by module 4 or not. DF6 is a controlling data file for module 6, it contains the number of input channels, the number of filtered channels, the number of input samples per segment, a flag for a time-window, a flag

for a spectral filter, the number of cross-spectrum points to be plotted for each analyzed pair, the number of time lags of the cross-correlation function to be plotted for each pair, flags to print the numerical values of the cross-spectrum and/or cross-correlation function for each analyzed pair, the sampling frequency, a parameter describing a spectral filter, the number of channel pairs to be correlated, the maximum data segment number for both scanning and scanned channels, the scanning channel numbers, the scanned channel numbers, number of data segments and segment numbers for both scanning and scanned channels, and flags to indicate whether each scanning and/or scanned channel has been filtered by module 4.

4.2.5 Examples

Example 4.1

Consider the analysis of human colonic Electrical Activity recorded from 4 sets of bipolar electrodes E1, E2, E3 and E4 placed subserosally on the descending and sigmoid colon. Fig. 4.5 depicts the signals obtained using a Beckman recorder with lower and upper cut-off frequencies set at 0.16 and 30 Hz respectively, where the top trace depicts the respiration signal. The simultaneous continuous-time signals were digitized using a 100 Hz sampling frequency.

The processing requirements are:

1. Reduce the sampling rate to 5 Hz and limit the band width to approximately 1 Hz.
2. Determine the frequency spectrum of each signal.
3. Determine the cross-spectrum and cross-correlation function of signal pairs (E1, E2), (E2, E3) and (E3, E4).

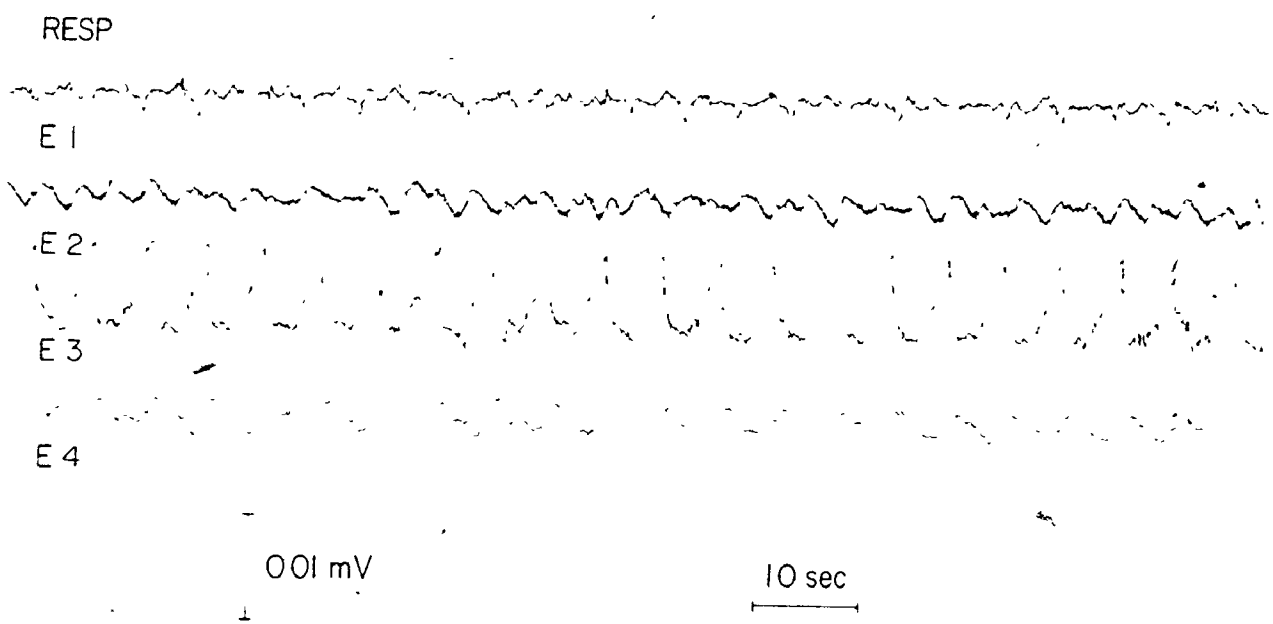

Fig. 4.5 Human Colonic Electrical Activity recorded from 4 sets of bipolar electrodes E1, E2, E3 and E4 placed subserosally on the taenia coli of descending (E1, E2) and sigmoid (E3, E4) colon. The top trace depicts the respiration signal.

The user-computer dialogue necessary to generate the controlling data files of the multichannel analysis processor is given in Fig. 4.6, the frequency spectrum of signal E_4 is shown in Fig. 4.7, while the cross-spectrum and cross-correlation function of signal pair (E2, E3) is given in Fig. 4.8.

Example 4.2

Consider the investigation of phase-relationships of the 3 cpm component of the human colonic Electrical Activity obtained from 3 sets of bipolar electrodes placed subserosally on the taenia coli of ascending colon (Bardakjian et al. 1976a) and recorded as described in Example 4.1. The processing requirements are:

1. Reduce the sampling rate to 5 Hz.
2. Perform narrow band-pass filtering from 2 to 4 cpm.

The user-computer dialogue necessary to generate the controlling data files of the multichannel analysis processor is given in Fig. 4.9, whereas the input continuous-time signals and the band-pass filtered signals are depicted in Fig. 4.10, wherein the signals are shown to be phase-unlocked.

4.3 An Interactive Processor for Modelling of Biological Rhythms

Populations of coupled nonlinear oscillators are used to model biological rhythms. Each oscillator can be stimulated by a user-specified stimulus at a user-specified time for a user-specified duration. The nonlinear differential equations prescribing a population of coupled oscillators are prescribed by the user.

```
GMPC
 ENTER NUMBER OF CHANNELS  5
 ENTER SAMPLING FREQUENCY  100
 ANALOG TO DIGITAL CONVERSION? YES
 ENTER SYSTEM CLOCK FREQUENCY  100
 ENTER DIGITIZATION TIME DURATION IN SEC  120
 DECIMATION? YES
 ENTER CONVERSION GAIN  1
 ENTER NUMBER OF DECIMATION STAGES  2
 ENTER DECIMATION RATIOS  5,4
 DIGITAL FILTERING? NO
 COMPUTATION OF FREQUENCY SPECTRA? YES
 ENTER NUMBER OF INPUT SAMPLES PER SEGMENT  300
 ENTER NUMBER OF PADDING ZEROS PER SEGMENT  724
 ENTER NUMBER OF TIME WINDOW  1
 ENTER NUMBER OF SPECTRUM WINDOW  2
 REMOVE DC COMPONENT? YES
 ENTER NUMBER OF CHANNELS TO BE ANALYZED  5
 ENTER CHANNEL NUMBER(S)  1,2,3,4,5
 FOR CHANNEL        1
 ENTER NUMBER OF SEGMENTS  1
 ENTER SEGMENT NUMBER(S)  1
 ENTER NUMBER OF SPECTRUM POINTS TO BE PLOTTED  120
 POWER SPECTRUM PRINTING? NO
 FOR CHANNEL        2
 ENTER NUMBER OF SEGMENTS  1
 ENTER SEGMENT NUMBER(S)  1
 ENTER NUMBER OF SPECTRUM POINTS TO BE PLOTTED  120
 POWER SPECTRUM PRINTING? NO
 FOR CHANNEL        3
 ENTER NUMBER OF SEGMENTS  1
 ENTER SEGMENT NUMBER(S)  1
 ENTER NUMBER OF SPECTRUM POINTS TO BE PLOTTED  120
 POWER SPECTRUM PRINTING? NO
 FOR CHANNEL        4
 ENTER NUMBER OF SEGMENTS  1
 ENTER SEGMENT NUMBER(S)  1
 ENTER NUMBER OF SPECTRUM POINTS TO BE PLOTTED  120
 POWER SPECTRUM PRINTING? NO
 FOR CHANNEL        5
 ENTER NUMBER OF SEGMENTS  1
 ENTER SEGMENT NUMBER(S)  1
 ENTER NUMBER OF SPECTRUM POINTS TO BE PLOTTED  120
 POWER SPECTRUM PRINTING? NO
 COMPUTATION OF CROSS-CORRELATIONS? YES
 ENTER NUMBER OF CHANNEL PAIRS TO BE CORRELATED  3
 ENTER SCANNING CHANNEL NUMBER(S)  1,2,3
 ENTER SCANNED CHANNEL NUMBER(S)  2,3,4
 ENTER NUMBER OF INPUT SAMPLES PER SEGMENT  300
 FOR SCANNING CHANNEL        1
 ENTER NUMBER OF SEGMENTS  1
 ENTER SEGMENT NUMBER(S)  1
 FOR SCANNED CHANNEL        2
 ENTER NUMBER OF SEGMENTS  1
 ENTER SEGMENT NUMBER(S)  1
 FOR SCANNING CHANNEL        2
 ENTER NUMBER OF SEGMENTS  1
 ENTER SEGMENT NUMBER(S)  1
 FOR SCANNED CHANNEL        3
 ENTER NUMBER OF SEGMENTS  1
 ENTER SEGMENT NUMBER(S)  1
 FOR SCANNING CHANNEL        3
 ENTER NUMBER OF SEGMENTS  1
 ENTER SEGMENT NUMBER(S)  1
 FOR SCANNED CHANNEL        4
 ENTER NUMBER OF SEGMENTS  1
 ENTER SEGMENT NUMBER(S)  1
 ENTER NUMBER OF FREQUENCY POINTS TO BE PLOTTED  120
 ENTER NUMBER OF TIME LAGS TO BE PLOTTED  60
 CROSS SPECTRUM PRINTING? NO
 CROSS-CORRELATION PRINTING? NO
STOP
```

Fig. 4.6 User-Computer dialogue for Example 4.1

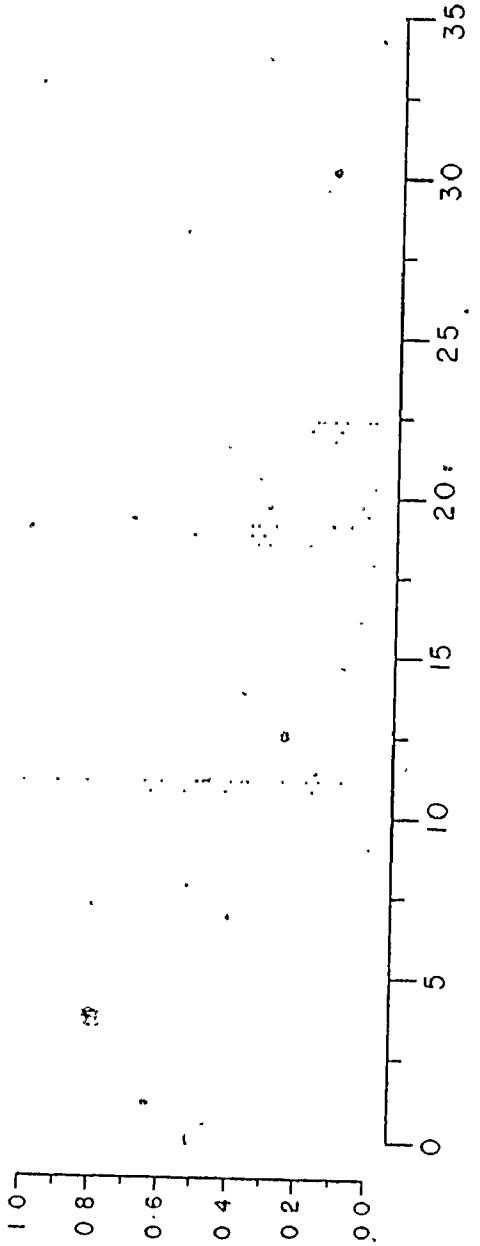

Fig. 4.7 The frequency spectrum of the signal recorded from E4 and computed with a frequency resolution of 0.293 cpm

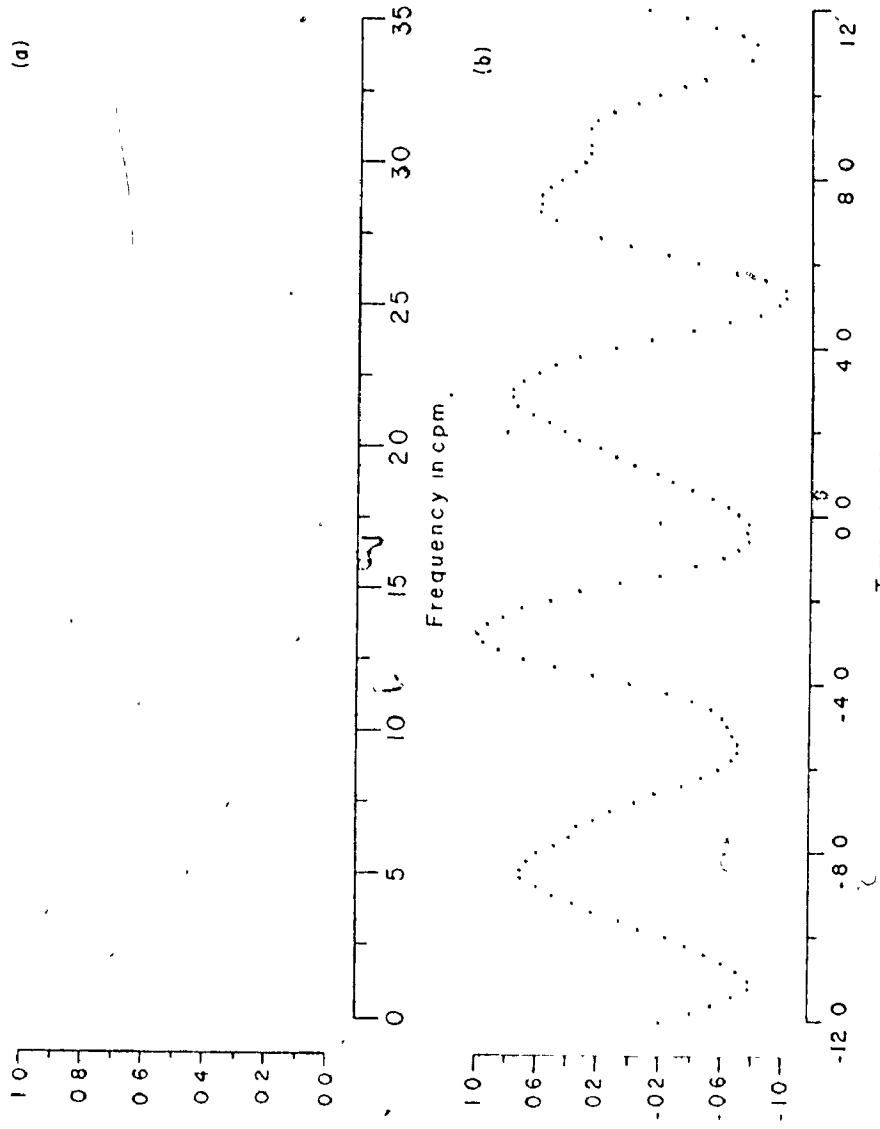

Fig. 4.8 (a) The cross-spectrum of signal pair recorded from E2 and E3 and computed with a frequency resolution of 0.293 cpm

(b) The cross-correlation function of signal pair recorded from E2 and E3 and computed with a time resolution of 0.2 sec

```
GMPC
 ENTER NUMBER OF CHANNELS  4
 ENTER SAMPLING FREQUENCY  100
 ANALOG TO DIGITAL CONVERSION? YES
 ENTER SYSTEM CLOCK FREQUENCY  100
 ENTER DIGITIZATION TIME DURATION IN SEC  600
 DECIMATION? YES
 ENTER CONVERSION GAIN  1
 ENTER NUMBER OF DECIMATION STAGES:  2
 ENTER DECIMATION RATIOS  5,4
 DIGITAL FILTERING? YES
 ENTER TUNEABILITY METHOD NUMBER  2
 ENTER NUMBER OF FILTERED CHANNELS  3
 ENTER CHANNEL NUMBER(S)  1,2,3
 ENTER NUMBER OF FILTERING STAGES  6
 FOR FILTERING STAGE        1
 ENTER 1 FOR LPF OR 2 FOR HPF  1
 ENTER PASS BAND EDGE FREQUENCY IN CPM  4
 FOR FILTERING STAGE        2
 ENTER 1 FOR LPF OR 2 FOR HPF  2
 ENTER PASS BAND EDGE FREQUENCY IN CPM  2
 FOR FILTERING STAGE        3
 ENTER 1 FOR LPF OR 2 FOR HPF  1
 ENTER PASS BAND EDGE FREQUENCY IN CPM  4
 FOR FILTERING STAGE        4
 ENTER 1 FOR LPF OR 2 FOR HPF  2
 ENTER PASS BAND EDGE FREQUENCY IN CPM  2
 FOR FILTERING STAGE        5
 ENTER 1 FOR LPF OR 2 FOR HPF  1
 ENTER PASS BAND EDGE FREQUENCY IN CPM  4
 FOR FILTERING STAGE        6
 ENTER 1 FOR LPF OR 2 FOR HPF  2
 ENTER PASS BAND EDGE FREQUENCY IN CPM  2
 COMPUTATION OF FREQUENCY SPECTRA? NO
 COMPUTATION OF CROSS-CORRELATIONS? NO
STOP
```

Fig. 4.9 User-Computer dialogue for Example 4.2

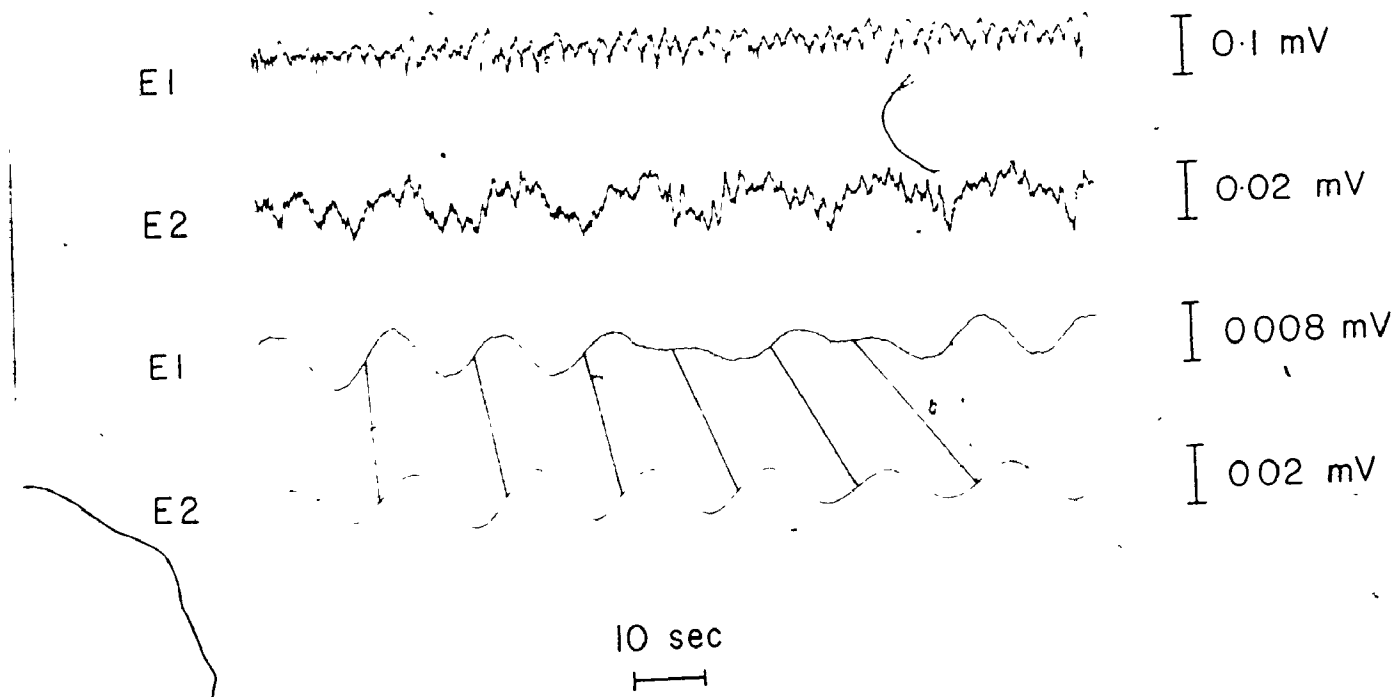

Fig. 4.10 Human Colonic Electrical Activity recorded from 2 (out of 3) sets of bipolar electrodes E1 and E2 placed subserosally on the taenia coli of ascending colon. The activity before (the two upper traces) and after (the two lower traces) band-pass filtering (2-4 cpm) is shown. Continuous lines join the zero crossings of waveforms.

4.3.1 A General Structure of the Modelling Processor

The modelling processor is compatible with the analysis processor in the sense that the output file (B1) of the former can be used as an input file to the latter, Fig. 4.12 depicts a general structure of the modelling processor.

The main program is a user-supplied program for dimensioning purposes and for summoning subroutine Rhythm which is a subroutine for organizing a user-computer dialogue that generates, or alternatively makes use of the information stored in previously generated, parameter files PF1, PF2, and PF3 containing the model parameters, stimulation parameters and initial conditions of simulation run, respectively. Rhythm also organizes the summoning of the other subroutines of the processor. Opus 1 is a subroutine for identifying the words Yes and No. Opus 2 is a subroutine for run-time printing or plotting of the computed time sequences (oscillator outputs) either on a line-printer or a CRT screen. Opus 3 is a subroutine for reading from or writing into the files PF1, PF2, and PF3. Opus 4 is a subroutine for the numerical solution of nonlinear ordinary simultaneous first-order differential equations using an automatic step change Merson differential equation solver (Christiansen 1970). Opus 5 is a user-supplied subroutine for prescribing the set of nonlinear ordinary simultaneous first-order differential equations characterizing a specific rhythm. Opus 6 is a subroutine for stimulating a user-specified oscillator by a user-specified stimulus (d.c., sinusoidal or rectangular) at a user-specified time for a user-specified duration. Opus 7 is a subroutine for listing the model parameters, stimulation parameters and initial conditions of simulation,

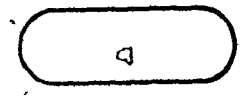

MAIN PROGRAM

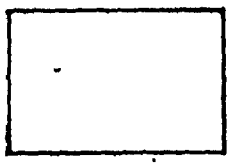

SUBROUTINE

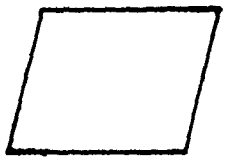

DATA FILE

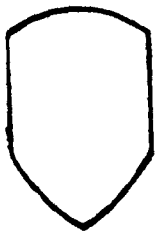

CRT SCREEN

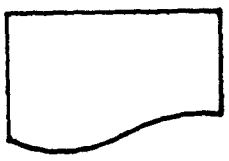

LINE PRINTER

Fig. 4.11 Charting symbols for modelling processor

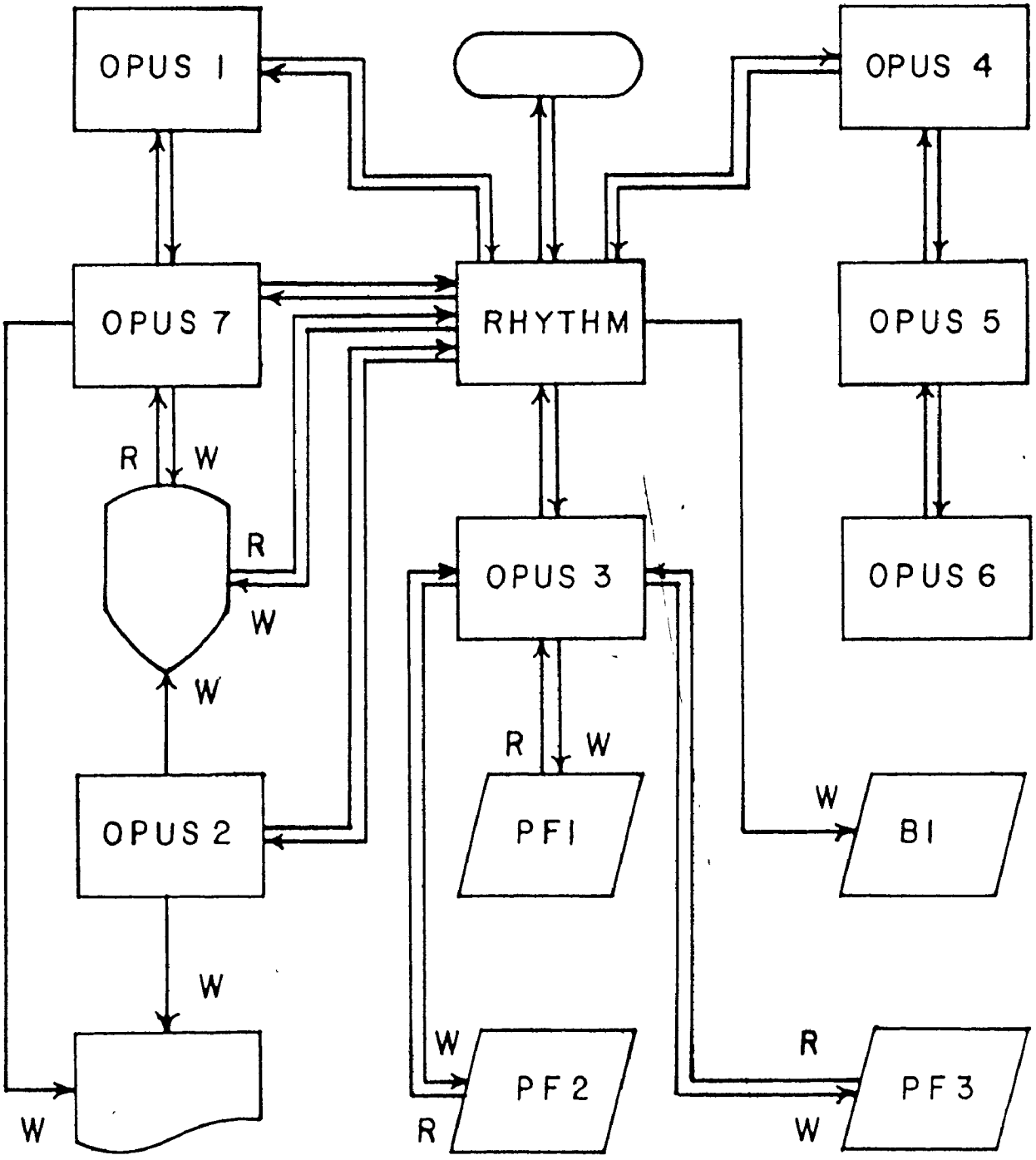

Fig. 4.12 A general structure of the modelling processor

on a line printer or a CRT screen. A Fortran listing of the modelling processor is given elsewhere (Bardakjian 1978).

4.3.2 Example 4.3

Consider the modelling of a rhythm by two bidirectionally-coupled generalized BVP oscillators prescribed by (Sarna, Daniel and Kingma 1972)

$$\dot{x}_i = p_j(p_{j+1}\, x_{i+1} + p_{j+2}\, x_i + p_{j+3}\, x_i^2 + p_{j+4}\, x_i^3 + p_{j+10} x_{i-2} + p_{j+11}\, x_{i+2})$$

$$\dot{x}_{i+1} = \frac{-1}{p_j}(p_{j+6}\, x_{i+1} + p_{j+7}\, x_i + p_{j+8}\, x_i^2 + p_{j+9} x_i^3 - p_{j+5})$$

where

$i = 1, 3$

$j = 1, 13$

and

$$\{ p_j \mid j=1,....24 \} = \{ 10, 1.344, 1, -0.644, -0.4636, -5, 0, 3.5, 0, 0, 0, 0.13, 10, 1.202, 1, -0.705, -0.5022, -5, 0, 3.5, 0, 0, 0.13, 0 \}$$

Apply a rectangular pulse of height 10 and width 5 sec to the first oscillator at the 48th second of simulated time.

A Fourier series expansion (truncated at the 20th harmonic component) of a rectangular wave where the period (100 sec) is larger than the stimulus duration (20 sec), is used to represent the stimulating pulse.

The user-supplied programs are depicted in Fig.4.13and the user-

computer dialogue is depicted in Fig. 4.14, whereas a listing of simulation parameters is depicted in Fig. 4.15 and the oscillator outputs are depicted in Fig. 4.16.

The cross spectra, phase lag spectra and time delay spectra of the outputs of the two oscillators were computed, via the analysis processor, for 6 consecutive time segments each of 20 sec duration (using $N_s = 256$ and $N_z = 236$). Their peak values are given in Table 4.1. It is to be noted that before the application of the stimulus, the two oscillators were synchronized at a frequency of 4.68 cpm, phase lag of 4.9° and time delay of 0.17 sec, whereas during the application of the stimulus their synchrony was lost (Table 4.1) and after the removal of the stimulus the two oscillator outputs gradually synchronized (Fig. 4.16) while their phase lag and time delay gradually returned to their values prior to the application of the stimulus.

4.4 Discussion

A multiple-input processor for the analysis of biological rhythms is described. The discrete-time and discrete-frequency analysis processes comprise decimation, tuneable IIR digital filtering, forward and inverse Discrete Fourier Transformation and Spectral digital filtering. Two methods for tuneable IIR digital filtering are described and a mathematical formulation of the analysis processor in terms of difference equations and Discrete Fourier Transform pairs along with a modular structure are given. The analysis processor is implemented as a modular user-oriented interactive computer program package that enables the tailoring of the processor through a user-computer dialogue

(a)

```
C
C       THIS IS A USER-SUPPLIED MAIN PROGRAM TO DIMENSION THE
C       ARRAYS "X","P","S","R","I1","I2" AND "I3"
C
        DIMENSION X(20),P(120),S(80),R(80),I1(10),I2(10),I3(12)
        CALL RHYTHM(X,P,S,R,I1,I2,I3)
        STOP
        END
```

(b)

```
C                    *********
C                    * OPUS5 *
C                    *********
C
C       THIS IS A USER-SUPPLIED SUBROUTINE TO DESCRIBE THE SET OF
C       FIRST ORDER SIMULTANEOUS DIFFERENTIAL EQUATIONS CHARACTERIZING
C       A SPECIFIC RHYTHM
C
        SUBROUTINE OPUS5(X,T,P,S,N,XDOT)
        DIMENSION X(1),XDOT(1),P(1),S(1)
        I2=1
        I3=1
        N1=N/2
        DO 4 I1=1,N1
        CALL OPUS6(I1,T,S,SA)
        X2=X(I2)*X(I2)
        X3=X2*X(I2)
        I4=I2-2
        IF(I4) 6,6,7
    6   I4=I1
    7   I5=I2+2
        IF(I5-N) 8,8,9
    9   I5=I1
    8   XDOT(I2)=P(I3)*(P(I3+1)*X(I2+1)+P(I3+2)*X(I2)+P(I3+3)*X2+P(I3+4)
   1    *X3+P(I3+10)*X(I4)+P(I3+11)*X(I5))+SA
        XDOT(I2+1)=-1 /P(I3)*(P(I3+6)*X(I2+1)+P(I3+7)*X(I2)+P(I3+8)*X2
   1    +P(I3+9)*X3-P(I3+5))
        I2=I2+2
    4   I3=I3+12
        RETURN
        END
```

Fig. 4.13 User-supplied programs
(a) Main program for dimensioning
(b) Subroutine Opus 5 for prescribing the population of oscillators

```
EX3
 ENTER NUMBER OF OSCILLATORS. 2
 ENTER NUMBER OF PARAMETERS PER OSCILLATOR: 12
 ENTER NUMBER OF STATE VARIABLES PER OSCILLATOR: 2
 USE SAVED STARTING CONDITIONS? NO
 ENTER INITIAL TIME ORIGIN  0
 ENTER INITIAL STEP SIZE OF INTEGRATION: 0.01
 ENTER SAMPLING PERIOD OF SOLUTION  1
 USE SAVED MODEL PARAMETERS? NO
 USE SAVED STIMULATION PARAMETERS? NO
 ENTER NUMBER OF SOLUTION SAMPLES. 120
 TERMINATE AFTER 120 SAMPLES? YES
 OUTPUT PLOTTING? YES
 HOW MANY OSCILLATORS TO BE MONITORED? 2
 ENTER NUMBER(S) OF OSCILLATORS  1,2
 ENTER MAXIMUM AMPLITUDE ESTIMATES  3 ,3
 ENTER MINIMUM AMPLITUDE ESTIMATES  -3 ,-3
 OUTPUT ON LINE PRINTER? YES
 ONLY OSCILLATOR OUTPUTS SAVED? YES
 MODEL PARAMETERS
 ENTER PARAMETERS OF OSCILLATOR 1
 10 ,1.344,1 ,-0 644,-0 4636,-5 ,0 ,3 5,0 ,0 ,0 ,0 13
 CHECK ENTERED PARAMETER VALUES? NO
 ENTER PARAMETERS OF OSCILLATOR 2
 10 ,1 202,1 ,-0 705,-0 5525,-5 ,0 ,3 5,0 ,0 ,0 13,0
 CHECK ENTERED PARAMETER VALUES? YES
 10 0000      1 2020      1 0000     -0 7050
 -0 5525     -5 0000      0 0000      3 5000
  0 0000      0 0000      0 1300      0 0000
 ANY CHANGES? YES
 HOW MANY PARAMETERS TO BE CHANGED? 1
 ENTER PARAMETER NUMBER(S)  5
 ENTER MODIFIED VALUE OF PARAMETER 5       -0 5022
 STIMULATION? YES
 HOW MANY OSCILLATORS TO BE STIMULATED? 1
 ENTER NUMBER(S) OF OSCILLATOR(S)  1
 FOR STIMULUS APPLIED TO OSCILLATOR 1
 ENTER TIME OF STIMULUS APPLICATION IN SEC  48.
 ENTER STIMULUS DURATION TIME IN SEC. 20
 DC STIMULUS? NO
 SINUSOIDAL STIMULUS? NO
 RECTANGULAR STIMULUS? YES
 ENTER STIMULUS AMPLITUDE. 10.
 ENTER STIMULUS PERIOD IN SEC  100.
 ENTER STIMULUS PULSE WIDTH IN SEC  5
 ENTER STIMULUS HARMONIC INDEX. 20
 LIST MODEL PARAMETERS? YES
 LIST STIMULATION PARAMETERS? YES
 LIST INITIAL CONDITIONS? YES
 LIST PARAMETERS OF ALL OSCILLATORS? YES
 PARAMETER LISTING ON LINE PRINTER? YES
 HOW MANY PARAMETERS LISTED PER LINE? 2
STOP
```

Fig. 4.14 User-computer dialogue for Example 4.3

```
NUMBER OF OSCILLATORS =   2
NUMBER OF PARAMETERS PER OSCILLATOR =  12
NUMBER OF STATE VARIABLES PER OSCILLATOR =  2
 SAMPLING PERIOD OF SOLUTION    1 000  SEC
INITIAL TIME =    0 000  SEC
INITIAL INTEGRATION STEP SIZE =  0 0100

PARAMETERS OF OSCILLATOR   1  ARE

MODEL PARAMETERS
      10 0000         1 3440
       1 0000         0 6440
       0 4536         5 0000
       0 0000         3 5000
       0 0000         0 0000
       0 0000         0 1300
STIMULATION PARAMETERS
      25 0000        48 0000
      68 0000        50 5000
      20 0000         0 5000
       0 0628         5 0000
INITIAL VALUES OF STATE VARIABLES
       1 0000         1 0000

PARAMETERS OF OSCILLATOR   2  ARE

MODEL PARAMETERS
      10 0000         1 2020
       1 0050         0 7050
       0 5022         5 0000
       0 0000         3 5000
       0 0000         0 0000
       0 1100         0.0000
STIMULATION PARAMETERS
       5 0000         0 0000
       0 0000         0 0000
       0 0000         0 0000
       0 0000         0 0000
INITIAL VALUES OF STATE VARIABLES
       1 0000         1 0000
```

Fig. 4.15 Listing of parameters. The stimulation parameters per oscillator consist of a flag to indicate presence and type of stimulus, application time in sec, removal time in sec, a time-shift factor equal to application time plus one half the pulse width, highest harmonic component in truncated fourier series, average value, angular frequency and pulse width, respectively.

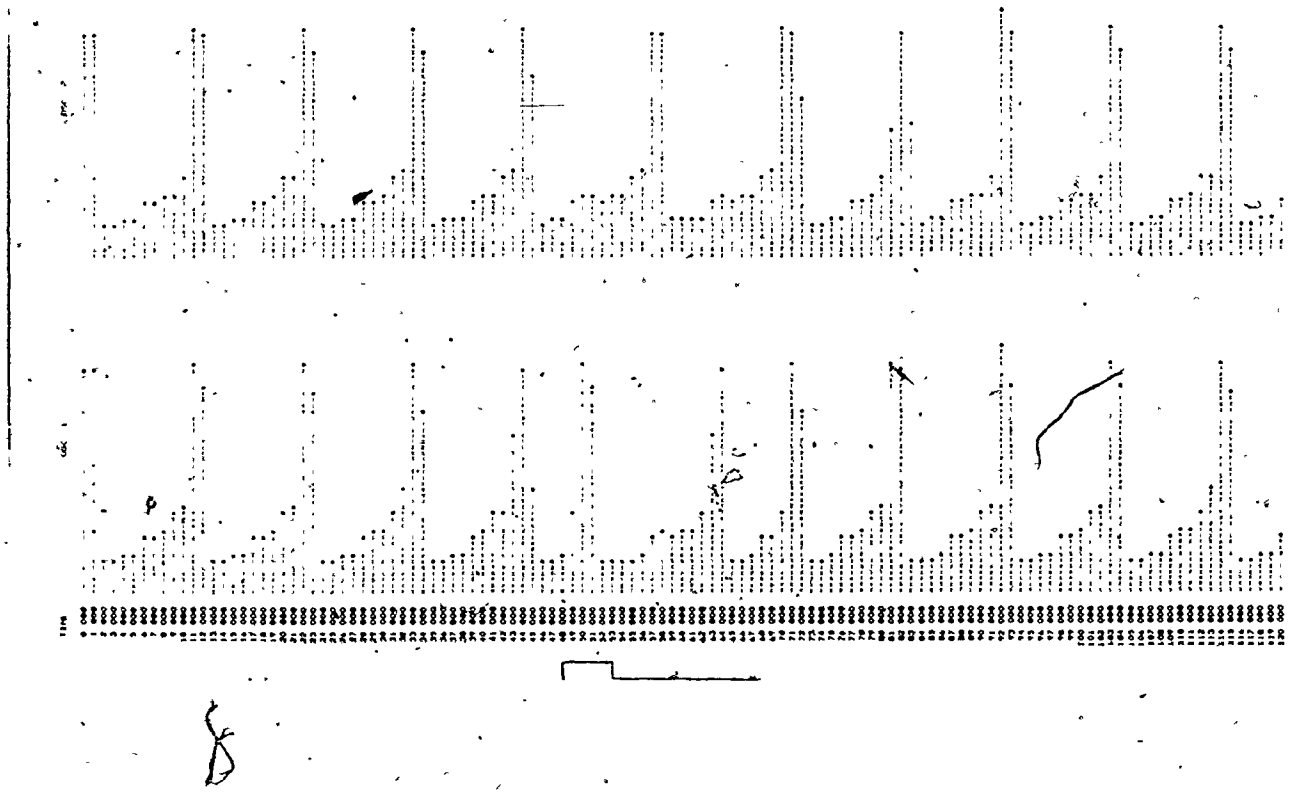

Fig. 4.16 Outputs of the two coupled oscillators of Example 4.3

TABLE 4.1

PEAK PHASE LAGS AND TIME DELAYS

FOR EXAMPLE 4.3

Time segment in sec		Peak common freq. in cpm	Intensity of peak common freq.	Phase-lag in degrees	Time delay in sec
Initial time	Final time				
0	20	4.68	0.36	4.944	0.176
20	40	4.68	0.49	4.971	0.177
40	60	3.28	0.13	-114.265	-5.804
60	80	4.68	0.16	- 55.977	-1.990
80	100	4.68	0.50	7.065	0.251
100	120	4.68	0.44	4.853	0.173

where the user responds with yes,no or a numeral. Narrow band-pass filtering enables investigation of spontaneous phase-relationships of different frequency components of analyzed signals. Two examples are given to illustrate the application of the analysis processor as a numerical approach to the spectral analysis of human colonic electrical activity.

Furthermore, an interactive processor for modelling of biological rhythms by populations of coupled nonlinear oscillators, where each oscillator can be selectively stimulated, is presented. The modelling processor enables an interactive investigation of the main features of the dynamic properties of a population of coupled nonlinear oscillators. The modelling and analysis processors are compatible in the sense that the output file of the former can be used as an input file to the latter. An example is given to illustrate the main features of the modelling processor and to elucidate the use of phase lag spectra and time delay spectra which can be computed via the analysis processor.

CHAPTER 5

MATHEMATICAL INVESTIGATION OF POPULATIONS OF COUPLED SROs

5.1 Introduction

Van der Pol (1927) described an analytical investigation of forced oscillations in a Van der Pol oscillator, thereafter, mathematical investigations of entrainment ans subharmonic entrainment of a Van der Pol oscillator by an external stimulus have been described (Haag 1962; Hayashi 1964; Sansone and Conti 1964; Butenin 1965; Andronov, Vitt and Khaikin 1966; Pavlidis 1973). Furthermore, populations of coupled Van der Pol oscillators have also been mathematically investigated (Minorsky 1962; Aggarwal and Richie 1966; Pavlidis 1973; Linkens 1974a, 1976a; Endo and Mori 1976, 1978).

Chua and Green (1972, 1974) described a method to synthesize the generic equation of a SRO having a prescribed periodic solution but they did not investigate a population of coupled SROs or external stimulation of a SRO. This chapter deals with the mathematical investigation of a population of coupled SROs in so far as its generic equation and synchronization are concerned. Also, entrainment and subharmonic entrainment of a SRO by an external stimulus are investigated.

5.2 The Generic Equation of a Population of Coupled SROs

In a population of coupled SROs containing N_p members, isolate

an nth oscillator from its neighbourhood and let its output (after isolation) be prescribed by

$$x_{1ni}(t) = a_{on} + b_{1n} \sin \omega_n t + \sum_{k=1}^{K_n} a_{kn} \cos k\omega_n t \qquad (5.1a)$$

where ω_n, b_{1n} and $\{ a_{kn} | \ k=0, 1, \ldots K_n \}$ are the intrinsic parameters of the nth oscillator. An alternative form of (5.1a) is

$$x_{1ni}(t) = a_{on} + b_{1n} \sin \omega_n t + \sum_{k=1}^{K_n} a_{kn} \ T_k(\cos \omega_n t) \qquad (5.1b)$$

where $T_k(.)$ is the kth Chebyshev polynomial of the first kind (Rivlin 1974).

To synthesize a generic equation for (5.1a) using a transformational synthesis approach (Chua and Green 1972, 1974; Bass 1975) which is summarized in Fig. 5.1, define the generic equation of an isolated fundamental nth oscillator to be prescribed by

$$\dot{u}_{1ni} = \omega_n [u_{2ni} + u_{1ni}(1 - u_{1ni}^2 - u_{2ni}^2)] \qquad (5.2a)$$

$$\dot{u}_{2ni} = \omega_n [-u_{1ni} + u_{2ni}(1 - u_{1ni}^2 - u_{2ni}^2)] \qquad (5.2b)$$

Excluding the point $u_{1ni} = u_{2ni} = 0$, (5.2a) and (5.2b) can be transformed via the polar coordinates

$$r_{ni}^2 = u_{1ni}^2 + u_{2ni}^2$$

$$\phi_{ni}^2 = \arctan \frac{u_{1ni}}{u_{2ni}}$$

and

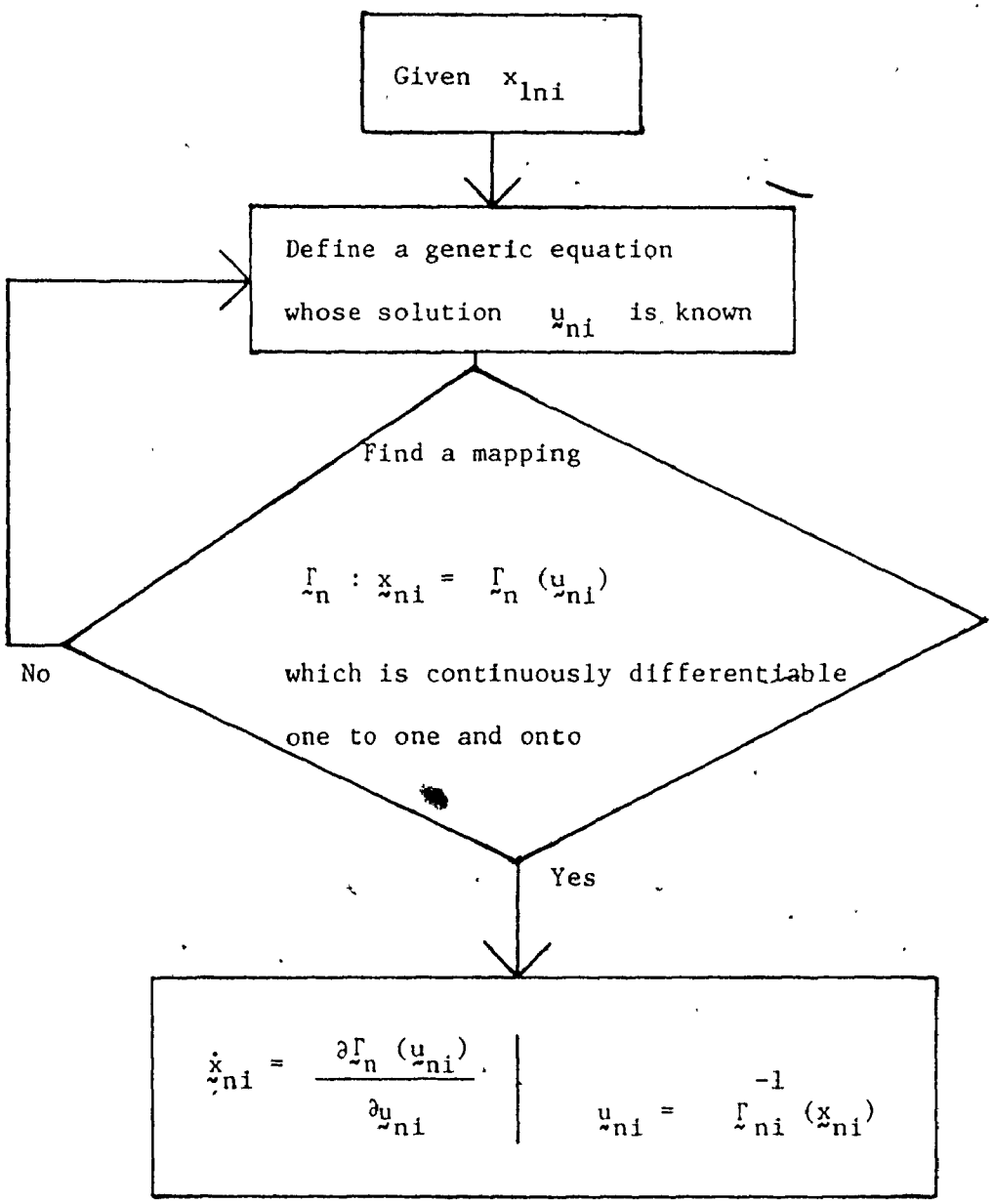

Fig. 5.1 A Transformational Synthesis Approach

$$\dot{r}_{ni} = \frac{1}{r_{ni}} \left(u_{1ni}\dot{u}_{1ni} + u_{2ni}\dot{u}_{2ni} \right)$$

into $$\dot{\phi}_{ni} = \frac{u_{2ni}\,\dot{u}_{1ni} - u_{1ni}\,\dot{u}_{2ni}}{u_{1ni}^2 + u_{2ni}^2}$$

into

$$\dot{r}_{ni} = \omega_n r_{ni} (1 - r_{ni}^2) \qquad (5.2c)$$

$$\dot{\phi}_{ni} = \omega_n \qquad (5.2d)$$

From (5.2c) it follows that

$$\dot{r}_{ni} \begin{cases} < 0, & r_{ni} > 1 \\ = 0, & r_{ni} = 1 \text{ or } r_{ni} = 0 \\ > 0, & 0 < r_{ni} < 1 \end{cases}$$

Excluding $r_{ni} = 0$, all other solutions approach $r_{ni} = 1$ as a limit at which the steady-state solution is (Saaty and Bram 1964; Sansone and Conti 1964; Chua and Green 1972, 1974)

$$u_{1ni} = \sin \omega_n t \qquad (5.3a)$$

$$u_{2ni} = \cos \omega_n t \qquad (5.3b)$$

Hence, the unit circle in a Cartesian plane $u_{1ni} - u_{2ni}$ is a limit cycle and the origin ($u_{1ni} = u_{2ni} = 0$) is an unstable focus.

Definition: An isolated fundamental nth oscillator can be represented as a moving state dot in the $u_{1ni} - u_{2ni}$ Cartesian plane (as shown in Fig. 5.2a) propelled by a vector field, representing the generic equation of the isolated funda-

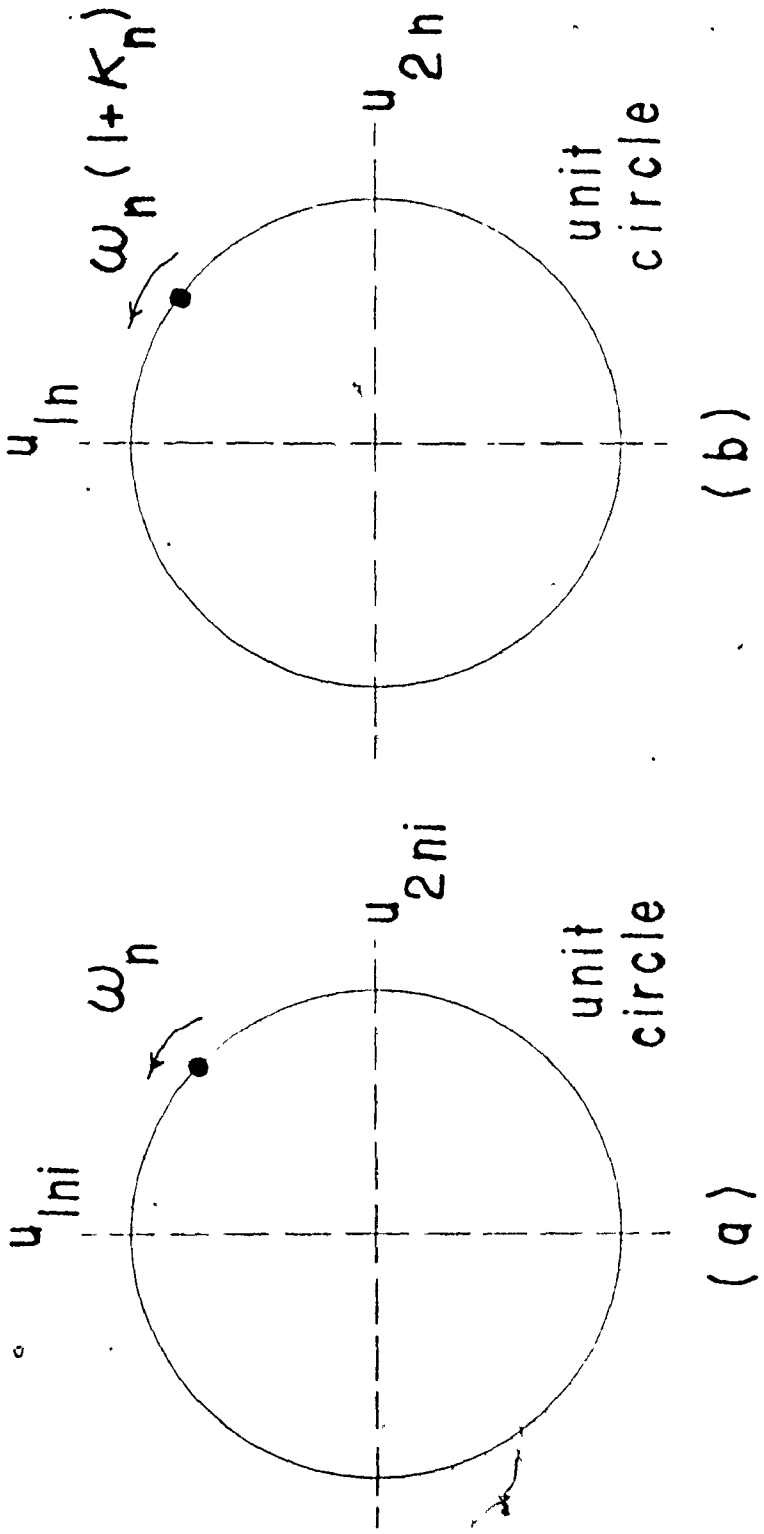

Fig. 5.2 Representation of the state of the fundamental nth oscillator.
(a) When isolated from its neighborhood.
(b) When coupled to its neighborhood.

mental nth oscillator, to approach the unit circle and (in the limit) rotate around the unit circle with an angular frequency ω_n unless the state dot was initially at the origin.

Examination of (5.1b), (5.3a) and (5.3b) leads to the following choice of a mapping $\underset{\sim}{\Gamma}_{ni}$ such that

$$x_{1ni} = a_{on} + b_{1n}\, u_{1ni} + \sum_{k=1}^{K_n} a_{kn}\, T_k(u_{2ni}) \qquad (5.4a)$$

$$x_{2ni} = u_{2ni} \qquad (5.4b)$$

and the inverse mapping $\underset{\sim}{\Gamma}_{ni}^{-1}$ such that

$$u_{1ni} = \frac{1}{b_{1n}} \left[x_{1ni} - a_{on} - \sum_{k=1}^{K_n} a_{kn}\, T_k\,(x_{2ni})\right] \qquad (5.4c)$$

$$u_{2ni} = x_{2ni} \qquad (5.4d)$$

From (5.4a) - (5.4d) it follows that for

$$b_{1n} \neq 0 \qquad (5.4e)$$

then the mapping $\underset{\sim}{\Gamma}_{ni} : \underset{\sim}{x}_{ni} = \underset{\sim}{\Gamma}_{ni}(\underset{\sim}{u}_{ni})$ is continuously differentiable, one-to-one, and onto.

Differentiation of (5.4a) and (5.4b) with respect to time and substitution from (5.2a), (5.2b), (5.4c) and (5.4d) leads to the following generic equation of an nth isolated SRO

$$\dot{x}_{1ni} = \omega_n[\{b_{1n}\}\{x_{2ni} + \rho_{ni}(1 - \rho_{ni}^2 - x_{2ni}^2)\}$$

$$+ \{-\rho_{ni} + x_{2ni}(1 - \rho_{ni}^2 - x_{2ni}^2)\}$$

$$\{\sum_{k=1}^{K_n} a_{kn} \frac{d\, T_k(x_{2ni})}{d\, x_{2ni}}\}] \tag{5.5a}$$

$$\dot{x}_{2ni} = \omega_n[-\rho_{ni} + x_{2ni}(1 - \rho_{ni}^2 - x_{2ni}^2)] \tag{5.5b}$$

where

$$\rho_{ni} = \frac{1}{b_{1n}}[x_{1ni} - a_{on} - \sum_{k=1}^{K_n} a_{kn}\, T_k(x_{2ni})] \tag{5.5c}$$

Next remove the isolation of the nth oscillator, thus letting it be coupled to its neighbourhood (as prior to its isolation) and define a type of coupling such that equations (5.2c) and (5.2d) are modified to

$$\dot{r}_n = \omega_n r_n(1 - r_n^2) \tag{5.6a}$$

$$\dot{\phi}_n = \omega_n(1 + \kappa_n) \tag{5.6b}$$

where

$$\kappa_n = \sum_{m \in I_{cn}} c_{mn}(x_{1m} - x_{1n}) \tag{5.6c}$$

I_{cn} is a coupling index set representing the neighbourhood of the nth oscillator

c_{mn} is the coupling factor representing the portion of the output of the mth oscillator which is being fed to the input of the nth oscillator

x_{1m} & x_{1n} are the outputs of the mth and nth coupled oscillators respectively

and a mapping Γ_n (similar to Γ_{ni}) such that

$$x_{1n} = a_{on} + b_{1n}u_{1n} + \sum_{k=1}^{K_n} a_{kn}\, T_k(u_{2n}) \tag{5.6d}$$

$$x_{2n} = u_{2n} \tag{5.6e}$$

along with an inverse mapping Γ_n^{-1} (similar to Γ_{ni}^{-1}) such that

$$u_{1n} = \frac{1}{b_{1n}} \left[x_{1n} - a_{on} - \sum_{k=1}^{K_n} a_{kn}\, T_k(x_{2n})\right] \tag{5.6f}$$

$$u_{2n} = x_{2n} \tag{5.6g}$$

The generic equation for a coupled fundamental nth oscillator can be obtained by transforming (5.6a) and (5.6b) via the Cartesian coordinates

$$u_{1n} = r_n \sin \phi_n$$

$$u_{2n} = r_n \cos \phi_n$$

and

$$\dot{u}_{1n} = \dot{r}_n \sin \phi_n + \dot{\phi}_n r_n \cos \phi_n$$

$$\dot{u}_{2n} = \dot{r}_n \cos \phi_n - \dot{\phi}_n r_n \sin \phi_n$$

into

$$\dot{u}_{1n} = \omega_n[u_{2n}(1 + \kappa_n) + u_{1n}(1 - u_{1n}^2 - u_{2n}^2)] \tag{5.7a}$$

$$\dot{u}_{2n} = \omega_n[-u_{1n}(1+\kappa_n) + u_{2n}(1-u_{1n}^2-u_{2n}^2)] \qquad (5.7b)$$

From (5.6a) it follows that excluding $r_n = 0$, all other solutions approach $r_n = 1$ as a limit, hence the unit circle in a Cartesian plane $u_{1n} - u_{2n}$ is a limit cycle and the origin is an unstable focus.

Definition: A coupled fundamental nth oscillator can be represented as a moving state dot in the $u_{1n} - u_{2n}$ Cartesian plane (as shown in Fig. 5.2b) propelled by a vector field, representing the generic equation of the coupled fundamental nth oscillator, to approach the unit circle and (in the limit) rotate around the unit circle with an instantaneous angular frequency $\omega_n(1 + \kappa_n)$ unless the state dot was initially at the origin.

Differentiation of (5.6d) and (5.6e) with respect to time and substitution from (5.7a), (5.7b), (5.6f) and (5.6g) leads to the following generic equation of a population of coupled SROs

$$\dot{x}_{1n} = \omega_n[\{b_{1n}\}\{x_{2n}(1+\kappa_n) + \rho_n(1-\rho_n^2-x_{2n}^2)\} + \{-\rho_n(1+\kappa_n) + x_{2n}(1-\rho_n^2-x_{2n}^2)\} \{\sum_{k=1}^{K_n} a_{kn} \frac{d\,T_k(x_{2n})}{d\,x_{2n}}\}] \qquad (5.8a)$$

$$\dot{x}_{2n} = \omega_n[-\rho_n(1+\kappa_n) + x_{2n}(1-\rho_n^2 - x_{2n}^2)] \qquad (5.8b)$$

where

$$\rho_n = \frac{1}{b_{1n}}[x_{1n} - a_{on} - \sum_{k=1}^{K_n} a_{kn}\, T_k(x_{2n})] \qquad (5.8c)$$

$$b_{1n} \neq 0$$

$$n = 1, 2, \ldots\ldots, N_p$$

5.3 Synchronization of a Population of Coupled SROs

In a population of coupled SROs containing N_p members, where

τ_n is the fundamental period of an nth member when isolated from its neighbourhood and is equal to $\frac{2\pi}{\omega_n}$

$\hat{\tau}_n$ is a particular fundamental period, under investigation, of an nth (coupled) member and is equal to $\frac{2\pi}{\hat{\omega}_n}$

$\hat{t}_{on}$ is the elapsed time until the beginning of the fundamental period $\hat{\tau}_n$

$\hat{\phi}_{on}$ is the phase angle corresponding to $\hat{t}_{on}$

let the output of an nth member be prescribed by

$$x_{1n}(t) = \hat{a}_{on} + \sum_{k=1}^{\hat{K}_n} (\hat{a}_{kn} \cos k\hat{\omega}_n t + \hat{b}_{kn} \sin k\hat{\omega}_n t) \qquad (5.9a)$$

for $\hat{t}_{on} \leq t \leq \hat{t}_{on} + \hat{\tau}_n$

whereby it is assumed that the parameters $\hat{\omega}_n$, $\hat{a}_{on}$ and $\{\hat{a}_{kn}, \hat{b}_{kn} | k=1, \ldots, \hat{K}_n\}$, corresponding to a fundamental period $\hat{\tau}_n$ remain

constant within the fundamental period $\hat{\tau}_n$ but may vary from period to period, that is they may vary with time in a step-wise manner.

Integration of equation (5.6b) along the limit cycle (the unit circle in the u_{1n} - u_{2n} plane) leads to the following

$$\int_{\hat{\phi}_{on}}^{\hat{\phi}_{on}+2\pi} d\phi_n = \omega_n \int_{\hat{t}_{on}}^{\hat{t}_{on}+\tau_n} (1+\kappa_n)dt \qquad (5.9b)$$

Substituting from (5.6c) and (5.9a) into (5.9b) and integrating, it follows that

$$\begin{aligned}\tau_n = \hat{\tau}_n + \sum_{m\varepsilon I_{cn}} c_{mn}\Big[&(\hat{a}_{om} - \hat{a}_{on})\,\hat{\tau}_n \\ &+ \sum_{k=1}^{\hat{K}_m} \frac{\hat{a}_{km}}{k\,\hat{\omega}_m}\{\sin k\,\hat{\omega}_m(\hat{t}_{on}+\hat{\tau}_n) - \sin k\,\hat{\omega}_n\hat{t}_{on}\} \\ &- \sum_{k=1}^{\hat{K}_n} \frac{\hat{a}_{kn}}{k\,\hat{\omega}_n}\{\sin k\,\hat{\omega}_n(\hat{t}_{on}+\hat{\tau}_n) - \sin k\hat{\omega}_n\hat{t}_{on}\} \\ &- \sum_{k=1}^{\hat{K}_m} \frac{\hat{b}_{km}}{k\hat{\omega}_m}\{\cos k\,\hat{\omega}_m(\hat{t}_{on}+\hat{\tau}_n) - \cos k\,\hat{\omega}_m\hat{t}_{on}\} \\ &+ \sum_{k=1}^{\hat{K}_n} \frac{\hat{b}_{kn}}{k\,\hat{\omega}_n}\{\cos k\,\hat{\omega}_n(\hat{t}_{on}+\hat{\tau}_n) - \cos k\,\hat{\omega}_n\hat{t}_{on}\}\Big] \qquad (5.9c)\end{aligned}$$

Substituting from $\hat{\omega}_n\hat{\tau}_n = 2\pi$ into (5.9c) and rearranging terms it follows that

$$\sum_{m\epsilon I_{cn}} \frac{c_{mn}}{\hat{\omega}_m} \sum_{k=1}^{\hat{K}_m} \frac{1}{k} [(\hat{b}_{km} \cos k \hat{\omega}_m \hat{t}_{on} - \hat{a}_{km} \sin k \hat{\omega}_m \hat{t}_{on})$$

$$(\cos k \hat{\omega}_m \hat{\tau}_n - 1) - (\hat{b}_{km} \sin k \hat{\omega}_m \hat{t}_{on}$$

$$+ \hat{a}_{km} \cos k \hat{\omega}_m \hat{t}_{on})(\sin k \hat{\omega}_m \hat{\tau}_n)]$$

$$= \hat{\tau}_n [1 + \sum_{m\epsilon I_{cn}} c_{mn} (\hat{a}_{om} - \hat{a}_{on})] - \tau_n \qquad (5.9d)$$

where

$$n = 1, \ldots, N_p$$

Theorem

In a population of bidirectionally coupled SROs containing N_p members, where the output of an nth member can be prescribed by (5.9a), the necessary and sufficient conditions for synchronization are

$$\hat{\tau}_n [1 + \sum_{m\epsilon I_{cn}} c_{mn} (\hat{a}_{om} - \hat{a}_{on})] - \tau_n = 0$$

for

$$\tau_n \neq \hat{\tau}_n \quad , \quad 0 < \hat{\tau}_n < \infty \quad \text{and} \quad n = 1, \ldots, N_p$$

Proof

Case 1: Let the population be synchronized, then

$$\hat{\tau}_n = \hat{\tau}_m \quad \text{and} \quad \hat{\omega}_m \hat{\tau}_n = 2\pi \qquad (5.10a)$$

where

$$m \epsilon I_{cn} \quad \text{and} \quad n = 1, \ldots, N_p$$

Substituting from (5.10a) into (5.9d), it follows that the left hand side of (5.9d) is equal to zero.

Case 2: Let the right hand side of (5.9d) be equal to zero, this gives rise to the following three possibilities

(i) $c_{mn} = 0, \quad m\varepsilon I_{cn}$

implying

$\hat{\tau}_n = \tau_n, \quad n = 1, \ldots, N_p$

which violates a premise of the theorem.

(ii) $\hat{a}_{km} = \hat{b}_{km} = 0$

implying

$\hat{\tau}_m = 0, \quad m\varepsilon I_{cn}, \; n = 1, \ldots, N_p$

which violates a premise of the theorem

(iii) $k\hat{\omega}_m\hat{\tau}_n = 2\pi i$

hence

$$k\frac{\hat{\tau}_n}{\hat{\tau}_m} = i \qquad (5.10b)$$

where

$k=1, \ldots, \hat{K}_m; \; m\varepsilon I_{cn}; \; n=1, \ldots, N_p$ and $i = 1, 2....$

also, due to bidirectional coupling

$k\hat{\omega}_n\hat{\tau}_m = 2\pi i$

hence

$$k\frac{\hat{\tau}_m}{\hat{\tau}_n} = i \qquad (5.10c)$$

where

$$k=1,\ldots,\hat{K}_n,\ n \in I_{cm},\ m=1,\ldots N_p \text{ and } i=1,2,\ldots$$

from (5.10b) and (5.10c) it follows that

$$\hat{\tau}_n = \hat{\tau}_m \qquad m \in I_{cn},\ n = 1, \ldots, N_p$$

hence, the population is synchronized. This completes the proof.

5.4 Entrainment and Subharmonic Entrainment of a SRO by an External Stimulus

Consider a population of SROs consisting of two unidirectionally coupled members with the first member representing the source of external stimulation as shown in Fig. 5.3. Substituting from the following

$$N_p = 2$$

$$I_{c1} \triangleq \{2\}$$

$$I_{c2} \triangleq \{1\}$$

$$c_{21} = 0$$

into (5.9d), it follows that

$$0 = \hat{\tau}_1 - \tau_1 \tag{5.11a}$$

$$\frac{c_{12}}{\hat{\omega}_1} \sum_{k=1}^{\hat{K}_1} \frac{1}{k} [(\hat{b}_{k1} \cos k\hat{\omega}_1 t_{o2} - \hat{a}_{k1} \sin k\hat{\omega}_1 t_{o2}) (\cos k\hat{\omega}_1 \hat{\tau}_2 - 1) - (\hat{b}_{k1} \sin k\hat{\omega}_1 t_{o2} + \hat{a}_{k1} \cos k\hat{\omega}_1 t_{o2}) (\sin k\hat{\omega}_1 \hat{\tau}_2)$$

$$= \hat{\tau}_2[1 + c_{12}(\hat{a}_{o1} - \hat{a}_{o2})] - \tau_2 \tag{5.11b}$$

When the second member is entrained or is under subharmonic entrainment by the first member then

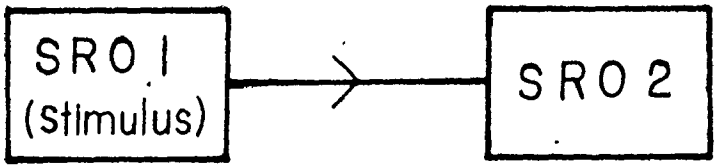

Fig. 5.3 Two unidirectionally coupled SROs representing external stimulation of a SRO

$$\hat{\tau}_2 = \ell\tau_1, \qquad \ell \geq 1 \qquad \text{where} \qquad (5.11c)$$

ℓ { = 1 for entrainment
> 1 for subharmonic entrainment

Substituting from (5.11a) and (5.11c) into (5.11b) and rearranging terms, it follows that

$$\hat{a}_{o2} = \frac{1}{c_{12}} \left(1 + c_{12}\, \hat{a}_{o1} - \frac{\tau_2}{\ell\tau_1}\right), \quad \ell \geq 1 \qquad (5.11d)$$

Case 1 : A d.c. stimulus

Let

$$x_{11}(t) = A_1$$

then, substituting from the following

$$a_{o1} = A_1$$

$$\frac{1}{\tau_1} = 0$$

into (5.11d), it follows that

$$\hat{a}_{o2} = \frac{1}{c_{12}} \left(1 + c_{12}\, A_1\right) \qquad (5.12a)$$

Case 2 : A sinusoidal stimulus

Let

$$x_{11}(t) = A_1 \sin \frac{2\pi}{\tau_1} t$$

then, substituting from the following

$$\hat{a}_{o1} = 0$$

into (5.11d), it follows that

$$\hat{a}_{o2} = \frac{1}{c_{12}} \left(1 - \frac{\tau_2}{\ell\tau_1}\right), \qquad \ell \geq 1 \qquad (5.12b)$$

Case 3 : A rectangular stimulus

Let (McMullen 1968)

$$x_{11}(t) = \frac{A_1 P_1}{\tau_1} + \frac{2A_1 P_1}{\tau_1} \sum_{n=1}^{\infty} \frac{\sin(n\pi P_1/\tau_1)}{(n\pi P_1/\tau_1)} \cos\left\{\frac{2\pi n}{\tau_1}\left(t - \frac{P_1}{2}\right)\right\}$$

where A_1 is the stimulus amplitude, P_1 is the stimulus pulse width and τ_1 is the stimulus period, then substituting from the following

$$\hat{a}_{o1} = \frac{A_1 P_1}{\tau_1}$$

into (5.11d), it follows that,

$$\hat{a}_{o2} = \frac{1}{c_{12}} \left[1 + \frac{1}{\ell\tau_1}(\ell c_{12} A_1 P_1 - \tau_2)\right], \qquad \ell \geq 1 \qquad (5.12c)$$

An alternative form of (5.12c) is

$$A_1 = \frac{\ell\tau_1(c_{12}\hat{a}_{o2} - 1) + \tau_2}{\ell\, c_{12}\, P_1}, \qquad \ell \geq 1 \qquad (5.12d)$$

which elucidates the relation between the stimulus amplitude and stimulus duration required for entrainment and subharmonic entrainment of a SRO, hence a theoretical strength-duration curve can be obtained and is depicted in Fig. 5.4 .

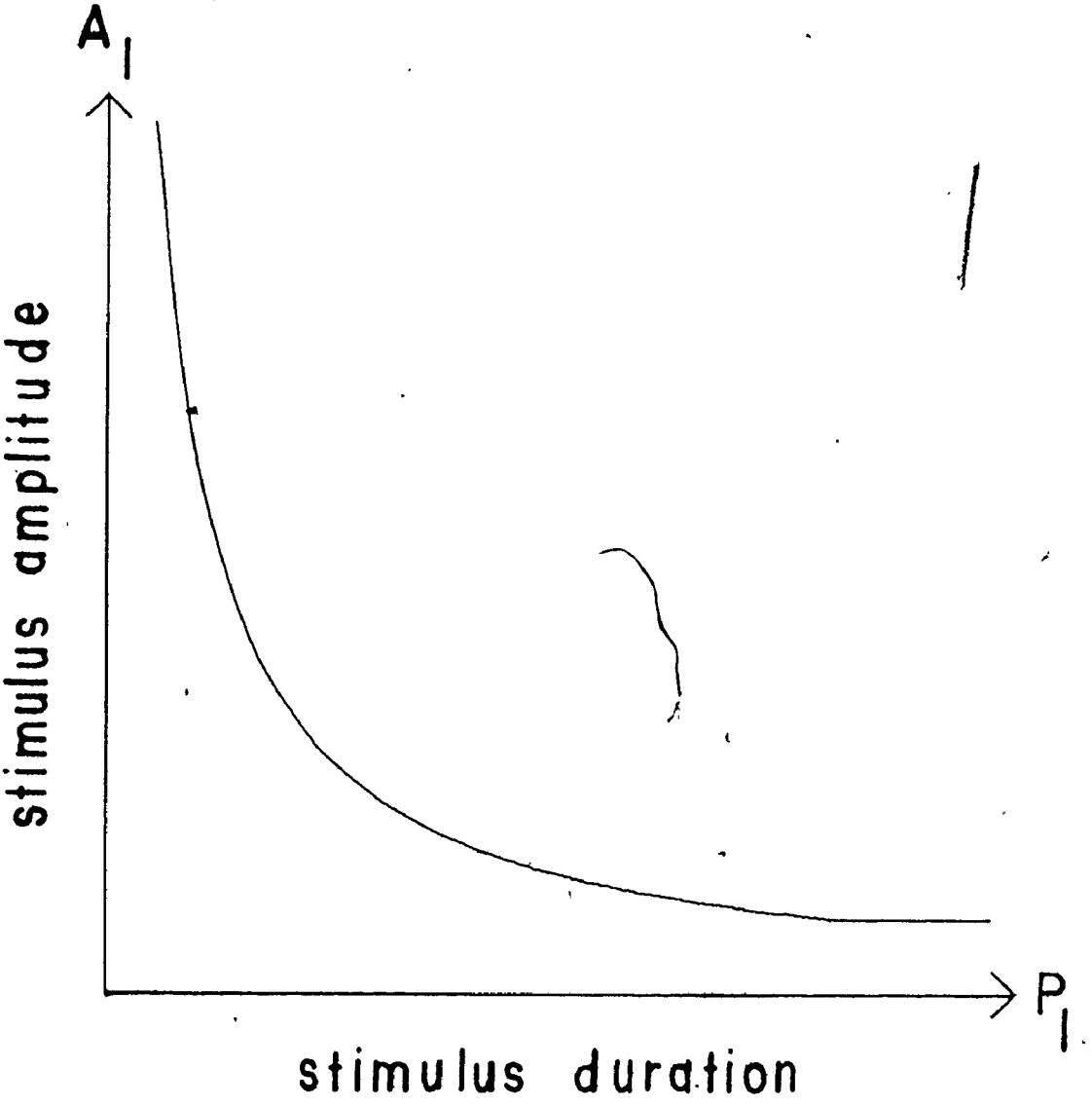

Fig. 5.4 Theoretical strength-duration curve for a SRO

5.5 Discussion

The type of coupling used, in equations (5.6a) and (5.6b), provided for relaxation characteristics since the frequency of a SRO was directly driven by the outputs of neighbouring SROs (as can be seen from Fig. 5.2b). The form of κ_n in equation (5.6c) was justified because when two oscillators were unidirectionally coupled to investigate entrainment and subharmonic entrainment of a SRO by an external rectangular stimulus, a theoretical strength-duration curve was obtained whose shape (as depicted in Fig. 5.4) resembled experimentally observed strength-duration curves for smooth muscle cells (Bozler 1938a; Davies and Sowton 1966). Also, other investigators (Aggarwal and Richie 1966; Grattarola and Torre 1977) of coupled systems have used a similar form of κ_n in their mathematical analyses.

From (5.10b) and (5.10c) it can be seen that if a population of SROs is unidirectionally coupled, then ℓth order synchronization is possible as can be further illustrated from (5.11d).

A justification for assuming a step-wise variation of the parameters $\hat{\omega}_n$, $\hat{a}_{on}$, $\{\hat{a}_{kn}, \hat{b}_{kn} \mid k = 1, \ldots, \hat{K}_n\}$ is that within the duration of a fundamental period $\hat{\tau}_n$ the variation of the parameters may be assumed to be negligible when the population is synchronized, since the time variations are more potent when the population is not synchronized.

The theorem of section 5.3 implies that two bidirectionally coupled sinusoidal oscillators (with zero average values) can be synchronized

only if their intrinsic frequencies are equal, this is in agreement with simulation results (Bardakjian and Sarna 1977). Furthermore, equation (5.12b) shows that if the output of a SRO is sinusoidal (with a zero average value), then it can be entrained or subharmonically entrained by an external sinusoidal stimulus (with a zero average value) if its intrinsic frequency is equal to or is a sub-multiple of the frequency of the sinusoidal stimulus.

For SROs entrained or subharmonically entrained by external rectangular stimuli, it can be seen from equation (5.12d) that for SROs having the same intrinsic frequency, the higher the coupled average ($\hat{a}_{o2}$) the higher the needed strength (or duration). Also, for SROs having the same coupled average value, the lower the intrinsic frequency the higher the needed stimulus strength (or duration). Furthermore, for SROs with the same intrinsic frequency and coupled average value, the lower the frequency of the stimulus the higher the needed stimulus strength (or duration.).

CHAPTER 6

ANALYSIS OF THE ECA IN HUMAN COLON

6.1 Introduction

The colon is a sacculated arched tube that constitutes the part of the large intestine extending from the cecum to the rectum, as shown in Fig. 6.1. In man (Haubrich 1964), it is customarily divided into an ascending colon about 20 cm in length, a transverse colon about 40-50 cm in length, a descending colon about 30 cm in length and a sigmoid colon about 15-50 cm in length. The circumference of the human colon progressively decreases from a maximum diameter of about 8.5 cm at the proximal ascending colon to a minimum diameter of about 2.5 cm at the sigmoid colon. It is to be noted that large variations in length and size of the human colon are often found. The muscular coat of the colonic wall consists of an inner circular muscle coat which is circumferentially oriented and an incomplete outer longitudinal muscle coat which proximally converges at the base of the vermiform appendix, and distally becomes complete over the rectum. The outer longitudinal muscle coat is represented by the taeniae coli which form three separate longitudinal muscular bands about 0.8 cm in width and situated in an equidistant manner around the circumference of the colon. The wall of the colon is characterized by haustra which are sacculations apparent between the taenia coli. In rabbits and guinea pigs (Daniel and Chapman 1963) the colonic longitudinal muscle coat is also incomplete being

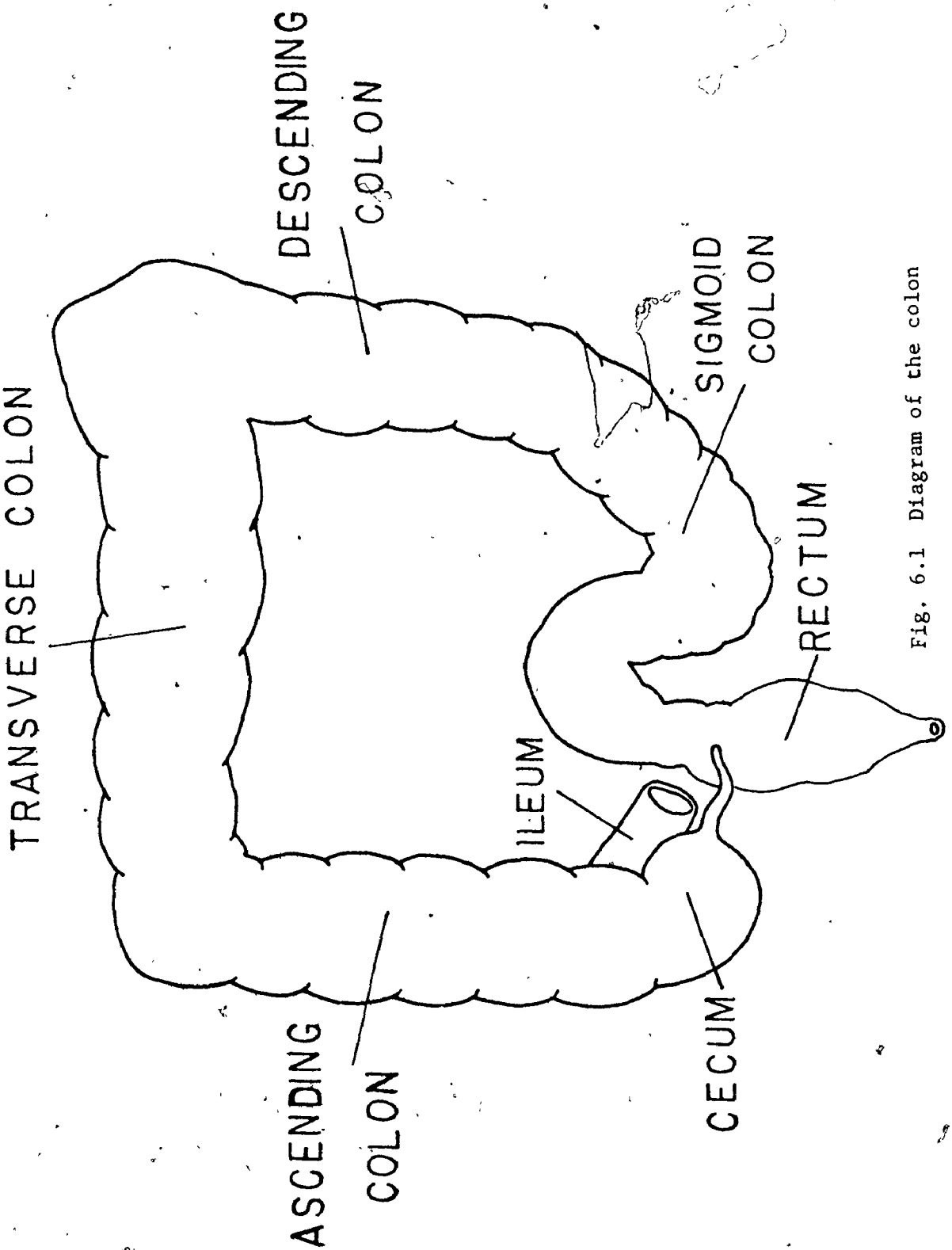

Fig. 6.1 Diagram of the colon

represented by the taenia coli, whereas in dogs it is complete.

Daniel (1975) cited the necessity of a system of controls in the colon to provide for orderly storage and movements of the semi-liquid luminal contents during transit from cecum to rectum in such a way as to allow for extraction of electrolytes and water for other changes in composition en route. Duthie (1974), Daniel (1975) and Christensen (1975) cited that myogenic, neural and hormonal controls collaborate in performing such a regulatory task. The myogenic control system in colon as in the rest of gastrointentinal tract in represented by the Electrical Control Activity. The presence of this activity in colonic smooth muscle cells has been reported in dogs (Alvarez and Mahoney 1922), rabbits (Alvarez and Mahoney 1922; Gillespie 1962a, 1962b; Couturier et al. 1969), guinea pigs (Bulbring, Burnstock and Holman 1958), cats (Christensen et al. 1969, 1971a, 1971b, 1972, 1974; Caprilli and Onori 1972) and man (Couturier et al. 1969; Provenzale and Pisano 1971; Vanasin et al. 1971; Taylor et al. 1974, 1975; Bardakjian et al. 1976a). An equivalence relationship between frequency of control waves, repetition rate of response potentials (when present) and frequency of muscular contractions was demonstrated in isolated smooth muscle strips from rabbit colon (Gillespie 1962a, 1962b), and cat colon (Caprilli and Onori 1972).

Mucosal (intraluminal) electrodes and/or serosal (extraluminal) electrodes have been used (Couturier et al. 1969; Provenzale and Pisano 1971; Vanasin et al. 1971, Taylor et al. 1974, 1975; Bardakjian et al. 1976a) to acquire electrical signals, which were subsequently amplified and filtered, as an indication of the in vivo electrical activity of the human colon. Visual analysis of the acquired records was not always adequate because of the irregularity of the colonic electrical activity as

compared to the gastric and small intestinal electrical activities (Daniel and Chapman 1963). Intraluminal pressure measurements have been used (Connell 1968) as an indication of the in vivo mechanical activity of the human distal colon.

This chapter deals with computer-aided analysis of the in vivo human colonic ECA acquired using serosal electrodes. An interactive analysis processor, described in Chapter 4, is used to determine the ECA frequency gradient along the human colon and also to determine whether or not the control waves are phase-locked in the longitudinal and circumferential directions.

6.2 Methods

6.2.1 Acquisition of Biological Data

The electrical activity in the smooth muscle cells of the human colon was recorded in vivo, using up to 6 bipolar electrode sets which were placed subserosally on the taenia coli of 16 patients undergoing elective cholecystectomy (The electrodes were implanted by Dr. W.E. Waterfall and Dr. J.F. Lind, Department of Surgery). Informed consent was obtained from each patient before surgery. Each bipolar electrode set consisted of two teflon-coated stainless steel wires (Mediwire Corporation), 0.01 inch in diameter and approximately 1 cm apart (the tip of each wire was bared by stripping off its teflon coat for a length of approximately 1 cm). The bipolar electrode sets were arranged (Fig. 6.2) in the following manner: 3 electrode sets were placed on the ascending colon of 5 patients and the transverse colon of 2 patients; 6 electrode sets were placed on the transverse colon of 2 patients; whereas 4 electrode sets were placed on the ascending colon of 1 patient,

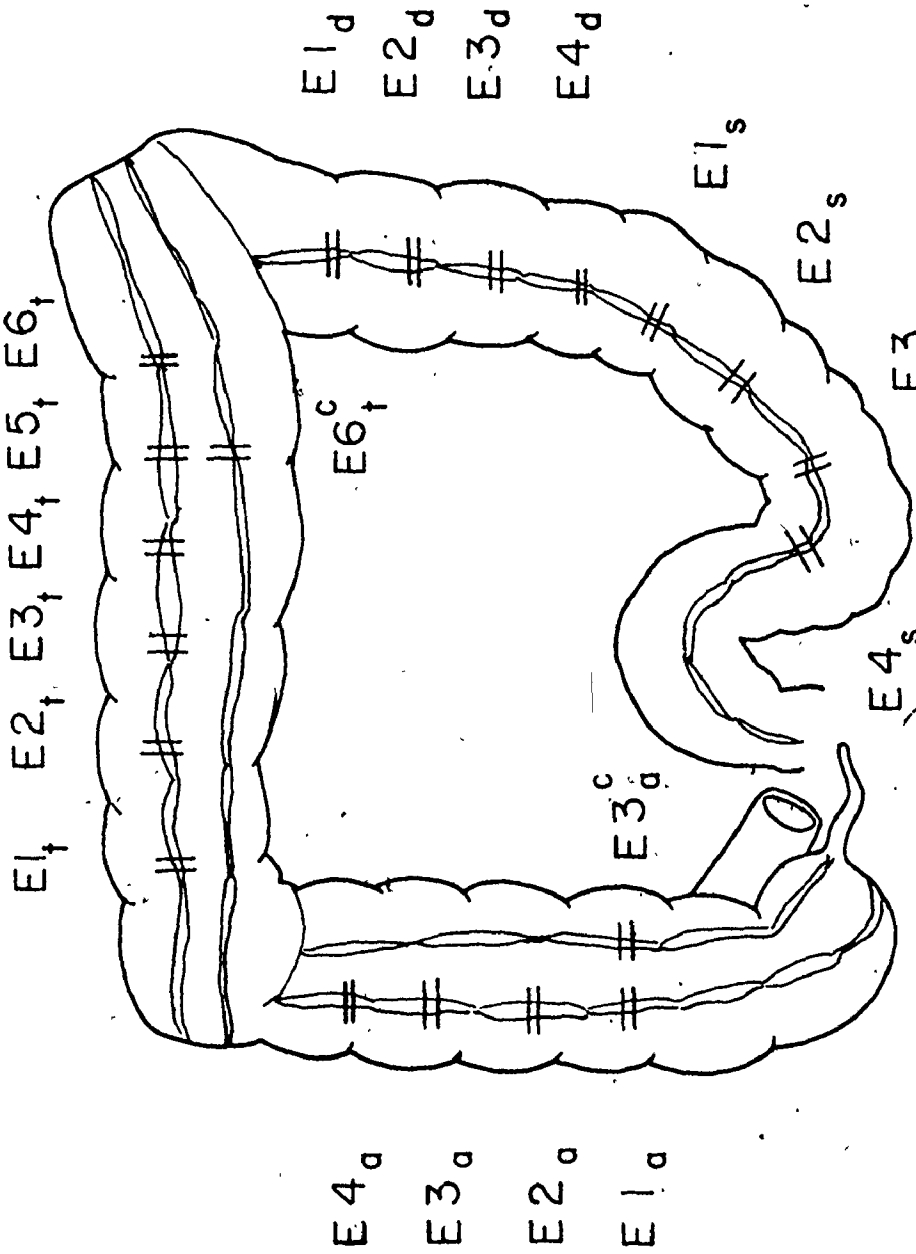

Fig. 6.2 Arrangement of electrodes

the transverse colon of 1 patient, the descending colon of 1 patient, the sigmoid colon of 2 patients and on both the descending and sigmoid colon in 2 patients. The electrode leads were brought out through the abdominal wall via a Penrose drain, routinely placed in the right flank and pulled out with it 5-7 days after operation.

The electrical activity acquired via the bipolar electrode sets was preprocessed (amplified and filtered) on an 8-channel Beckman recorder (type R611) with lower and upper cut-off frequencies set at 0.16 and 30 Hz respectively. Respiration was monitored using a Beckman type pneumogram placed around the patient's chest during recording. The preprocessed colonic electrical activity and the monitored respiration signal were simultaneously recorded on paper and on magnetic tape (using an 8-channel Hewlett Packard FM tape recorder-Model 3968A). Whenever possible, two recordings (each lasting for at least 1 hour) were made daily, one in the morning and one in the afternoon. Some recordings lasted for about 3 hours to determine the effect of feeding in which case only 1 recording per day was made.

6.2.2 Computer-Aided Analysis of Biological Data

For processing on the NOVA 830 minicomputer, using the interactive analysis processor described in chapter 4, the continuous-time signals recorded on magnetic tape were digitized via an 8-channel analog to-digital converter using a 100 Hz sampling rate (to account for the 30 Hz upper cut-off frequency of the Beckman recorder) in module 1. Decimation was necessary since using 1024 samples (this limit on the number of samples was imposed by the relatively small memory of the minicomputer used) at a 100 Hz sampling frequency in a Fast Fourier

Transform algorithm gave a frequency resolution of 0.0975 Hz which was unacceptable because the colonic frequency of interest was found to be in the range of 0.05-0.2 Hz. Using two decimation stages having decimation ratios of 5 and 4 respectively, in module 2, reduced the sampling frequency to 5 Hz and the upper cut-off frequency to 1.1 Hz (Table 3.1). To obtain the power spectra via Discrete Fourier Transformations, 10 minute segments of data (1 minute at a time using 724 padding zeros to obtain a resolution of 0.005 Hz), were used in module 5. The spectral filter with the coefficient set { 0.25,-0.25 } was used for spectral smoothing. To obtain the common frequencies (cross spectra) between different control waves,10 minute segments of data (1 minute at a time using 724 padding zeros to obtain a resolution of 0.005 Hz) were used in module 6. The plots of power and cross spectra were normalized such that the frequency component with the largest strength was made equal to 1, meanwhile, the absolute strength of each frequency component was printed on the right hand margin of each plot (See Bardakjian 1978b for program details). To investigate phase-locking between different control waves, module 4 was used for tuneable bandpass IIR digital filtering to extract the frequency component of interest and the filtered signals were displayed using a 4-channel digital-to-analog converter and a Beckman recorder.

6.3 Results

6.3.1 Characteristics of Human Colonic ECA

The ECA in human colon was continuously present with waxing and waning of the amplitude of control waves [manifesting in certain segments of the records (e.g. Fig. 6.14) where the activity could not be

(visually) noticed]. The ECA frequency varied from cycle to cycle and between different electrode sites. The temporal variation of the ECA frequency implied that in the power spectra, the energy was distributed in frequency bands (Fig. 6.4) where each frequency band generally spread over 1-2 cycles/min (cpm). The waveshape of the control waves was nonsinusoidal thus giving rise to harmonic frequency components. An nth harmonic peak frequency is defined as $nf_p \pm f_r$ where f_p is the fundamental peak frequency and f_r is the frequency resolution of the power spectrum. Up to fourth harmonic peak frequencies as well as multiple fundamental peak frequencies during the same segment of data (Figs. 6.7 & 6.19) were prominent in several recordings.

In the ascending colon (Figs. 6.3-6.7) the fundamental peak frequencies as well as their intensities varied from minute to minute and between different electrode sites. The fundamental peak frequencies were within a lower frequency range of 2-7 cpm and a higher frequency range of 8-12 cpm. The mean fundamental peak frequencies (6 patients) are given in Table 6.1 and the presence of second harmonic peak frequencies is described in Table 6.2. The control waves were not phase-locked over a 10 minute period (Figs. 4.10 & 6.5) either in the longitudinal direction (6 patients) or in the circumferential direction (1 patient).

In the transverse colon (Figs. 6.8-6.11) the temporal and spatial variation of the fundamental peak frequencies and their intensities were less prominent than in the rest of the colon. The fundamental peak frequencies were within a frequency range of 9-12 cpm. The mean fundamental peak frequencies (4 patients) are given in Table 6.3 and the presence of second harmonic peak frequencies is described in Table 6.4. The

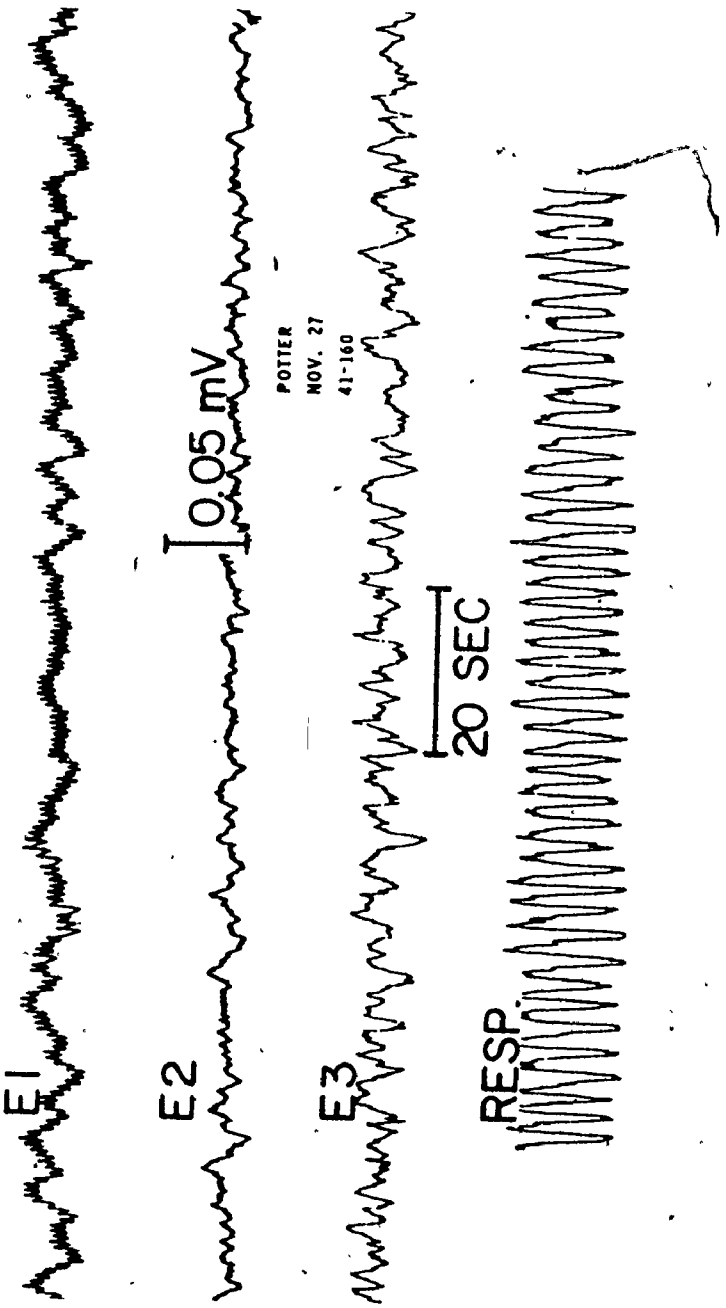

Fig. 6.3 a Human colonic electrical activity recorded from 3 sets of bipolar electrodes placed subserosally on the taenia coli of ascending colon. Electrode sets E1 and E2 were placed in the longitudinal direction whereas E1 and E3 were placed in the circumferential direction.

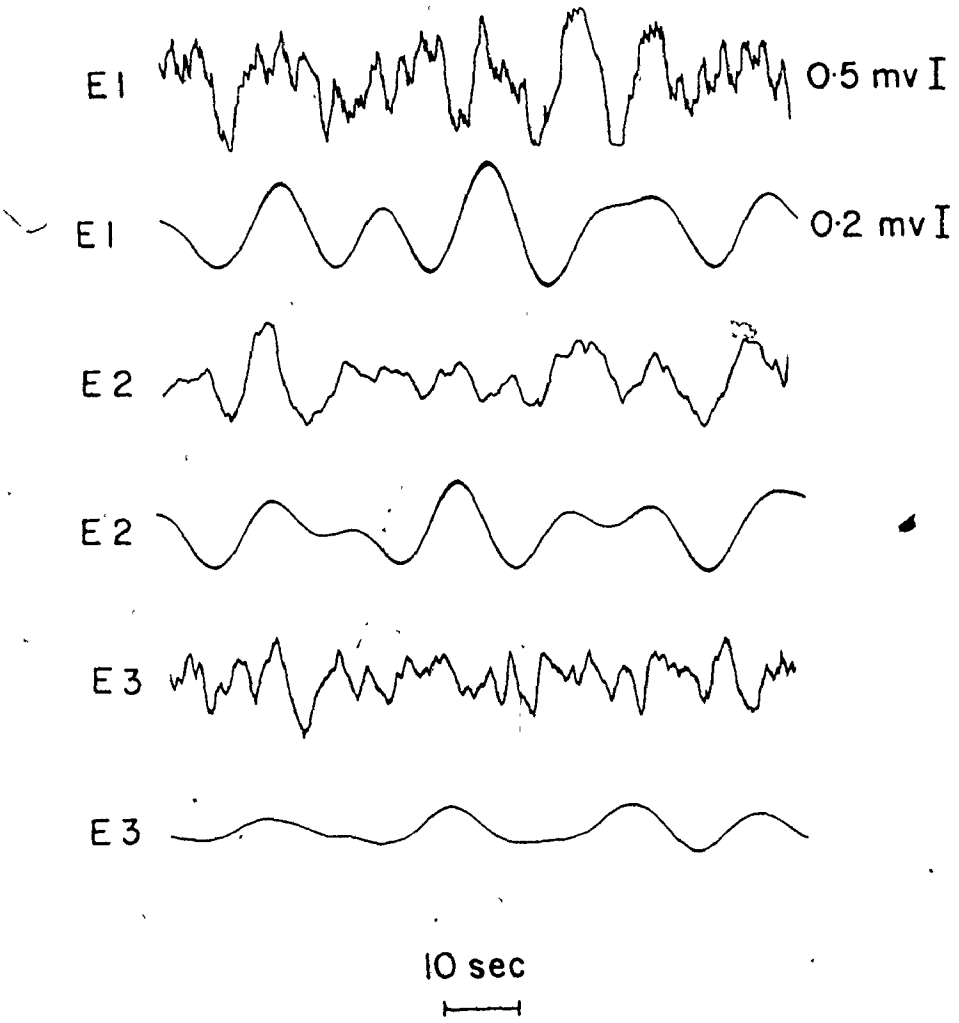

Fig. 6.3 b Human colonic electrical activity recorded from the ascending colon of the same patient of Fig. 6.3 a. For each electrode, the activity before and after low-pass filtering (f_c = 0.275 Hz) and decimation is shown in the top and bottom traces, respectively.

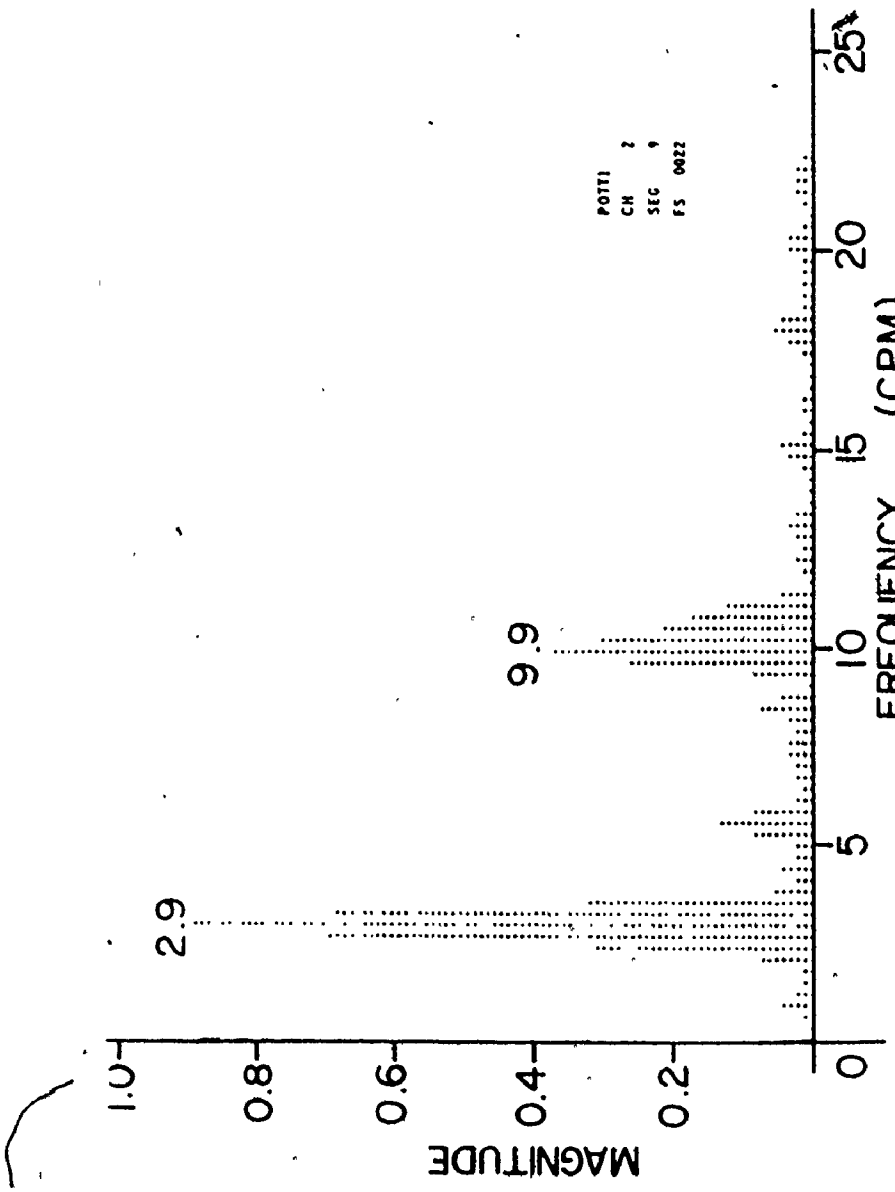

Fig. 6.4 a The power spectrum of a signal recorded from E1 in the ascending colon of the patient of Fig. 6.3, computed with a frequency resolution of 0.293 cpm

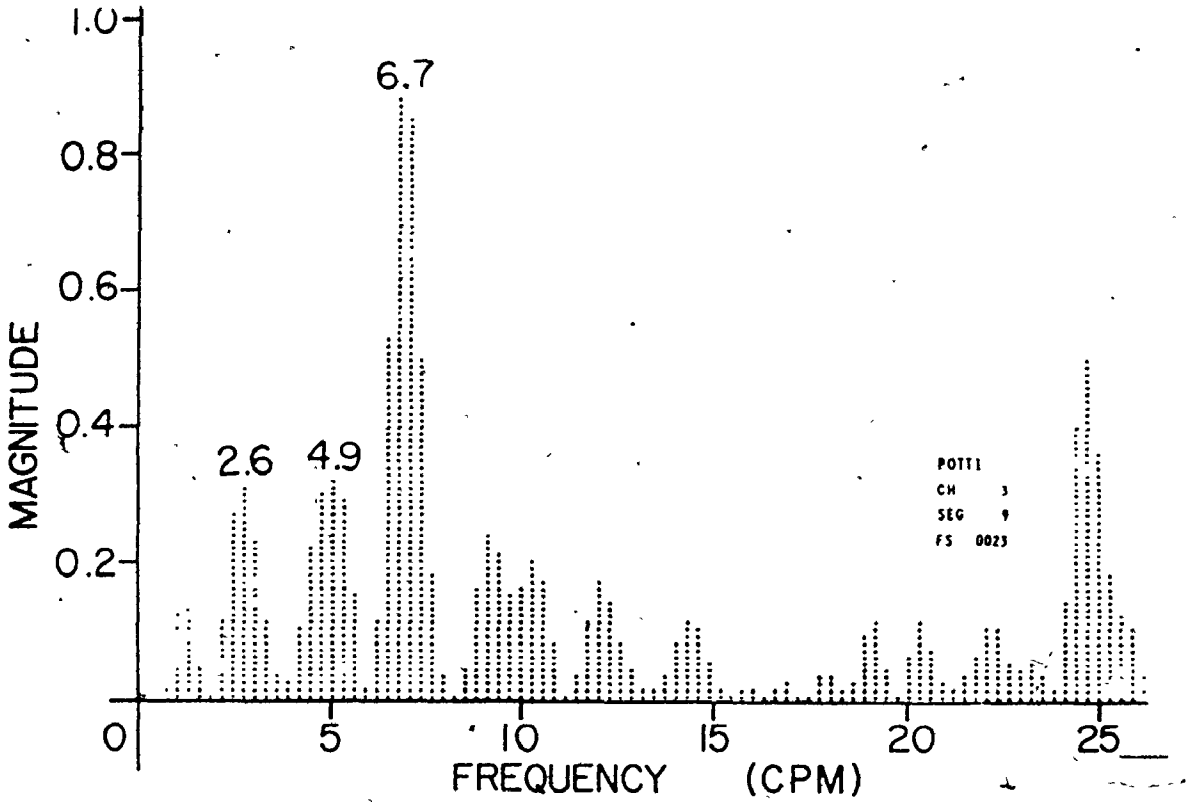

Fig. 6.4 b The power spectrum of a signal recorded from E2 in the ascending colon of the patient of Fig. 6.3, computed with a frequency resolution of 0.293 cpm

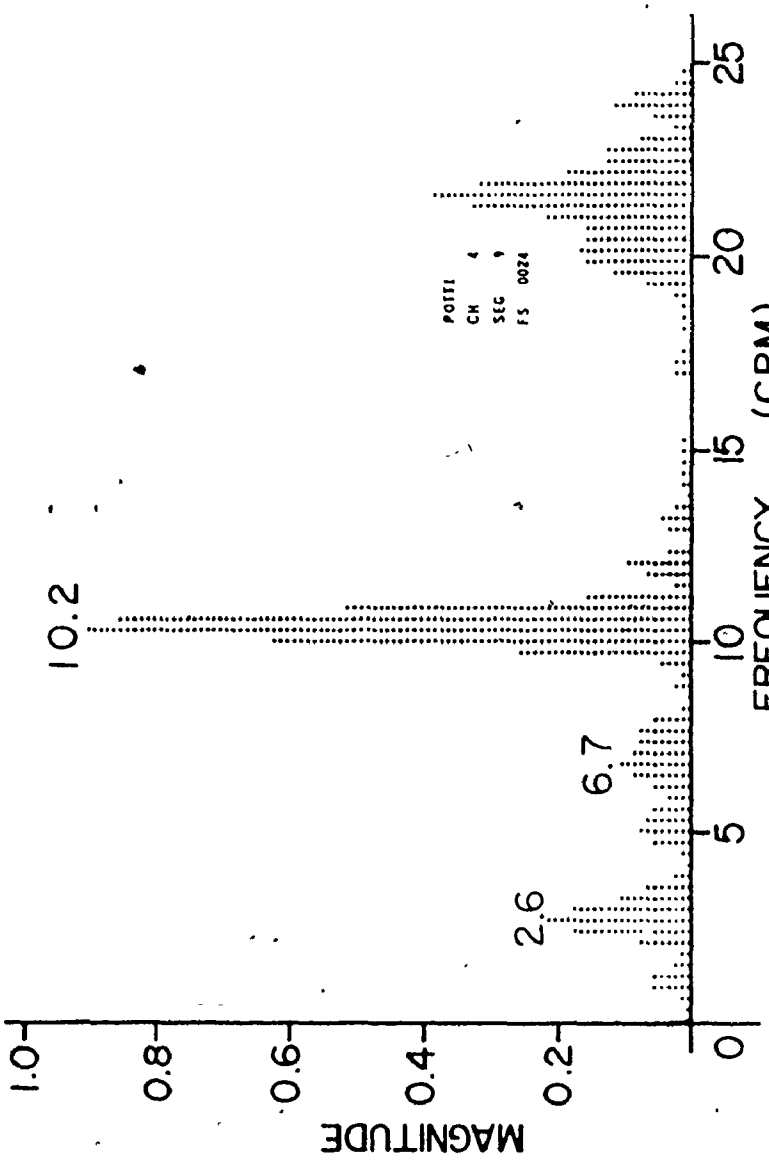

Fig. 6.4 c The power spectrum of a signal recorded from E3 in the ascending colon of the patient of Fig. 6.3, computed with a frequency resolution of 0.293 cpm

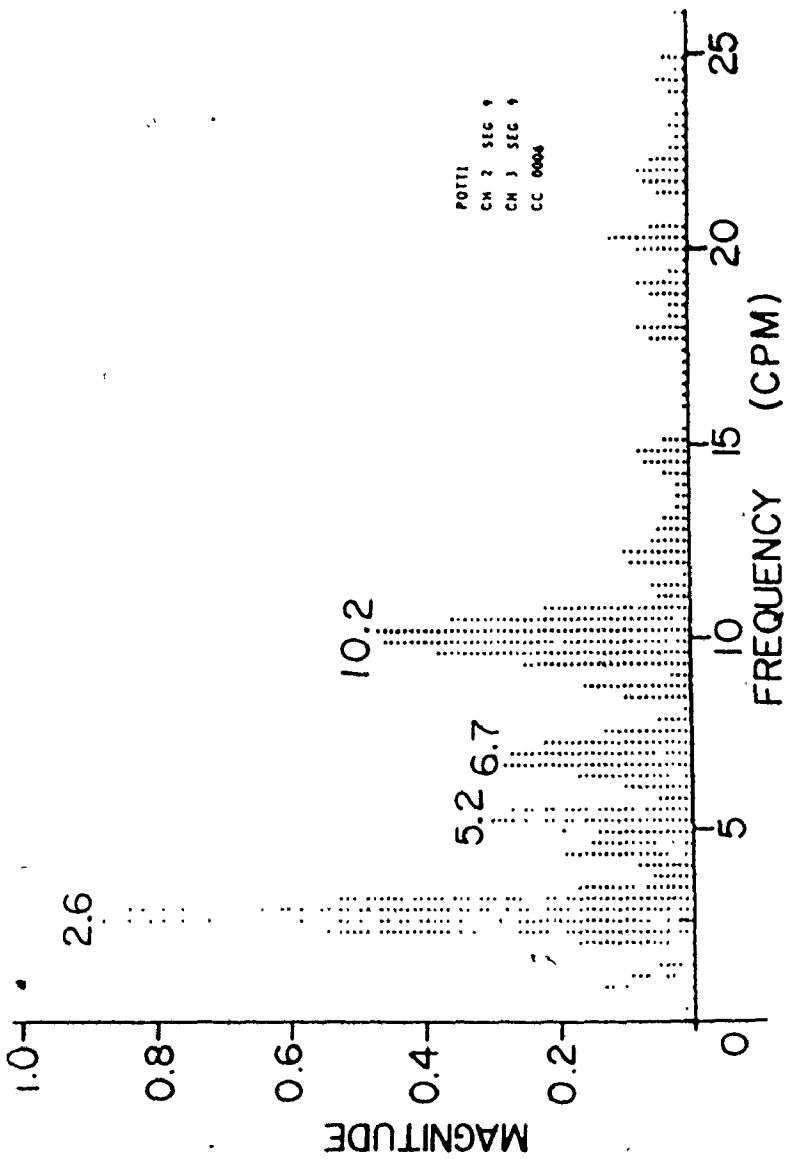

Fig. 6.4 d The cross spectrum of signal pair recorded from E1 and E2 in the ascending colon of the patient of Fig. 6.3, computed with a frequency resolution of 0.293 cpm

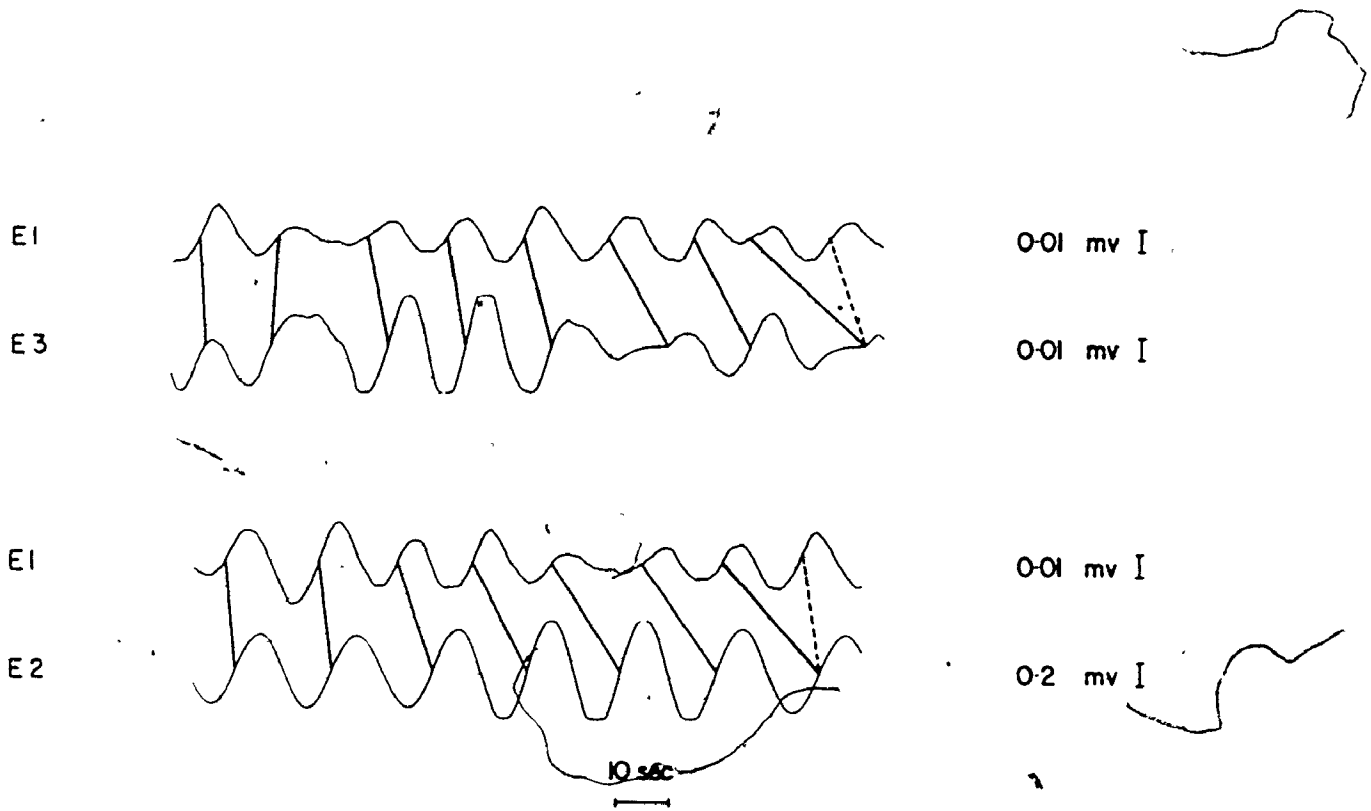

Fig. 6.5 Phase-lag variation of human colonic ECA recorded from the ascending colon of the patient of Fig. 6.3 and band-pass filtered (2-4 cpm). E1 and E3 were in the circumferential direction whereas E1 and E2 were in the longitudinal direction. Continuous lines join the zero crossings of waveforms.

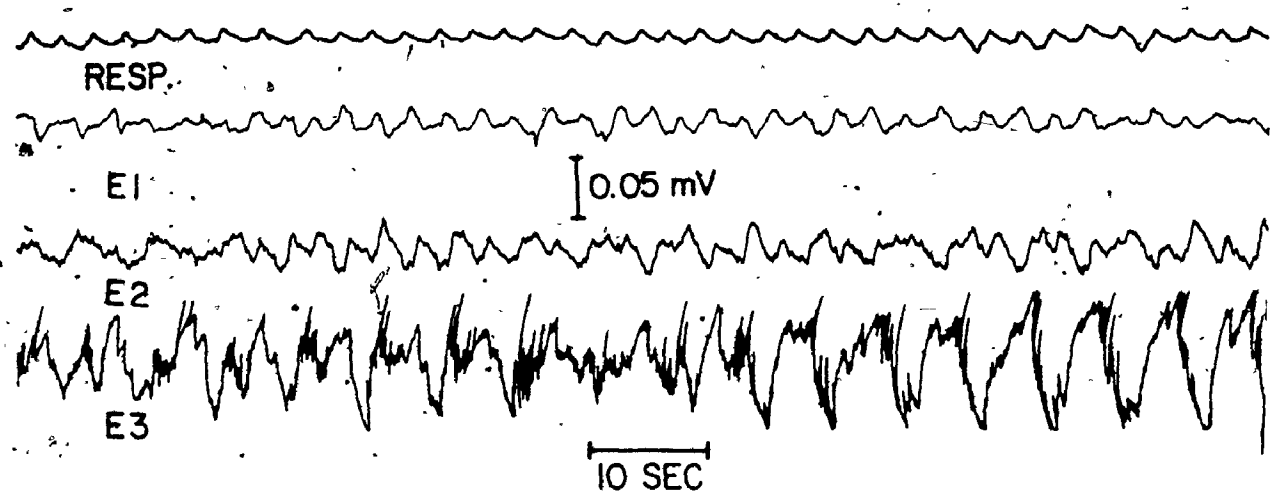

Fig. 6.6 Human colonic electrical activity recorded from 3 sets of bipolar electrodes placed subserosally, in the longitudinal direction, on the taenia coli of ascending colon

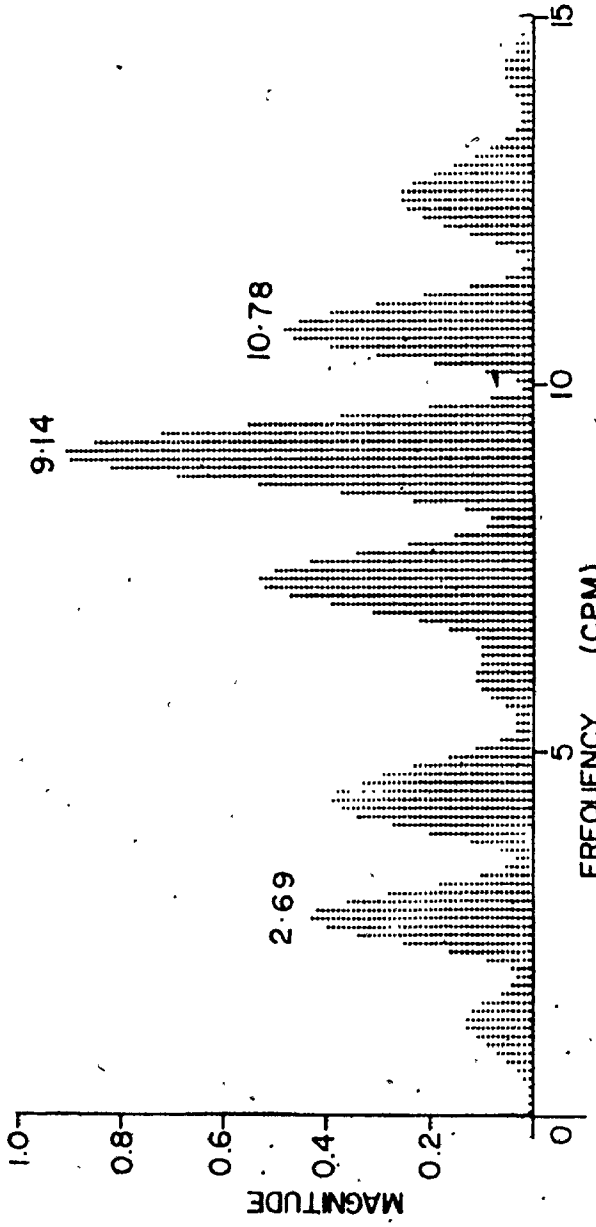

Fig. 6.7 The power spectrum of a signal recorded from E2 in the ascending colon of the patient of Fig. 6.6, computed with a frequency resolution of 0.293 cpm

TABLE 6.1

MEAN FUNDAMENTAL PEAK FREQUENCIES

IN ASCENDING COLON

Number of patients	Number of observations	Lower freq. range 2-7 cpm		higher freq. range 8-12 cpm	
		Mean	standard deviation	Mean	standard deviation
1	48	3.67	± 1.28	9.68	± 1.11
1	30	4.56	± 1.43	9.67	± 1.05
1	44	4.11	± 1.47	9.76	± 1.05
1	42	4.80	± 1.13	10.20	± 1.07
1	30	4.24	± 1.39	10.05	± 1.06
1	40	4.55	± 1.54	10.36	± 0.90
6	234	4.29	± 1.43	9.95	± 1.08

TABLE 6.2

PRESENCE OF SECOND HARMONIC FREQUENCY

COMPONENT IN ASCENDING COLON

Number of patients	number of observations	lower freq. range 2-7 cpm		higher freq. range 8-12 cpm	
		% ℓ	%h	% ℓ	%h
1	45	46.66	22.22	33.33	22.22
1	28	14.28	57.14	21.42	28.57
1	40	32.50	10.00	37.50	7.50
1	42	47.61	14.28	30.95	9.52
1	30	16.66	36.66	30.00	10.00
1	40	25.00	42.50	17.50	37.50
6	225	32.44	28.44	28.88	19.11

where

% ℓ denotes the percentage of time in which intensity of second harmonic is less than the intensity of fundamental but greater than 10% of it.

and

%h denotes the percentage of time in which intensity of second harmonic is greater than the intensity of fundamental

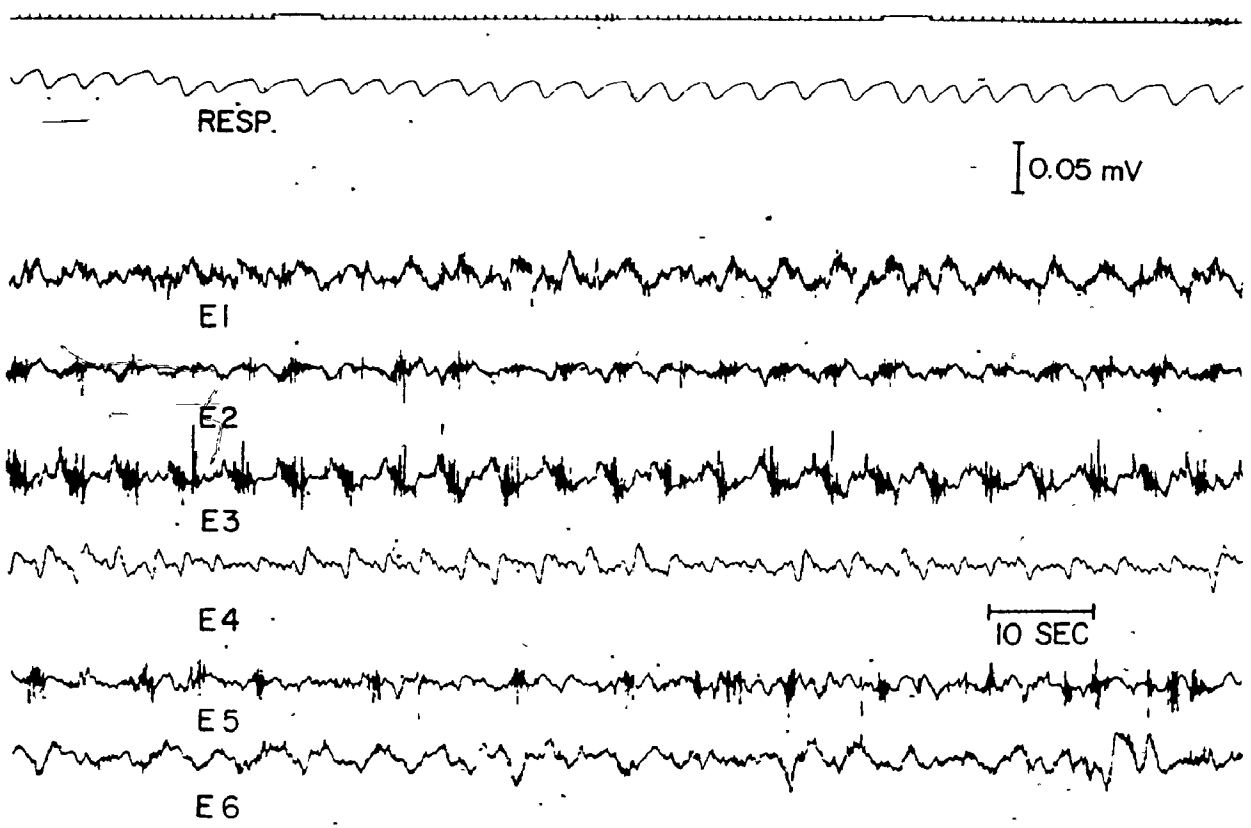

Fig. 6.8 Human colonic electrical activity recorded from 6 sets of bipolar electrodes placed subserosally on the taenia coli of transverse colon

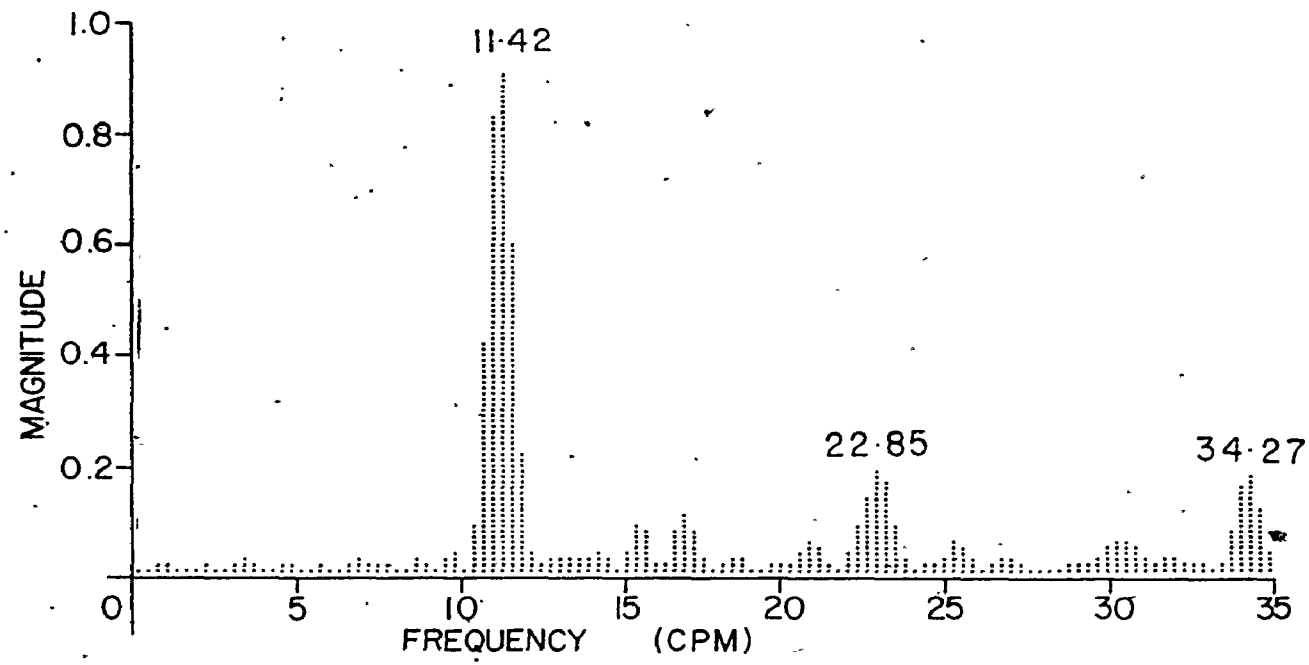

Fig. 6.9 The power spectrum of a signal recorded from E2 in the transverse colon of the patient of Fig. 6.8, computed with a frequency resolution of 0.293 cpm

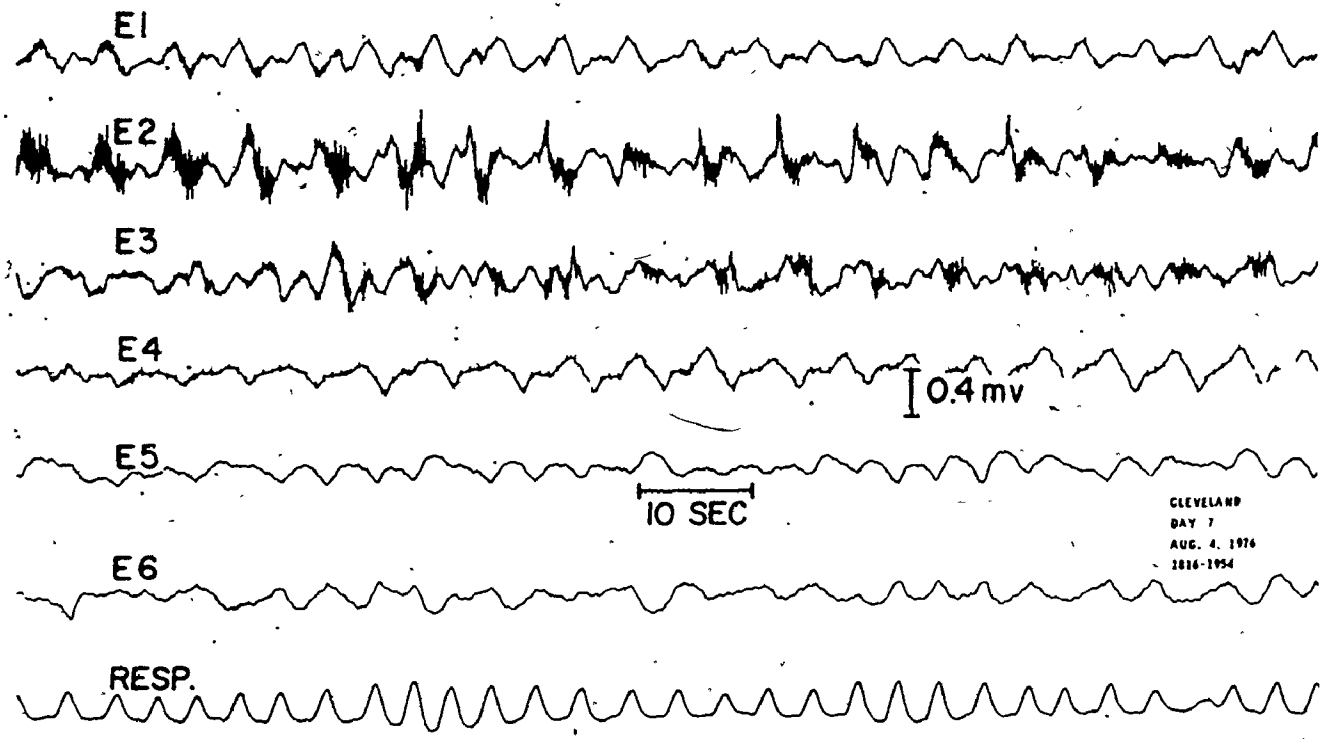

Fig. 6.10 Human colonic electrical activity recorded from 6 sets of bipolar electrodes placed subserosally on the taenia coli of transverse colon. Electrode sets E1-E5 were placed in the longitudinal direction whereas E5 and E6 were placed in the dircumferential direction.

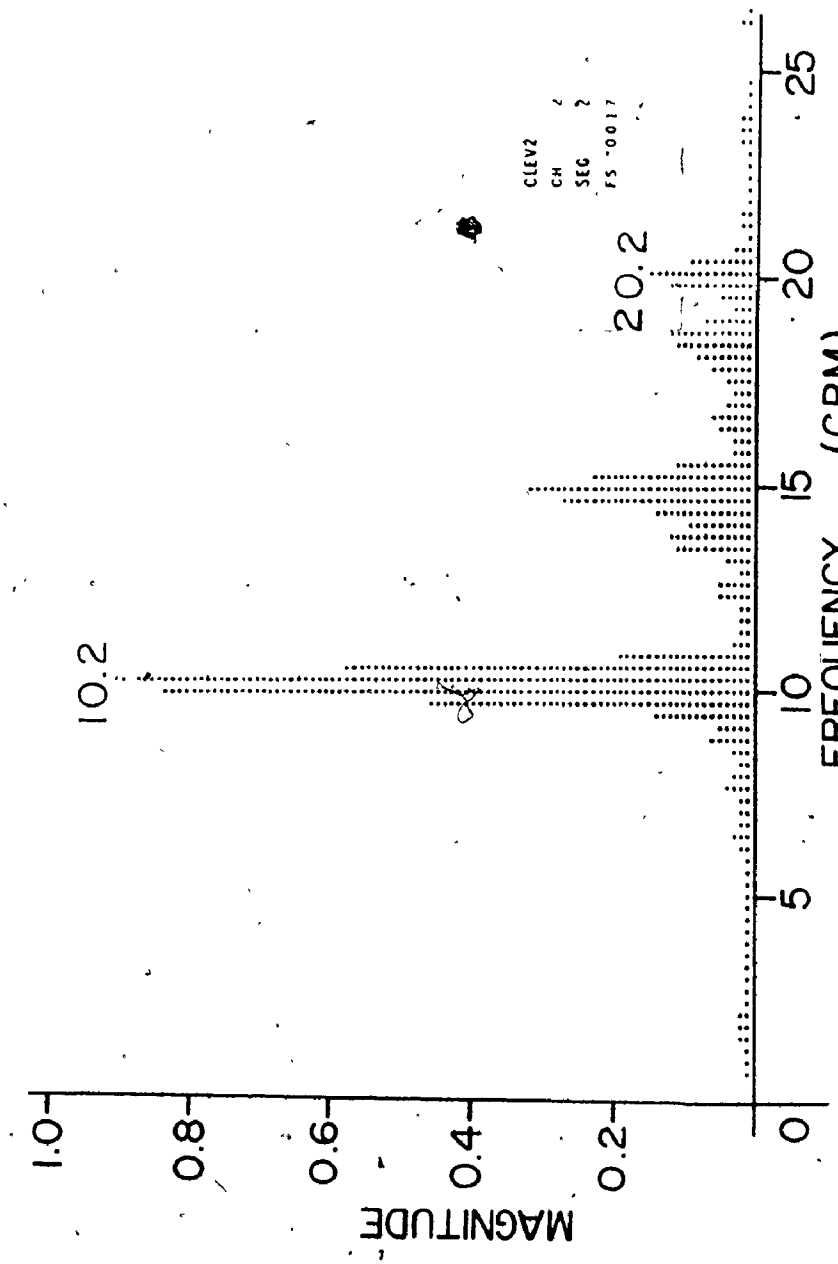

Fig. 6.11 a The power spectrum of a signal recorded from E2 in the transverse colon of the patient of Fig. 6.10

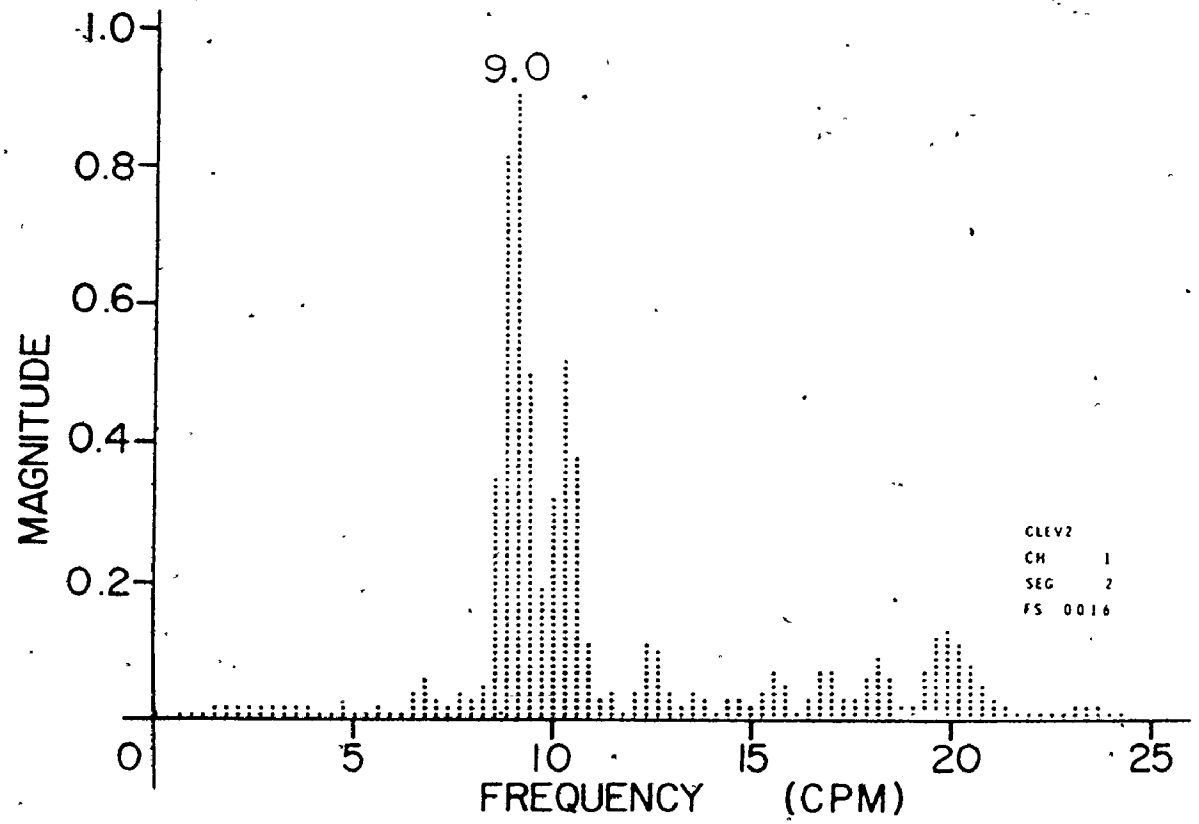

Fig. 6.11 b The power spectrum of a signal recorded from E1 in the transverse colon of the patient of Fig. 6.10, computed with a frequency resolution of 0.293 cpm

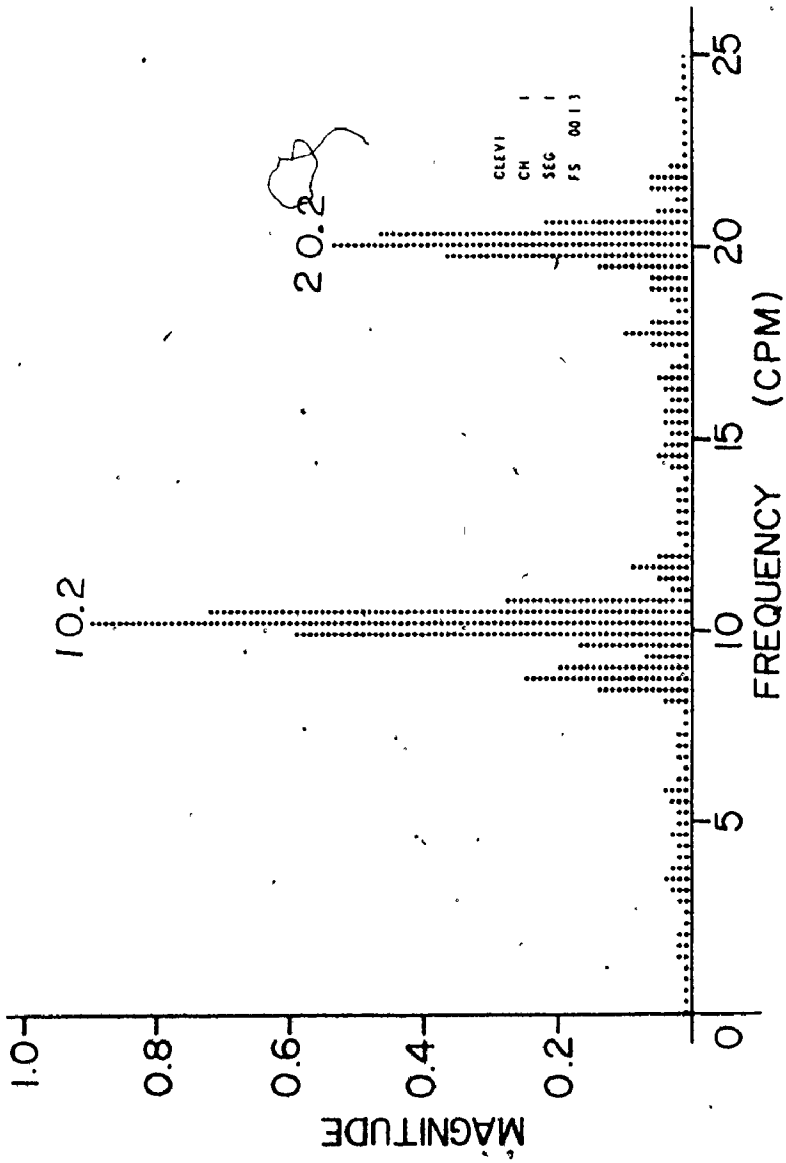

Fig. 6.11 The power spectrum of a signal recorded from E1 in the transverse colon of the patient of Fig. 6.10, computed with a frequency resolution of 0.293 cpm

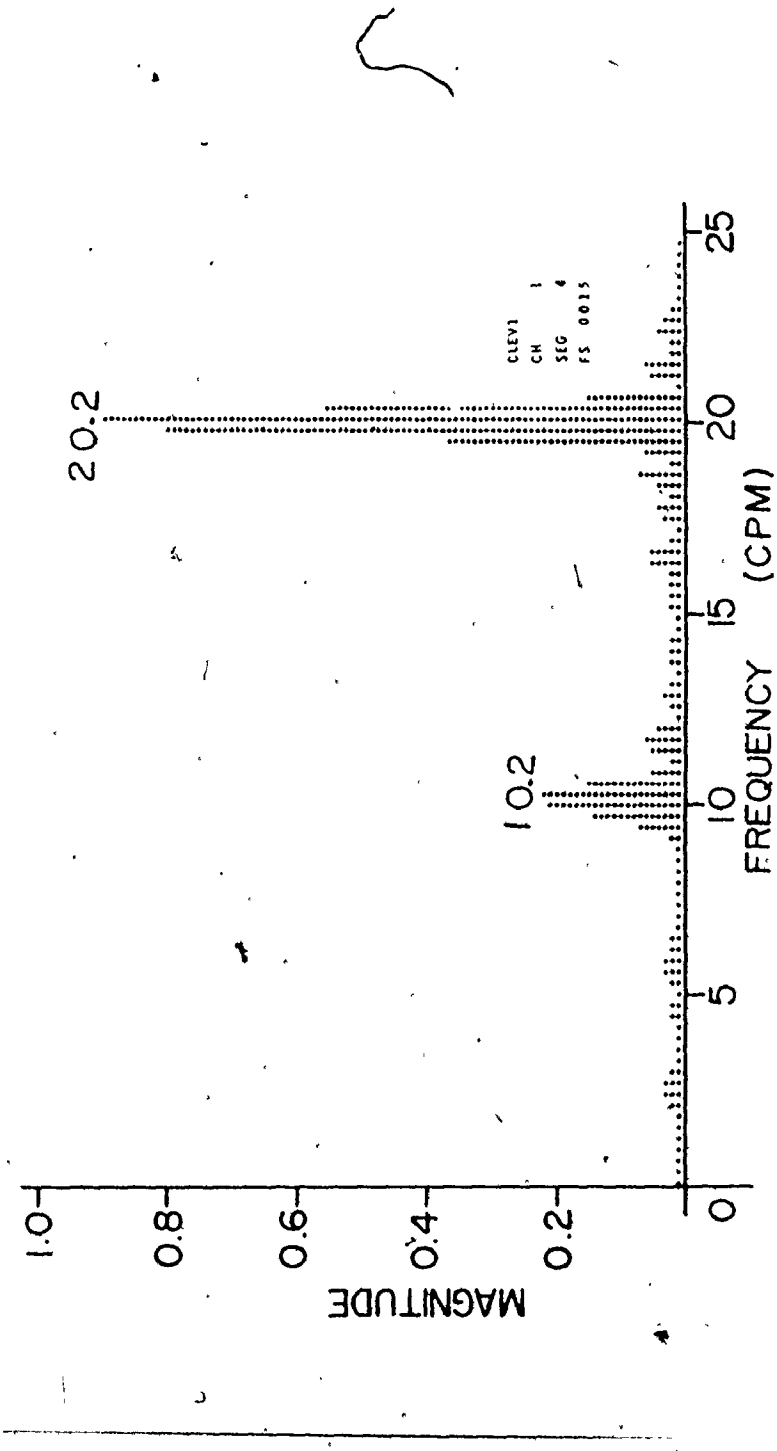

Fig. 6.11 d The power spectrum of a signal recorded from E1 in the transverse colon of the patient of Fig. 6.10, computed with a frequency resolution of 0.293 cpm

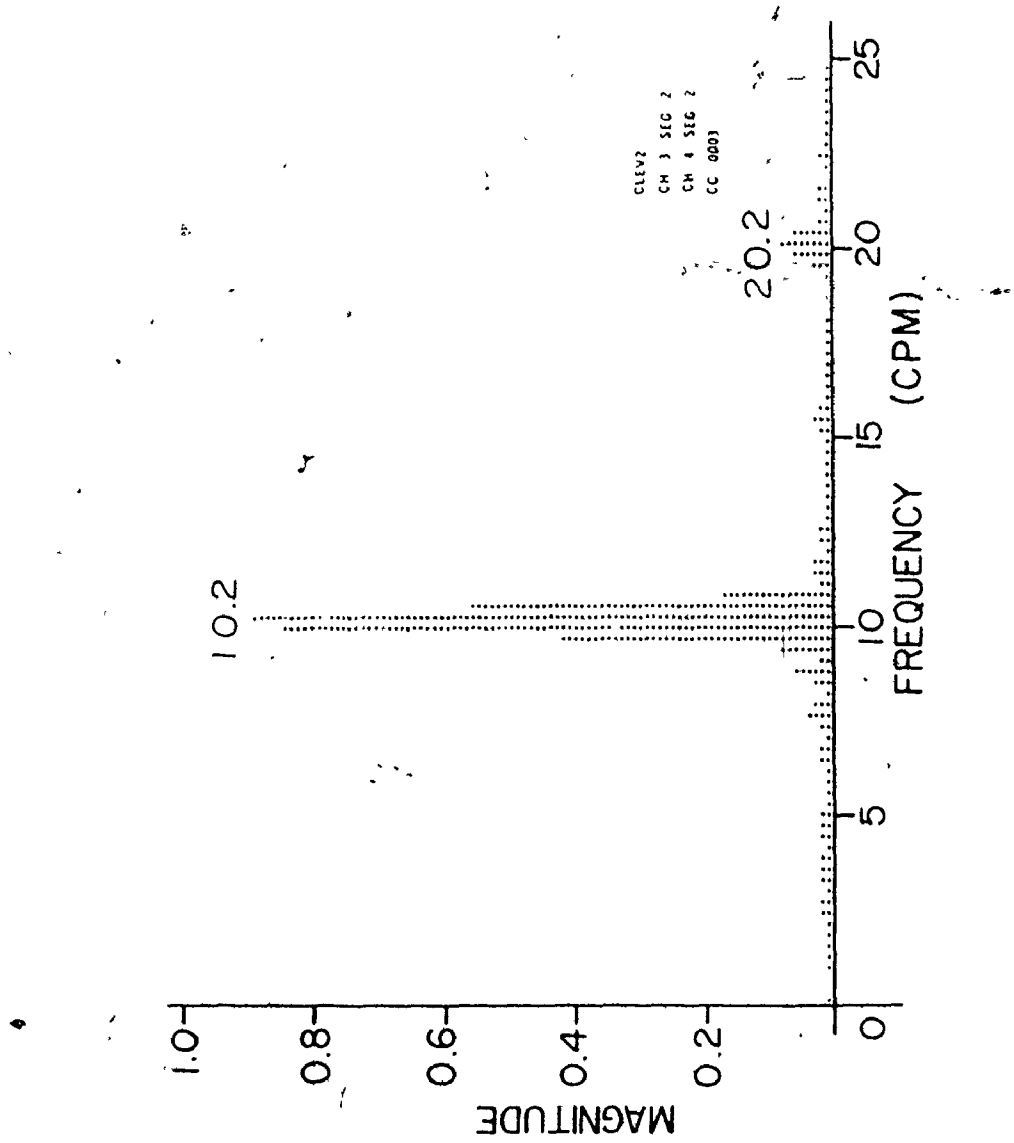

Fig. 6.11 e The cross spectrum of signal pair recorded from E3 and E4 in the transverse colon of the patient of Fig. 6.10, computed with a frequency resolution of 0.293 cpm

TABLE 6.3

MEAN FUNDAMENTAL PEAK FREQUENCY

IN TRANSVERSE COLON

Number of Patients	number of observations	higher freq. range 10-12 cpm	
		Mean	Standard deviation
1	89	10.90	± 0.83
1	65	9.95	± 0.80
1	9	10.67	± 0.88
1	56	10.46	± 0.93
4	219	10.50	± 0.94

TABLE 6.4

PRESENCE OF SECOND HARMONIC FREQUENCY

CONPONENT IN TRANSVERSE COLON

Number of patients	Number of observations	higher freq. range 8-12 cpm	
		% ℓ	%h
1	64	43.75	17.18
1	56	41.07	10.71
1	9	33.33	11.11
1	89	44.94	13.48
4	218	43.11	13.76

where

% ℓ denotes the percentage of time in which intensity of second harmonic is less than the intensity of fundamental but greater than 10% of it.

and

% h denotes the percentage of time in which intensity of second harmonic is greater than the intensity of fundamental

control waves were not phase-locked over a 10 minute period either in the longitudinal direction (4 patients) or in the circumferential direction (1 patient). In one patient the control waves remained phase-locked (in the longitudinal direction) for periods of time extending up to 10 minutes. The waxing and waning of the amplitude of control waves was less pronounced in the transverse colon than in the rest of the colon.

In the descending colon (Figs. 6.12-6.15) the fundamental peak frequencies as well as their intensities varied in time and space. The fundamental peak frequencies were (as in the ascending colon) within a lower frequency range of 2-7 cpm and a higher frequency range of 8-12 cpm. The mean fundamental peak frequencies (3 patients) are given in Table 6.5 and the presence of second harmonic peak frequencies is described in Table 6.6. The control waves were not phase-locked over a 10 minute period (3 patients) in the longitudinal direction. In one patient (Figs. 6.14 and 6.15) the frequency of the ECA and its characteristics were much the same as in the transverse colon, for the fundamental peak frequencies were in the higher frequency range of 8-12 cpm and the control waves remained phase-locked (in the longitudinal direction) for periods of time extending up to 5 minutes.

In the sigmoid colon (Figs. 6.14-6.17) the fundamental peak frequencies as well as their intensities, also, varied from minute to minute and between different electrode sites. The fundamental peak frequencies were (as in the ascending colon) within a lower frequency range of 2-7 cpm and a higher frequency range of 8-12 cpm. The mean fundamental peak frequencies (4 patients) are given in Table 6.7 and the presence of second harmonic peak frequencies is described in Table 6.8.

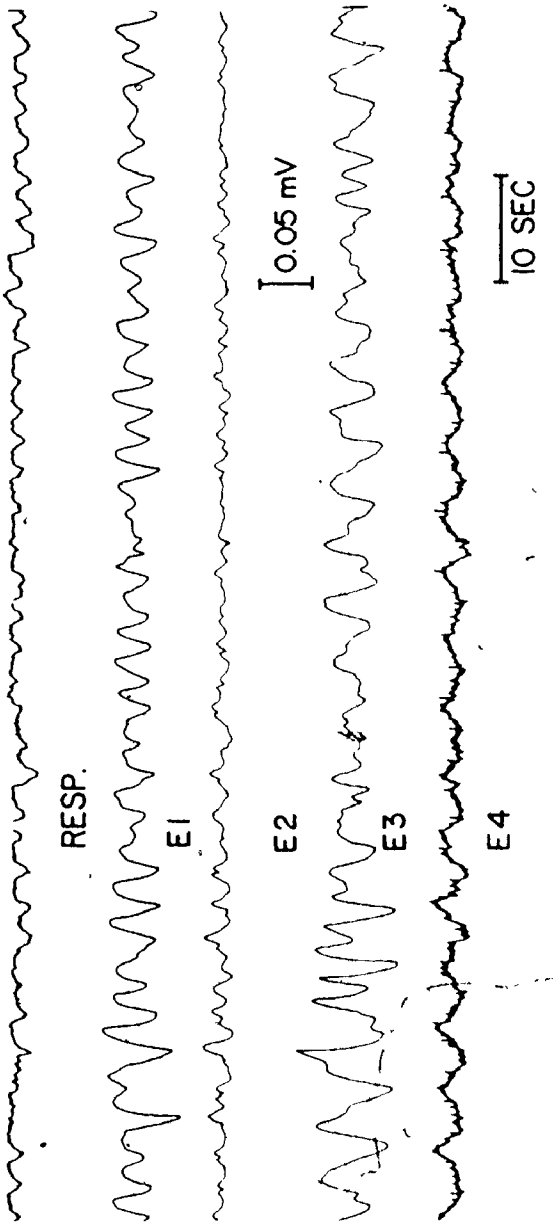

Fig. 6.12 Human colonic electrical activity recorded from 4 sets of bipolar electrodes placed subserosally on the taenia coli of descending colon

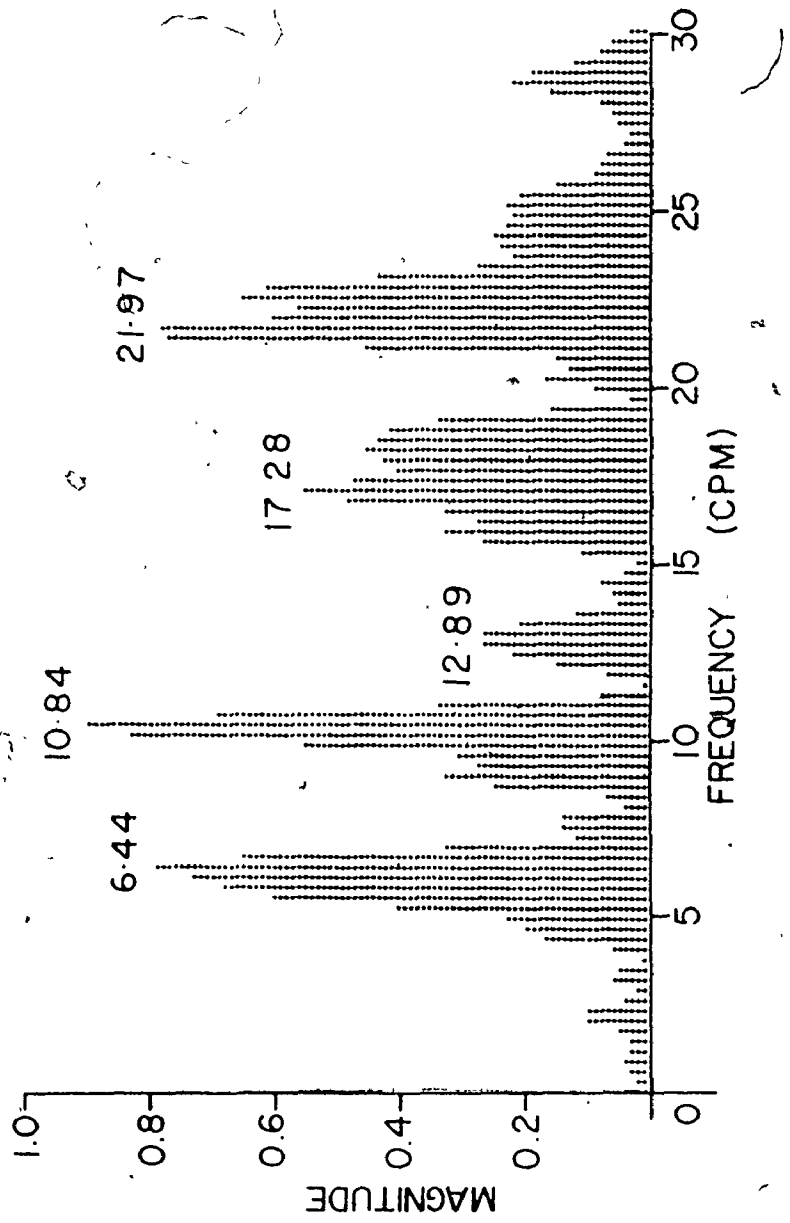

Fig. 6.13 The power spectrum of a signal recorded from E4 in the descending colon of the patient of Fig. 6.12, computed with a frequency resolution of 0.293 cpm

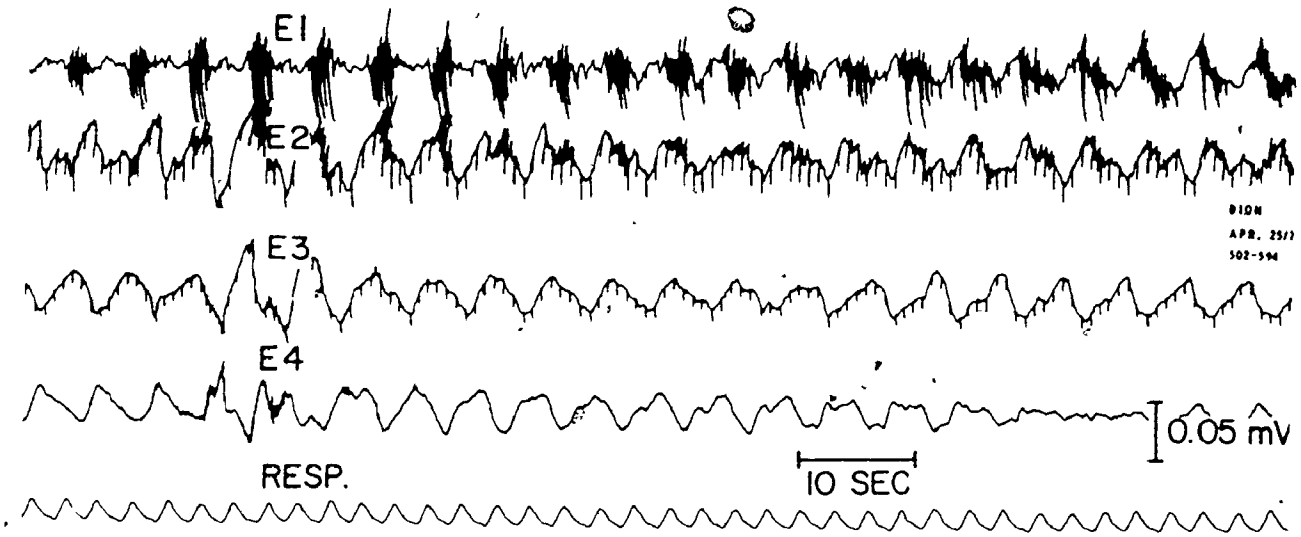

Fig. 6.14 Human colonic electrical activity recorded from 4 sets of bipolar electrodes placed subserosally on the taenia coli of descending and sigmoid colon. E1 and E2 were placed in the descending colon whereas E3 and E4 were placed in the sigmoid colon.

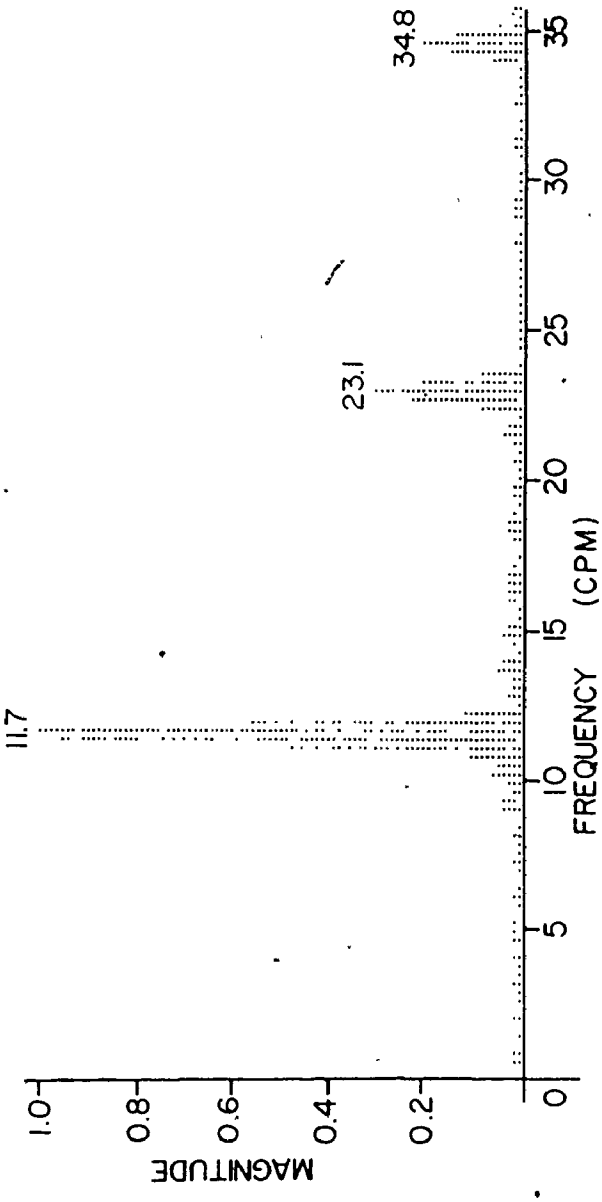

Fig. 6.15 The power spectrum of a signal recorded from E1 in the descending colon of the patient of Fig. 6.14, computed with a frequency resolution of 0.293 cpm

TABLE 6.5

MEAN FUNDAMENTAL PEAK FREQUENCIES

IN DESCENDING COLON

Number of patients	Lower freq. range 2-7 cpm			higher freq. range 8-12 cpm		
	number of observations	Mean	Std. deviation	number of observations	mean	Std. deviation
1	20	3.86	±1.09	20	10.14	±1.06
1	-	-	-	64	11.32	±0.56
1	59	4.88	±1.31	59	10.38	±0.71
3	79	4.62	±1.33	143	10.77	±0.87

TABLE 6.6

PRESENCE OF SECOND HARMONIC FREQUENCY

COMPONENT IN DESCENDING COLON

number of patients	lower freq. range 2-7 cpm			higher freq. range 8-12 cpm		
	number of observations	% ℓ	%h	number of observations	% ℓ	%h
1	19	31.57	31.57	19	15.78	10.52
1	-	-	-	63	52.38	17.46
1	59	16.94	45.76	59	30.50	11.86
3	78	20.51	42.30	141	38.29	14.18

where

% ℓ denotes the percentage of time in which the intensity of second harmonic is less than the intensity of the fundamental but greater than 10% of it.

and

%h denotes the percentage of time in which the intensity of second harmonic is greater than the intensity of fundamental

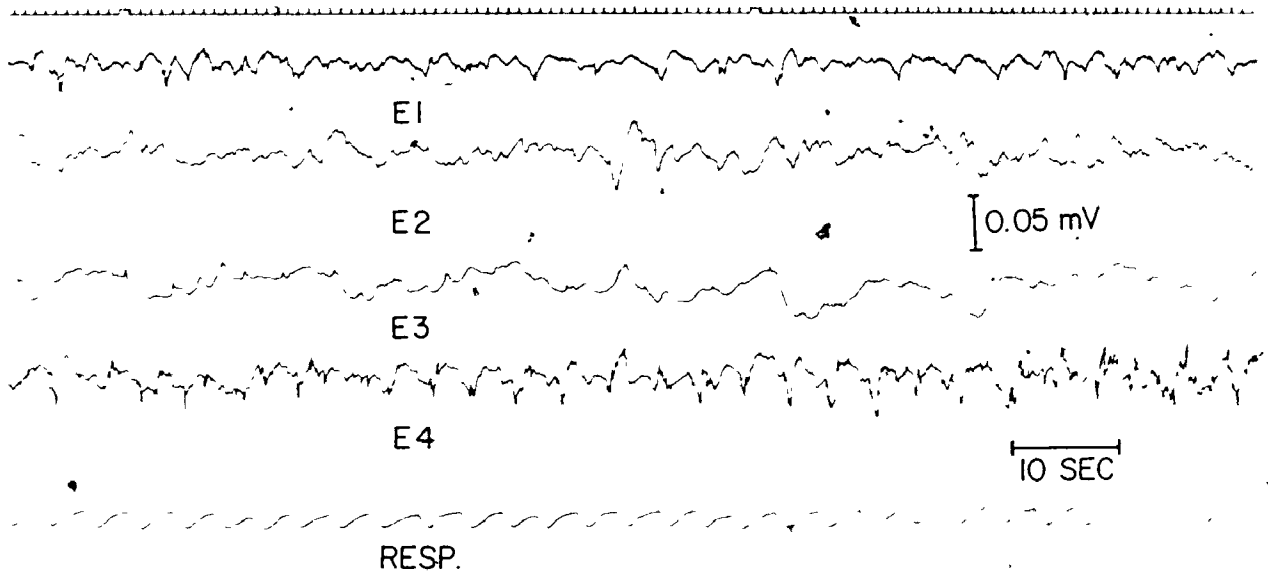

Fig. 6.16 Human colonic electrical activity recorded from 4 sets of bipolar electrodes placed subserosally on the taenia coli of sigmoid colon

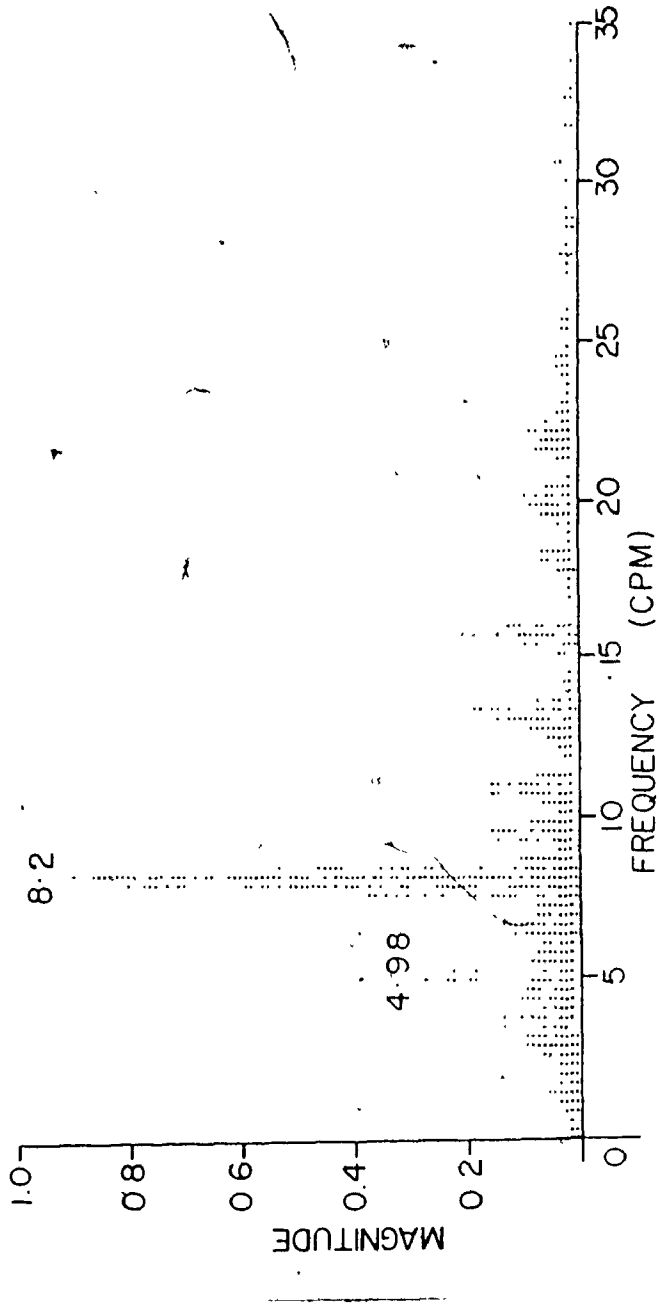

Fig. 6.17 a The power spectrum of a signal recorded from E2 in the sigmoid colon of the patient of Fig. 6.16, computed with a frequency resolution of 0.293 cpm

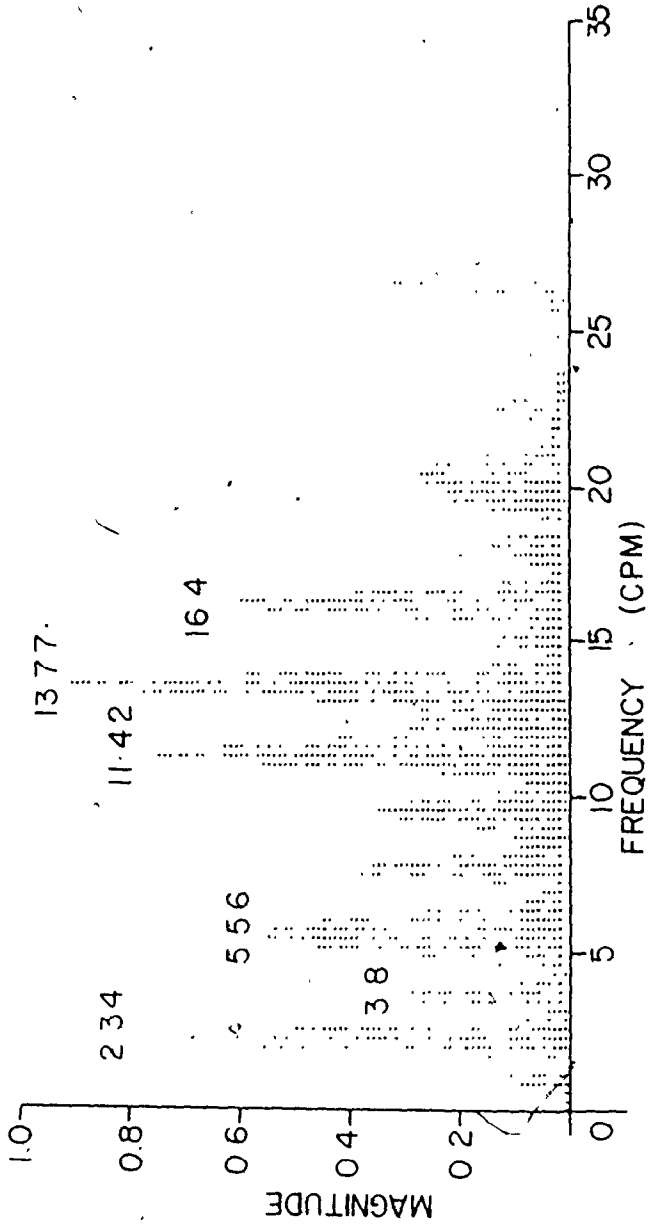

Fig. 6.17 b The power spectrum of a signal recorded from E4 in the sigmoid colon of the patient of Fig. 6.16, computed with a frequency resolution of 0.293 cpm

TABLE 6.7

MEAN FUNDAMENTAL PEAK FREQUENCIES

IN SIGMOID COLON

Number of Patients	lower freq. range 2-7 cpm			higher freq. range 8-12 cpm		
	number of observations	mean	standard deviation	number of observations	mean	standard deviation
1	19	4.00	±1.23	19	10.28	±0.67
1	-	-	-	64	10.89	±0.32
1	44	4.63	±1.15	44	10.19	±0.83
1	83	3.93	±1.29	83	10.00	±1.02
4	146	4.15	±1.28	210	10.34	±0.88

TABLE 6.8

PRESENCE OF SECOND HARMONIC FREQUENCY

COMPONENT IN SIGMOID COLON

number of patients	lower freq. range 2-7 cpm			higher freq. range 8-12 cpm		
	number of observations	%ℓ	%h	number of observations	%ℓ	%h
1	19	26.31	21.05	19	47.36	5.26
1	-	-	-	64	32.81	0.00
1	44	22.72	36.36	44	43.18	11.36
1	83	30.12	16.86	83	44.57	6.02
4	146	27.39	23.28	210	40.95	5.23

where

% ℓ denotes the percentage of time in which the intensity of second harmonic is less than the intensity of fundamental but greater than 10% of it.

and

%h denotes the percentage of time in which the intensity of second harmonic is greater than the intensity of fundamental.

The control waves were not phase-locked over a 10 minute period (4 patients) in the longitudinal direction whereas in one patient (Figs. 6.14 and 6.15) the frequency of the ECA and its phase-locking pattern in the longitudinal direction were the same as in the transverse colon.

6.3.2 Relationship Between ECA Frequency and Repetition Rate of Response Potentials in Human Colon

In addition to Electrical Control Activity, two other types of electrical activities were observed in the human colon. The first activity was ERA (Figs. 6.8, 6.14 & 6.20) which was related to the ECA in a similar manner to that in stomach and small intestine. The second activity, wherein the duration of a group of consecutive spikes was longer than that of a control cycle (Figs. 6.18 & 6.19) was called Segmental Response Activity (SRA) since it has been associated with segmental contractions in the human distal colon (Sarna et al., unpublished).

In Figs. 6.8, 6.9, 6.14, 6.15, 6.20 & 6.21 when the strongest frequency component (the one with the highest intensity) of the control waves was the fundamental frequency, the repetition rate of response potentials was the same as that of the fundamental frequency. In Figs. 6.20 & 6.21 when the strongest frequency component of the control wave was the second harmonic, the repetition rate of the response potentials was the same as that of the second harmonic frequency component (the repetition rate of response potentials changed in the same patient within a 4 minute period). However, there were instances (in all patients) when the repetition rate of response potentials was less than that of the strongest frequency component of the corresponding control wave (which is consistent with the definitions of chapter 1).

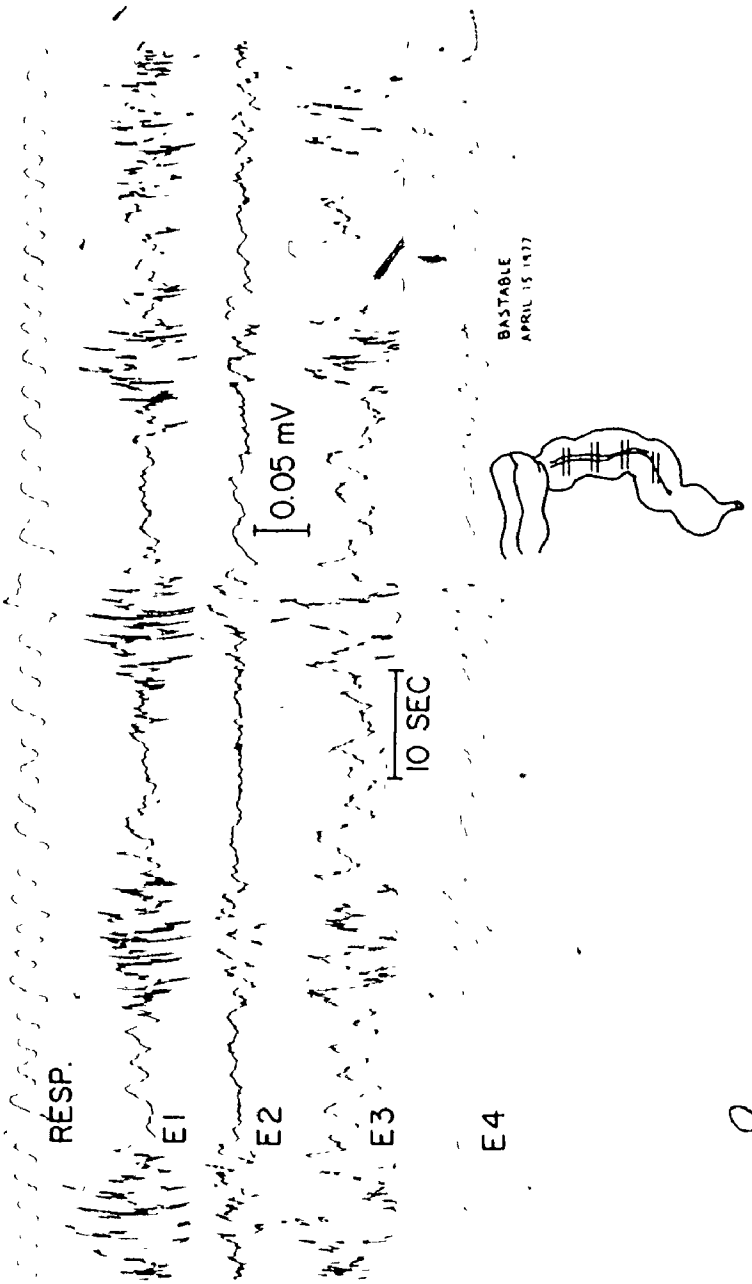

Fig. 6.18 a Human colonic electrical activity recorded from 4 sets of bipolar electrodes placed subserosally on the taenia coli of descending and sigmoid colon. E1 and E2 were placed in the descending colon whereas E3 and E4 were placed in the sigmoid colon.

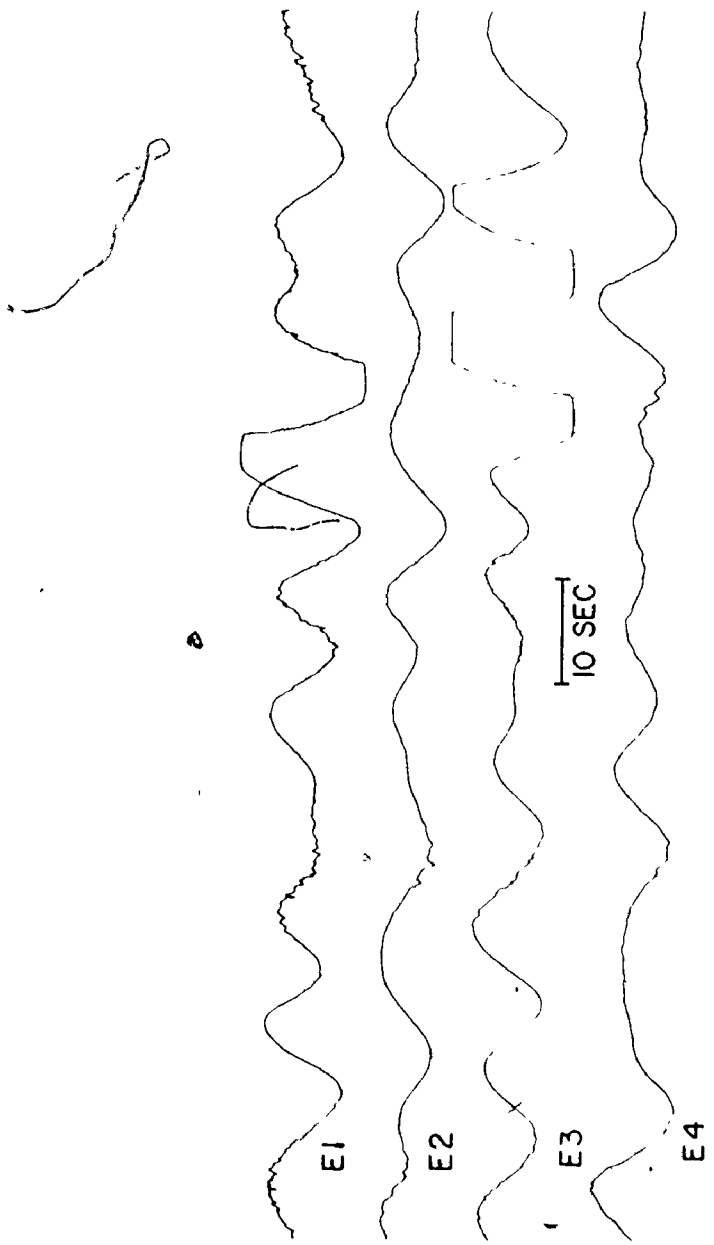

Fig. 6.18 b Band-pass filtering (2-5 cpm) of the human colonic electrical activity of Fig. 6.18 a

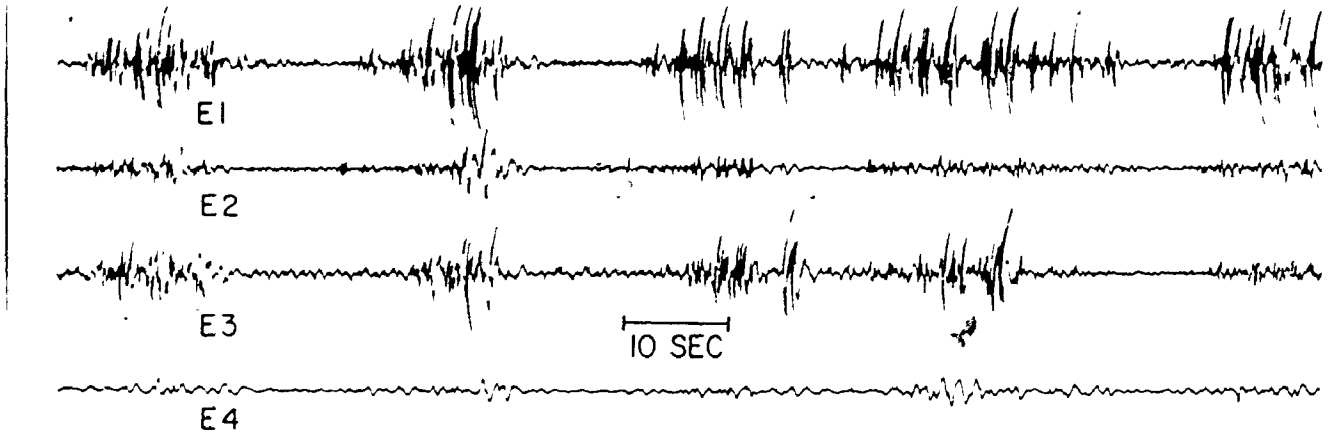

Fig. 6.18 c High-pass filtering (f_c = 20 cpm) of the human colonic electrical activity of Fig. 6.18 a

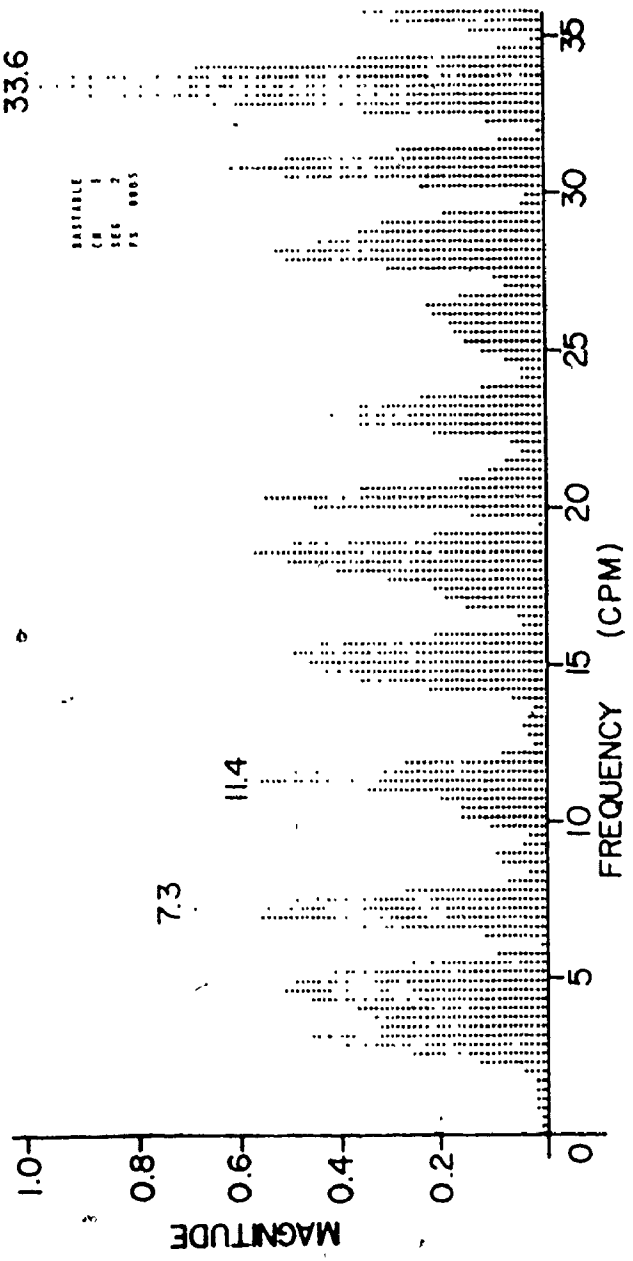

Fig. 6.19 a The power spectrum of a signal recorded from E1 in the descending colon of the patient of Fig. 6.18, computed with a frequency resolution of 0.293 cpm

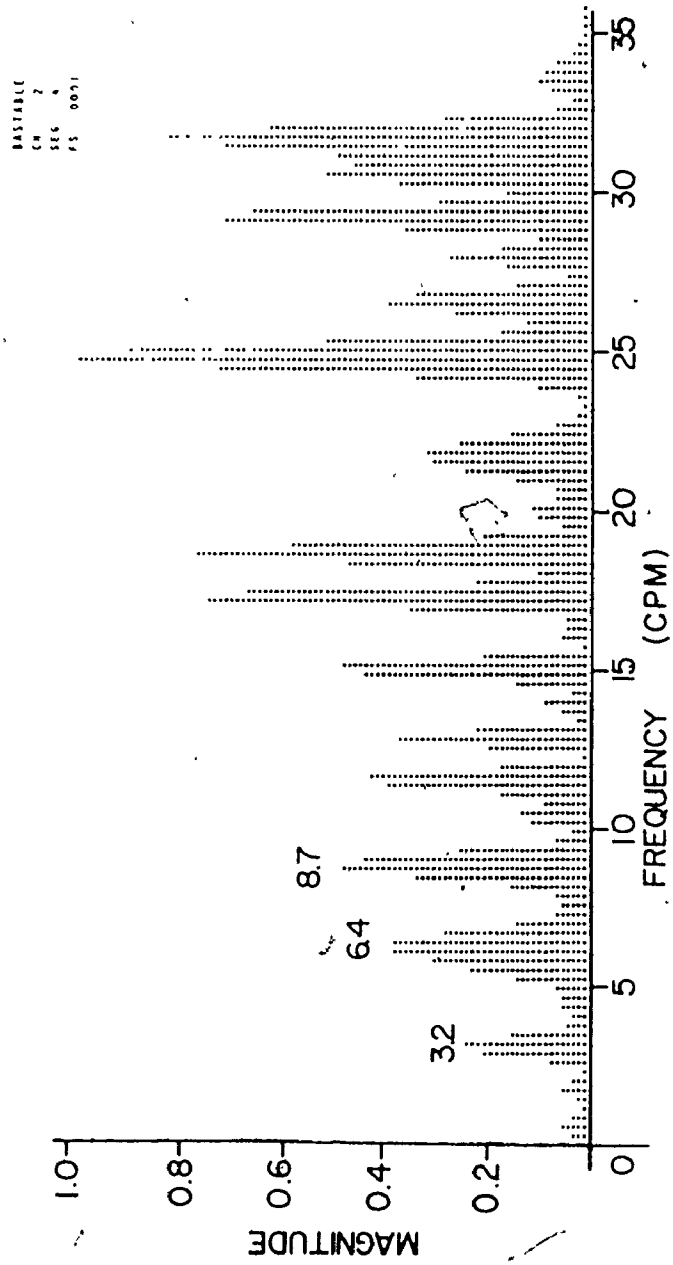

Fig. 6.19 b The power spectrum of a signal recorded from E2 in the descending colon of the patient of Fig. 6.18, computed with a frequency resolution of 0.293 cpm

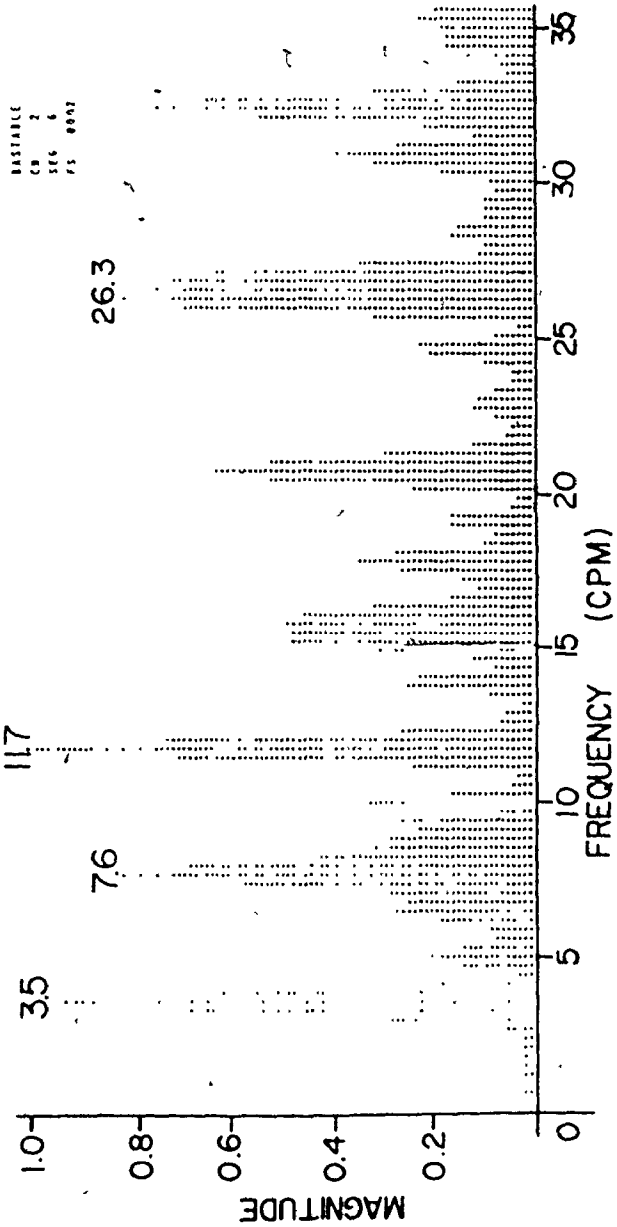

Fig. 6.19 c The power spectrum of signal recorded from E2 in the descending colon of the patient of Fig. 6.18, computed with a frequency resolution of 0.293 cpm

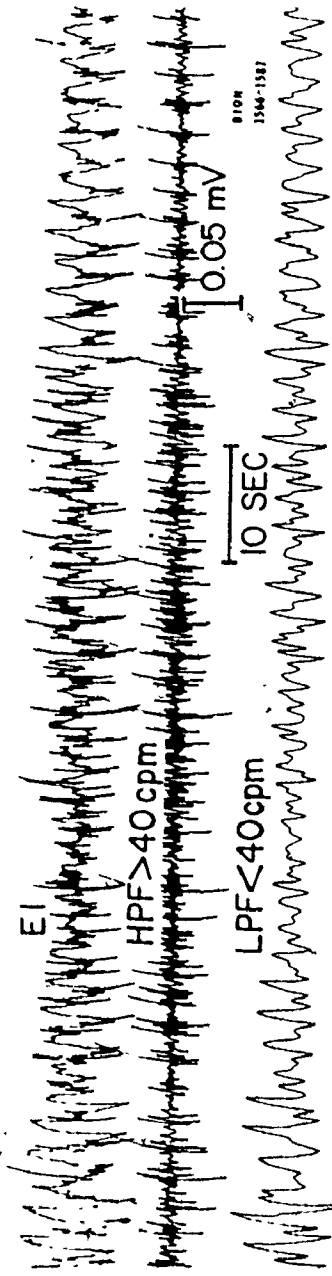

Fig. 6.20 Human colonic electrical activity recorded from E1 in the descending colon of the patient of Fig. 6.14

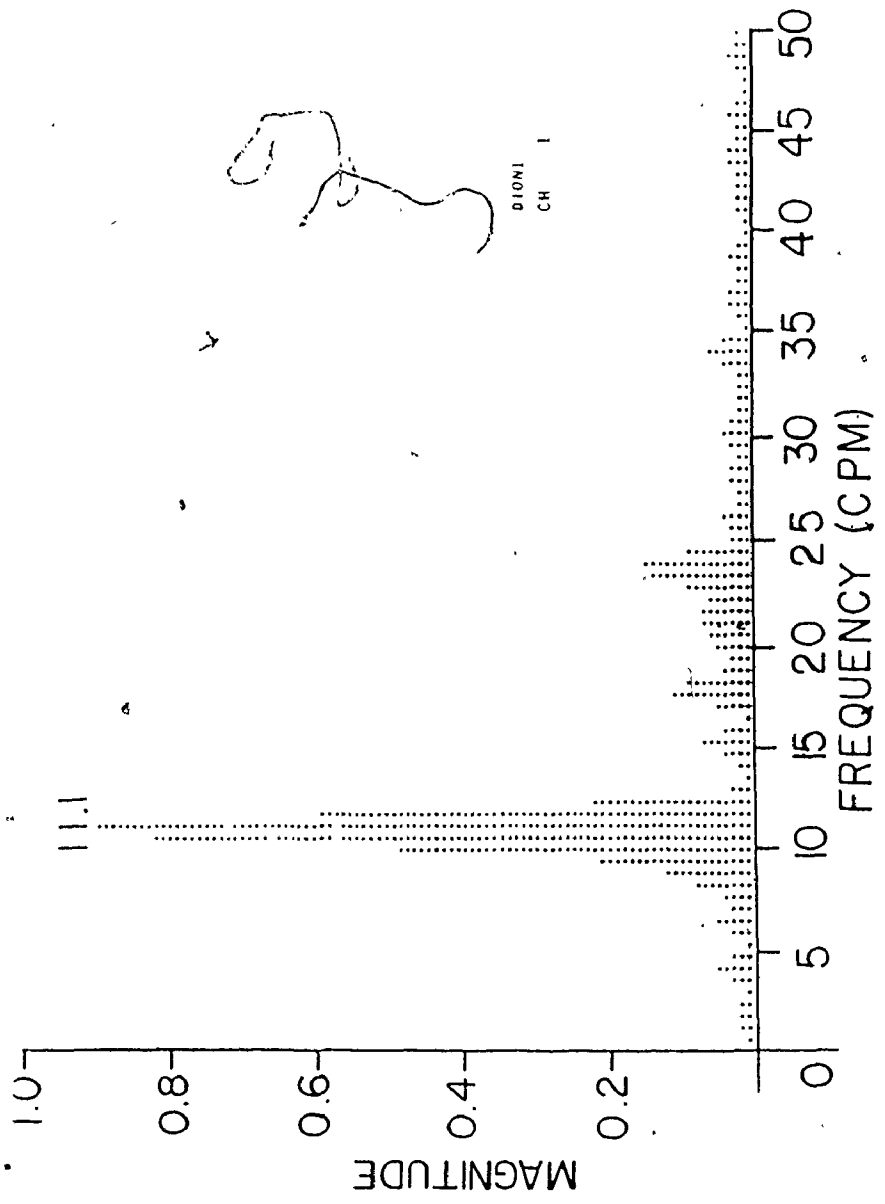

Fig. 6.21 a The power spectrum of the signal recorded from E1 of Fig.. 6.20 computed over a 0.5 minute time segment in the first quarter time interval

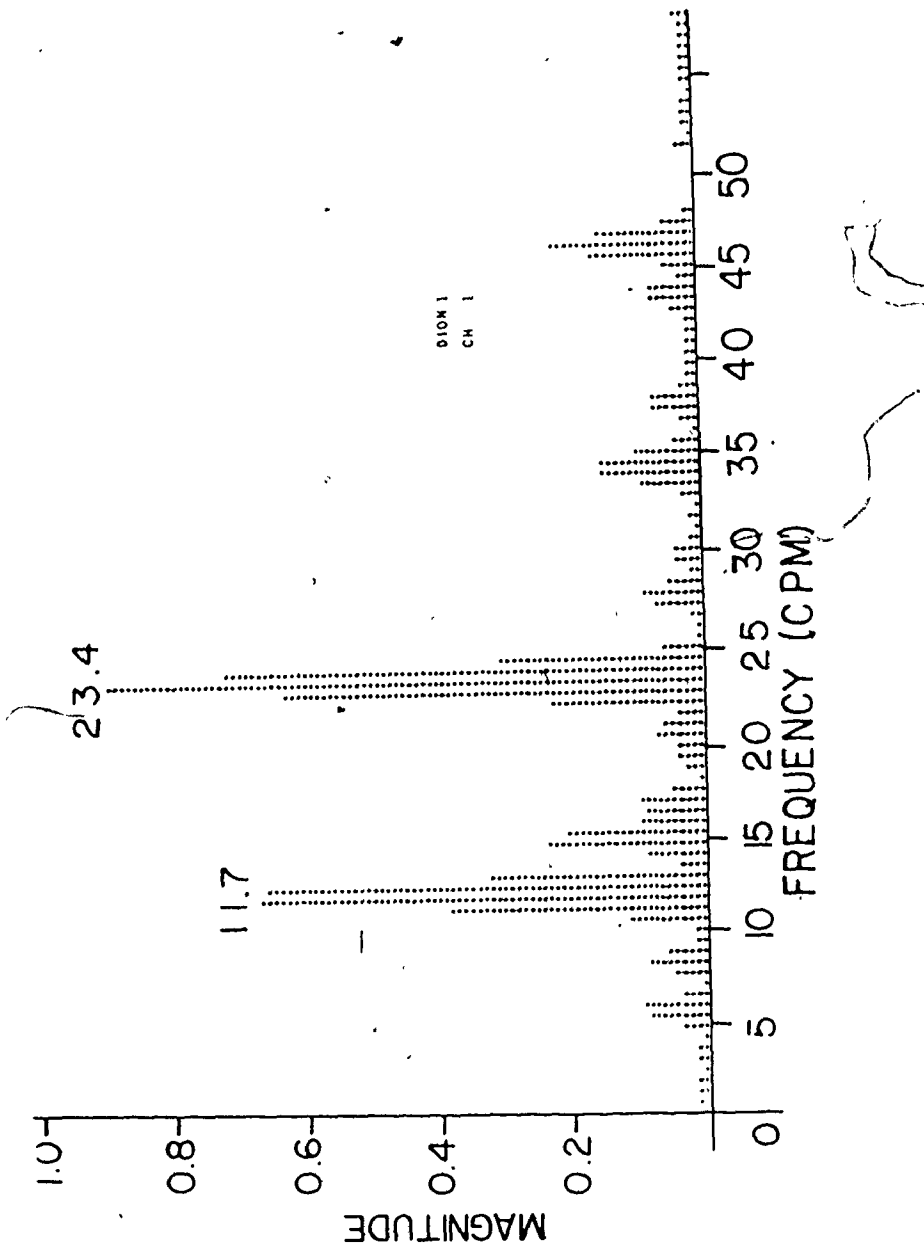

Fig. 6.21 b The power spectrum of the signal recorded from E1 of Fig. 6.20 computed over a 0.5 minute time segment in the second quarter time interval

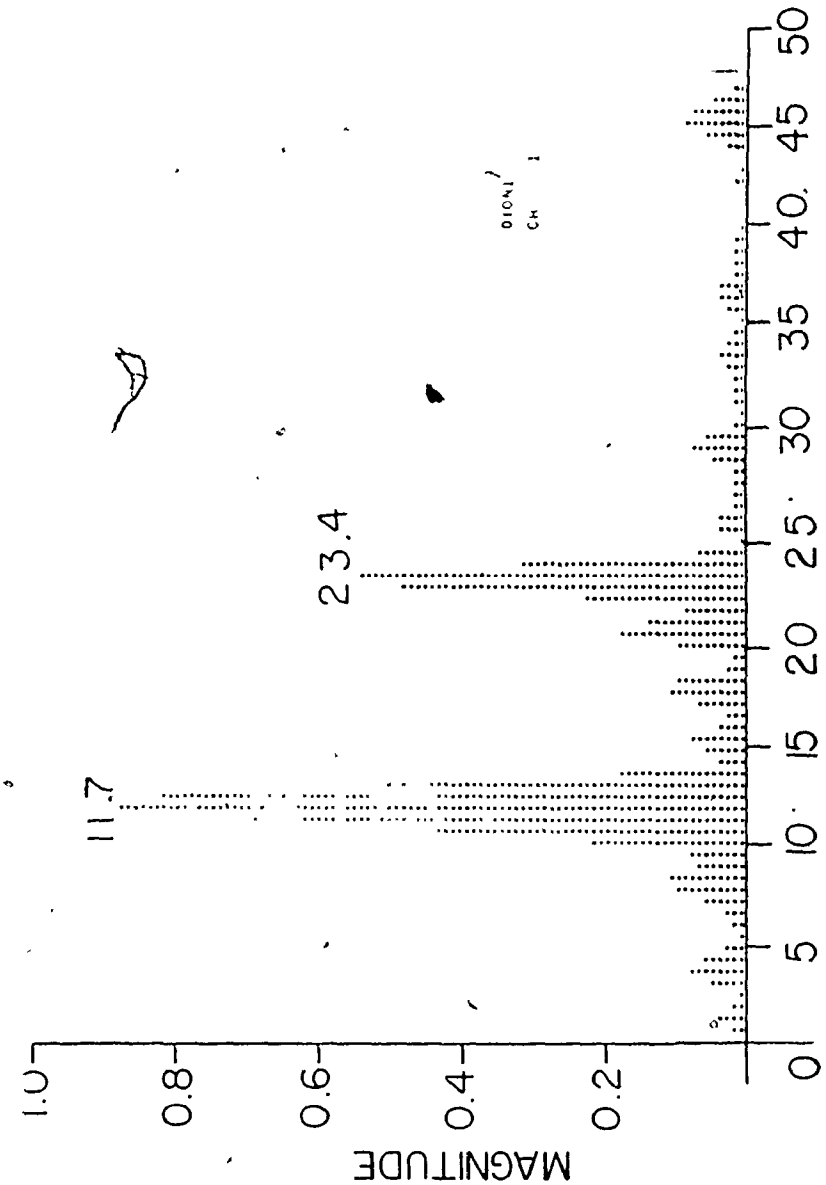

Fig. 6.21 c The power spectrum of the signal recorded from E1 of Fig. 6.20 computed over a 0.5 minute time segment in the third quarter time interval

6.3.3 Effects of Morphine and Feeding

An intramuscular injection (10 patients) of morphine (5-10 mg) or Demoral (75-100 mg) produced ERA (Fig. 6.22) 5-20 minutes after the injection without changing the ECA frequency.

Feeding (10 patients) produced intermittent ERA and SRA (Fig. 6.23) within a 3 hour period (with SRA mainly in transverse, descending and sigmoid colon) without changing the ECA frequency. Feeding immediately produced ERA (in the transverse colon of one patient and sigmoid colon of one patient) and SRA (in the descending and sigmoid colon of one patient), without changing the ECA frequency, thereafter intermittent ERA and SRA were observed within a 3 hour period.

6.4 Discussion

The ECA was found to be continuously present in the human colon but with waxing and waning of the amplitude of control waves. Provenzale and Pisano (1971) reported a similar finding whereas Taylor et. al. (1974, 1975) reported the presence of silent periods, wherein the human colonic ECA was not present, however in their illustrative records no such periods were prominent but rather an irregular control wave (with waxing and waning amplitude and time varying frequency) seemed to be present.

The role of the human colonic ECA is hypothesized to be similar to that in the stomach and small intestine, that is, to control the appearance of ERA, and hence of muscular contractions, in time and space. Furthermore, it is hypothesized that the frequency components of a control wave and their intensities form a major factor in determining the repetition rate of the response potentials since they determine the portions

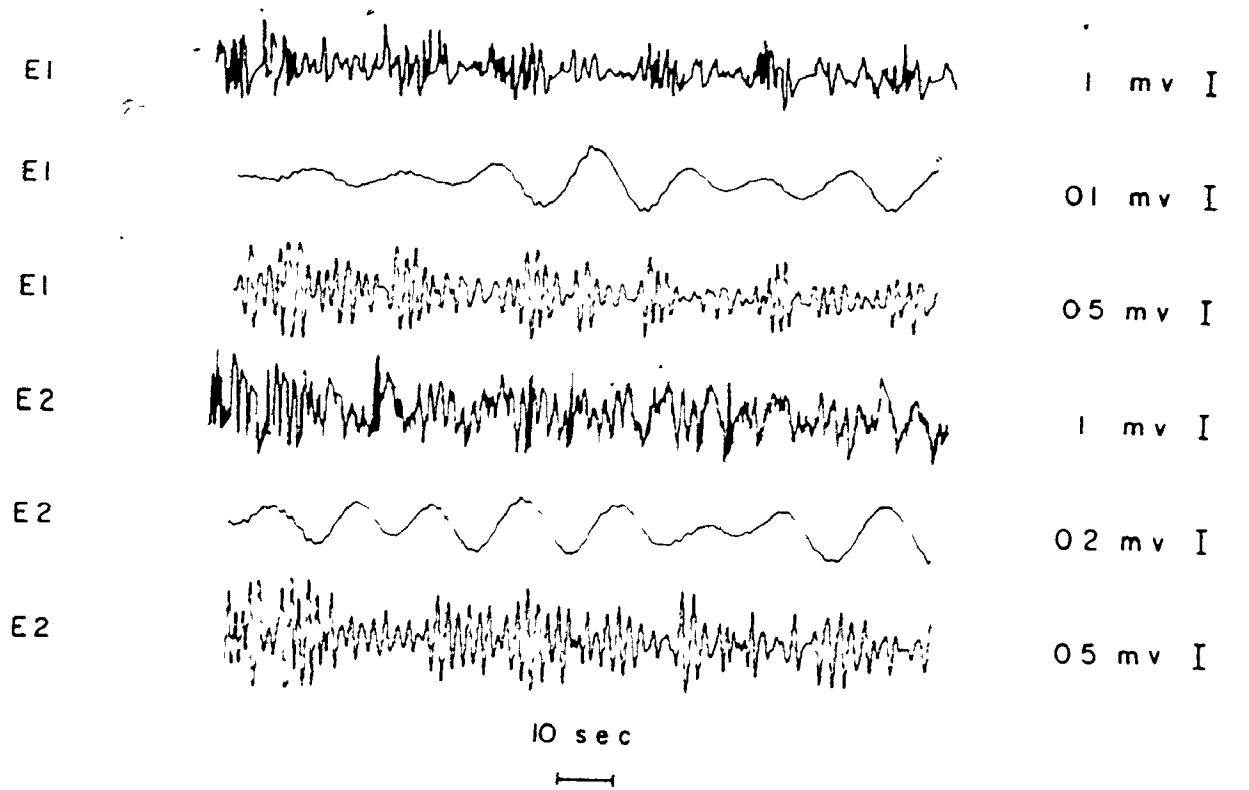

Fig. 6.22 a Human colonic electrical activity recorded from the ascending colon 10 minutes after an intramuscular injection of morphine (10 mg). For each electrode, the middle trace is low-pass filtered (f_c = 0.275 Hz) whereas the lower trace is high-pass filtered (f_c = 20 cpm).

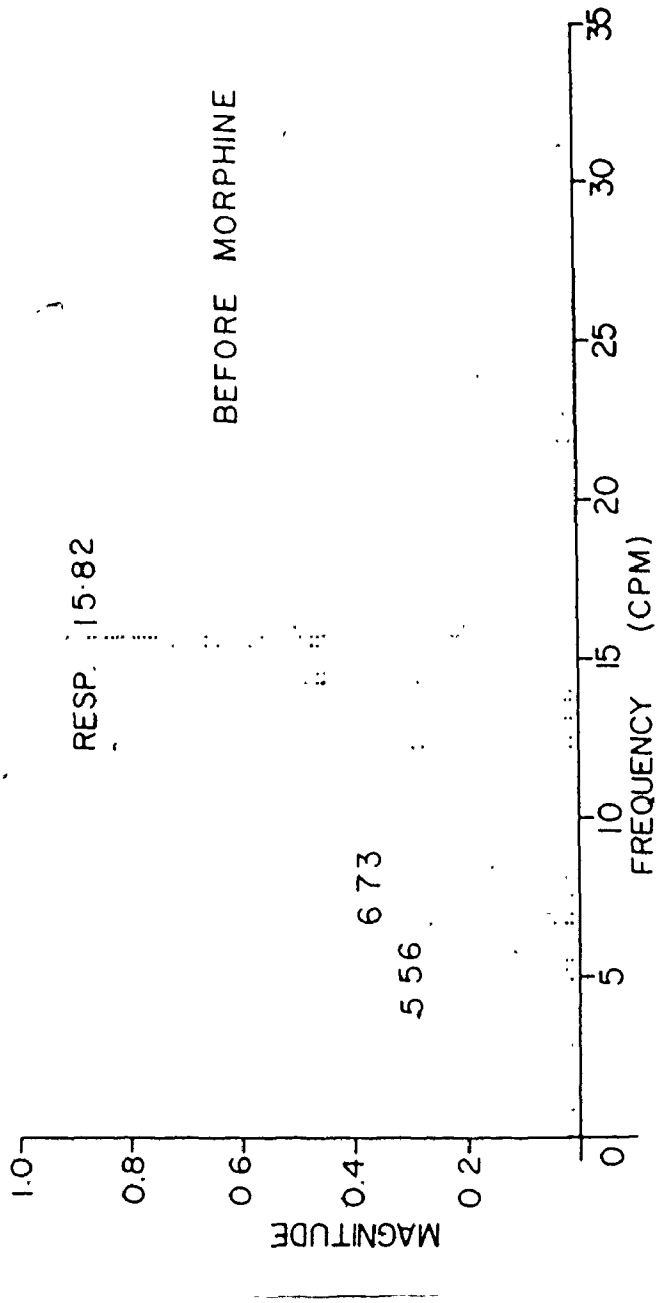

Fig. 6.22 b The power spectrum of a signal recorded from E2, before the morphine injection, computed with a frequency resolution of 0.293 cpm

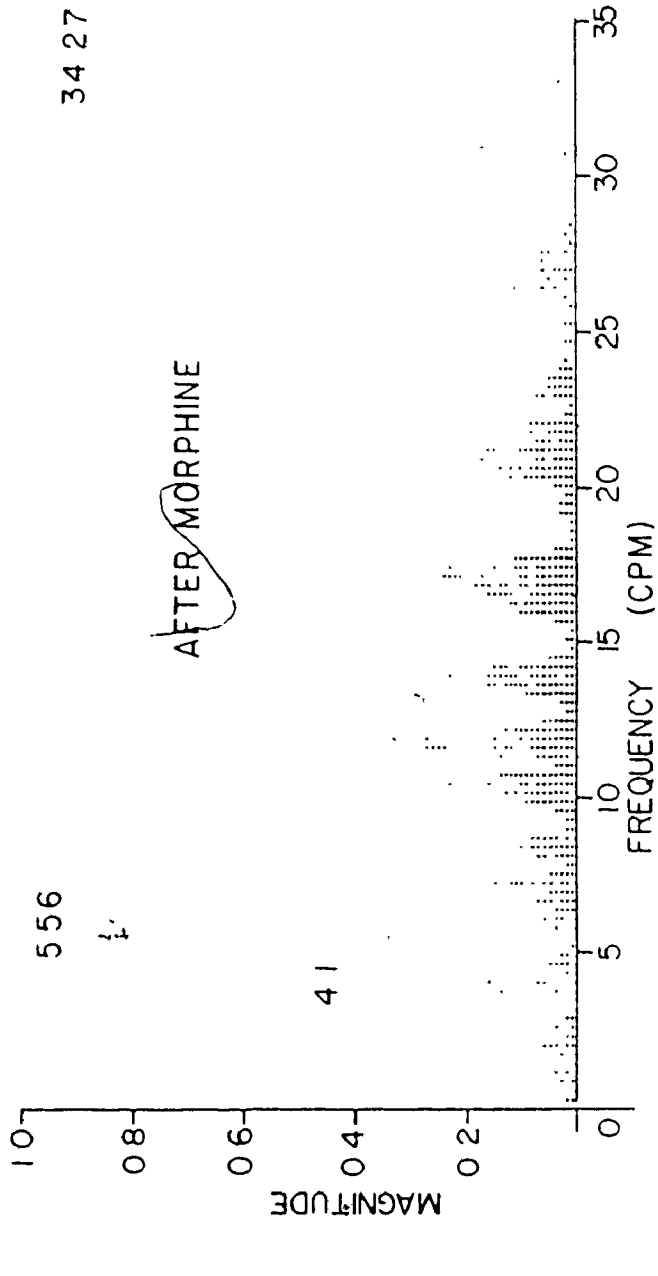

Fig. 6.22 c The power spectrum of a signal recorded from E2, after the morphine injection, computed with a frequency resolution of 0.293 cpm

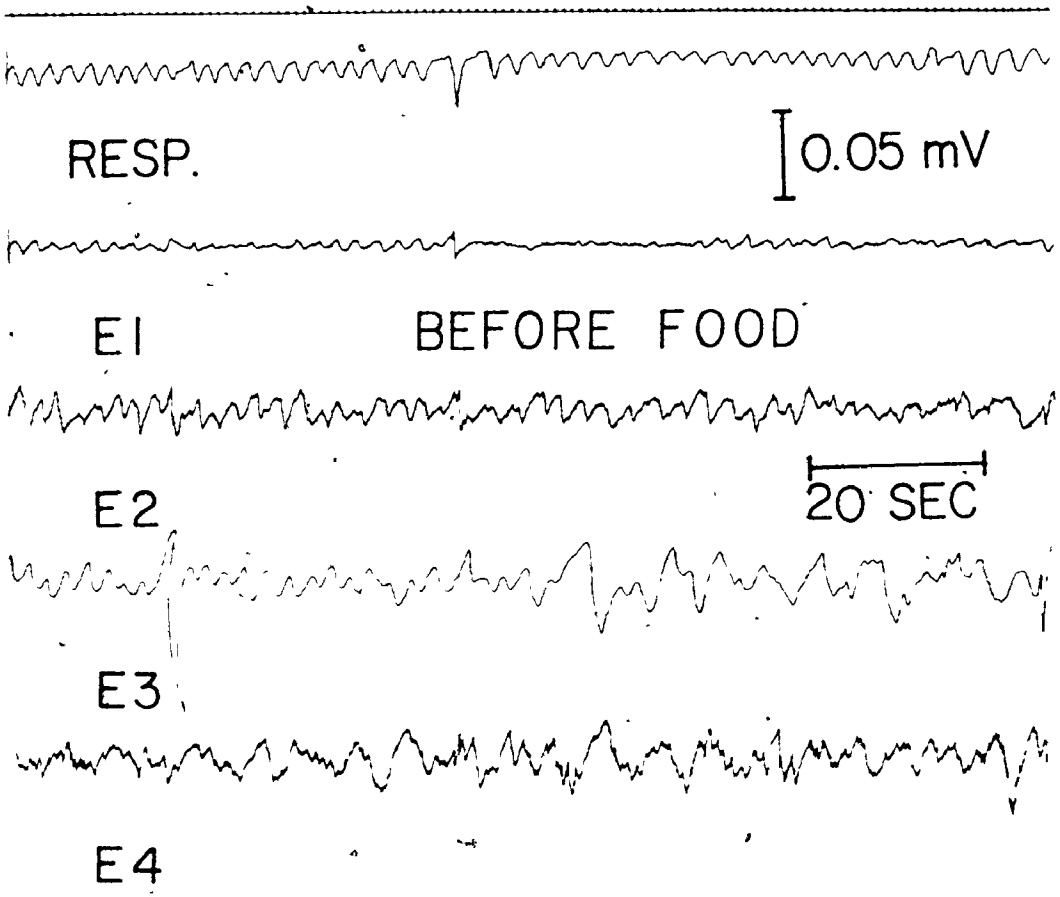

Fig. 6.23 a Human colonic electrical activity recorded from the descending and sigmoid colon, of the patient of Fig. 6.16, before food

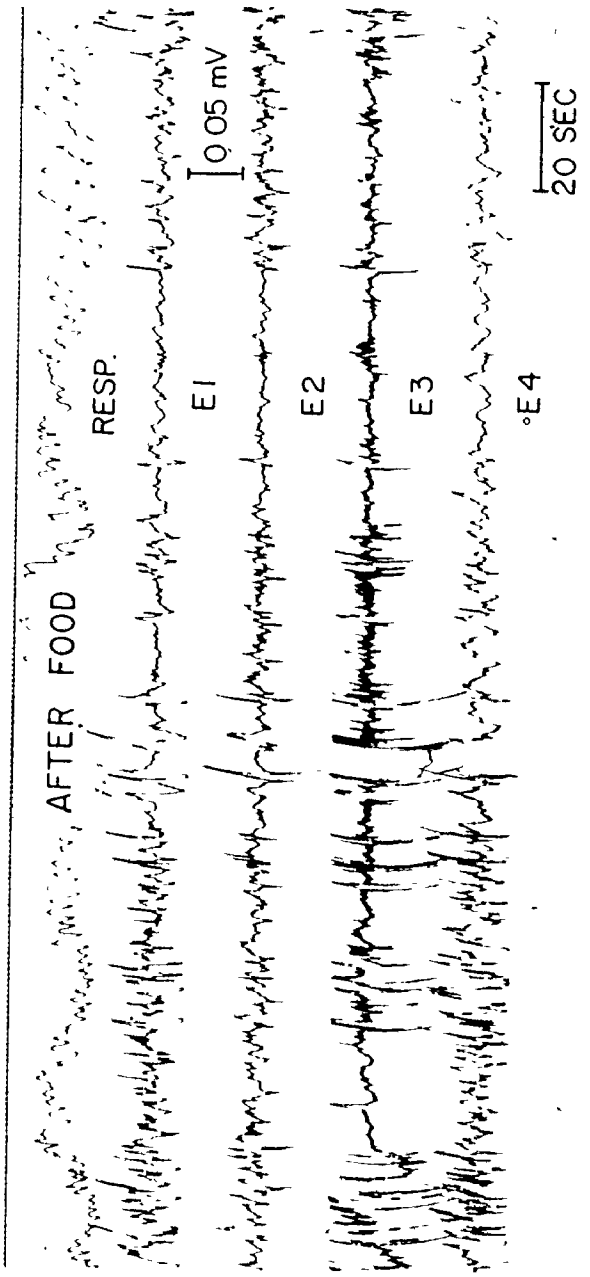

Fig. 6.23 b Human colonic electrical activity recorded from the descending and sigmoid colon of the patient of Fig. 6.16, immediately after eating

of the control cycle which exceed an excitation threshold (Golenhofen 1970, page 339) above which response potentials appear.

The excitation threshold may be influenced by other factors as well such as neural and hormonal inputs.

The analysis results may be summarized as follows:

1. The ECA is continuously present in the human colon with waxing and waning of the amplitude of control waves.
2. The control waves are not continuously phase-locked in either the longitudinal direction (ascending, transverse, descending, and sigmoid colon) or in the circumferential direction (ascending and transverse colon), but remain phase-locked for longer durations in the transverse colon.
3. The control waves have fundamental peak frequencies in the range of 9-12 cpm in the transverse colon, whereas their fundamental peak frequencies in the rest of the colon lie within a lower frequency range of 2-7 cpm and a higher frequency range of 8-12 cpm.
4. Multiple fundamental peak frequencies as well as up to fourth harmonic peak frequencies of the control waves are prominent (mainly in ascending, descending and sigmoid colon). The intensities of the harmonic peak frequencies may be larger than those of the fundamental peak frequencies.
5. In the power spectra of the human colonic ECA both the frequency components and their intensities vary in time and space.
6. The repetition rate of response potentials, when present, at any one site is less than or equal to that of the strongest frequency component of the control wave at that site.

CHAPTER 7

A MODEL OF THE ECA IN HUMAN COLON

7.1 Introduction

Christensen et al. (1969, 1971a, 1971b, 1972, 1974) demonstrated that the ECA in isolated cat colon is myogenic in nature and behaves like a system of coupled relaxation oscillators. Vanasin et al. (1971) reported the presence of control waves in isolated muscle strips from human taenia coli, whose frequencies were not the same in different strips obtained from different regions of the taenia coli and also were not the same as the in vivo frequencies in comparable intact regions, suggesting that the ECA in human colon may also behave like a system of coupled relaxation oscillators.

Linkens et al. (1976b) used two oscillator rings connected in parallel, where each ring contained four bidirectionally coupled Van der Pol oscillators, to model the ECA in human rectosigmoid. The oscillators could oscillate in three different modes and these could be switched by direct injection of either external switching stimuli or white noise, or alternatively, by random changes within the model by perturbing one or more of the intrinsic frequencies., To reproduce periods of no electrical activity, summation of the outputs of adjacent oscillators was necessary, thus attributing the periods of no electrical activity to the summative effects of extracellular recording. Introducing an additional

parameter into the Van der Pol equation forced the no electrical activity mode without the need for summation of adjacent oscillator outputs but required an in situ decrease in that parameter value to zero in order to reproduce periods of electrical activity. Alternatively they used two bidirectionally coupled "hard-excited" relaxation oscillators, where each oscillator was represented by a modified Van der Pol equation to obtain different modes of oscillation without the need for a ring structure or for summation of adjacent oscillator outputs but an external switching stimulus was still necessary. One of the main features of their model was the presence of periods of no electrical activity, this feature was not present in our data of the ECA in human colon (see Chapter 6).

This chapter presents a model of the ECA in human colon using bidirectionally coupled rings of bidirectionally coupled SROs (see chapter 5). The parameters of a SRO at any one site are the coefficients of a truncated Fourier series representation of the control wave at that site when it is electrically isolated from its neighbouring oscillators and may be experimentally estimated using Fast Fourier Transformation of time sequences acquired from electrically isolated muscle strips. Non-physiological inputs to the SROs are not required to simulate any of the observed characteristics of human colonic ECA.

7.2 The Generic Equation

A value of $K_n = 4$ was chosen (which was found to be adequate in reproducing the observed features of the human colonic ECA) and substituted in equations (5.8a) and (5.8c) to obtain the model's generic equation, namely,

$$\dot{x}_{1n} = \omega_n[\{b_{1n}\}\{x_{2n}(1 + \kappa_n) + \rho_n(1 - \rho_n^2 - x_{2n}^2)\}$$

$$+ \{-\rho_n(1 + \kappa_n) + x_{2n}(1 - \rho_n^2 - x_{2n}^2)\}$$

$$\{a_{1n} - 3a_{3n} + 4(a_{2n} - 4a_{4n})x_{2n}$$

$$+ 12a_{3n}x_{2n}^2 + 32a_{4n}x_{2n}^3\}] \qquad (7.1a)$$

$$\dot{x}_{2n} = \omega_n[-\rho_n(1 + \kappa_n) + x_{2n}(1 - \rho_n^2 - x_{2n}^2)] \qquad (7.1b)$$

where

$$\rho_n = \frac{1}{b_{1n}}[a_{2n} - a_{0n} - a_{4n} + x_{1n} - (a_{1n} - 3a_{3n})x_{2n}$$

$$-2(a_{2n} - 4a_{4n})x_{2n}^2 - 4a_{3n}x_{2n}^3$$

$$-8\,a_{4n}\,x_{2n}^4] \qquad (7.1c)$$

$$\kappa_n = \sum_{m \in I_{cn}} c_{mn}(x_{1m} - x_{1n}) \qquad (7.1d)$$

$$n = 1, \ldots, N_p$$

All symbols are as defined in Chapter 5.

7.3 The Model Structure

An interacting population of 99 SROs was used to simulate the in vivo features of the ECA in human colon. The population was arranged in a tubular structure of 33 bidirectionally coupled rings where each ring consisted of 3 bidirectionally coupled SROs as shown in Fig. 7.1. The first 9 rings (comprising SROs 1-27) simulated the ECA in

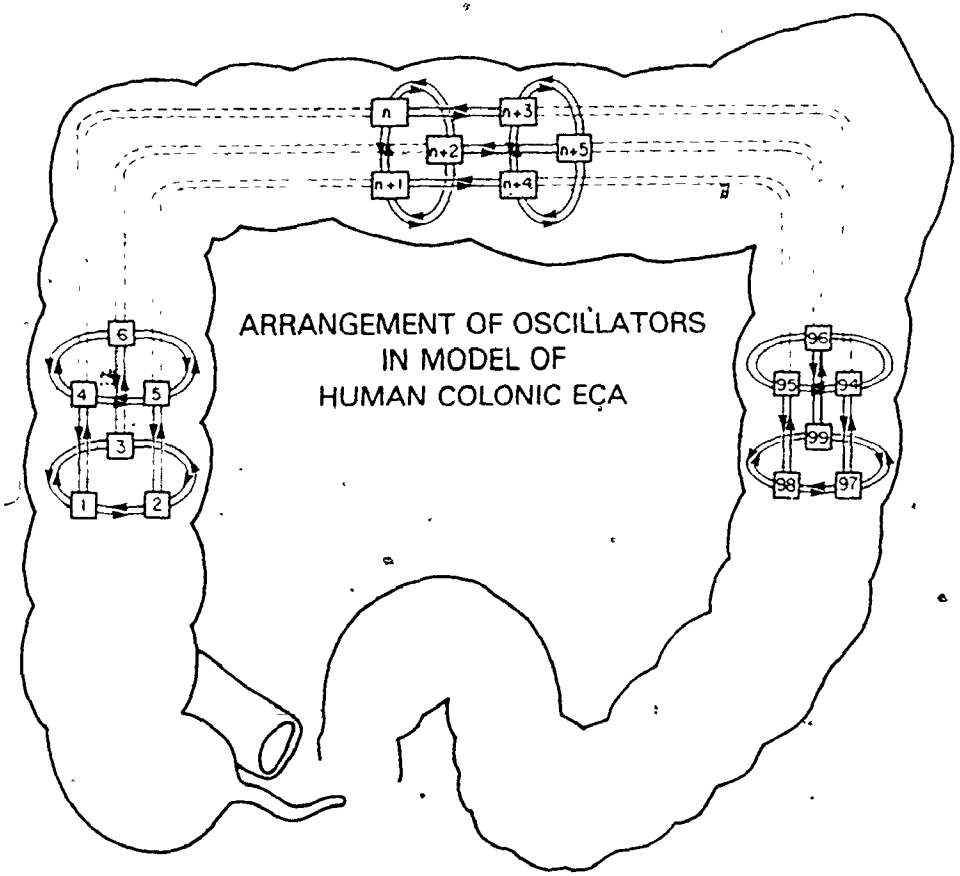

Fig. 7.1 Arrangement of oscillators in model of human colonic ECA

ascending colon and the next 12 rings (comprising SROs 28-63) simulated the ECA in transverse colon, whereas the last 12 rings (comprising SROs 64-99) simulated the ECA in descending and sigmoid colon. The model parameters, which comprise the intrinsic parameters of the SROs and their coupling factors, are given in Table 7.1. The intrinsic frequency gradients in the longitudinal and circumferential directions are depicted in Fig. 7.2.

7.4 The Simulation Program

A user-oriented interactive computer program package SISYPHUS was developed using Fortran as the programing language and implemented on NOVA 830 minicomputer. A fortran listing is given elsewhere (Bardakjian 1978b). The package contains a main program which organizes a "user-computer" dialogue which allows the user to respond to computer instructions by entering numbers specifying the number of oscillators in the population along with the intrinsic parameters and coupling factors associated with each oscillator, also, the parameters necessary for the numerical algorithm such as the time segment for which the solution is to be computed, the time intervals between successive solution samples and the initial step size, or entering words (Yes or No), which are identified by subroutine YON, to activate options such as writing only the output variables (in order to save space) rather than all the state variables into a disk file and run-time monitoring of the computation in a graphical or tabular form. Stimulation options allow each oscillator to be stimulated by a specified stimulus at a specified time and for a specified duration. For each time sample in the specified time segment at which the solution is to be computed, the set of first order non-linear

TABLE 7.1

THE MODEL PARAMETERS

Oscillator Numbers			Intrinsic freq. in cpm			$a_{2i}=a_{2j}=a_{2k}$	$a_{3i}=a_{3j}=a_{3k}$	$a_{4i}=a_{4j}=a_{4k}$	$c_{ij}=c_{ji}=c_{jk}=c_{kj}=c_{ki}=c_{ik}$	$c_{ip}=c_{pi}=c_{jq}=c_{qj}=c_{kr}=c_{rk}$
i	j	k	f_i	f_j	f_k					
1	2	3	2.75	2.5	3	2	0.8	0.4	0.1	0.1
4	5	6	3	2.75	3.5	0.8	2	0.4	0.101	0.101
7	8	9	4	3.5	4.5	2	0.8	0.4	0.102	0.102
10	11	12	5	4.5	5.5	2	0.8	0.4	0.103	0.103
13	14	15	6	5.5	6.5	0.8	0.4	0.2	0.104	0.104
16	17	18	7	6.5	7.5	0.8	0.4	0.2	0.105	0.105
19	20	21	8	7.5	8.5	0.8	0.4	0.2	0.106	0.106
22	23	24	9	8.5	9.5	0.8	0.4	0.2	0.108	0.108
25	26	27	10	9.5	10.5	0.2	0.8	0	0.11	0.11
28	29	30	10.2	10.4	10.6	0.8	0.2	0	0.112	0.112
31	32	33	10.4	10.2	10.8	0.8	0.2	0	0.114	0.114
34	35	36	10.6	10.8	11	0.8	0.2	0	0.116	0.116
37	38	39	10.8	10.6	11.2	0.8	0.2	0	0.118	0.118
40	41	42	11	11.2	11.4	0.8	0.4	0	0.12	0.12
43	44	45	11.2	11.4	10.8	0.2	0.8	0	0.125	0.125
46	47	48	11.4	11.2	11	0.8	0.4	0	0.13	0.13

contd.....

Table 7.1 (continued)

Oscillator Numbers			Intrinsic freq. in cpm			$a_{2i}=a_{2j}=a_{2k}$	$a_{3i}=a_{3j}=a_{3k}$	$a_{4i}=a_{4j}=a_{4k}$	$c_{ij}=c_{ji}=c_{jk}=c_{kj}=c_{ki}=c_{ik}$	$c_{ip}=c_{pi}=c_{jq}=c_{qj}=c_{kr}=c_{rk}$
i	j	k	f_i	f_j	f_k					
49	50	51	11.3	11	10.8	0.8	0.4	0	0.135	0.135
52	53	54	11.4	11.2	11	0.2	0.8	0	0.14	0.14
55	56	57	11.2	11.4	11.3	0.8	0.4	0	0.145	0.145
58	59	60	11	11.2	11.4	0.8	0.4	0	0.15	0.15
61	62	63	10.8	10.6	11.2	0.2	0.8	0	0.155	0.155
64	65	66	10.6	10.8	11	0.8	0.4	0	0.16	0.16
67	68	69	10.4	10.2	10.8	0.8	0.2	0	0.165	0.165
70	71	72	10.2	10.4	10.6	0.8	0.2	0	0.17	0.17
73	74	75	10	9.5	10.5	0.8	0.2	0	0.172	0.172
76	77	78	9	8.5	9.5	0.8	0.2	0	0.174	0.174
79	80	81	8	7.5	8.5	0.8	0.2	0	0.176	0.176
82	83	84	7	6.5	7.5	0.8	0.2	0	0.178	0.178
85	86	87	6	5.5	6.5	0.8	0.2	0	0.18	0.18
88	89	90	5	4.5	5.5	2	0.4	0	0.182	0.182
91	92	93	4	3.5	4.5	2	0.4	0	0.184	0.184
94	95	96	3	2.75	3.5	0.4	2	0.2	0.186	0.186
97	98	99	2.75	2.5	3	0.2	0.4	2	0.188	0

where

$p = i + 3$ for all i
$q = j + 3$ for all j
$r = k + 3$ for all k

and $a_{0n} = a_{1n} = b_{1n} = 1$ for $n = 1,\ldots,99$

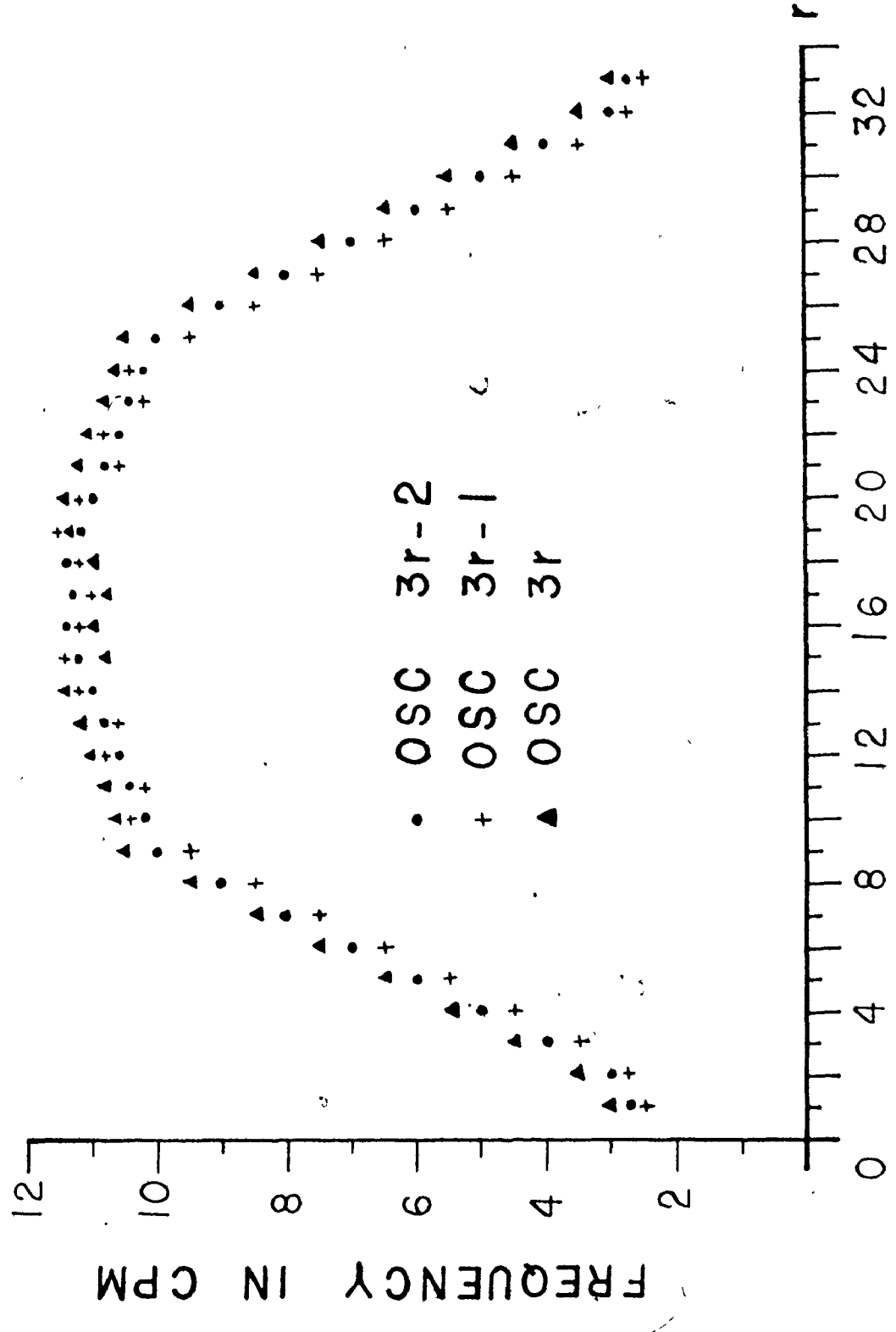

Fig. 7.2 Intrinsic frequency gradients in the longitudinal (along the r axis) and circumferential directions of ECA model

differential equations (7.1), prescribed by the subroutine F, is numerically solved via subroutine DASCRU using an automatic step change Merson differential equation solver (Christiansen 1970). Figure 7.3 depicts the calling sequence of the subroutines DASCRU and F by SISYPHUS. After the solution is computed for the specified time, the user has the option of terminating the simulation run or continuing the computation of solution for another segment of time (with or without changing one or more of the model or stimulation parameters). When the simulation run is terminated the model parameters, the stimulation parameters and the final conditions of the simulation run are saved in appropriate disk files which may be used to initiate subsequent simulation runs at a later date. The outputs of the oscillators are also saved in a disk file appropriate for output display either by using a digital-to-analog converter and a chart recorder or using a graphics package on a CRT screen of a computer terminal or a line printer.

7.5 Simulation Results

For the coupled population, the outputs of all oscillators are depicted in Appendix II. Eight oscillator outputs representing a few sites in the model's ascending, transverse, descending, and sigmoid colon are depicted in Fig. 7.4 whereas their power spectra are depicted in Fig. 7.5 and their limit cycles in Fig. 7.6. The fundamental and harmonic peak frequencies as well as their intensities varied in time and space. The fundamental peak frequencies were within a frequency range of 9-12 cpm in the model's transverse colon, whereas they were within a lower frequency range of 2-7 cpm and a higher frequency range of 8-12 cpm in the model's ascending, descending and sigmoid colon. The

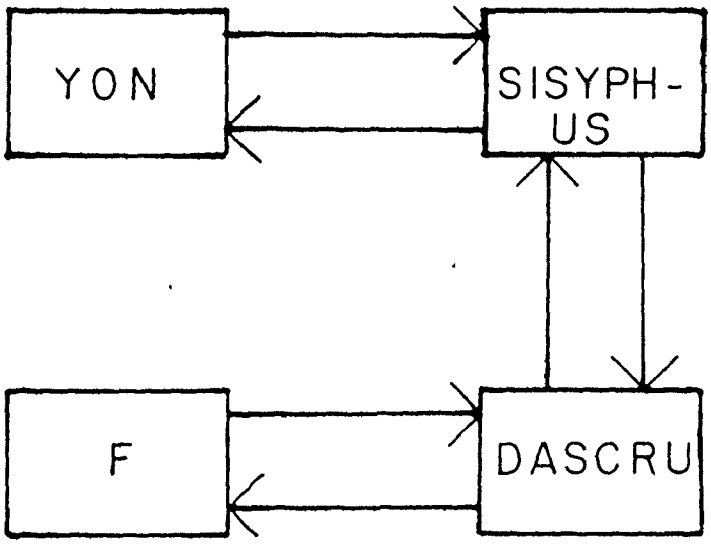

Fig. 7.3 A general structure of the simulation program SISYPHUS

Fig. 7.4 Oscillator outputs from the coupled population. For each oscillator output, the maximum amplitude is normalized to unity and the simulated time segment is of 2 minutes duration.

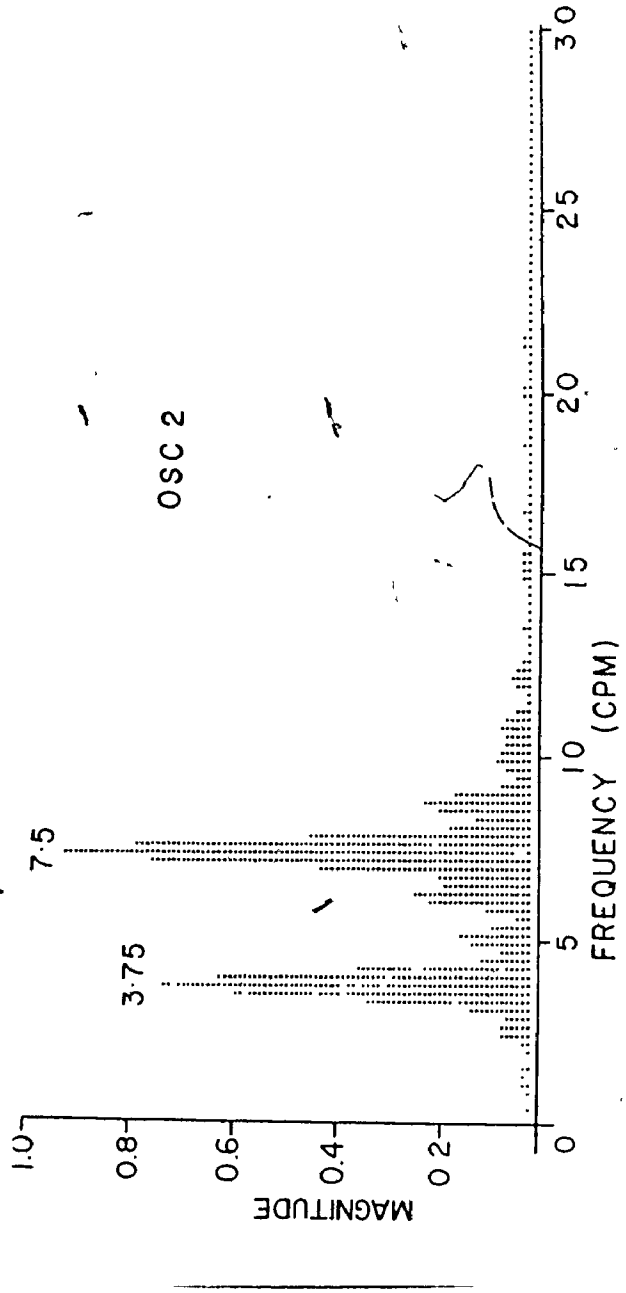

Fig. 7.5 a The power spectrum of an output from oscillator 2 in the model's ascending colon, computed with a frequency resolution of 0.234 cpm

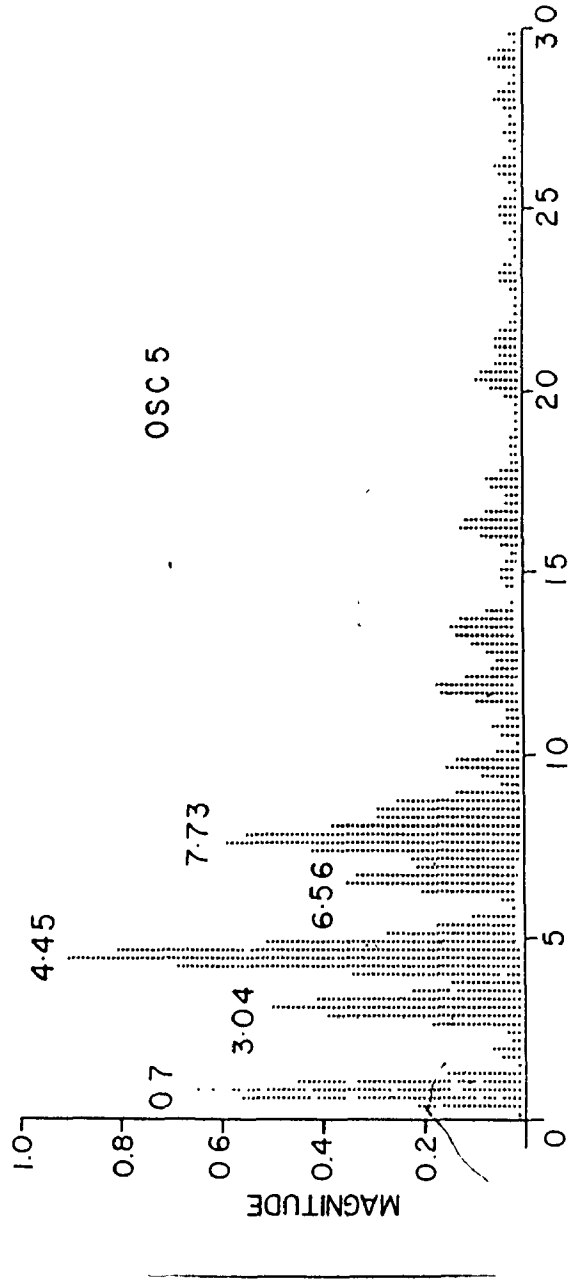

Fig. 7.5 b The power spectrum of an output from oscillator 5 in the model's ascending colon, computed with a frequency resolution of 0.234 cpm

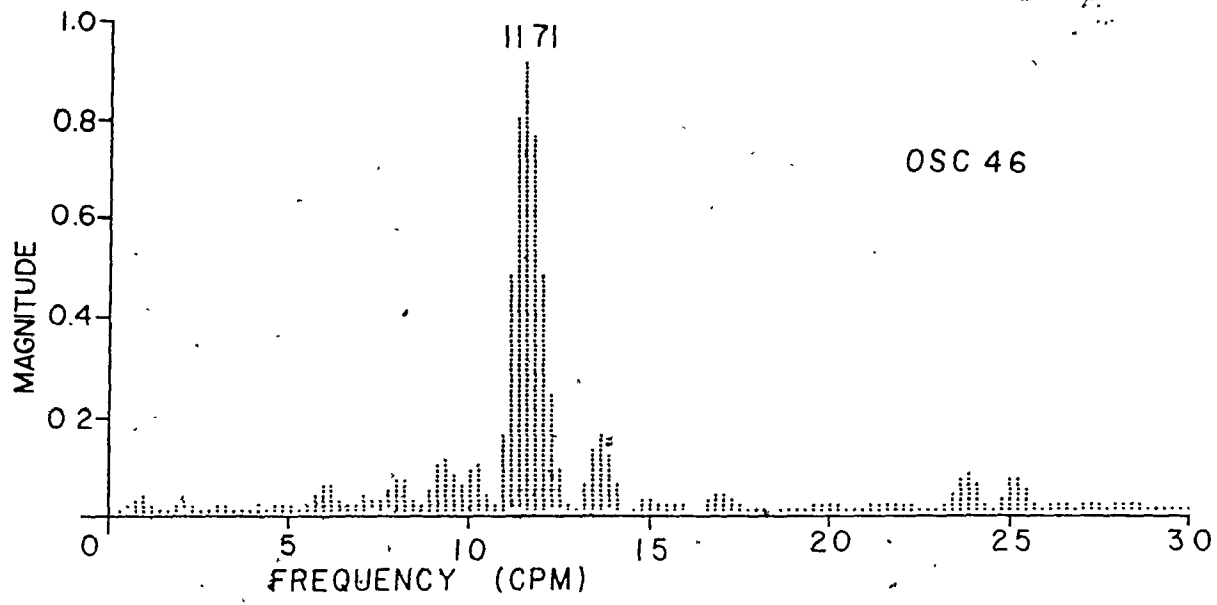

Fig. 7.5 c The power spectrum of an output from oscillator 46 in the model's transverse colon; computed with a frequency resolution of 0.234 cpm

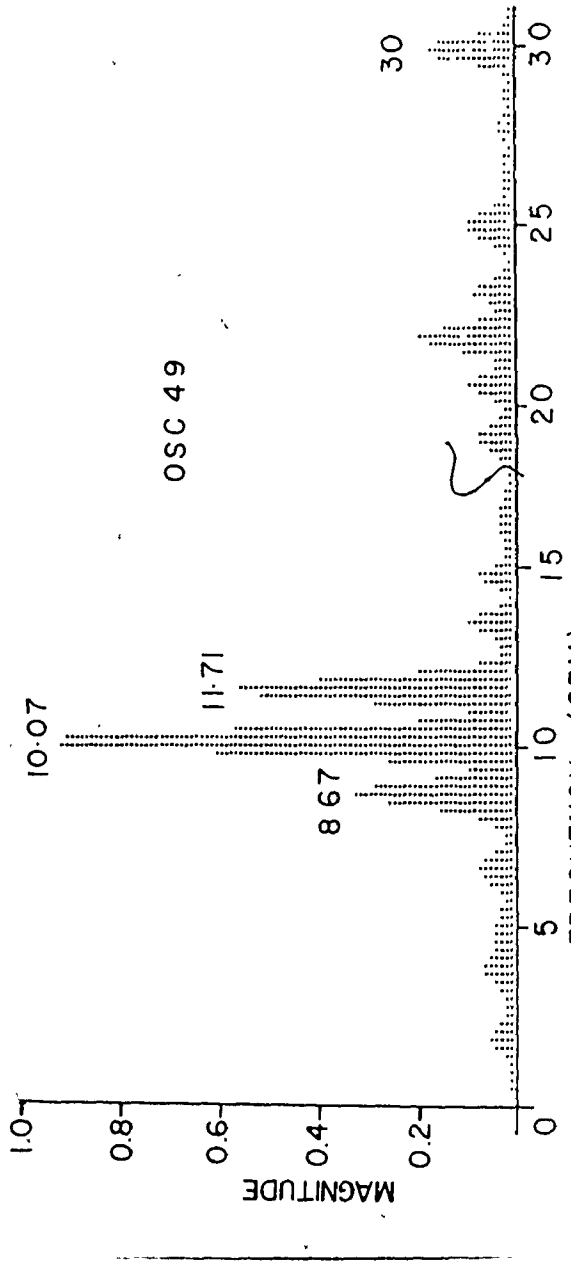

Fig. 7.5 d The power spectrum of an output from oscillator 49 in the model's transverse colon, computed with a frequency resolution of 0.234 cpm

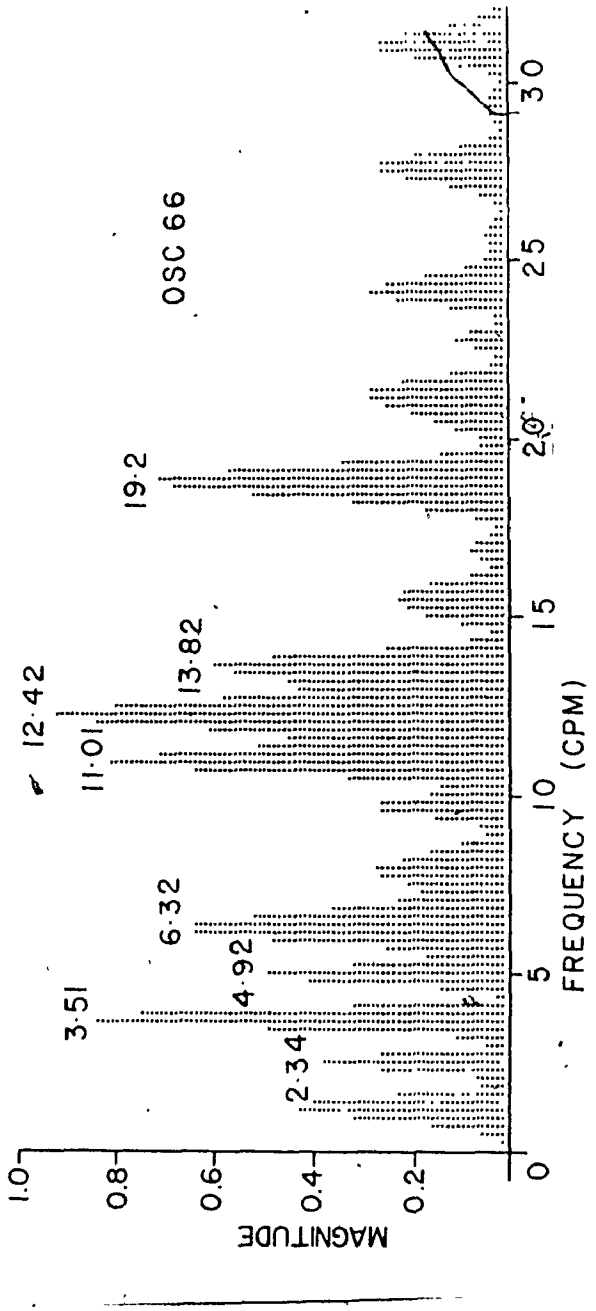

Fig. 7.5 e The power spectrum of an output from oscillator 66 in the model's descending colon, computed with a frequency resolution of 0.234 cpm

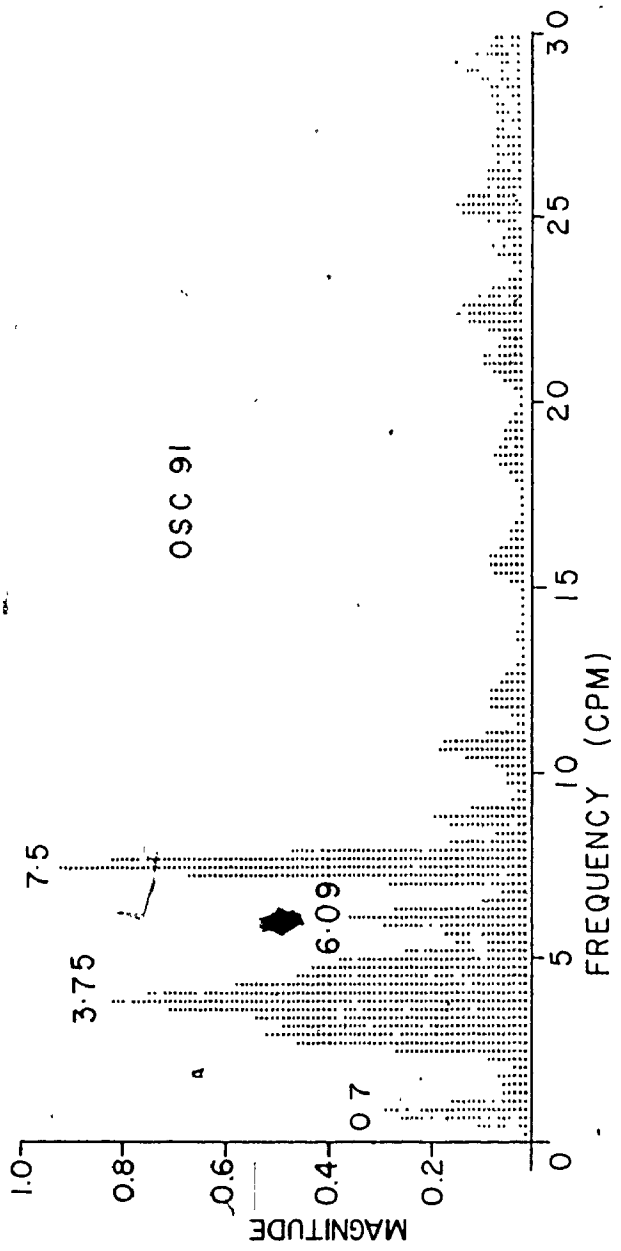

Fig. 7.5 f The power spectrum of an output from oscillator 91 in the model's sigmoid colon, computed with a frequency resolution of 0.234 cpm

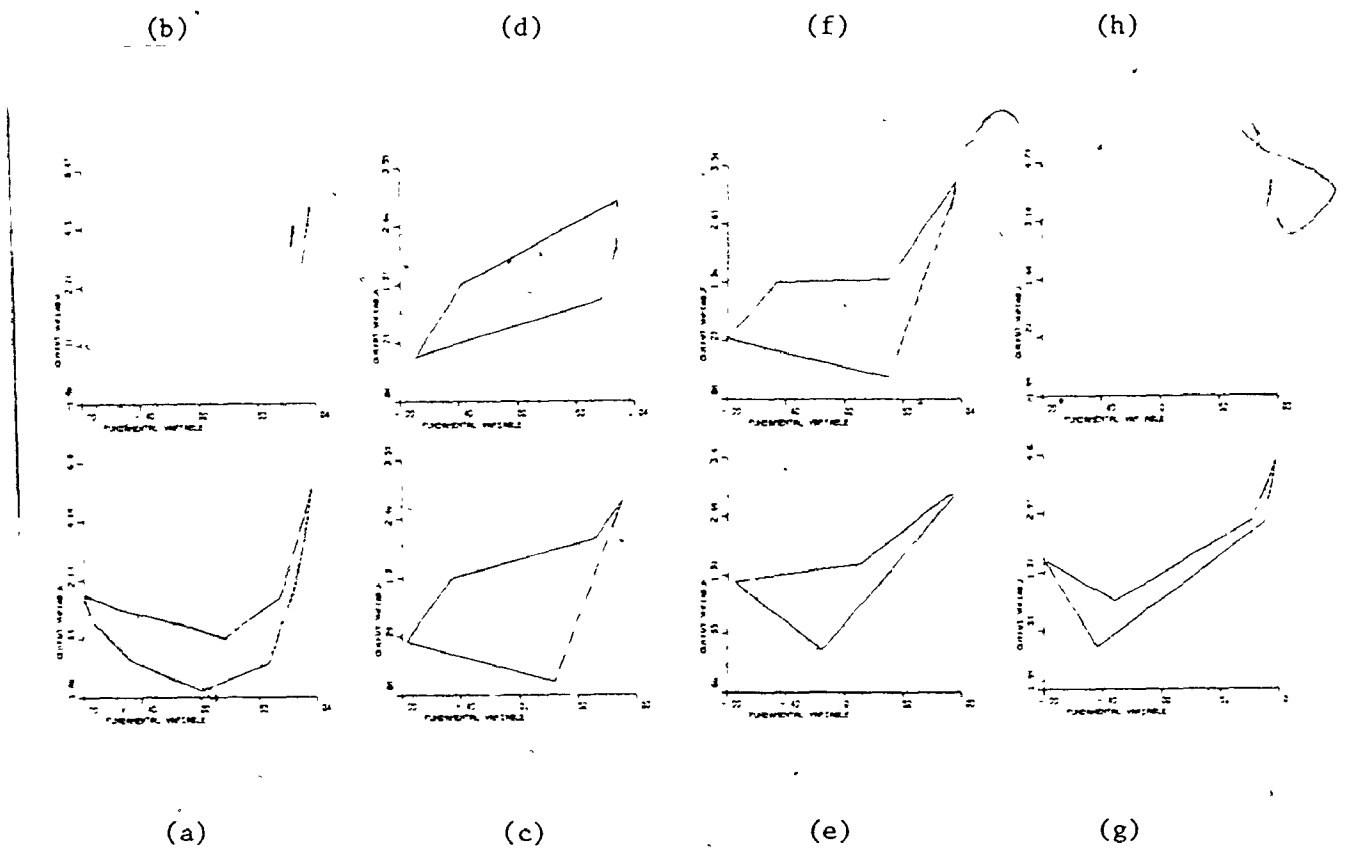

Fig. 7.6 Limit cycles of oscillators from the coupled population.
(a) osc. 2 (b) osc. 5 (c) osc. 46 (d) osc. 49
(e) osc. 63 (f) osc. 66 (g) osc. 88 and (h) osc. 91

mean fundamental peak-frequencies are given in Table 7.2 and the presence of second harmonic peak frequencies is described in Table 7.3. The oscillator outputs were not phase-locked over a 10 minute period either in the longitudinal direction or in the circumferential direction (Fig. 7.7, Appendix II).

When the population was uncoupled by reducing all the coupling factors to zero, the outputs of all oscillators were as depicted in Appendix III. Eight representative oscillator outputs (corresponding to the oscillators in Fig. 7.4) are depicted in Fig. 7.8 whereas their power spectra are depicted in Fig. 7.9 and their limit cycles in Fig. 7.10.

In the simulation runs, the sampling frequency used in computing the oscillator outputs was 1 Hz .

7.5.1 Effects of Recording Instruments

The analog preprocessing effects of the recording instruments used in biological data acquisition were investigated in two ways

1. A digital simulator of the RC input-coupler (Appendix IV), with a time constant of 1 sec corresponding to a lower cut-off frequency of 0.16 Hz, was used to digitally process the oscillator outputs (eight of which are depicted in Fig. 7.11).
2. The oscillator outputs from the coupled population were converted into an analog form (using a digital-to-analog converter) and recorded by a Beckman recorder (whose lower and upper cut-off frequencies were set at 0.16 and 30 Hz respectively). Fig. 7.12 depicts eight of the recorded oscillator outputs.

TABLE 7.2

MEAN FUNDAMENTAL PEAK FREQUENCIES

IN MODEL

region	Oscillator numbers	Lower freq. range 2-7 cpm			higher freq. range 8-12 cpm		
		number of observations	Mean	std. deviation	number of observations	Mean	std. deviation
Ascending	1,4,7 10,13,16, 19	56	4.57	±1.57	56	9.48	±0.95
Transverse	37,40,43, 46,49,52, 53	-	-	-	55	10.90	±0.92
Descending and Sigmoid	66,67,68, 70,73,90 91,94,97 98	76	4.31	±1.36	76	10.07	±1.04

TABLE 7.3

PRESENCE OF SECOND HARMONIC

FREQUENCY COMPONENT IN MODEL

region	oscillator numbers	lower freq. range 2-7 cpm			higher freq. range 8-12 cpm		
		number of observations	%ℓ	%h	number of observations	%ℓ	%h
Ascending	1,4,7, 10,13,16, 19.	56	42.85	14.28	56	26.78	1.78
Transverse	37,40, 43,46,49 52,53	-	-	-	55	47.27	1.81
Descending & Sigmoid	66, 67, 68, 70,73,90, 91,94,97, 98	76	30.26	15.78	76	32.89	10.52

where

%ℓ denotes the percentage of time in which intensity of second harmonic is less than the intensity of fundamental but greater than 10% of it.

and

%h denotes the percentage of time in which intensity of second harmonic is greater than the intensity of fundamental.

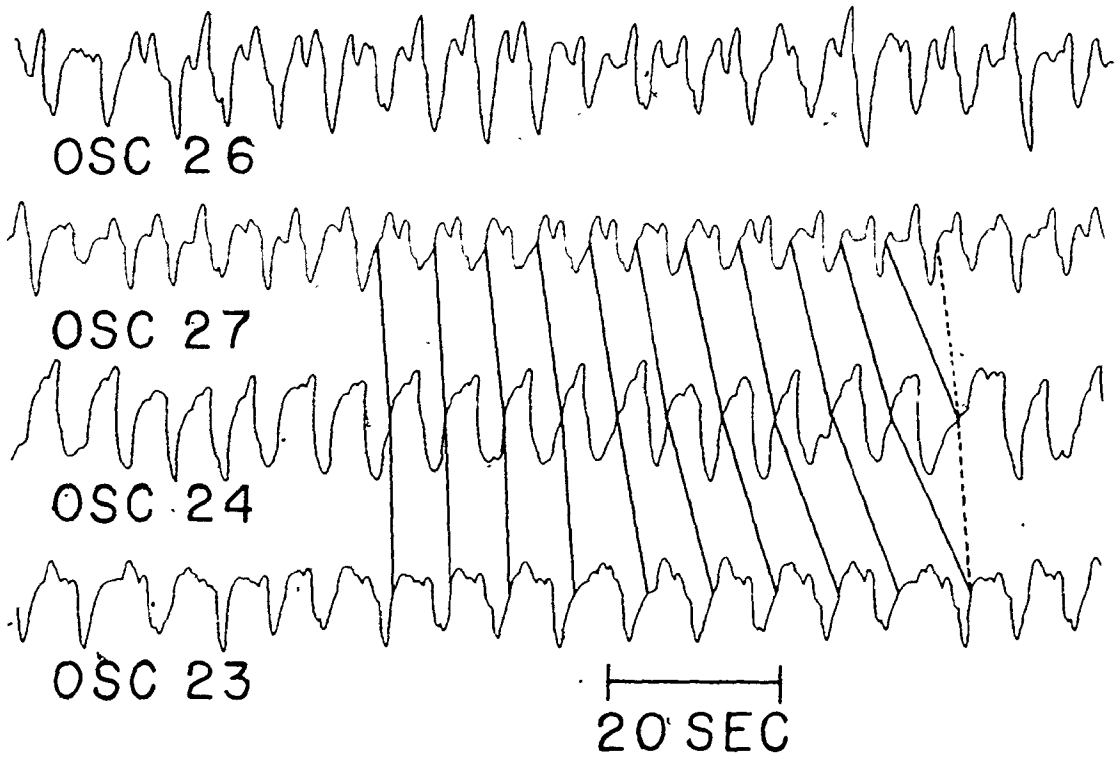

Fig. 7.7 Phase-lag variations in the model's ascending colon. Osc. 23 & Osc. 24 are in the circumferential direction whereas Osc. 24 & Osc. 27 are in the longitudinal direction. Continuous lines join the zero crossings of waveforms.

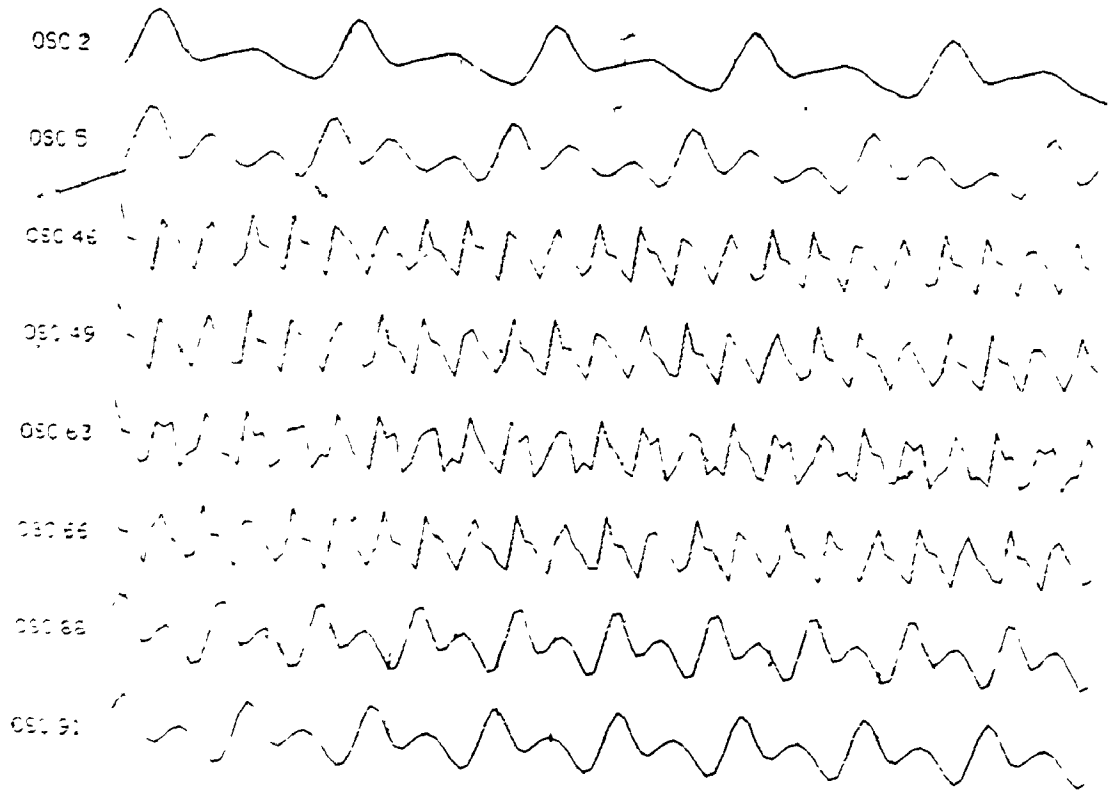

Fig. 7.8 Oscillator outputs from the uncoupled population. For each oscillator output the maximum amplitude is normalized to unity and the simulated time segment is of 2 minutes duration.

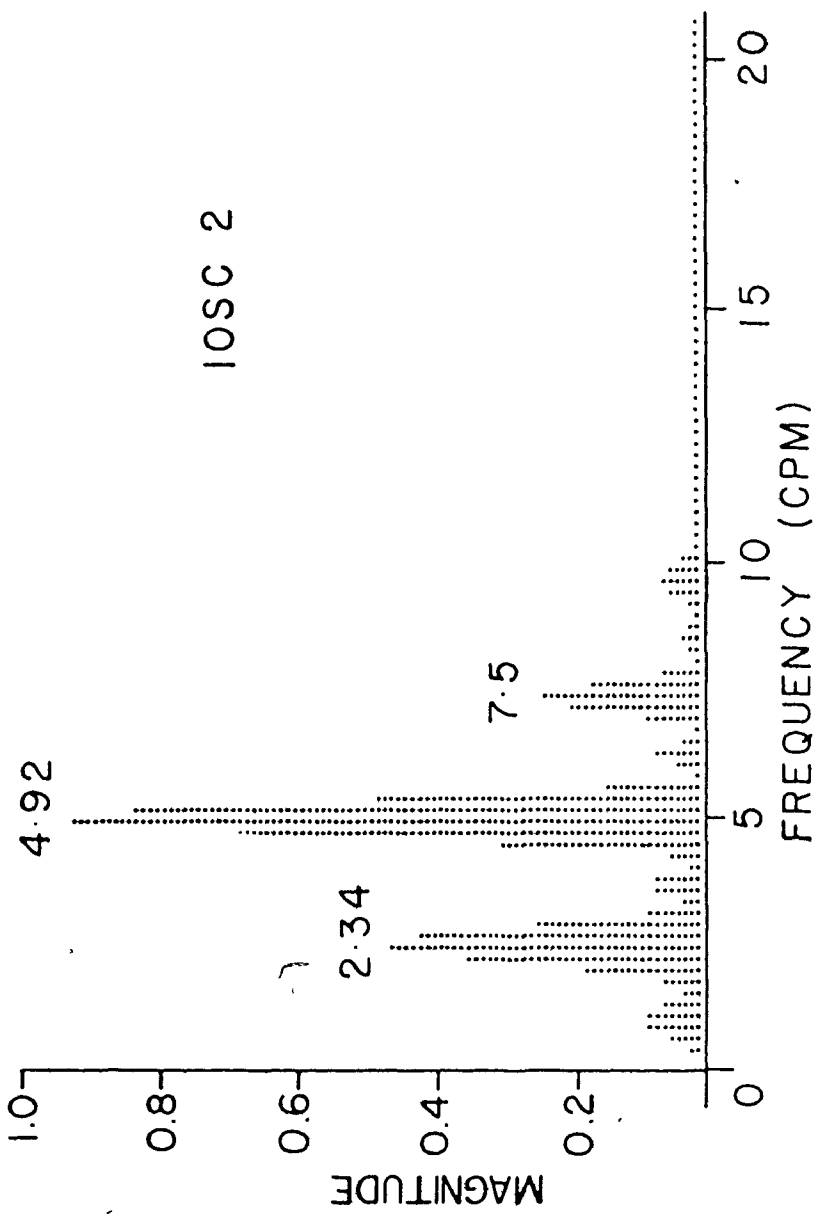

Fig. 7.9 a The power spectrum of an output from intrinsic oscillator 2 in the uncoupled population, computed with a frequency resolution of 0.234 cpm

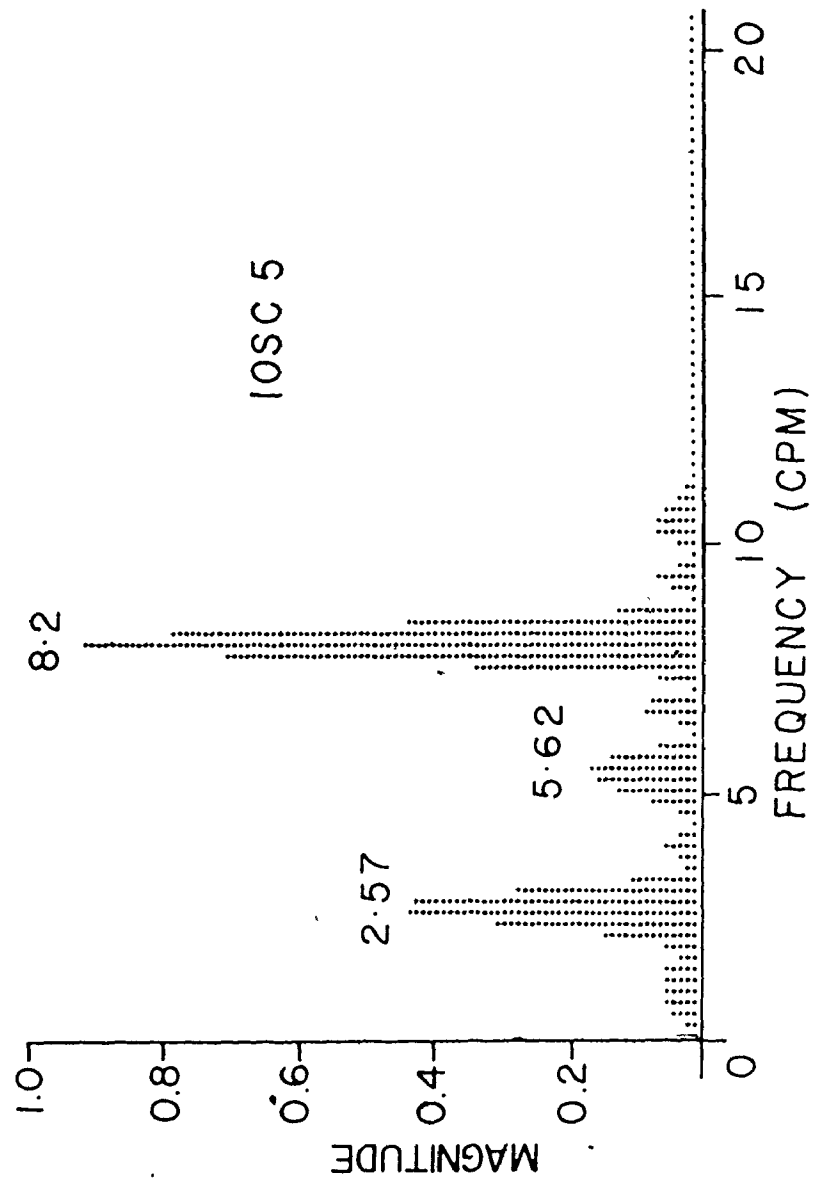

Fig. 7.9 b The power spectrum of an output from intrinsic oscillator 5 in the uncoupled population, computed with a frequency resolution of 0.234 cpm

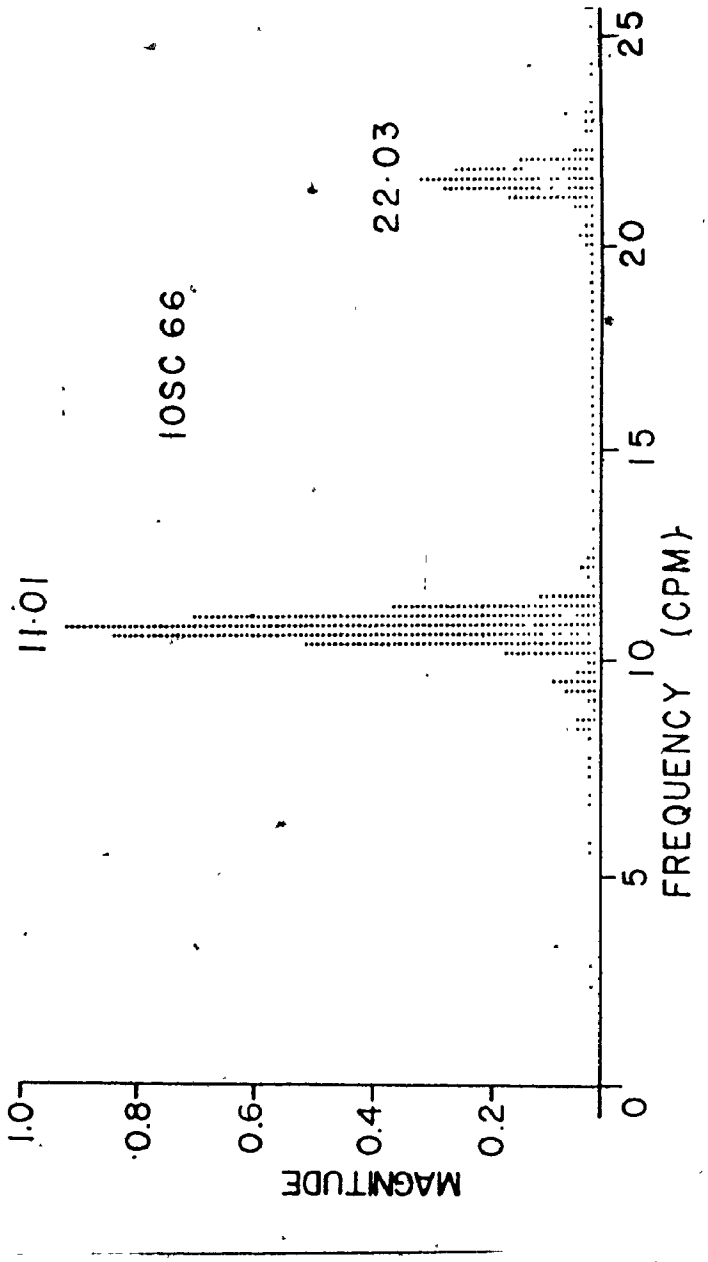

Fig. 7.9 c The power spectrum of an output from intrinsic oscillator 66 in the uncoupled population, computed with a frequency resolution of 0.234 cpm

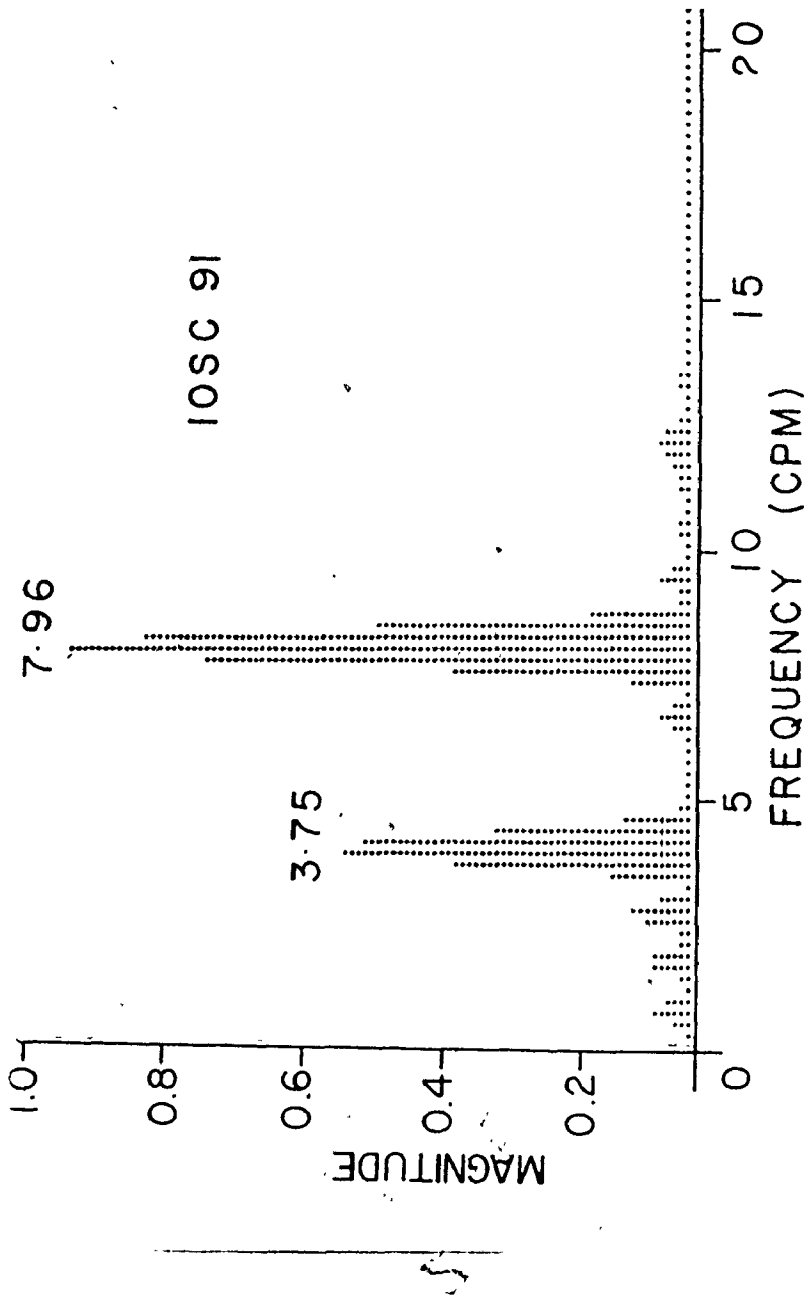

Fig. 7.9 d The power spectrum of an output from intrinsic oscillator 91 in the uncoupled population, computed with a frequency resolution of 0.234 cpm

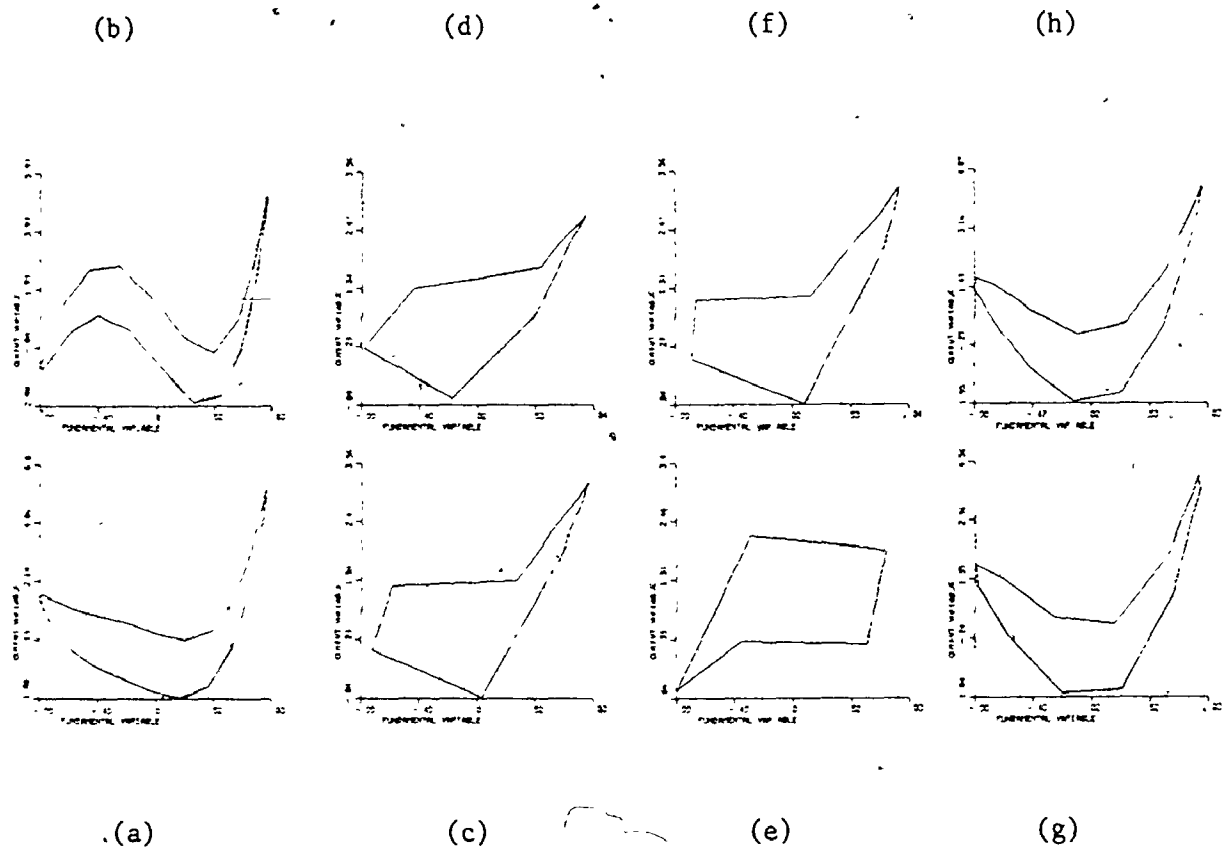

Fig. 7.10 Limit cycles of oscillators from the uncoupled population.
(a) osc. 2 (b) osc. 5 (c) osc. 46 (d) osc. 49
(e) osc. 63 (f) osc. 66 (g) osc. 88 and (h) osc. 91

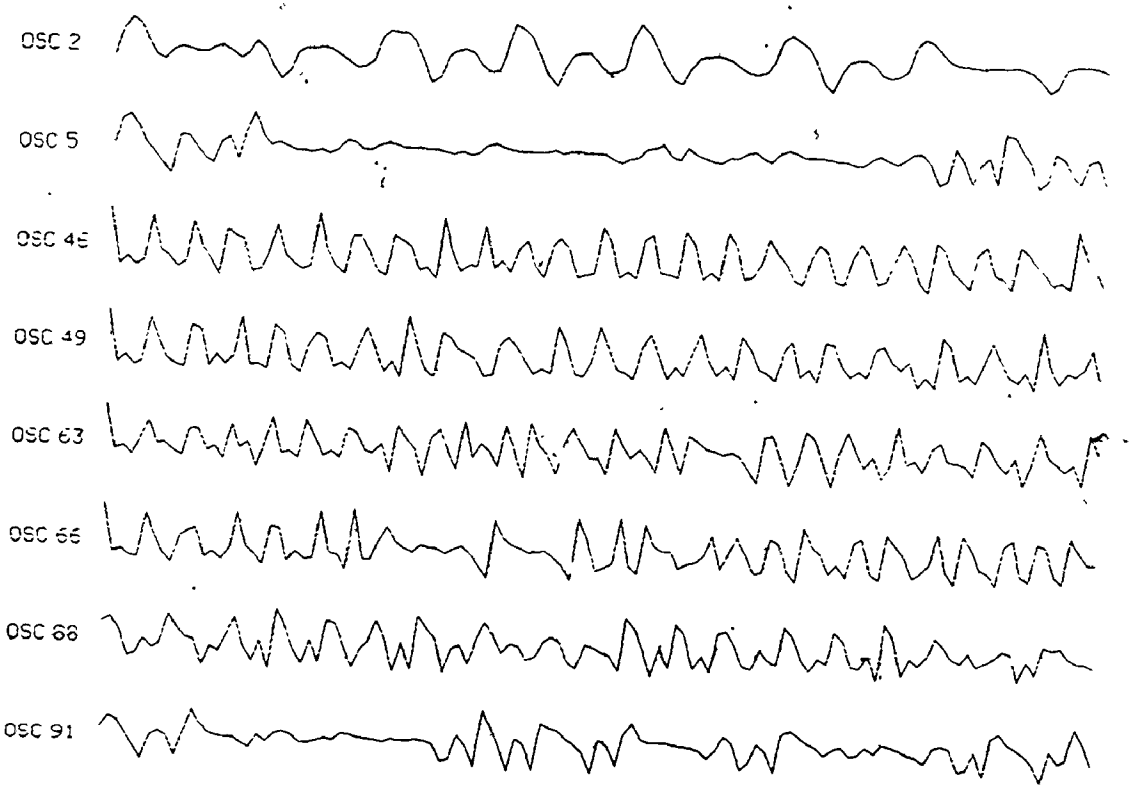

Fig. 7.11 Oscillator outputs from the coupled population after processing by a simulator of an RC input coupler. For each oscillator output, the maximum amplitude is normalized to unity and the simulated time segment is of 2 minutes duration.

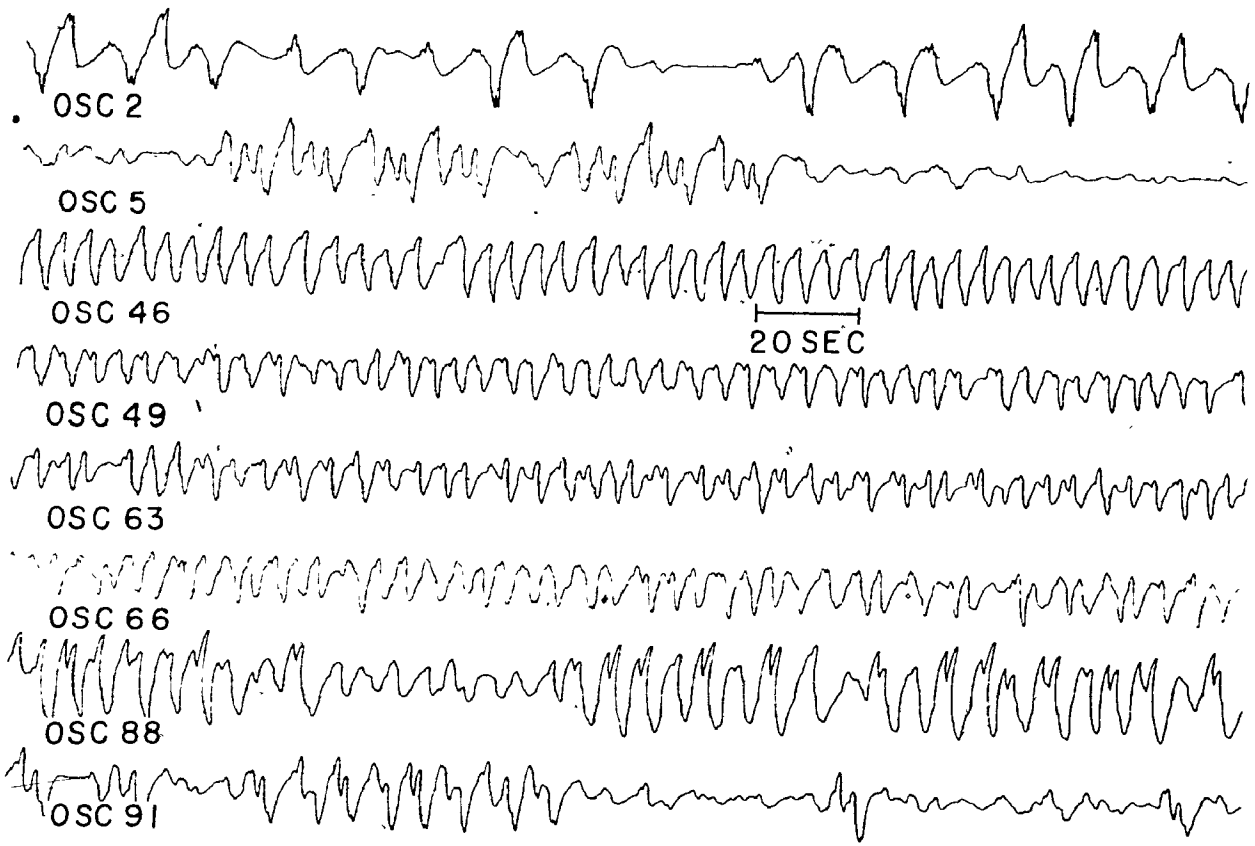

Fig. 7.12 Oscillator output from the coupled population recorded by a Beckman recorder after conversion to an analog form via a digital-to-analog converter

7.5.2 Effects of External Stimulation

To study the effects of external stimulation, a rectangular stimulus (amplitude = 0.8, period = 1 sec and pulse width = 0.3 sec) was applied to oscillator 44 in the model's transverse colon (for a stimulus duration = 1 min). The outputs of oscillators in the neighbourhood of the stimulated oscillator before, during and after stimulus application are depicted in Fig. 7.13 while their fundamental peak frequencies are given in Table 7.4. The effect of external stimulation of oscillator 44 was to increase its fundamental peak frequency (from 11.9 cpm before stimulus application to 15.8 cpm during stimulus application) without appreciably affecting the fundamental peak frequencies of its neighbouring oscillators.

7.5.3 Effects of Transection

A partial longitudinal transection in the model's proximal transverse colon was simulated by uncoupling (by reducing the bi-directional coupling factors to zero) of oscillators 37 & 38, 40 & 41, 43 & 44, 46 & 47 and 49 & 50 respectively. The outputs of oscillators in the neighbourhood of the transection site, before and after transection, are depicted in Fig. 7.14 whereas their fundamental peak frequencies are given in Table 7.5. There was no discernible change in fundamental peak frequencies after transection.

A complete circumferential transection in the model's proximal transverse colon was simulated by reducing the bidirectional coupling factors (between oscillators 43 & 46, 44 & 47 and 45 & 48 respectively) to zero. The outputs of oscillators in the neighbourhood of the transection site before and after transection, are depicted in Fig. 7.15 whereas

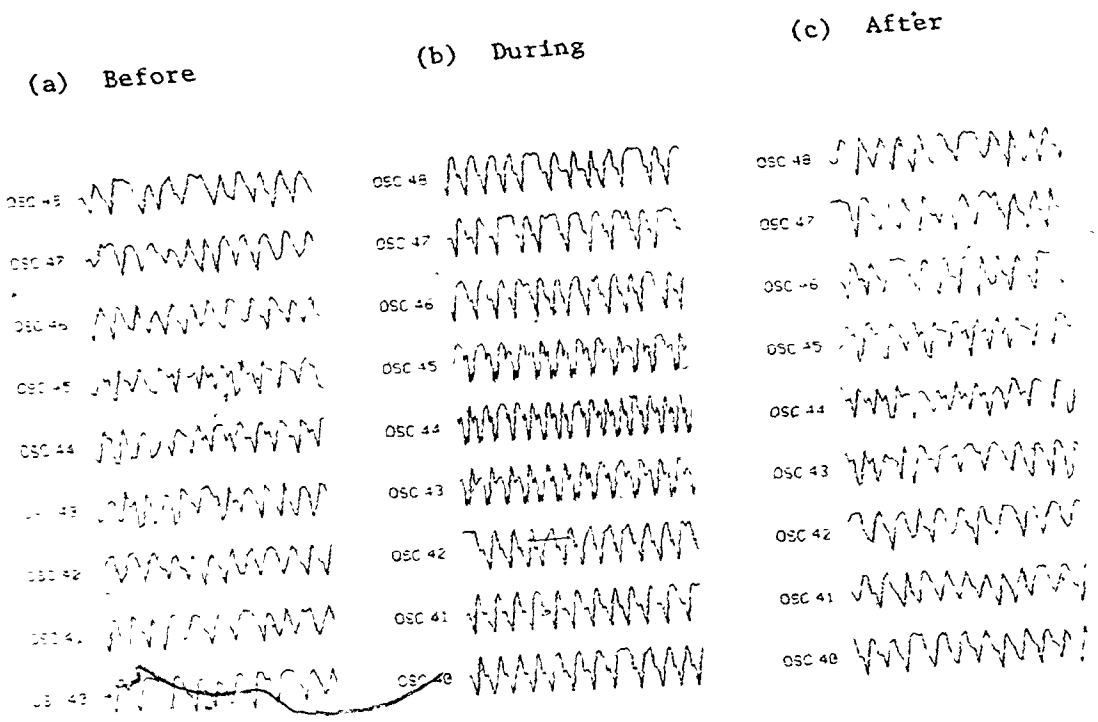

Fig. 7.13 Effects of stimulation of oscillator 44 in the coupled population by a rectangular stimulus (amplitude 0.8, period = 1 sec and pulse width = 0.3 sec). For each oscillator output, the maximum amplitude is normalized to unity and the simulated time segment is of 1 minute duration.

TABLE 7.4

FUNDAMENTAL PEAK FREQUENCIES BEFORE, DURING AND AFTER STIMULATION OF OSCILLATOR 44

Oscillator Number	Fundamental Peak Frequency in cpm		
	Before Stimulation	During Stimulation	After Stimulation
40	11.25	11.13	11.06
41	11.01	12.01	11.95
42	11.71	12.3	10.78
43	12.18	12.59	12.42
44	11.95	15.82	12.18
45	11.48	11.71	11.25
46	12.42	12.59	13.12
47	12.18	10.25	12.89
48	12.89	11.71	12.89

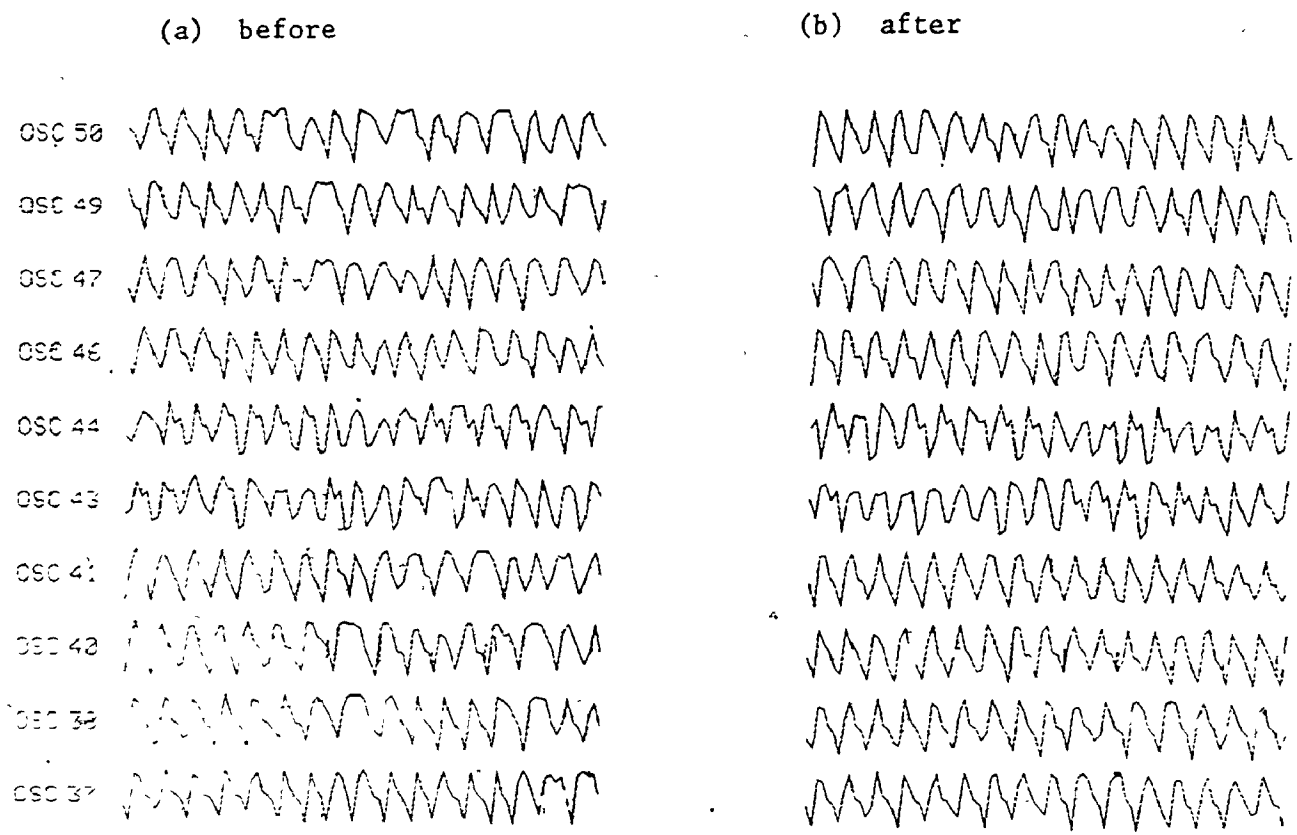

Fig. 7.14 Effects of a partial longitudinal transection between oscillators 37 & 38, 40 & 41, 43 & 44, 46 & 47 and 49 & 50 in the coupled population. For each oscillator output, the maximum amplitude is normalized to unity and the simulated time segment is of 1.5 minutes duration.

TABLE 7.5

FUNDAMENTAL PEAK FREQUENCIES BEFORE AND AFTER PARTIAL LONGITUDINAL TRANSECTION BETWEEN OSCILLATORS 37, 40, 43, 46, 49 AND 38, 41, 44, 47, 50

Oscillator Number	Fundamental Peak Frequencies in cpm	
	Before Transection	After Transection
37	11.95	11.06
38	10.31	11.48
40	11.25	11.71
41	11.01	11.71
43	12.18	11.95
44	11.95	11.71
46	12.42	11.95
47	12.18	12.18
49	12.42	11.95
50	10.07	12.42

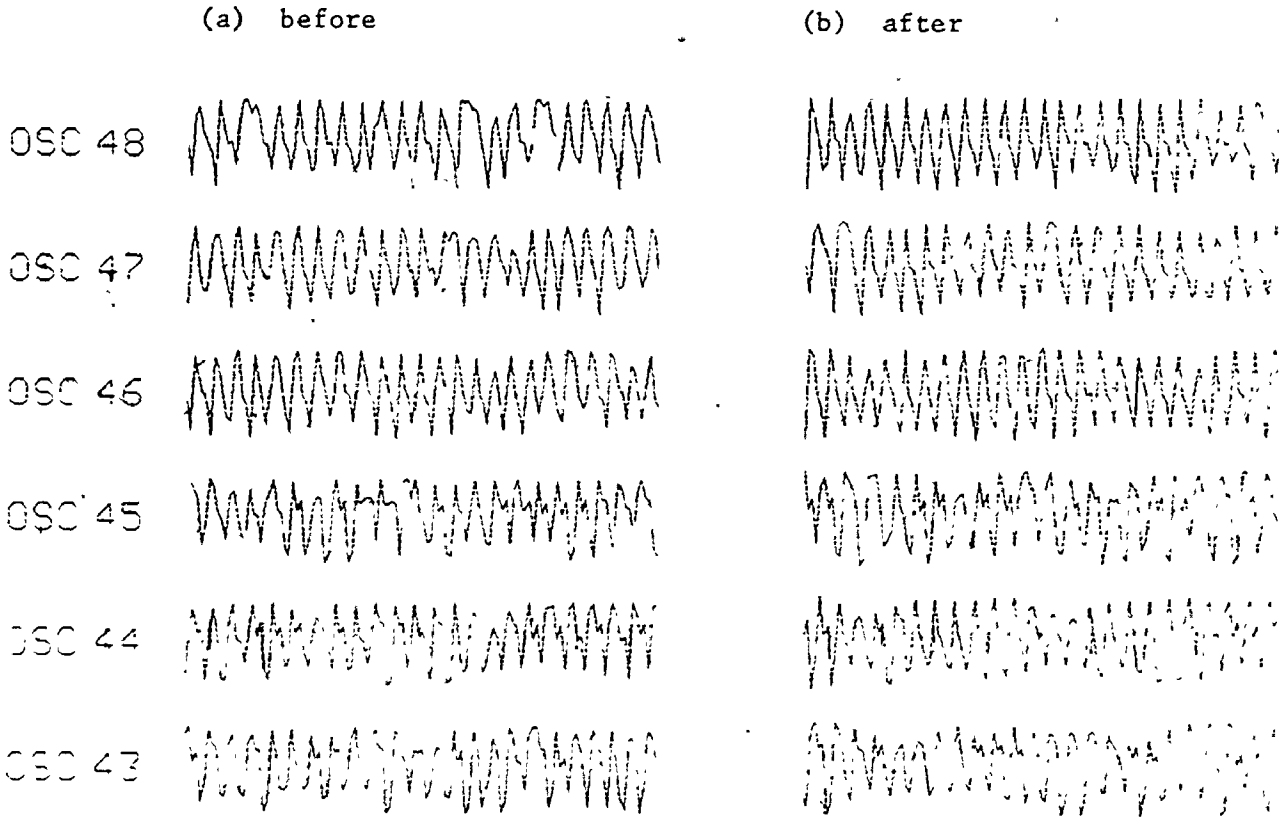

Fig. 7.15 Effects of a complete circumferential transection in the model's transverse colon between oscillators 43 & 46, 45 & 47 and 44 & 48 in the coupled population. For each oscillator output, the maximum amplitude is normalized to unity and the simulated time segment is of 2 minutes duration.

their fundamental peak frequencies are given in Table 7.6. There was no discernible change in fundamental peak frequencies after transection. A complete circumferential transection in the model's sigmoid colon was simulated by uncoupling of oscillators 85 & 88, 86 & 89 and 87 & 90 respectively. The outputs of oscillators in the neighbourhood of the transection site, before and after transection are depicted in Fig. 7.16 whereas their fundamental peak frequencies are given in Table 7.7. There was no discernible change in fundamental peak frequencies after transection.

A partial colectomy and an end-to-end anastomosis (Ottinger 1974) was simulated by removing oscillators 28-81 from the coupled population and amalgamating the two remaining populations into a unified population through bidirectional coupling (with each coupling factor = 0.05 since an end-to-end anastomosis provides for weak coupling) of oscillators 25 & 82, 26 & 83 and 27 & 84 respectively. The corresponding oscillator outputs, before and after the simulated colectomy and anastomosis, are depicted in Fig. 7.17 whereas their fundamental peak frequencies are given in Table 7.8. There was no discernible change in fundamental peak frequencies of comparable oscillators but the total number of oscillators was reduced to 45. A colectomy and an end-to-end anastomosis is used for surgical management of some diseases of the colon such as diverticular disease and ulcerative colitis and for removal of segments of the colon for interposing at other levels of the digestive tract (as in esophageal substitution) since the colon seems to be relatively dispensable and a partial or total colectomy seems to be well tolerated (Ottinger 1974).

TABLE 7.6

FUNDAMENTAL PEAK FREQUENCIES BEFORE AND AFTER

COMPLETE CIRCUMFERENTIAL TRANSECTION

DISTAL TO OSCILLATORS 43, 44 & 45

Oscillator number	Fundamental Peak Frequency in cpm	
	Before Transection	After Transection
43	12.18	11.95
44	11.95	12.42
45	11.48	10.78
46	12.42	12.42
47	12.18	11.48
48	12.89	12.42

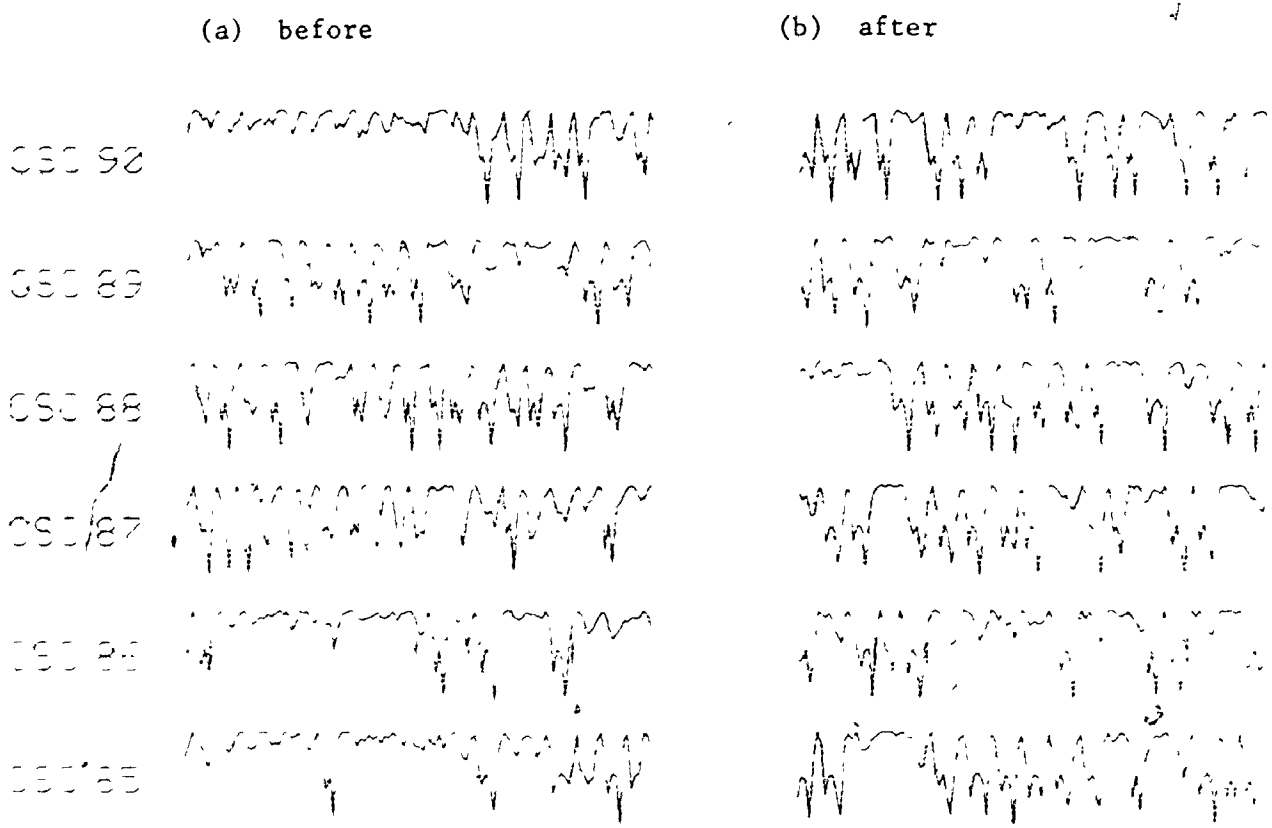

Fig. 7.16 Effects of a complete circumferential transection in the model's distal colon between oscillators 85 & 88, 86 & 89 and 87 & 90 in the coupled population. For each oscillator output, the maximum amplitude is normalized to unity and the simulated time segment is of 2 minutes duration.

TABLE 7.7

FUNDAMENTAL PEAK FREQUENCIES BEFORE AND AFTER COMPLETE CIRCUMFERENTIAL TRANSECTION DISTAL TO OSCILLATORS 85, 86 & 87

Oscillator Number	Fundamental Peak, Frequency in cpm			
	Before Transection		After Transection	
	lower freq. range 2-7 cpm	higher freq. range 8-12 cpm	lower freq. range 2-7 cpm	higher freq. range 8-12 cpm
85	3.28	7.73	5.15	8.2
86	3.98	9.6	3.98	9.37
87	2.34	7.73	2.57	8.2
88	4.21	9.14	4.21	9.14
89	5.62	10.07	6.32	10.78
90	2.81	9.37	2.1	9.14

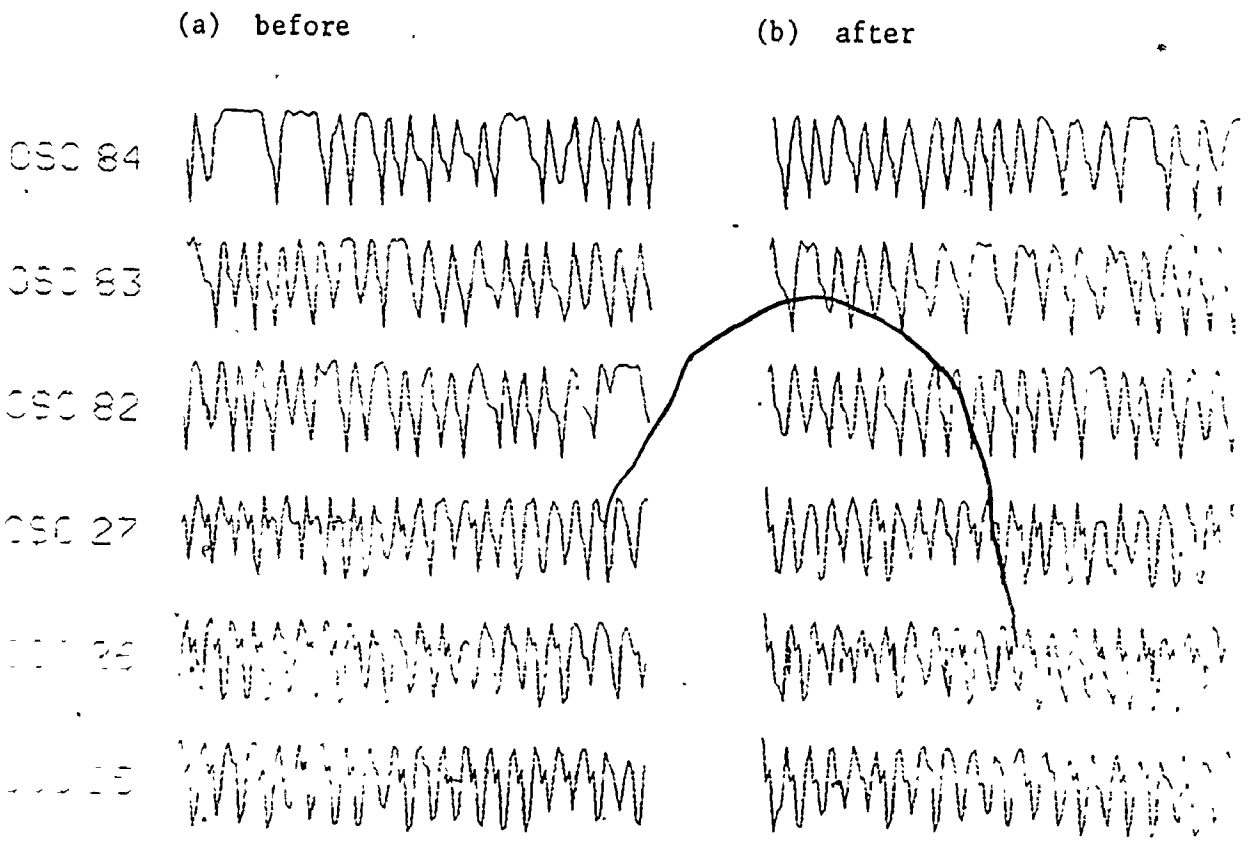

Fig. 7.17 Effects of a simulated partial colectomy (oscillators 28-81 removed) and an end-to-end anastomosis (oscillators 25 & 82, 26 & 83 and 27 & 84 coupled back together with a coupling factor of 0.05). For each oscillator output, the maximum amplitude is normalized to unity and the simulated time segment is of 2 minutes duration.

TABLE 7.8

FUNDAMENTAL PEAK FREQUENCIES BEFORE

AND AFTER SIMULATED PARTIAL COLECTOMY

AND END-TO-END ANASTOMOSIS

Oscillator number	Fundamental Peak Freq. in cpm			
	Before Operation		After Operation	
	lower freq. range 2-7 cpm	higher freq. range 8-12 cpm	lower freq. range 2-7 cpm	higher freq. range 8-12 cpm
25	3.28	10.31	2.34	10.31
26	2.34	10.31	2.34	9.84
27	5.85	10.54	5.15	10.78
82	4.92	11.25	5.85	10.07
83	5.85	10.07	6.79	10.54
84	3.98	10.54	4.21	10.31

7.6 An Extension of ECA Model to Include ERA

An extension of the generic equation of ECA model (7.1a)-(7.1d) to include ERA is given in Appendix V. An oscillator, which is isolated from its neighbouring oscillators, is represented by a fourth-order nonlinear differential equation with four state variables described as follows:

The output variable: is the oscillator output including both the control wave and ERA.

The control variable: is the variable representing the control wave.

The fundamental variable: is the variable whose frequency determines the fundamental frequency of the control wave.

The response variable: is the variable representing the ERA.

Fig. 7.18 depicts the four state variables for an oscillator which is isolated from its neighbouring oscillators and whose intrinsic parameters are

$$a_{01} = a_{11} = b_{11} = d_{01} = d_{11} = e_{01} = e_{11} = 1$$

$$a_{31} = a_{41} = d_{21} = d_{31} = d_{41} = 0$$

$$a_{21} = 2$$

$$f_{11} = 12$$

$$f_{21} = 480$$

and all coupling factors are zero, whereas Fig. 7.19 depicts the two-dimensional limit cycles.

Response potentials appear when the amplitude of the control variable exceeds an excitation threshold (governed by the parameter e_{01}). The portions of the control variable that exceed this excitation threshold are

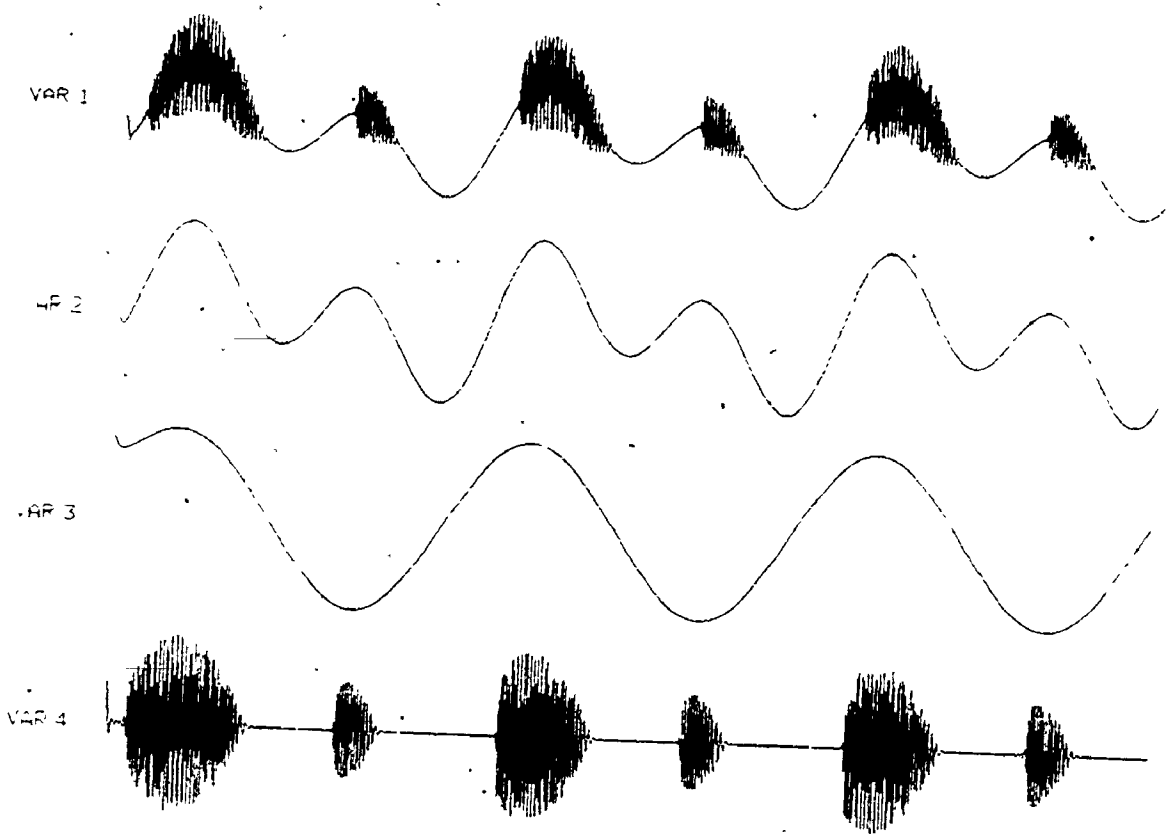

Fig. 7.18 The four state variables of an oscillator exhibiting ECA and ERA. For each state variable the maximum amplitude is normalized to unity and the simulated time segment is of 15 sec duration.

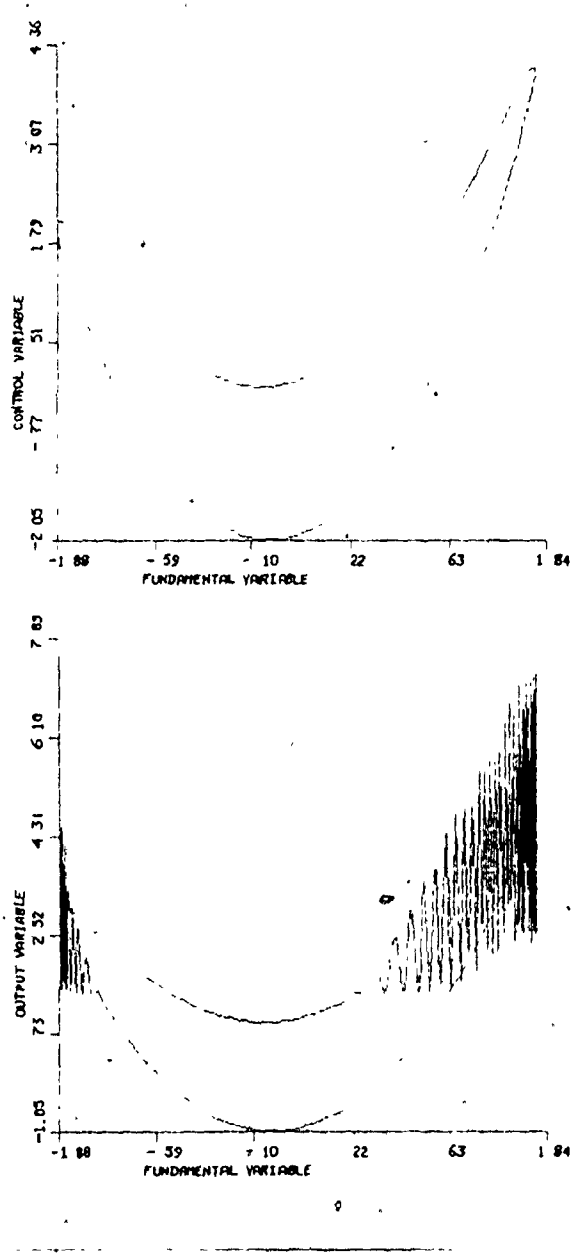

Fig. 7.19 Limit cycles of an oscillator exhibiting ECA and ERA

determined by the frequency components of the control variable. The strongest frequency component of the control wave is the second harmonic and the repetition rate of response potentials is equal to that of the second harmonic frequency component of the control variable.

7.7 Discussion

The ECA in human colon will be assumed to originate in the smooth muscle cells of the colonic wall since no conclusive experimental evidence is, as yet, available regarding its genesis in the longitudinal and/or circular muscle cells. Although a rhythmic electrical activity had been recorded from isolated strips of human taenia coli (Vanasin et al. 1971) guinea pig taenia coli (Bülbring et al. 1958), longitudinal muscle of rabbit colon (Gillespie 1962a) and circular muscle of cat colon (Christensen et al. 1969), more in vitro investigations need to be carried out to determine its precise generating musculature in the human colon.

Linkens et al. (1976b) proposed three models of the ECA in human rectosigmoid using synchronous populations of coupled Van der Pol oscillators where the oscillator outputs were strictly phase-locked. Their demonstrative models were of a strip of rectosigmoid (and not the whole colon) since they consisted mainly of either two bidirectionally coupled oscillators having the same intrinsic frequencies and coupling factors, or one or two rings connected in parallel where each ring contained four bidirectionally coupled oscillators having the same intrinsic frequencies and coupling factors. The following features of their models do not have an acceptable physiological premise

1. To produce the postulated three stable modes of oscillation, either the initial starting conditions of the simulation run had to be changed

or alternatively, an external stimulus had to be applied intermittently to switch between the three modes.

2. The dependence of the coupled frequency, in a synchronous population of oscillators, on the initial phase-shift between individual oscillators.

3. The manifestation of a coupled frequency, in a synchrouous population of oscillators having the same intrinsic frequency, which is lower than the common intrinsic frequency.

The proposed model of ECA in human colon is qualitative in nature and the intrinsic frequency gradient was hypothesized since no biological data regarding the intrinsic frequency gradient of the ECA in human colon is available. Hence, the choice of the intrinsic frequency gradient was governed mainly by the attempt to reproduce the observed in vivo features of the ECA in human colon. It was found that such a gradient reproduces a waxing and waning phenomena in the coupled population (as can be seen from Figs. 7.4 and 7.12). The number of rings and the number of oscillators per ring were arbitrarily chosen but were found to be adequate to reproduce the in vivo features of the human colonic ECA.

The model reproduced the following main features 1. The continuous presence of control waves but with a waxing and waning of their amplitudes. 2. No continuous phase-locking in either the longitudinal or circumferential direction, but the control waves remained temporarily phase-locked for longer periods of time in the transverse colon than in ascending, descending or sigmoid colon. 3. A coupled frequency gradient resembling the in vivo frequency gradient in the human colon. 4. Presence of multiple frequency components as well as second, third and fourth harmonic frequency components, of the control waves, whose

intensities may be larger than that of the fundamental frequency components. 5. The frequency components, of the control waves, and their intensities vary in time and space.

It is to be noted that the in vivo time varying features of the ECA in human colon were simulated by the model without the need of any run-time parameter adjustments or the need to apply external stimuli. An explanation of this phenomena may be attributed to lack of synchronization of the coupled population due to insufficient coupling between oscillators (for the assumed intrinsic frequency gradient). Stimulation and transection of the model were investigated in order to predict the effects of such manoeuvers but comparable biological experiments were not feasible.

The waxing and waning phenomena can be explained by envisaging that, for the duration of the phenomena, the state dot in $u_{1n} - u_{2n}$ space (Fig. 5.2b) rotates around the unit circle at a slow instantaneous angular velocity, propelled by a vector field representing its generic equation. This is demonstrated in Fig. 7.6b where the trajectory of the state dot is represented by an arc for a time duration which is sufficient for it to be represented by a complete limit cycle.

In summary, a tubular structure of bidirectionally coupled rings of bidirectionally coupled relaxation oscillators existing in the smooth muscle cells of the colonic wall is proposed as a model of the ECA in the human colon.

CHAPTER 8

CONCLUSIONS

This thesis covers the areas of digital signal processing and modelling of a biological rhythm, whereby a tubular structure of bidirectionally coupled rings of bidirectionally coupled relaxation oscillators existing in the smooth muscle cells of the colonic wall is proposed as a model of the ECA in human colon.

An interactive analysis processor for multistage filtering and decimation, tuneable IIR digital filtering along with power and cross spectra computation was developed and implemented in a modular form to enable tailoring of the processor to fit a given requirement. Optimal IIR digital filters were designed either by using the bilinear z-transformation method, where the approximation problem is solved in the s-domain and then transforming the solution into the z-domain, or alternatively, by using a least pth optimization strategy in conjunction with a function minimization algorithm, where the approximation problem is solved in the z-domain directly, hence, enabling arbitrary specifications on the magnitude characteristics of the digital filter transfer function. Also, optimal IIR filters with finite-word-length coefficients were designed by a discrete optimization method using a branch and bound strategy in conjunction with a function minimization algorithm. Tuneable IIR digital filters were designed either through algebraic transformations of a prototype analog low-pass elliptic filter, then transforming the

s-domain solution into a z-domain solution by the bilinear z-transformation, or alternatively, through spectral transformations of a prototype low-pass optimal IIR digital filter. A multistage decimator having a different cut-off frequency at each decimation stage but using the same IIR digital filter coefficients, was developed and bounds on some design parameters were derived to optimize the multistage decimator.

An interactive processor for modelling of a biological rhythm by a population of coupled relaxation oscillators where each oscillator can be selectively stimulated, was developed in such a way as to enable using the analysis processor to process both the biological and simulated data in a consistent manner. Although the biological rhythm of concern in this thesis is the ECA in human colon, the interactive analysis and modelling processors are general enough to warrant their usage for other biological rhythms as well [actually, they have been routinely used for processing rhythms from different levels of the digestive tract (Sarna et al., unpublished)].

The ECA in the human colon was found to be continuously present with waxing and waning of the amplitude of control waves but no "silent" periods with zero electrical activity were observed. The characteristics of human colonic ECA varied in time and space hence resulting in irregular organizational patterns that are not amenable to visual analysis, which may partially explain the various interpretations of different investigators (e.g. Provenzale and Pisano 1971; Taylor et al. 1974,1975). The cycle-to-cycle variation of the frequency of control waves caused the energy to appear spreading over frequency bands in the power spectra (which were computed over a one minute interval). Multiple fundamental

peak frequencies along with harmonic peak frequencies were present in the power spectra of the control waves. The intensities of the harmonic peak frequencies were at times larger than those of the fundamental peak frequencies; this is relevant in ERA organizational patterns since the repetition rate of response potentials (when present) was less than or equal to the strongest frequency component of the corresponding control wave. Both the frequency components and their intensities varied in time and space. Furthermore, the control waves were not continuously phase-locked in either the longitudinal or the circumferential directions.

The human colonic ECA is hypothesized to control the appearance of ERA (and hence of colonic muscular contractions) in time and space. The presence of multiple fundamental peak frequencies and harmonic peak frequencies of the ECA, whose intensities varied in time and space, suggests that the rate of colonic muscular contractions also varies in time and space. Also, assuming that the ERA appears at a relatively fixed phase of the control cycle, then the absence of continuous phase-locking of the control waves (with an aboral phase lag) in the longitudinal direction suggests that the dominant activity in the human colon is mixing (rather than aborally propulsive) contractions. Furthermore, temporary phase-locking of the control waves (with a temporary aborally-decreasing frequency gradient of the ECA), in a certain region of the colon, would cause the appearance of aborally propulsive contractions in that region.

A population of coupled SROs was used to model the observed features of human colonic ECA. The computer model reproduced the observed variations of the ECA characteristics in time and space without the need for any externally applied stimuli [as those used by Linkens et al. (1976b)],

but rather due to the lack of synchrony of the coupled population. The intrinsic parameters of a SRO are the coefficients of a truncated Fourier series representation of a control wave acquired from an electrically isolated muscle strip, behaving like a relaxation oscillator, hence they may be estimated experimentally.

A mathematical investigation of a population of coupled SROs helped to elucidate some of the underlying interactions and pointed out the relevance of the average values of control waves of a synchronous population of SROs as they constituted a major factor in the conditions necessary for synchronization. This led to the derivation of conditions of entrainment of a SRO by different external stimuli; whereby for rectangular stimuli, the theoretical strength-duration curves resembled (qualitatively) the ones observed in practice (Bozler 1938a).

The waxing and waning phenomena is explained by envisaging that, for the duration of the phenomena, the state dot of a coupled fundamental oscillator rotates around its limit cycle at a slow instantaneous angular velocity, propelled by a vector field representing its generic equation.

No discernible effects of simulated transection or simulated partial colectomy with an end-to-end anastomosis of the computer model were observed, hence suggesting that removal of parts of colon will not have drastic effects on the remaining parts (when coupled back together). This is in agreement with the practical observation that a partial colectomy and an end-to-end anastomosis is reasonably well tolerated (Ottinger 1974).

A mathematical investigation of external stimulation as well as stimulation of the computer model suggests the possibility of electronic pacing of the colon (for management of some disorders in colonic motility).

The limitations of this study may be summarized as follows:

1. The ECA in human colon is assumed to originate in the smooth muscle cells of the colonic wall without further specifying the musculature (longitudinal and/or circular) of its genesis.
2. The intrinsic frequency gradient of human colonic ECA is hypothesized because of the unavailability of biological data. Hence, the choice of the intrinsic frequency gradient was governed mainly by the attempt to qualitatively reproduce the observed in vivo features of ECA in (intact) human colon.
3. An arbitrary number of oscillators and hypothesized intrinsic parameters of SROs were used in the model but were found adequate to reproduce, qualitatively, the observed characteristics of the human colonic ECA.

Improvements and suggestions for future work may be summarized as follows:

1. Intracellular studies of human colonic muscle strips to determine whether the ECA is generated in the longitudinal and/or circular muscle cells. Also, to determine the relationships between the electrical activity of the longitudinal and circular muscle cells.
2. In vitro studies of muscle strips acquired from different regions of the human colon to determine the intrinsic frequency gradient of the ECA in human colon. Then the intrinsic paramters of the SROs can be routinely computed via a frequency analysis to determine the coefficients of a truncated Fourier series representation of the electrical signals acquired from the different muscle strips.
3. Animal studies to investigate the neural and hormonal influences on the ECA characteristics and organizational patterns. Also, to

investigate the effects of various operations (e.g. transection, resection of colonic segments, providing links between various colonic segments and electrical stimulation) to compare with the effects of similar operations on a comparable computer model.

4. To take into consideration the time varying characteristics of the control waves and develop analysis procedures (possibly new transforms from the time-domain into some suitable domain) for signals with time varying amplitude, frequency and phase.

5. To develop a model of both the ECA and ERA in the human colon.

The applications and practical importance of this study may be summarized as follows:

1. The development and implementation of interactive processors for the analysis and simulation of biological rhythms aids researchers in the field as it provides them with an interactive tool. Furthermore, a consistent analysis of biological and simulated data is provided, and since the modelling processor is geared specifically towards biological rhythms it provides some attractive features (such as stimulation at a specified time for a specified duration by a specified stimulus) that are not readily available in a more general simulation language [such as ISL (Interactive Simulation Language)].

2. Interactive computer modules for analyzing the gastrointestinal electrical signals aid both the researcher and the clinician in sifting useful information about the myogenic control systems in the gastrointestinal tract. Also, establishing a data base aids in clinical diagnosis of certain gastrointestinal disorders.

3. The introduction and mathematical investigation of a population of

coupled SROs provides researchers in the field with a foundation for elucidating the complex interactions, coupling mechanisms, synchronization and external stimulation of such coupled populations used to model a biological rhythm. Admittedly, a purely mathematical analysis of oscillatory high-order nonlinear systems is not always feasible due to the inherent difficulties encountered in solving high-order nonlinear differential equations, hence, a combination of mathematical analysis and computer simulation seems to be fruitful.

4. A computer model of the ECA in human colon can be used for teaching purposes by simulation of normal and disease conditions also simulation of surgical and/or pharmacological interventions. It can also aid in diagnosing certain colonic disorders and eventually it may aid in suggesting a treatment of those disorders through pharmacological and/or surgical interventions or electrical stimulation by electronic oscillators. Surgical interventions may involve resecting certain oscillators and/or providing appropriate links amongst certain oscillators which may have been uncoupled because of other operations or lesions. Pharmacological interventions may involve giving drugs or hormones that may alter membrane characteristics by changing the intrinsic parameters of oscillators or may alter the coupling between cells. Electrical stimulation may involve implanting colonic pace makers (in a manner similar to cardiac pace makers) to normalize the ECA frequencies and produce desired ECA organizational patterns.

APPENDIX I

PARTIAL DERIVATIVES OF THE GENERALIZED LEAST PTH OBJECTIVE FUNCTION WITH RESPECT TO THE IIR DIGITAL FILTER COEFFICIENTS

Partial differentiation of the generalized least pth objective function (2.3) with respect to the IIR digital filter coefficient vector $\underset{\sim}{c}$ yields

$$\nabla U(\underset{\sim}{c},\psi,\xi,p) = \Big[\sum_{i\in K_u} \Big\{ \frac{e_\mu(\underset{\sim}{c},\psi_i) - \xi}{M(\underset{\sim}{c},\xi)} \Big\}^g + \sum_{i\in K_\ell} \Big\{ \frac{-e_1(\underset{\sim}{c},\psi_i) - \xi}{M(\underset{\sim}{c},\xi)} \Big\}^g \Big]^{\frac{1}{g}-1}$$

$$\Big[\sum_{i\in K_u} \Big\{ \frac{-e_u(\underset{\sim}{c},\psi_i) - \xi}{M(\underset{\sim}{c},\xi)} \Big\}^{g-1} \nabla e_u(\underset{\sim}{c},\psi_i) - \sum_{i\in K_\ell} \Big\{ \frac{-e_1(\underset{\sim}{c},\psi_i) - \xi}{M(\underset{\sim}{c},\xi)} \Big\}^{g-1} \nabla e_1(\underset{\sim}{c},\psi_i) \Big] \tag{I.1}$$

where

$$\nabla = \Big[\frac{\partial}{\partial c_1} \quad \frac{\partial}{\partial c_2} \quad \frac{\partial}{\partial c_3} \quad \frac{\partial}{\partial c_4} \quad \cdots\cdots \quad \frac{\partial}{\partial c_{4k+1}} \Big]^T$$

and all other symbols as defined in Chapter 2. If the transfer function is chosen to be of the cascade form then

$$\frac{\partial}{\partial c_{4k-3}} e_u(\underset{\sim}{c}, \psi) = w_u(\psi) \; |H(z)| \; \mathrm{Re}\left\{\frac{z^{-1}}{1 + c_{4k-3} z^{-1} + c_{4k-2} z^{-2}}\right\} \quad (I.2)$$

$$\frac{\partial}{\partial c_{4k-2}} e_u(\underset{\sim}{c}, \psi) = w_u(\psi) \; |H(z)| \; \mathrm{Re}\left\{\frac{z^{-2}}{1 + c_{4k-3} z^{-1} + c_{4k-2} z^{-2}}\right\} \quad (I.3)$$

$$\frac{\partial}{\partial c_{4k-1}} e_u(\underset{\sim}{c}, \psi) = -w_u(\psi) \; |H(z)| \; \mathrm{Re}\left\{\frac{z^{-1}}{1 + c_{4k-1} z^{-1} + c_{4k} z^{-2}}\right\} \quad (I.4)$$

$$\frac{\partial}{\partial c_{4k}} e_u(\underset{\sim}{c}, \psi) = -w_u(\psi) \; |H(z)| \; \mathrm{Re}\left\{\frac{z^{-2}}{1 + c_{4k-1} z^{-1} + c_{4k} z^{-2}}\right\} \quad (I.5)$$

for $k = 1, \ldots, K$ and

$$\frac{\partial}{\partial c_{4K+1}} e_u(\underset{\sim}{c}, \psi) = w_u(\psi) \; \frac{|H(z)|}{c_{4K+1}} \quad (I.6)$$

On the other hand if the transfer function is chosen to be of the parallel form then

$$\frac{\partial}{\partial c_{4k-3}} e_u(\underset{\sim}{c}, \psi) = w_u(\psi) \; |H(z)| \; \mathrm{Re}\left\{\frac{1}{H(z)\,[1 + c_{4k-1} z^{-1} + c_{4k} z^{-2}]}\right\} \quad (I.7)$$

$$\frac{\partial}{\partial c_{4k-2}} e_u(\underset{\sim}{c}, \psi) = w_u(\psi) \; |H(z)| \; \mathrm{Re}\left\{\frac{z^{-1}}{H(z)\,[1 + c_{4k-1} z^{-1} + c_{4k} z^{-2}]}\right\} \quad (I.8)$$

$$\frac{\partial}{\partial c_{4k-1}} e_u(\underset{\sim}{c},\psi) = - w_u(\psi) \, |H(z)| \, \mathrm{Re}\left\{\frac{c_{4k-3} z^{-1} + c_{4k-2} z^{-2}}{H(z) \, [1 + c_{4k-1} z^{-1} + c_{4k} z^{-2}]^2}\right\} \quad \text{(I.9)}$$

$$\frac{\partial}{\partial c_{4k}} e_u(\underset{\sim}{c}, \psi) = - w_u(\psi) \, |H(z)| \mathrm{Re}\left\{\frac{c_{4k-3} z^{-2} + c_{4k-2} z^{-3}}{H(z) \, [1 + c_{4k-1} z^{-1} + c_{4k} z^{-2}]^2}\right\} \quad \text{(I.10)}$$

and

$$\frac{\partial}{\partial c_{4K+1}} e_u(\underset{\sim}{c},\psi) = w_u(\psi) \, |H(z)| \, \mathrm{Re}\left\{\frac{1}{H(z)}\right\}. \quad \text{(I.11)}$$

$$k = 1, \ldots\ldots, K$$

Whereas for both the cascade and parallel forms of the transfer function,

$$\underset{\sim}{\nabla} e_\ell(\underset{\sim}{c},\psi) = \frac{w_\ell(\psi)}{w_u(\psi)} \underset{\sim}{\nabla} e_u(\underset{\sim}{c},\psi) \quad \text{(I.12)}$$

APPENDIX II

THE OUTPUTS OF ALL OSCILLATORS IN A POPULATION OF COUPLED SROs

For each oscillator output, the maximum amplitude is normalized to unity and the simulated time segment is of 2 minutes duration.

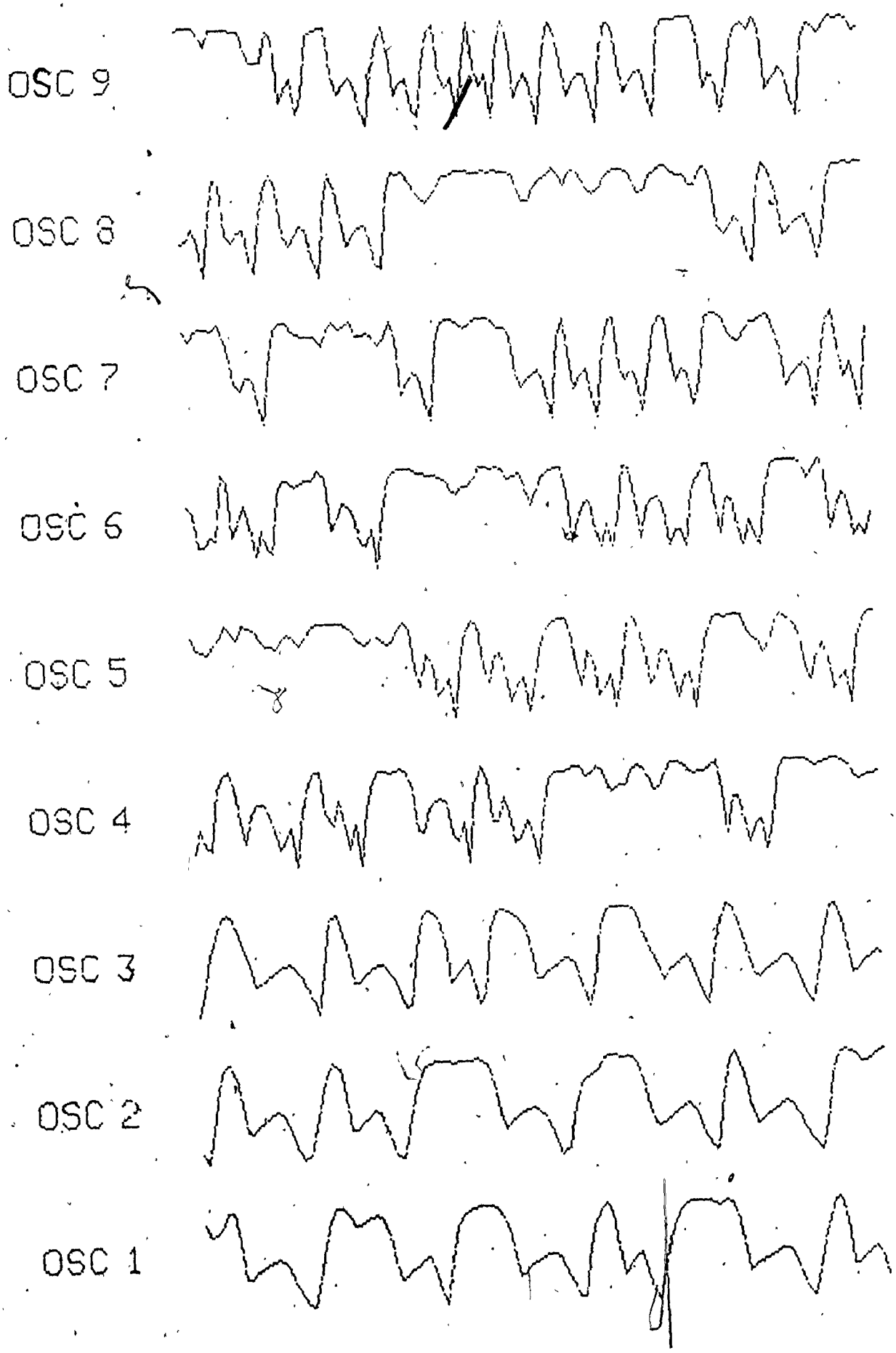
OSC 9
OSC 8
OSC 7
OSC 6
OSC 5
OSC 4
OSC 3
OSC 2
OSC 1

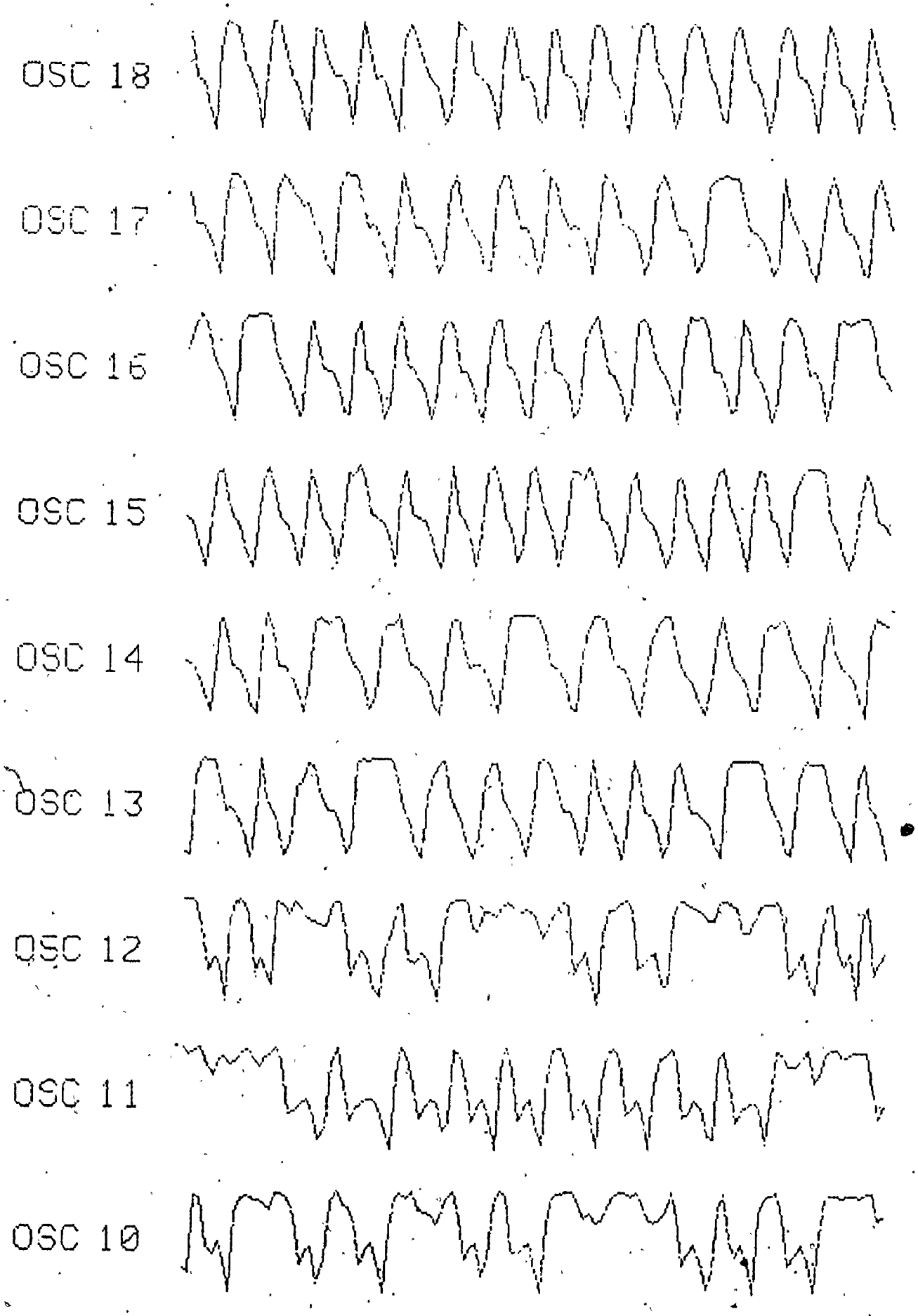
OSC 18
OSC 17
OSC 16
OSC 15
OSC 14
OSC 13
OSC 12
OSC 11
OSC 10

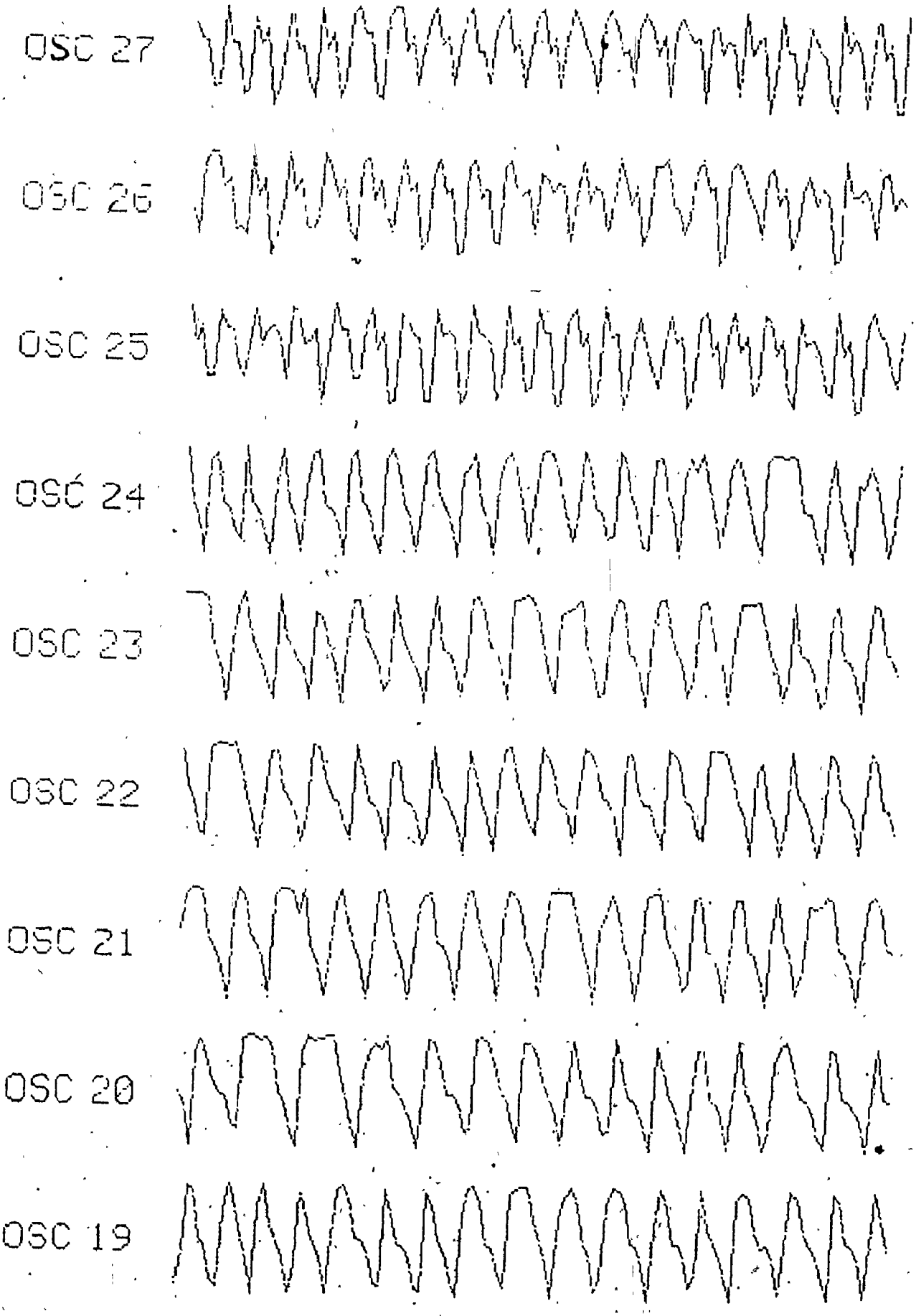
OSC 27
OSC 26
OSC 25
OSC 24
OSC 23
OSC 22
OSC 21
OSC 20
OSC 19

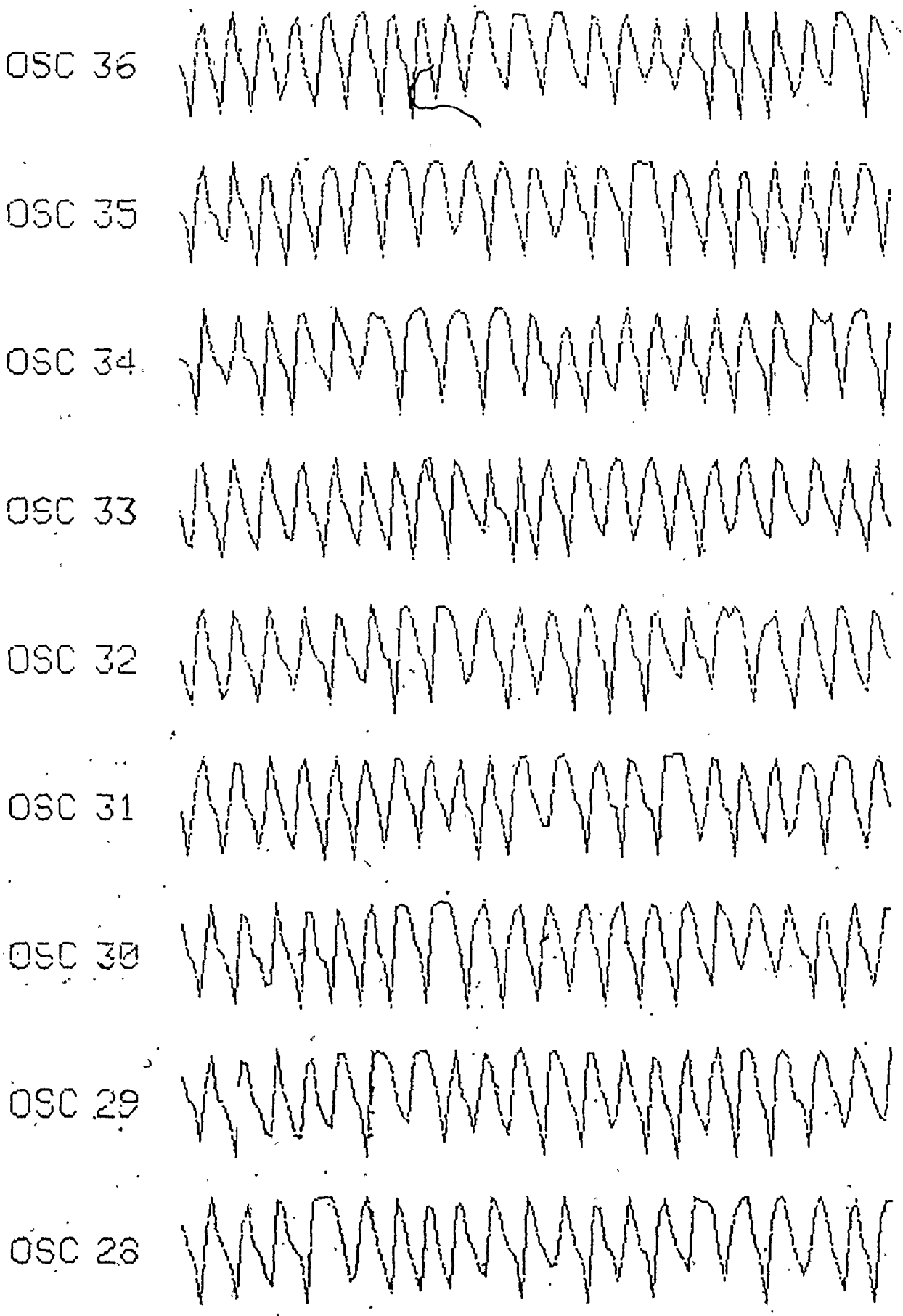
OSC 36
OSC 35
OSC 34
OSC 33
OSC 32
OSC 31
OSC 30
OSC 29
OSC 28

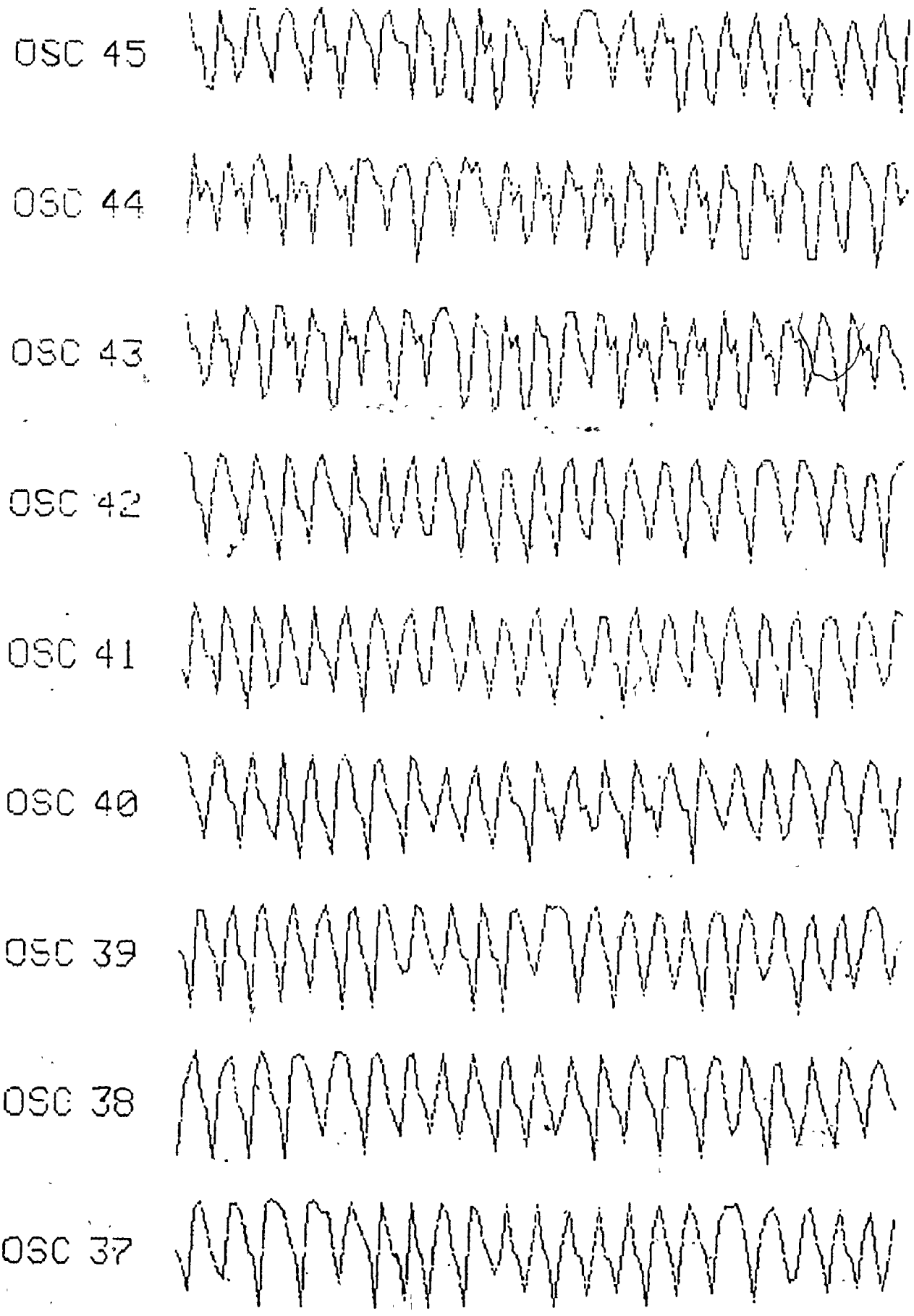
OSC 45
OSC 44
OSC 43
OSC 42
OSC 41
OSC 40
OSC 39
OSC 38
OSC 37

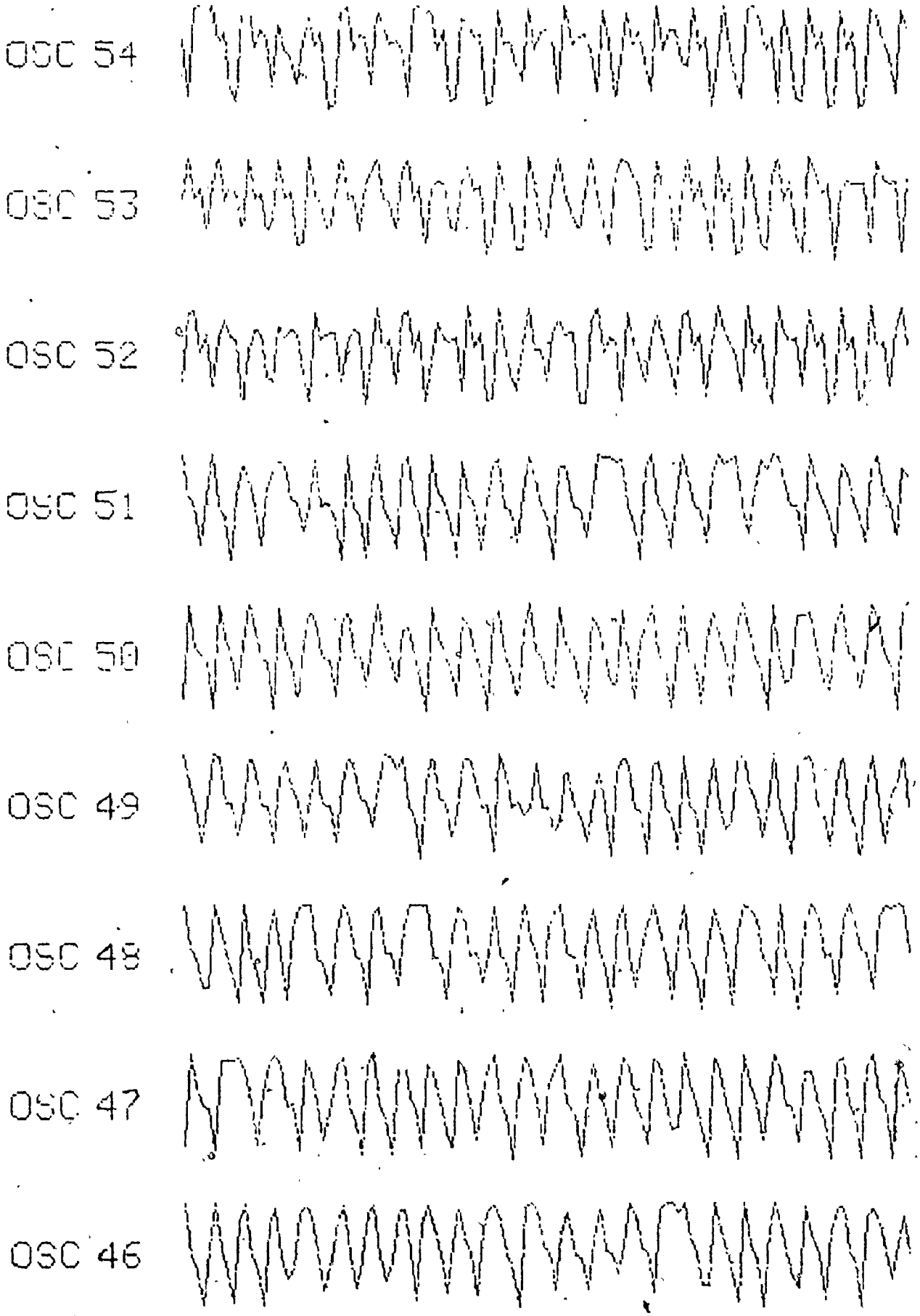
OSC 54
OSC 53
OSC 52
OSC 51
OSC 50
OSC 49
OSC 48
OSC 47
OSC 46

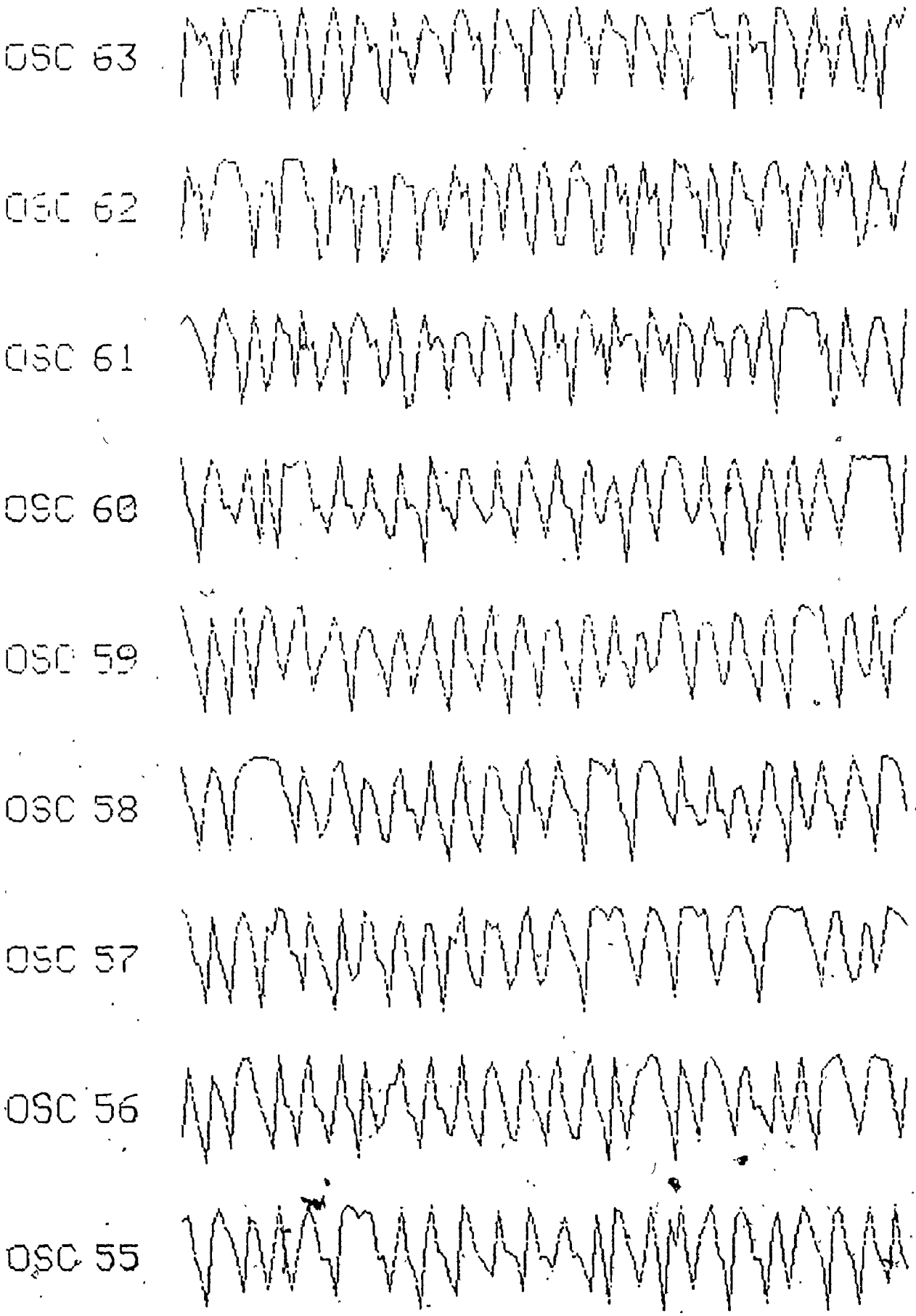
OSC 63
OSC 62
OSC 61
OSC 60
OSC 59
OSC 58
OSC 57
OSC 56
OSC 55

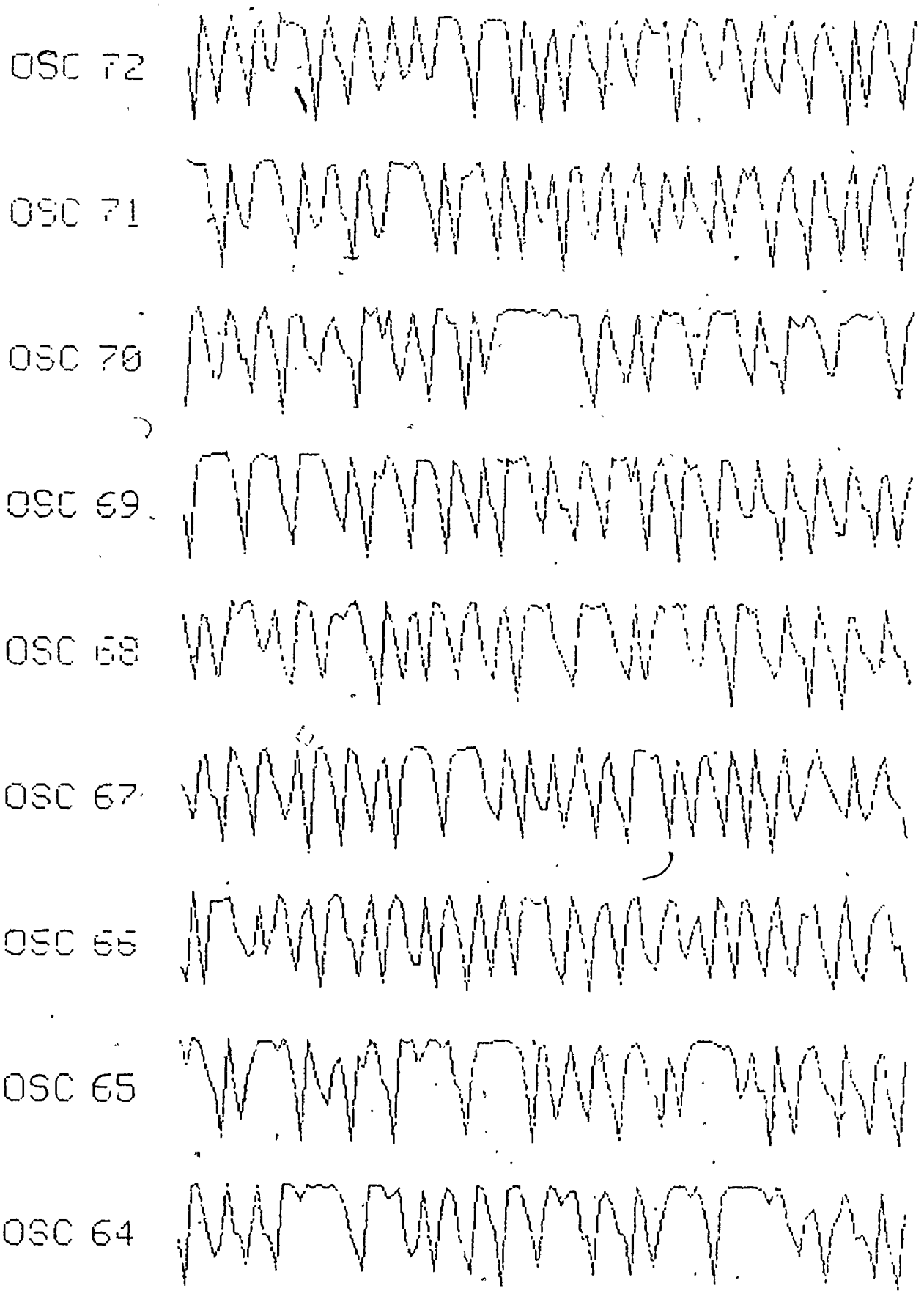
OSC 72
OSC 71
OSC 70
OSC 69
OSC 68
OSC 67
OSC 66
OSC 65
OSC 64

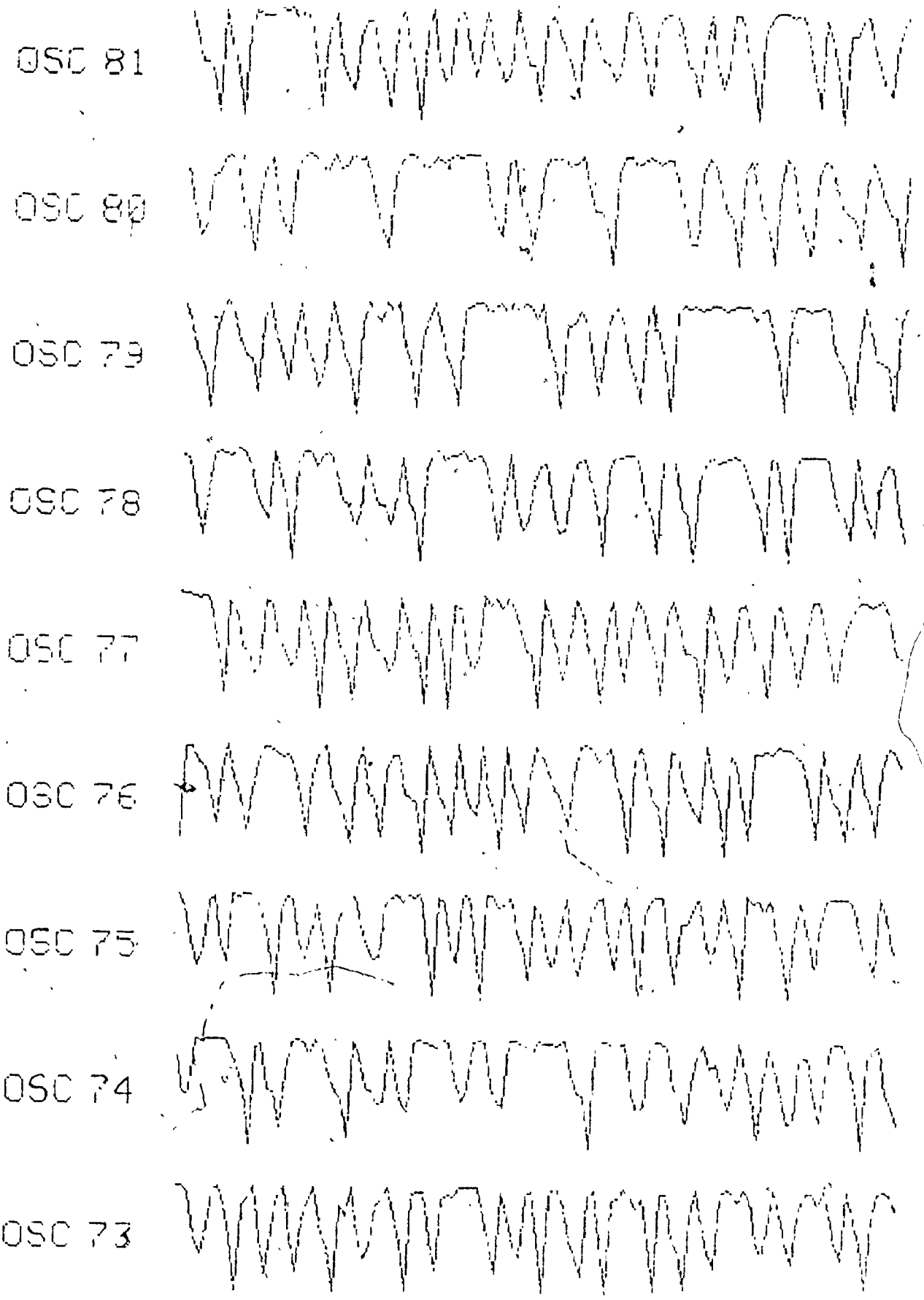
OSC 81
OSC 80
OSC 79
OSC 78
OSC 77
OSC 76
OSC 75
OSC 74
OSC 73

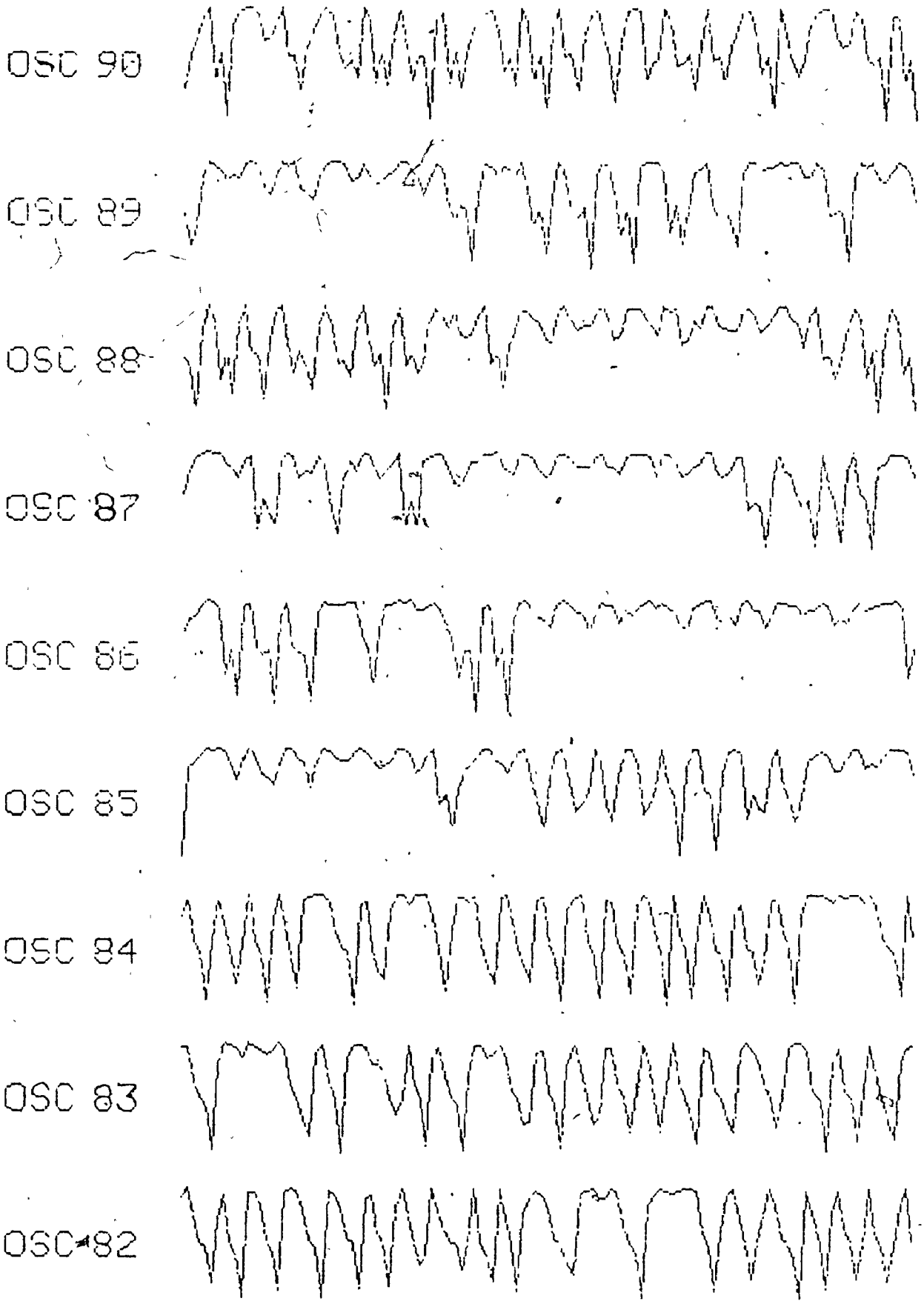
OSC 90
OSC 89
OSC 88
OSC 87
OSC 86
OSC 85
OSC 84
OSC 83
OSC 82

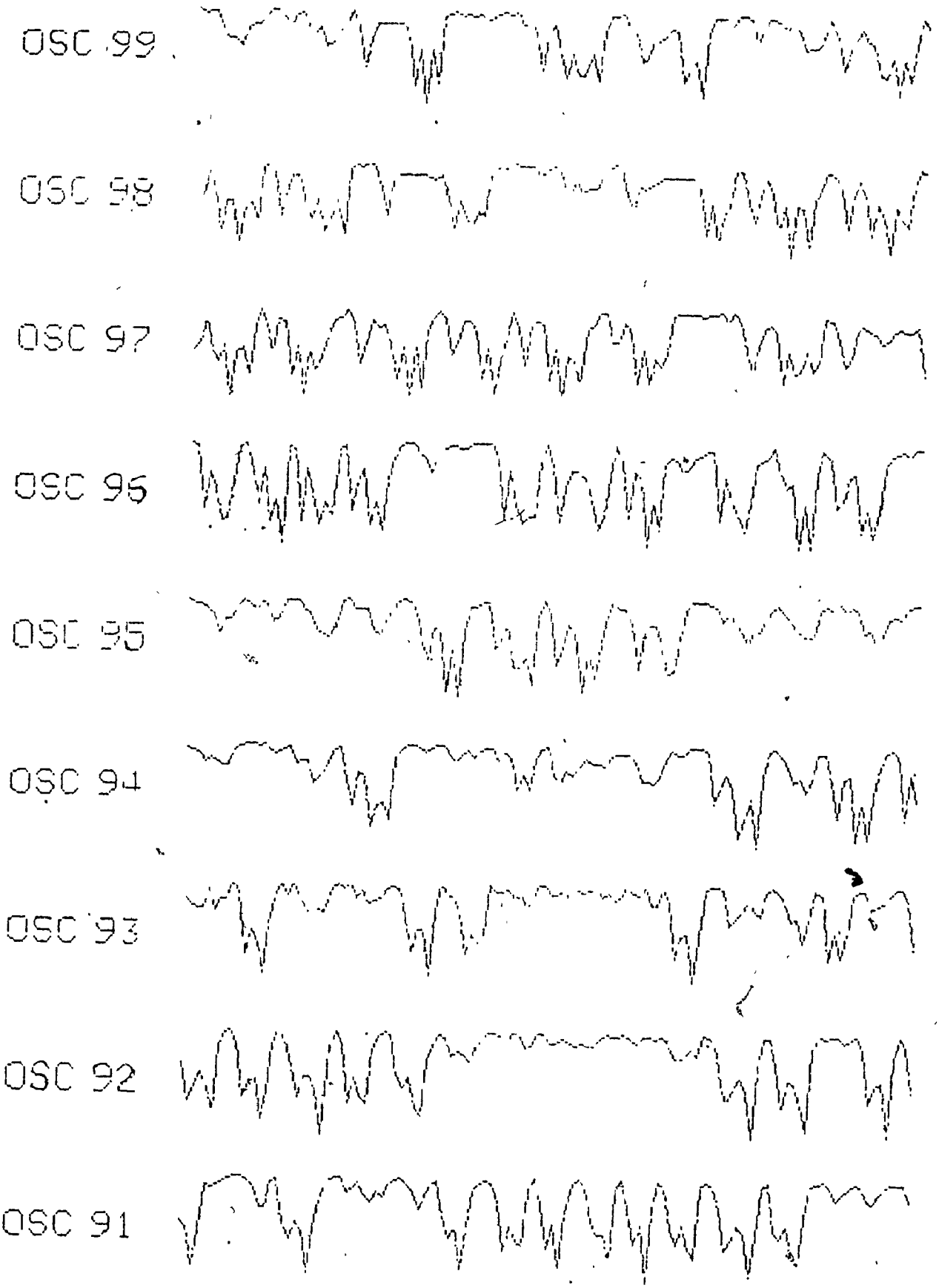
OSC 99
OSC 98
OSC 97
OSC 96
OSC 95
OSC 94
OSC 93
OSC 92
OSC 91

APPENDIX III

THE OUTPUTS OF ALL OSCILLATORS IN A POPULATION OF UNCOUPLED SROs

For each oscillator output, the maximum amplitude is normalized to unity and the simulated time segment is of 2 minutes duration.

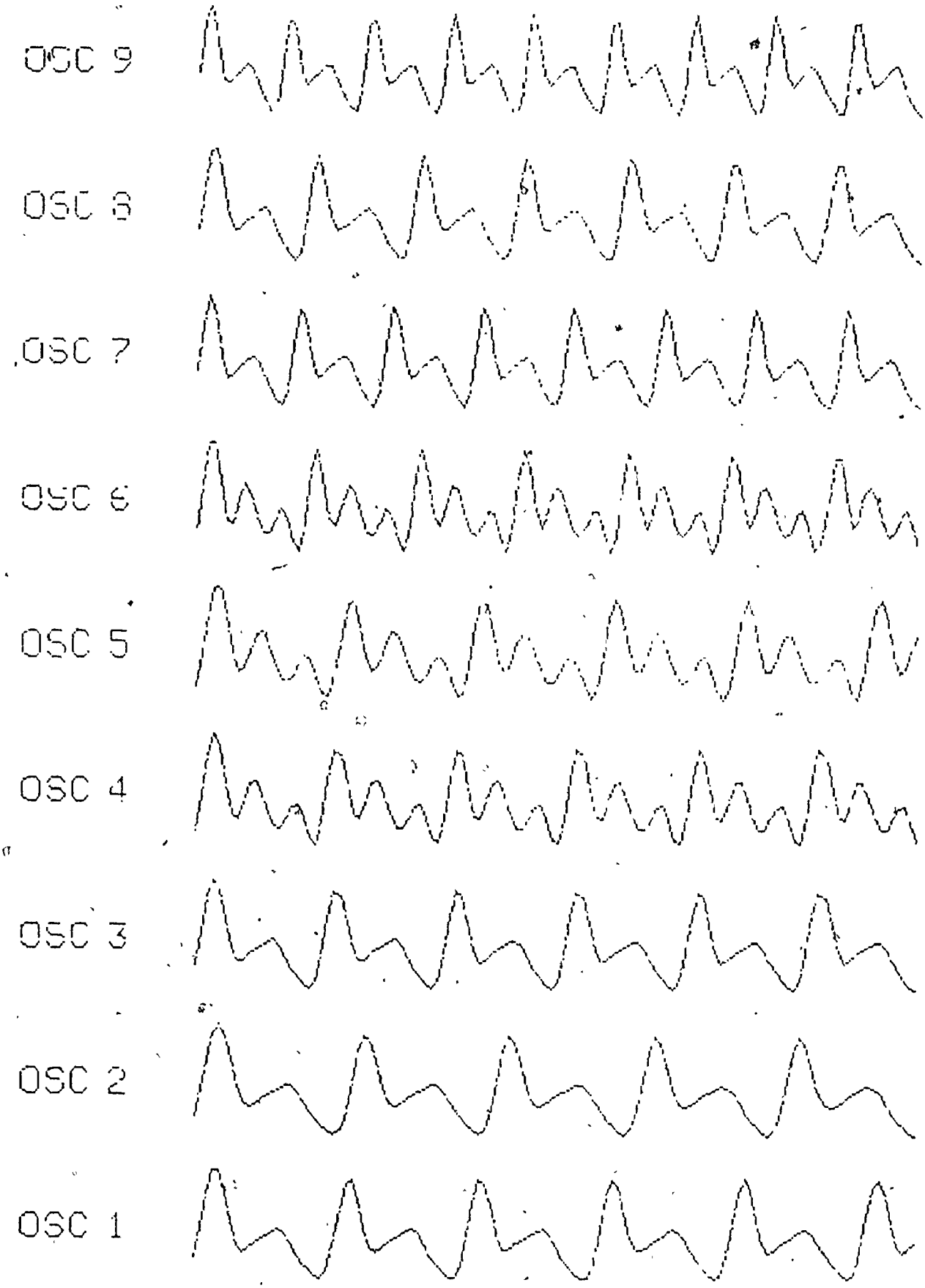
OSC 9
OSC 8
OSC 7
OSC 6
OSC 5
OSC 4
OSC 3
OSC 2
OSC 1

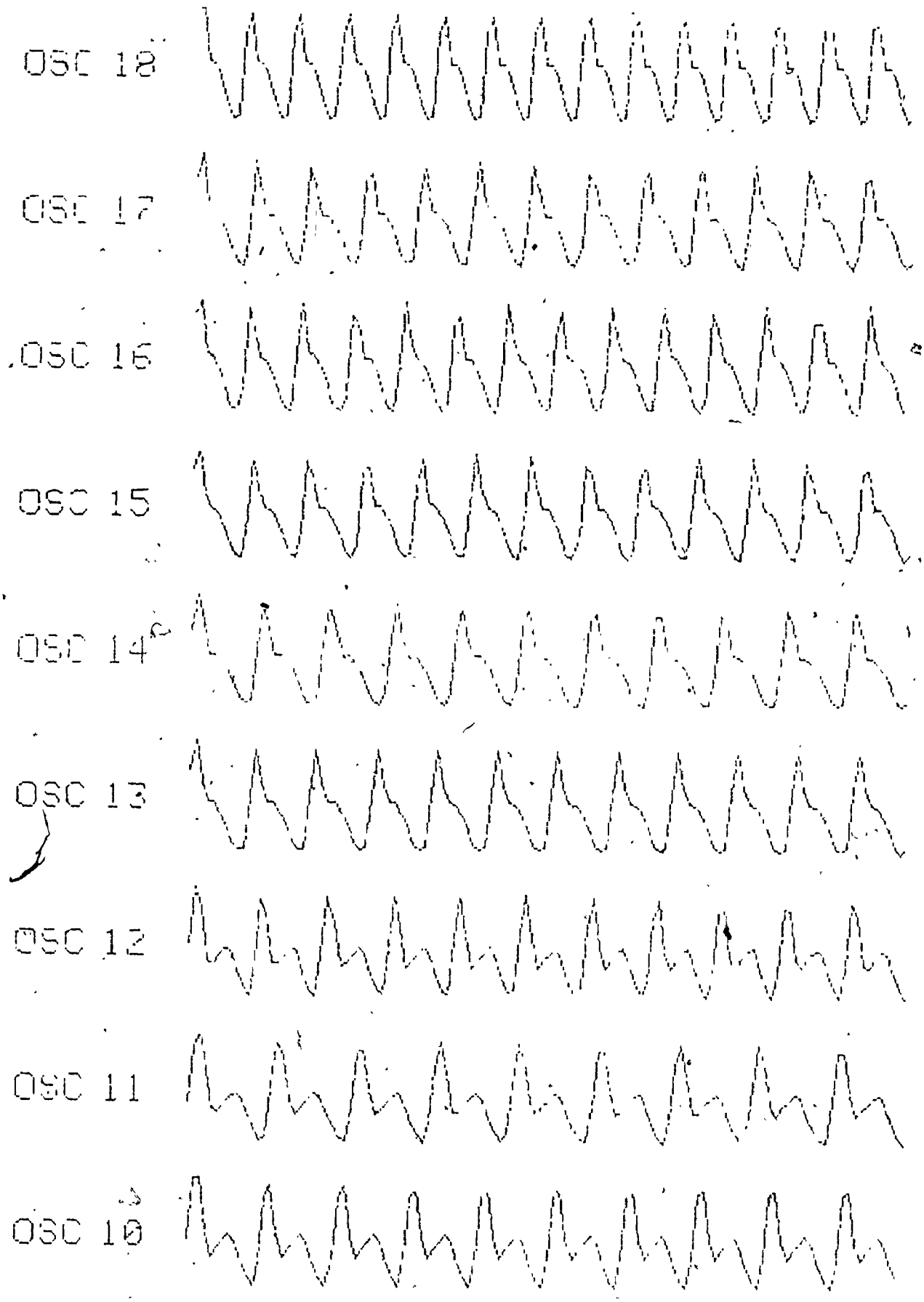
OSC 18
OSC 17
OSC 16
OSC 15
OSC 14
OSC 13
OSC 12
OSC 11
OSC 10

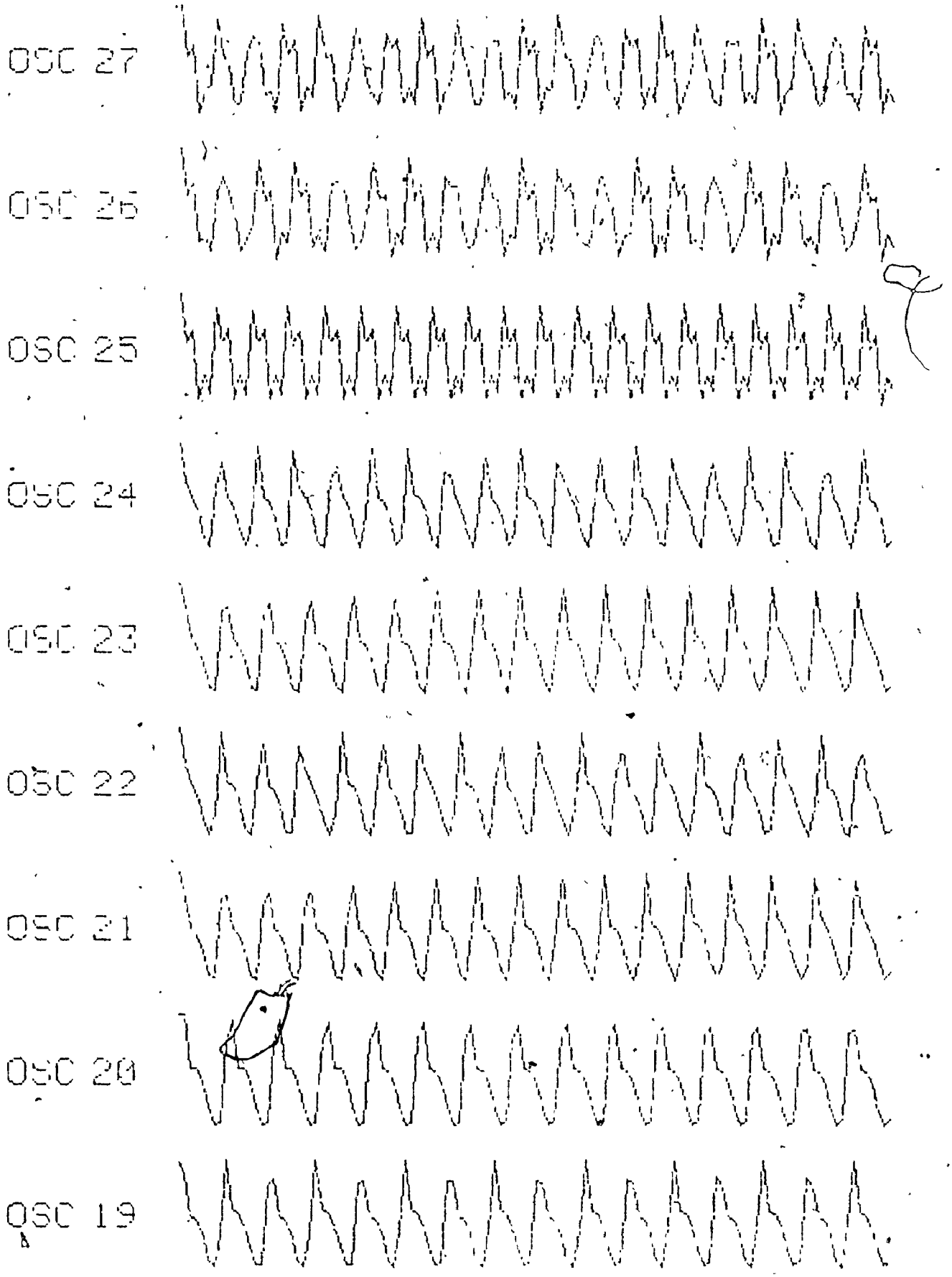
OSC 27
OSC 26
OSC 25
OSC 24
OSC 23
OSC 22
OSC 21
OSC 20
OSC 19

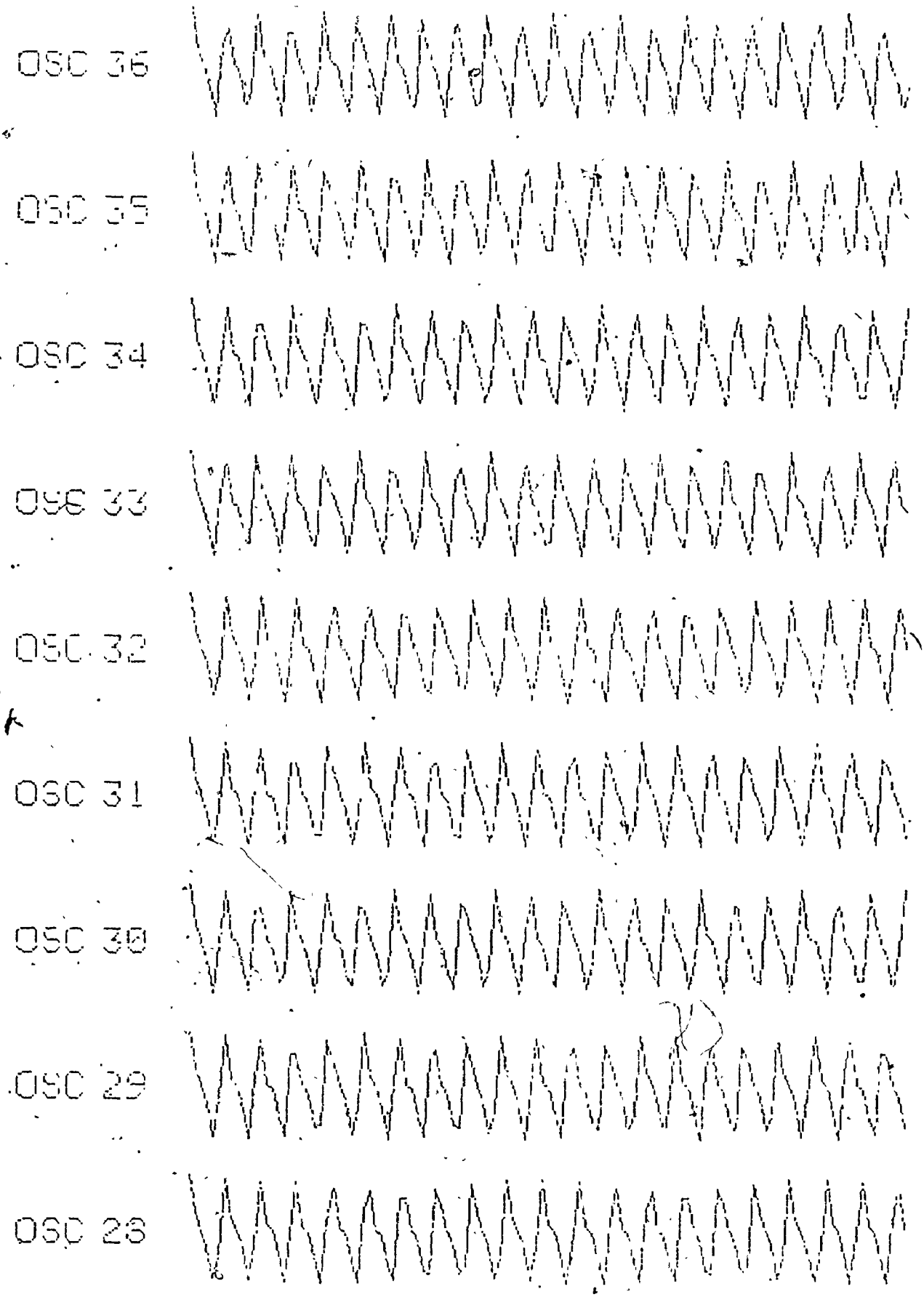
OSC 36
OSC 35
OSC 34
OSC 33
OSC 32
OSC 31
OSC 30
OSC 29
OSC 28

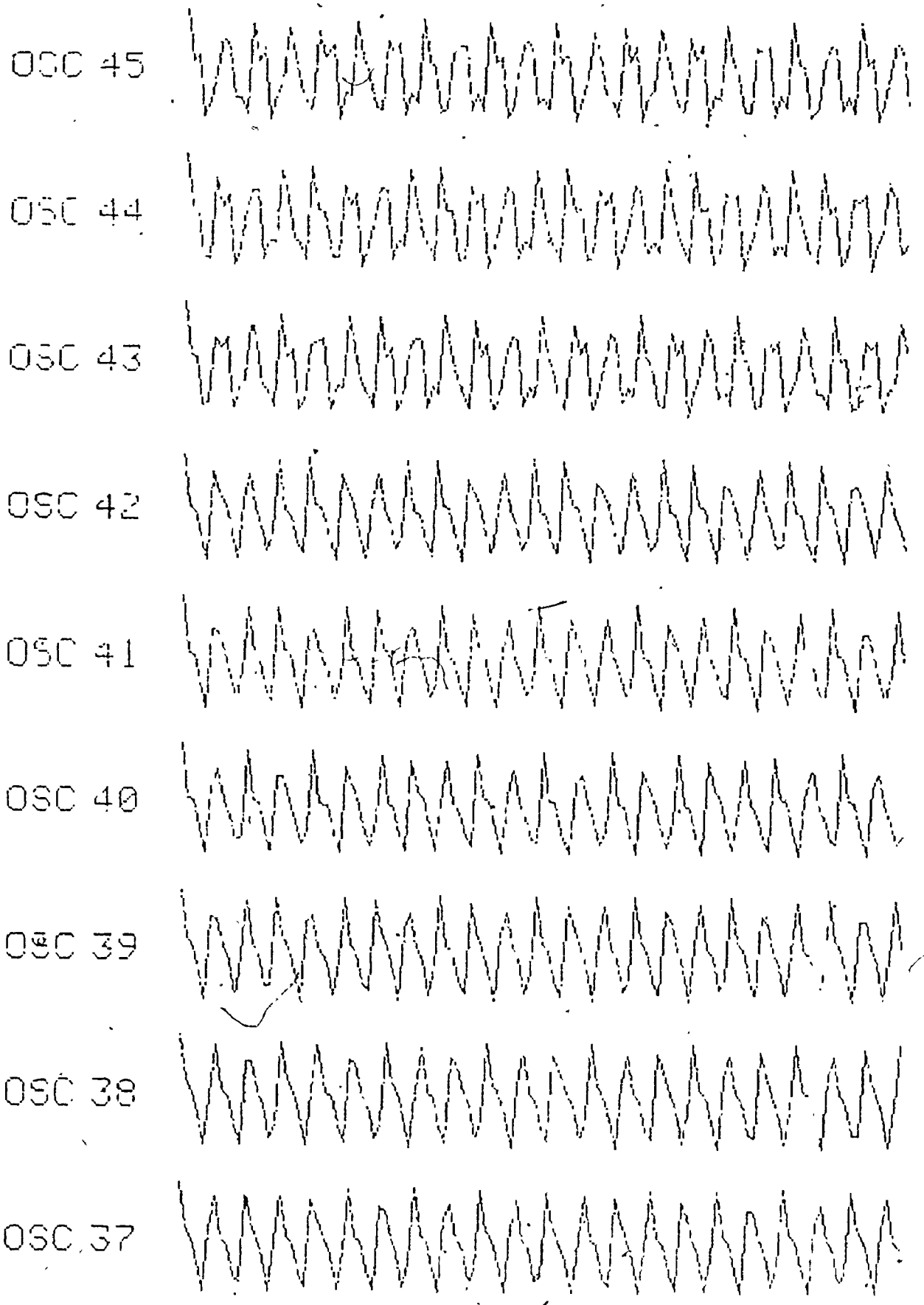
OSC 45
OSC 44
OSC 43
OSC 42
OSC 41
OSC 40
OSC 39
OSC 38
OSC 37

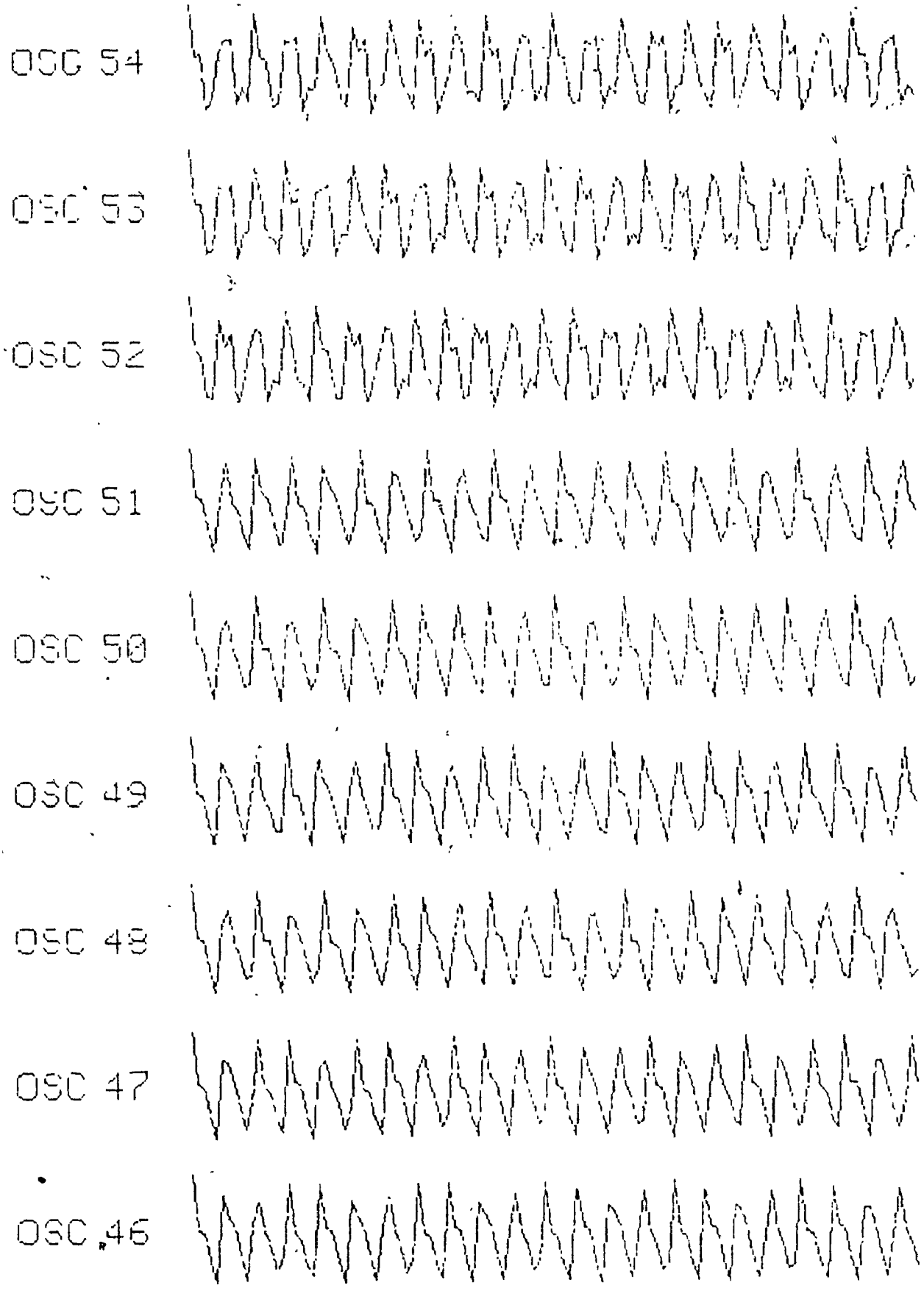
OSC 54
OSC 53
OSC 52
OSC 51
OSC 50
OSC 49
OSC 48
OSC 47
OSC 46

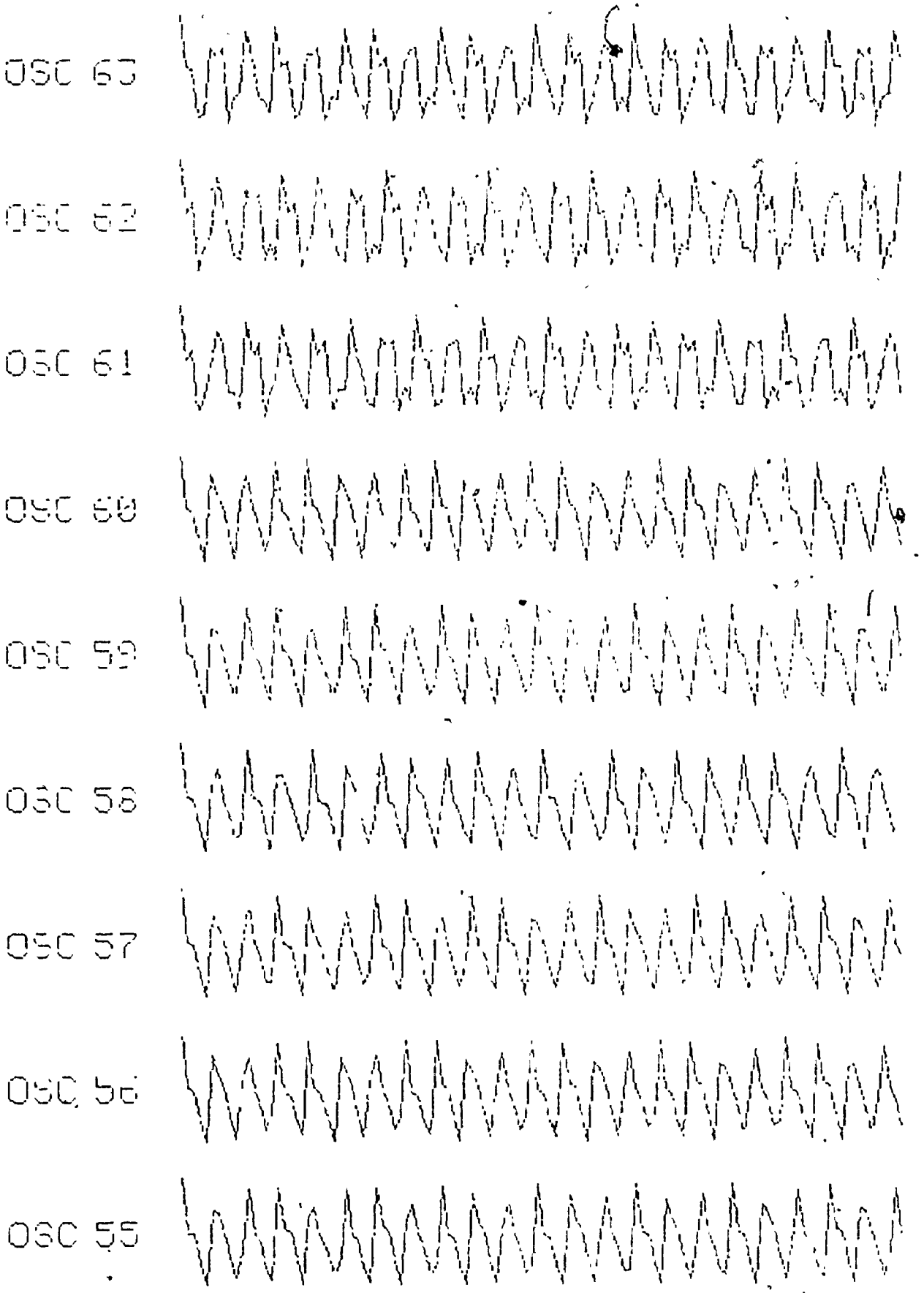
OSC 63
OSC 62
OSC 61
OSC 60
OSC 59
OSC 58
OSC 57
OSC 56
OSC 55

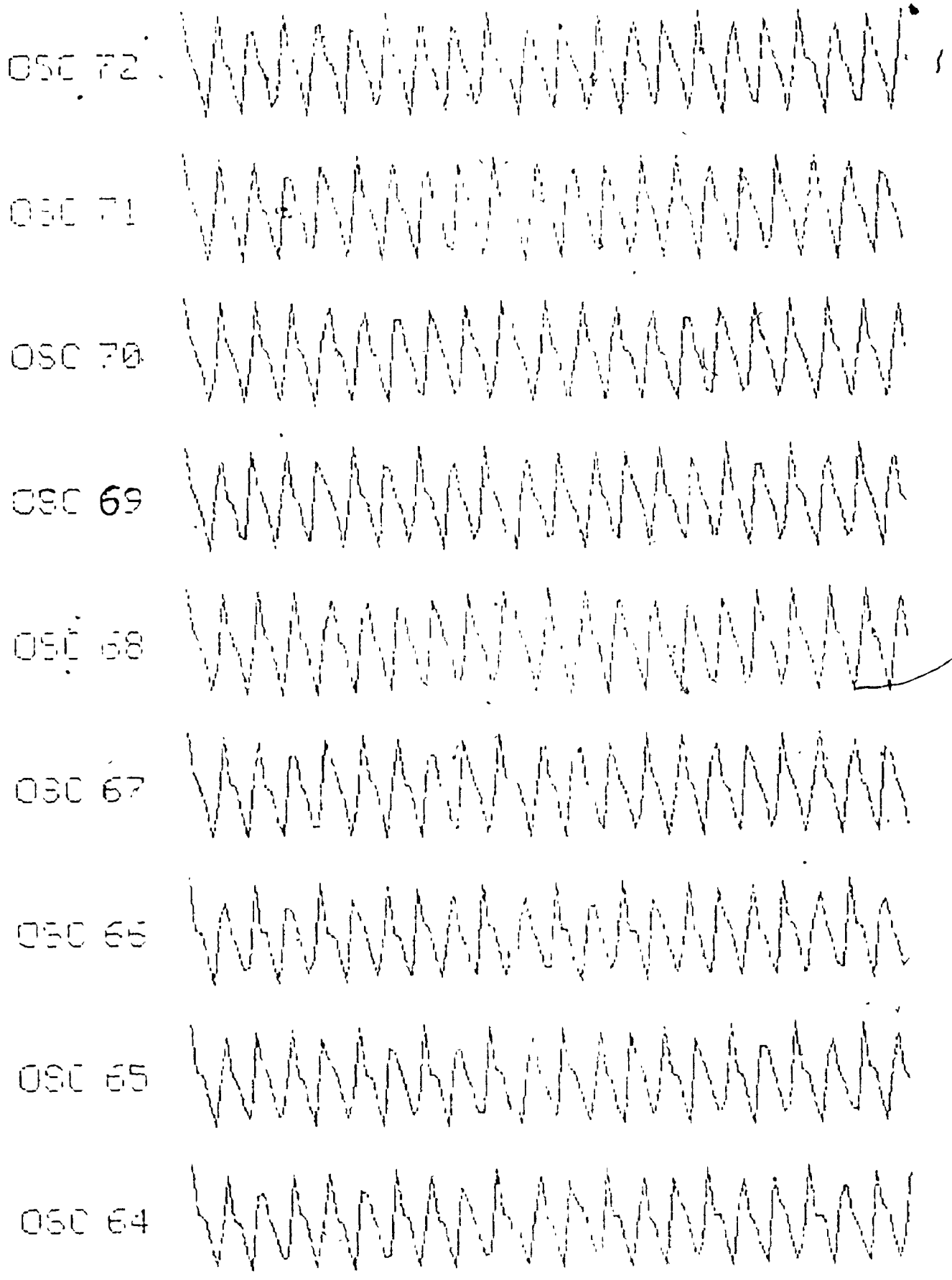
OSC 72
OSC 71
OSC 70
OSC 69
OSC 68
OSC 67
OSC 66
OSC 65
OSC 64

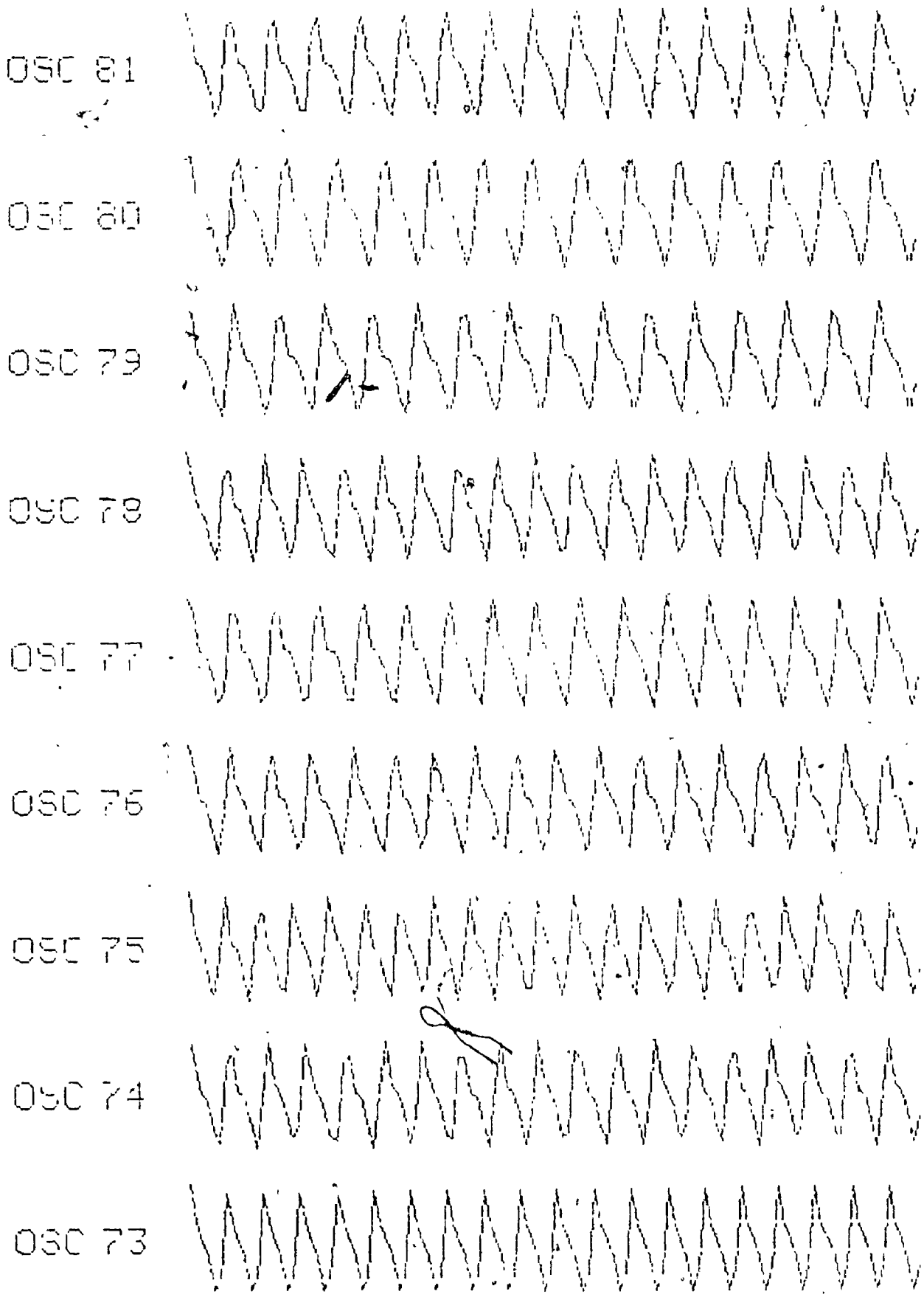
OSC 81
OSC 80
OSC 79
OSC 78
OSC 77
OSC 76
OSC 75
OSC 74
OSC 73

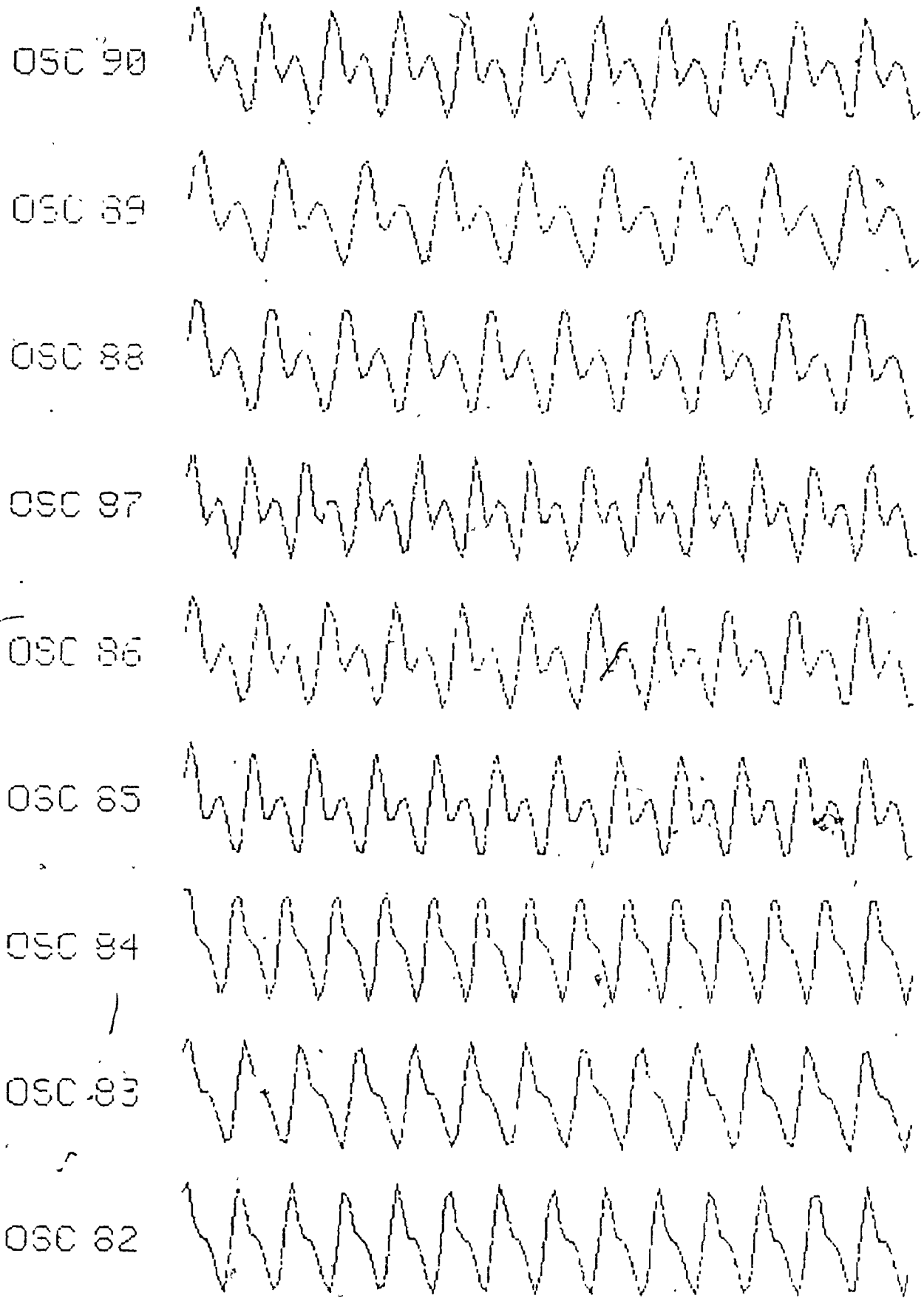
OSC 90
OSC 89
OSC 88
OSC 87
OSC 86
OSC 85
OSC 84
OSC 83
OSC 82

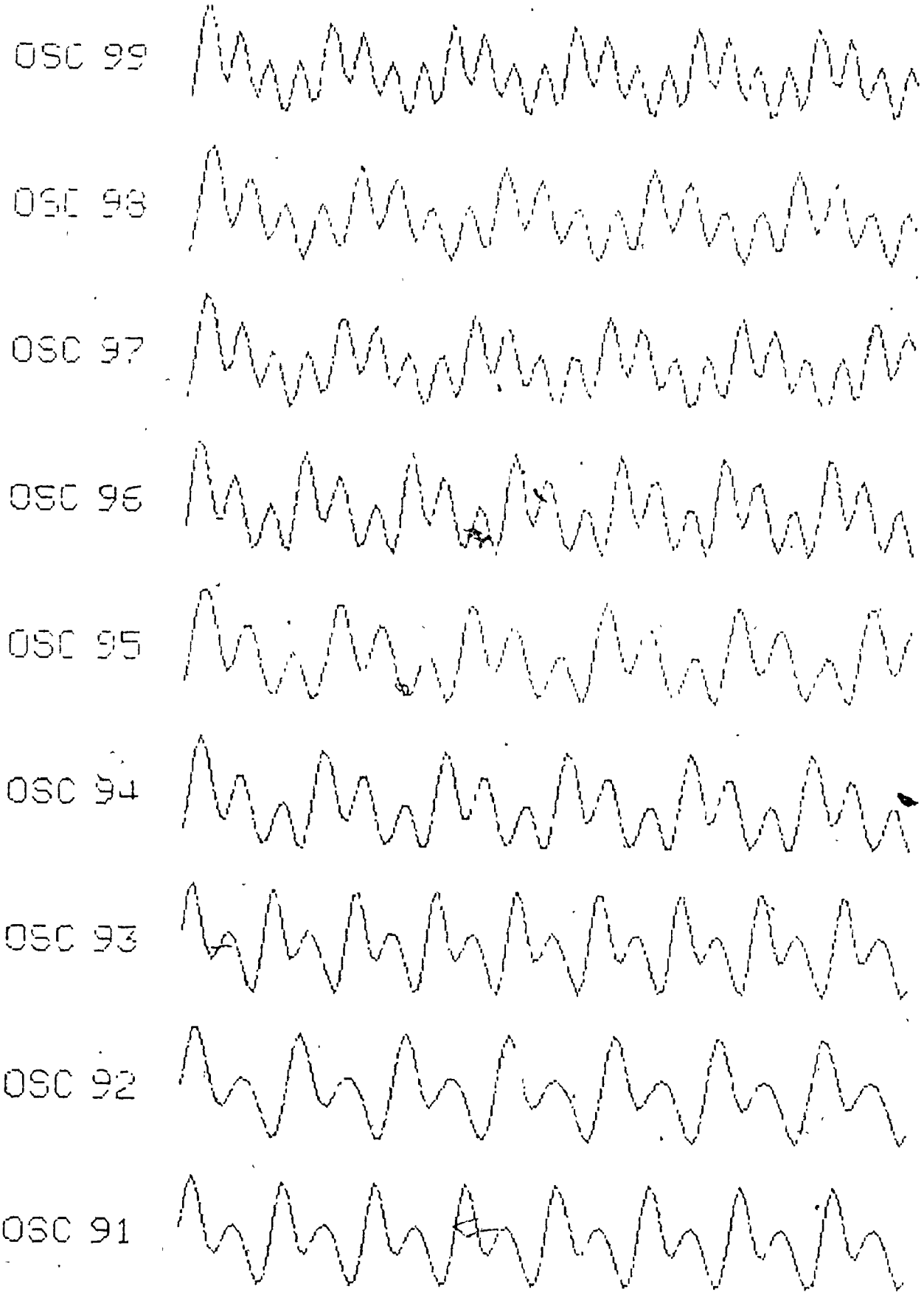
OSC 99
OSC 98
OSC 97
OSC 96
OSC 95
OSC 94
OSC 93
OSC 92
OSC 91

APPENDIX IV

A DIGITAL SIMULATOR OF AN ANALOG INPUT COUPLER

The transfer function of an analog, high-pass, one section RC network consisting of a series capacitance C and a shunt resistance R is

$$H(s) = \frac{s T_c}{1 + s T_c} \qquad \text{(IV.1)}$$

where

$T_c = RC$

and

f_c is the lower cut-off frequency

The transfer function of the digital simulator of an analog input coupler [whose transfer function is prescribed by (IV.1) and whose lower cut-off frequency is f_c] is obtained via the bilinear z-transformation as follows:

Let

ω_d denote the digital angualr frequency

ω_a' denote the prewarped analog angular frequency

T_c' denote the prewarped analog time constant

and τ_s denote the sampling frequency

then

$$\omega_d = 2\pi f_c \qquad \text{(IV.2)}$$

and

$$\omega'_a = \frac{2}{\tau_s} \tan\left(\frac{\omega_d \tau_s}{2}\right) \qquad \text{(IV.3)}$$

Since

$$\omega'_a T'_c = 2\pi f_c T_c \qquad \text{(IV.4)}$$

therefore, substituting from (IV.2) and (IV.3) into (IV.4) one gets

$$T'_c = \frac{\pi f_c T_c \tau_s}{\tan(\pi f_c \tau_s)} \qquad \text{(IV.5)}$$

Replacing T_c by T'_c and s by z in (IV.1), one gets the transfer function of the digital simulator

$$H(z) = G \frac{1 - z^{-1}}{1 + g z^{-1}} \qquad \text{(IV.6)}$$

where

$$G = \frac{2 T'_c}{\tau_s + 2T'_c}$$

and

$$g = \frac{\tau_s - 2T'_c}{\tau_s + 2T'_c}$$

APPENDIX V

AN EXTENSION OF THE GENERIC EQUATION OF ECA MODEL TO INCLUDE ERA

An extension of the generic equation of ECA model (7.1a) - (7.1d) to include ERA, by using a fourth-order nonlinear differential equation to represent each uncoupled oscillator, is prescribed by

$$\dot{x}_{1n} = \omega_{1n}[\{b_{1n}\}\{x_{3n}(1 + \kappa_n) + \rho_{1n}(1 - \rho_{1n}^2 - x_{3n}^2)\}$$
$$+\{-\rho_{1n}(1 + \kappa_n) + x_{3n}(1 - \rho_{1n}^2 - x_{3n}^2)\}\{a_{1n} - 3a_{3n}$$
$$+ 4(a_{2n} - 4a_{4n})x_{3n} + 12a_{3n}x_{3n}^2 + 32a_{4n}x_{3n}^3\}]$$
$$+\omega_{2n}[\{e_{1n}\}\{x_{4n}(1 + x_{2n}) + \rho_{2n}(x_{2n} - e_{0n} - \rho_{2n}^2 - x_{4n}^2)\}$$
$$+\{-\rho_{2n}(1 + x_{2n}) + x_{4n}(x_{2n} - e_{0n} - \rho_{2n}^2 - x_{4n}^2)\}$$
$$\{d_{1n} - 3d_{3n} + 4(d_{2n} - 4d_{4n})x_{4n} + 12d_{3n}x_{4n}^2 + 32d_{4n}x_{4n}^3\}] \qquad (V.1)$$

$$\dot{x}_{2n} = \omega_{1n}[\{b_{1n}\}\{x_{3n}(1 + \kappa_n) + \rho_{1n}(1 - \rho_{1n}^2 - x_{3n}^2)\}$$
$$+\{-\rho_{1n}(1 + \kappa_n) + x_{3n}(1 - \rho_{1n}^2 - x_{3n}^2)\}\{a_{1n} - 3a_{3n}$$
$$+ 4(a_{2n} - 4a_{4n})x_{3n} + 12a_{3n}x_{3n}^2 + 32a_{4n}x_{3n}^3\}] \qquad (V.2)$$

$$\dot{x}_{3n} = \omega_{1n}[-\rho_{1n}(1 + \kappa_n) + x_{3n}(1 - \rho_{1n}^2 - x_{3n}^2)] \qquad (V.3)$$

$$\dot{x}_{4n} = \omega_{2n}[-\rho_{2n}(1 + x_{2n}) + x_{4n}(x_{2n} - e_{0n} - \rho_{2n}^2 - x_{4n}^2)] \qquad (V.4)$$

where

$$\rho_{1n} = \frac{1}{b_{1n}} [a_{2n} - a_{0n} - a_{4n} + x_{2n} - (a_{1n} - 3a_{3n}) x_{3n}$$

$$- 2(a_{2n} - 4a_{4n}) x_{3n}^2 - 4a_{3n} x_{3n}^3 - 8a_{4n} x_{3n}^4] \quad (V.5)$$

$$\rho_{2n} = \frac{1}{e_{1n}} [d_{2n} - d_{0n} - d_{4n} - x_{2n} + x_{1n} - (d_{1n} - 3d_{3n}) x_{4n}$$

$$- 2(d_{2n} - 4d_{4n}) x_{4n}^2 - 4d_{3n} x_{4n}^3 - 8d_{4n} x_{4n}^4] \quad (V.6)$$

$$\kappa_n = \sum_{m \epsilon I_{cn}} c_{mn} (x_{1m} - x_{1n}) \quad (V.7)$$

$$\omega_{1n} = \frac{\pi}{30} f_{1n} \quad (V.8)$$

$$\omega_{2n} = \frac{\pi}{30} f_{2n} \quad (V.9)$$

also,

x_{1n} is the output variable of nth oscillator

x_{2n} is the control variable of nth oscillator

x_{3n} is the fundamental variable of nth oscillator

x_{4n} is the response variable of nth oscillator

I_{cn} is the coupling index of nth oscillator

and f_{1n}, f_{2n}, b_{1n}, e_{0n}, e_{1n}, $\{a_{kn}, d_{kn} \mid k = 0, 1, \ldots.4\}$ are the intrinsic parameters of nth oscillator.

REFERENCES

Aggarwal J.K. and Richie C.G. (1966), "On coupled Van der Pol oscillators", IEEE Trans. Circuit Theory, vol. CT-13, pp. 465-466.

Alvarez W.C. and Mahoney L.J. (1922), "Action current in stomach and intestine", Am. J. Physiol., vol. 58, pp. 476-493.

Andronov A.A., Vitt A.A. and Khaikin S.E. (1966), Theory of oscillators, Reading, Mass.: Addison-Wesley.

Avenhaus E. (1972), "On the design of digital filters with coefficients of limited word lengths", IEEE Trans. Audio Electroacoust., vol. AU-20, pp. 206-212.

Bandler J.W. and Charalambous C. (1972), "Practical least pth optimization of networks", IEEE Trans. Microwave Theory Tech.,vol. MTT-20, pp. 834-840.

Bandler J.W. and Bardakjian B.L. (1973a), "Least pth optimization of recursive digital filters", Proc. IEEE Int. Symp. on Circuit Theory, Toronto, Canada, pp. 377-380.

Bandler J.W. and Bardakjian B.L. (1973b), "Least pth optimization of recursive digital filters", IEEE Trans. Audio Electroacoust., vol. AU-21, pp. 460-470.

Bandler J.W. and Charalambous C. (1973c), "On conditions for optimality in least pth approximation with $p \to \infty$ ", J. Optimiz. Theory and Appl., vol. 11, pp. 556-566.

Bandler J.W., Bardakjian B.L. and Chen J.H.K. (1974a), "Design of recursive digital filters with optimum-word-length coefficients", Proc. 8th Princeton Conf. on Information Sciences and Systems, Princeton, N.J., pp. 126-131.

Bandler J.W. and Charalambous C. (1974b), "Nonlinear programming using minimax techniques", J. Optimiz. Theory and Appl., vol. 13, pp. 607-619.

Bandler J.W. and Chen J.H.K. (1975a), "DISOPT-A general program for continuous and discrete nonlinear programming problems", Int. J. Syst. Sci., vol. 6, pp. 665-680.

Bandler J.W., Bardakjian B.L. and Chen J.H.K. (1975b), "Design of recursive digital filters with optimized-word-length coefficients", Computer Aided Design, vol. 7, pp. 151-156.

Bandler J.W., Charalambous C., Chen J.H.K. and Chu W.Y. (1976), "New results in the least pth approach to minimax design", IEEE Trans. Microwave Theory Tech., vol. MTT-24, pp. 116-119.

Bardakjian B.L., Sarna S.K., Waterfall W.E., Daniel E.E. and Lind J.F. (1976a), "Control function of human colonic electrical activity analyzed by computer", Gastroenterology, vol. 70, pp. A-3/861.

Bardakjian B.L. and Sarna S.K. (1976b), "A multiple-input algorithmic processor for multistage decimation and filtering", Proc. 29th ACEMB, Boston, Mass., pp. 415.

Bardakjian B.L. and Sarna S.K. (1977), "Interactive modules for simulation of coupled biological oscillators", Proc. IEEE Int. Conf. on Cybernetics and Society, Washington D.C., pp. 465-467.

Bardakjian B.L. and Sarna S.K. (1978a), "An optimal processor for multistage decimation and filtering ", IEEE Trans. Acoust., Speech, Signal Processing, submitted for publication.

Bardakjian B.L. (1978b), "Program listings of interactive processors for analysis and modelling of biological rhythms", Internal Report in Biomedical Engineering, BME-4, Hamilton, Canada: McMaster University.

Basar E. and Eroglu C., (1976), "Spectral analysis of spontaneous activity in smooth muscles", in Physiology of Smooth Muscle, edited by Bülbring E. and Shuba M.F., New York: Raven Press, pp. 137-146.

Bass P. (1965), "Electric activity of smooth muscle of the gastrointestinal tract", Gastroenterology, vol. 49, pp. 391-394.

Bass S.C. (1975), "The mathematical and laboratory generation of prescribed periodic waveforms", IEEE Trans. Circuits and Systems, vol. CAS-22, pp. 603-610.

Beauchamp K.G. (1973), Signal processing: using analog and digital techniques. London: George Allan and Unwin.

Bozler E. (1938a), "Electrical stimulation and conduction of excitation in smooth muscle", Am. J. Physiol., vol. 122, pp. 614-623.

Bozler E. (1938b), "Action potentials of visceral smooth muscle", Am. J. Physiol., vol. 124, pp. 502-510.

Bozler E. (1939), "Electrophysiological studies on the motility of the gastrointestinal tract", Am. J. Physiol., vol. 127, pp. 301-307.

Bozler E. (1941), "Action potentials and conduction of excitation in muscle", Biol. Symposia, vol. 3, pp. 95-110.

Bruce J.D. (1968), "Discrete fourier transforms, linear filters, and spectrum weighting", IEEE Trans. Audio Electroacoust., vol. AU-16, pp. 495-499.

Buck J.B. (1935), "Synchronous flashing of fireflies experimentally induced", Science, vol. 81, no. 2101, pp. 339-340.

Buck J.B. (1937), "Flashing of fireflies in Jamaica", Nature, vol. 139, no. 3523, pp. 801.

Buck J.B. (1938), "Synchronous rhythmic flashing of fireflies", Quart. Rev. Biol., vol. 13, no. 3, pp. 301-314.

Buck J. and Buck E. (1966), "Biology of synchronous flashing of fireflies", Nature, vol. 211, no. 5049, pp. 562-564.

Bülbring E., Burnstock G. and Holman M.E. (1958), "Excitation and conduction in the smooth muscle of the isolated taenia coli of the guinea pig", J. Physiol., vol. 142, pp. 420-437.

Burnstock G., Holman M.E. and Prosser C.L. (1963), "Electrophysiology of smooth muscle", Physiol. Rev., vol. 43, pp. 482-527.

Butenin N.V. (1965), Elements of the theory of nonlinear oscillations. Boston, Mass.: Blaisdell.

Caprilli R. and Onori L. (1972), "Origin, transmission and ionic dependence of colonic electrical slow waves", Scand. J. Gastroent., vol. 7, pp. 65-74.

Charalambous C. and Bandler J.W. (1973), "New algorithms for network optimization", IEEE Trans. Microwave Theory Tech., vol. MTT-21, pp. 815-818.

Charalambous C. (1974a), "Minimax design of recursive digital filters", Comput. Aided Des., vol. 6, pp. 73-81.

Charalambous C. and Best M.J. (1974b), "Optimization of recursive digital filters with finite word lengths", IEEE Trans. Acoust., Speech, Signal Proc., vol. ASSP-22, pp. 424-431.

Charalambous C. (1975), "Minimax optimization of recursive digital filters using recent minimax results", IEEE Trans. Acoust., Speech, Signal Proc., vol. ASSP-23, pp. 333-345.

Charalambous C. and Bandler J.W. (1976), "Nonlinear minimax optimization as a sequence of least pth optimization with finite values of p", Int. J. Syst. Sci., vol. 7, pp. 377-391.

Chen J.H.K. (1974), "DISOPT-A general program for continuous and discrete nonlinear programming problems", Internal Report in Simulation Optimization and Control, SOC-29, Hamilton, Canada: McMaster University.

Christensen J., Caprilli R. and Lund G.F. (1969), "Electric slow waves in circular muscle of cat colon", Am. J. Physiol., vol. 217, pp. 771-776.

Christensen J. and Hauser R.L. (1971a), "Longitudinal axial coupling of slow waves in proximal cat colon", Am. J. Physiol., vol. 221, pp. 246-250.

Christensen J. and Hauser R.L. (1971b), "Circumferential coupling of electric slow waves in circular muscle of cat colon", Am. J. Physiol., vol. 221, pp. 1033-1037.

Christensen J. and Rasmus S.C. (1972), "Colon slow waves: size of oscillators and rates of spread", Am J. Physiol., vol. 223, pp. 1330-1333.

Christensen J., Auras S. and Hauser R.L. (1974),"Migrating spike bursts and electrical slow waves in the cat colon: effect of sectioning", Gastroenterology, vol. 66, pp. 240-247.

Christensen J. (1975), "Myoelectric control of the colon", Gastroenterology, vol. 68, pp. 601-609.

Christian E. and Eisenmann E. (1966), Filter design tables and graphs. New York: John Wiley.

Christiansen J. (1970), "Numerical solution of ordinary simultaneous differential equations of the first-order using a method of automatic step change", Numerische Mathematik, vol. 14, pp. 317-324.

Chu W.Y. (1974), "Extrapolation in least pth approximation and nonlinear programming", Internal Report in Simulation, Optimization and Control, SOC-71, Hamilton, Canada: McMaster University.

Chua L.O. and Green D.N. (1972), "Synthesis of nonlinear systems having prescribed periodic solutions", Memorandum in Electronics Research Laboratory, ERL-M350, Berkeley: University of California.

Chua L.O. and Green D.N. (1974), "Synthesis of nonlinear periodic systems" IEEE Trans. Circuits and Systems, vol. CAS-21, pp. 286-294.

Connell A.M. (1968), "Motor action of the large bowel", in Handbook of Physiology, Alimentary Canal, vol. 4: Motility, edited by Code C.F., Washington D.C.: American Physiological Society, pp. 2075-2091.

Constantinides A.G. (1967), "Frequency transformations for digital filters", Elec. Lett., vol. 3, pp. 487-489.

Constantinides A.G. (1968), "Frequency transformations for digital filters", Elec. Lett. vol. 4, pp. 115-116.

Constantinides A.G. (1970), "Spectral transformations for digital filters", Proc. IEE , vol, 117, pp. 1585-1590.

Cooley, J.W. and Tukey J.W. (1965), " An algorithm for the machine calculation of complex Fourier series", Math. of Comput., vol. 19, pp. 297-301.

Couturier D., Roze C., Couturier-Turpin M.H. and Debray C. (1969), "Electromyography of the colon in situ: an experimental study in man and in the rabbit", Gastroenterology, vol. 56, pp. 317-322.

Crochiere R.E. and Rabiner L.R. (1975), "Optimum FIR digital filter implementations for decimation, interpolation, and narrow-band filtering", IEEE Trans. Acoust., Speech, Signal Proc., vol. ASSP-23, pp. 444-456.

Dakin R.J. (1966), "A tree-search algorithm for mixed integer programming problems", Comput. J., vol. 8, pp. 250-255.

Daniel E.E. and Chapman K.M. (1963), "Electrical activity of the gastrointestinal tract as an indication of mechanical activity ", Am. J. Digest. Dis., vol.8, pp. 54-102.

Daniel E.E. (1975), "Electrophysiology of the colon", Gut, vol. 16, pp. 298-329.

Davies J.G. and Sowton E. (1966), "Electrical threshold of the human heart", Brit. Heart J., vol. 28, pp. 231-239.

De Haan R.L. (1967), "Spontaneous activity of cultured heart cells", in Factors influencing myocardial contractility, edited by Tanz R.D.,

Kavaler F. and Roberts J., New York: Academic Press, pp. 217-230.

Deczky A.G. (1972), "Synthesis of recursive digital filters using the minimum p-error criterion", IEEE Trans. Audio Electroacoust., vol. AU-20, pp. 257-263.

Diamant N.E. and Bortoff A. (1969a), "Nature of the intestinal slow-wave frequency gradient", Am. J. Physiol., vol. 216, pp. 301-307.

Diamant N.E. and Bortoff A. (1969b), "Effects of transection on the intestinal slow-wave frequency gradient", Am. J. Physiol., vol. 216, pp. 734-743.

Diamant N.E., Rose P.K. and Davison E.J. (1970), "Computer simulation of intestinal slow-wave frequency gradient", Am. J. Physiol., vol. 219, pp. 1684-1690.

Douglas D.M. (1949), "The decrease in frequency of contraction of the jejunum after transplantation to the ileum", J. Physiol., vol. 110, pp. 66-75.

Duthie H.L. (1974), "Electrical activity of gastrointestinal smooth muscle", Gut, vol. 15, pp. 669-681.

Endo T. and Mori S. (1976), "Mode analysis of a multimode ladder oscillator", IEEE Trans. Circuits and Systems, vol. CAS-23, pp. 100-113.

Endo T. and Mori S. (1978), "Mode analysis of a ring of a large number of mutually coupled Van der Pol oscillators", IEEE Trans. Circuits and Systems, vol. CAS-25, pp. 7-18.

Fitzhugh R. (1961), "Impusles and physiological states in theoretical models of nerve membrane", Biophys. J., vol. 1, pp. 445-466.

Fletcher R. and Powell M.J.D. (1963), "A rapidly convergent descent method for minimization", Comput. J., vol. 6, pp. 163-168.

Fletcher R. (1970), "A new approach to variable metric algorithms", Comput. J., vol. 13, pp. 317-322.

Fletcher R. (1972), "Fortran subroutines for minimization by quasi-Newton methods", Atomic Energy Research Establishment, Harwell, Berkshire, England, Report AERE-R7125.

Gillespie J.S. (1962a), "Spontaneous mechanical and electrical activity of stretched and unstretched intestinal smooth muscle cells and their response to sympathetic nerve stimulation", J. Physiol., vol. 162, pp. 54-75.

Gillespie J.S. (1962b), "The electrical and mechanical responses of intestinal smooth muscle cells to stimulation of their extrinsic parasympathetic nerves", J. Physiol., vol. 162, pp. 76-92.

Gold B. and Rader C.M. (1969), Digital processing of signals. New York: McGraw-Hill, Chapter 3.

Golenhofen K. (1970), "Slow rhythms in smooth muscle (minute-rhythm)", in Smooth Muscle, edited by Bülbring E., Brading A.F., Jones A.W. and Tomita T., Baltimore: Williams and Wilkins, pp. 316-342.

Golenhofen K. (1976), "Spontaneous activity and functional classification of mammalian smooth muscle", in Physiology of Smooth Muscle, edited by Bülbring E. and Shuba M.F., New York: Raven Press, pp. 91-97.

Grattarola M. and Torre V. (1977), "Necessary and sufficient conditions for synchronization of nonlinear oscillators with a given class of coupling", IEEE Trans. Circuits and Systems, vol. CAS-24, pp. 209-215.

Guillemin E.A. (1957), Synthesis of passive networks. New York: John Wiley.

Haag J. (1962), Oscillatory motions. Belmont, Calif.: Wadsworth.

Haneda Y. (1955), "Luminous organisms of Japan and The Far East", in The luminescence of biological systems, edited by Johnson F.H., Washington D.C.: American Association for the Advancement of Science, pp. 335-385.

Harvey E.N. (1940), Living light. Princeton, New Jersey: Princeton University Press.

Haubrich W.S. (1964), "Anatomy of the colon", in Gastroenterology, vol. 2, edited by Bockus H.L., Philadelphia: W.B. Saunders, pp. 595-618.

Hayashi C. (1964), Nonlinear oscillations in physical systems. New York: McGraw-Hill.

Haykin S.S. (1972), "A unified treatment of recursive digital filtering", IEEE Trans. Automatic Control. vol. AC-17, pp. 113-116.

Helms H.D. (1971), "Digital filters with equiripple or minimax responses", IEEE Trans. Audio Electroacoust., vol. AU-19, pp. 87-93.

Jensen D. (1966), "The hagfish", Scient. Am., vol. 214, no. 2, pp. 82-90.

Kaiser J.F. (1966), "Digital filters", in Systems analysis by digital computer, edited by Kuo F.F. and Kaiser J.F., New York: John Wiley.

Liénard A. (1928), "Étude des oscillations entretenues", Rev. Gén. Élec., vol. 23, pp. 901-912, 946-954.

Linkens D.A. (1974a), "Analytical solution of large numbers of mutually coupled nearly sinusoidal oscillators", IEEE Trans. Circuits. and Systems, vol. CAS-21, pp. 294-300.

Linkens D.A. and Cannell A.E. (1974b), "Interactive graphics analysis of gastrointestinal electrical signals", IEEE Trans. Biomed.Eng., vol. BME-21,pp. 335-339.

Linkens D.A. (1976a), "Stability of entrainment conditions for a particular form of mutually coupled Van der Pol oscillators", IEEE Trans. Circuits and Systems, vol. CAS-23, pp. 113-121.

Linkens D.A., Taylor I. and Duthie H.L. (1976b), "Mathematical modeling of the colorectal myoelectrical activity in humans", IEEE Trans. Biomed. Eng., vol. BME-23, pp. 101-110.

Lynn P.A. (1971), "Recursive digital filters for biological signals", Med. biol. Engng., vol. 9, pp. 37-43.

McMullen C.W. (1968), Communication theory principles. New York: Macmillan Chapter 1.

Milton G.W. and Smith A.W.M. (1956), "The pacemaking area of the duodenum", J. Physiol., vol. 132, pp. 100-114.

Minorsky N. (1962), Nonlinear oscillations. Princeton, New Jersey: D. Van Nostrand.

Nelsen T.S. and Becker J.C. (1968), "Simulation of the electrical and mechanical gradient of the small intestine", Am. J. Physiol., vol. 214, pp. 749-757.

Oppenheim A.V. and Schafer R.W. (1975), Digital signal processing. Englewood Cliffs, New Jersey: Prentice-Hall, Chapter 5.

Oppenheim A.V., Mecklenbrauker W.F.G. and Mersereau R.M. (1976), "Variable cutoff linear phase digital filters", IEEE Trans. Circuits Syst., vol. CAS-23, pp. 199-203.

Ottinger L.W. (1974), Fundamentals of colon surgery. Boston: Little, Brown and Company.

Pavlidis T. (1973), Biological oscillators: Their mathematical analysis.

New York: Academic Press.

Popovic J.R. and Bandler J.W. (1973), "A general program for discrete least pth approximation", Internal Report in Simulation, Optimization and Control, SOC-20, Hamilton, Canada: McMaster University.

Popovic J.R., Bandler J.W. and Charalambous C. (1974), "General programs for least pth and near minimax approximation", Int. J. Syst. Sci., vol. 5, pp. 907-932.

Prosser C.L., Weems W.A. and Connor J.A. (1976), "Types of slow rhythmic activity in gastrointestinal muscles", in Physiology of Smooth Muscle, edited by Bülbring E. and Shuba M.F., New York: Raven Press, pp. 99-109.

Provenzale L. and Pisano M. (1971), "Methods for recording electrical activity of the human colon in vivo", Am. J. Digest. Dis., vol. 16, pp. 712-722.

Puestow C.B. (1933), "Studies on the origin of the automaticity of the intestine: the action of certain drugs on isolated intestinal transplants", Am. J. Physiol. vol. 106, pp. 682-688.

Rabiner L.R., Cooley J.W., Helms H.D., Jackson L.B., Kaiser J.F., Rader C.M., Schafer R.W., Steiglitz K. and Weinstein C.J. (1972) "Terminology in digital signal processing", IEEE Trans. Audio Electroacoust., vol. AU-20, pp. 322-337.

Rabiner L.R., Kaiser J.F., Herrmann O. and Dolan M.T. (1974), "Some comparisons between FIR and IIR digital filters", Bell Syst. Tech. J., vol. 53, pp. 305-331.

Rabiner L.R. and Gold B. (1975), Theory and applications of digital signal processing. Englewood Cliffs, New Jersey: Prentice-Hall.

Rivlin T.J. (1974), The Chebyshev polynomials. New York: John Wiley.

Roberge F.A. and Nadeau R.A. (1966), "Simulation of sinus node activity by an electronic relaxation oscillator", Can. J. Physiol. Pharmacol., vol. 44, pp. 301-315.

Saaty T.L. and Bram J. (1964), Nonlinear mathematics. New York: McGraw-Hill, Chapter 4.

Sablatash M. (1971), "Approximation theory for digital filters", IEEE Trans. Circuit Theory, vol. CT-18, pp. 741-743.

Sansone G. and Conti R. (1964), Nonlinear differential equations. New York: Macmillan.

Sarna, S.K., Daniel E.E. and Kingma Y.J. (1971), "Simulation of slow-wave electrical activity of small intestine", Am. J. Physiol., vol. 221, pp. 166-175.

Sarna S.K., Daniel E.E. and Kingma Y.J. (1972), "Simulation of the electrical control activity of the stomach by an array of relaxation oscillators", Am. J. Digest. Dis., vol. 17, pp. 299-310.

Sarna S.K. (1975a), "Models of smooth muscle electrical activity", in Methods in Pharmacology, edited by Daniel E.E. and Paton D.M., New York: Plenum Press, pp. 519-540.

Sarna S.K. (1975b), "Gastrointestinal electrical activity: terminology", Gastroenterology, vol. 68, pp. 1631-1635.

Schafer R.W. and Rabiner L.R. (1973), "A digital signal processing approach to interpolation", Proc. IEEE , vol. 61, pp. 692-702.

Schüssler W. and Winkelnkemper W. (1970), "Variable digital filters", Arch. Elek. Übertragung, vol. 24, pp. 524-525.

Speckhart F.H. and Green W.L. (1976), A guide to using CSMP-the continuous system modeling program. Englewood Cliffs, New Jersey : Prentice-Hall.

Steiglitz K. (1965), "The equivalence of digital and analog signal processing", Inform. Contr., vol. 8, pp. 455-467.

Steiglitz K. (1970), "Computer-aided design of recursive digital filters", IEEE Trans. Audio Electroacoust., vol. AU-18, pp. 123-129.

Steiglitz K. (1971), "Designing short-word recursive digital filters", Proc. 9th Allerton Conf. Circuit and System Theory, Urbana, Ill,, pp. 778-788.

Steiglitz K. (1974), An introduction to discrete systems. New York: John Wiley.

Stephenson, R.E. (1971), Computer simulation for engineers. New York: Harcourt Brace Jovanovich.

Storzbach, W.H. (1972), "On the design of recursive digital filters with minimum coefficient word length", Proc. of Int. Symp. on Circuits Theory, North Hollywood, Calif., pp. 279-282.

Suk M. and Mitra S.K. (1972), "Computer-aided design of digital filters with finite word length", IEEE Trans. Audio Electro-acoust., vol. AU-20, pp. 356-363.

Taylor I.,Duthie H.L., Smallwood R., Brown B.H. and Linkens D.A. (1974), "The effect of stimulation on the myoelectrical activity of the rectosigmoid in man", Gut, vol. 15, pp. 599-607.

Taylor I.,Duthie H.L., Smallwood R. and Linkens D.A. (1975), "Large bowel myoelectrical activity in man", Gut, vol. 16, pp. 808-814.

Van der Pol B. (1926), "On relaxation oscillations", Phil. Mag., vol. 2, pp. 987-992.

Van der Pol B. (1927), "Forced oscillations in a circuit with nonlinear resistance", Phil. Mag.,vol. 3, pp. 65-80.

Van der Pol B. and Van der Mark J. (1928), "The heart beat considered as a relaxation oscillator and an electrical model of the heart", Phil. Mag., Suppl. 6, pp. 763-775.

Van der Pol B. (1940), "Biological rhythms considered as relaxation oscillations", Acta Med. Scand., Suppl. 108, pp. 76-87.

Vanasin B., Ustach T.J. and Schuster M.M. (1971), "Motor and electrical activity in human colon in vitro and in vivo", Gastroenterology, vol. 60, pp. 728.

Weaver C.S., Von der Groeben J., Mantey P.E., Toole J.G., Cole Jr. C.A., Fitzgerald J.W. and Lawrence R.W. (1968), "Digital filtering with applications to electrocardiogram processing", IEEE Trans. Audio Electroacoust. , vol. AU-16, pp. 350-391.

Winfree A.T. (1967), "Biological rhythms and the behavior of populations of coupled oscillators", J. Theoret. Biol., vol. 16, pp. 15-42.